FAIRCHILD SPACE AND DEFENSE SYSTEMS
A Division of Fairchild Camera and Instrument Corporation
300 Robbins Lane, Syosset, New York

Technical Summary Report

MARTIAN ORBITAL PHOTOGRAPHIC STUDY

Contract NAS8-21025

Job No. 2174
FSDS Report S&T-C67-3 FSDS-S/T-C67-3
30 December 1967

Submitted to:
NATIONAL AERONAUTICS AND SPACE ADMINISTRATION
GEORGE C. MARSHALL SPACE FLIGHT CENTER
Huntsville, Alabama, 35812

Prepared by:
R. Bashe,
Program Manager

S. Kennedy,
Project Engineer

Approved by:
E. E. Honeywell, Manager
Advanced Programs

J. J. Marcinek, Director
Divisional Systems & Technology

MARTIAN ORBITAL PHOTOGRAPHIC STUDY

ABSTRACT

A comprehensive study program aimed at achieving a more precise definition of realistic Martian orbital photographic experiment objectives and instrumentation techniques for the early orbital missions is described.

Photographic experiment objectives, photo sensor subsystems, and system tradeoff considerations are presented. Photo sensor system and support instrumentation requirements, as related to the scientific mission objectives, are discussed in terms of the geographic and environmental characteristics of the planet Mars.

A detailed review of those particular areas of scientific inquiry concerning the planet Mars which can be investigated by means of orbital photographic sensors is given. Surface features requiring either high or medium resolution imaging capability for analysis are delineated. Specific areas for high resolution Martian coverage are suggested.

The relationships between relevant orbital parameters and mission constraints to the imaging system design criteria are developed. Current state-of-the-art and realizable capabilities of optical subsystems and various film, electro-optical and other sensor devices are discussed in detail. System coverage, resolution, sensitivity, format size, multispectral capability and stereo capability are evaluated. Also considered are system assessments of data acquisition, conversion and transmission requirements and techniques. The results of photo system tradeoff studies are presented.

ACKNOWLEDGEMENT

This report was prepared under NASA Contract NAS8-21025 for Marshall Space Flight Center by Fairchild Space and Defense Systems (FSDS), a Division of Fairchild Camera and Instrument Corporation.

Fairchild Space and Defense Systems is indebted to Drs. D. Hale and L. Wood of Marshall Space Flight Center for their guidance and general assistance during this program. Special mention must also be made of the valuable cooperation of personnel from Ames Research Center, Jet Propulsion Laboratory, Boeing Company, General Electric Company and numerous instrumentation manufacturers.

The authors are grateful to the following FSDS personnel, who contributed to the preparation of the information and results presented in this report: S. Abrahams, A. D. Becassio, J. Bennardo, P. Reichel, D. Seyka and J. Waltzer. Sincere appreciation is expressed to management and consultant personnel for their advice and review.

Robert Bashe
Program Manager

TABLE OF CONTENTS

Section	Title	Page
	ABSTRACT	-ii-
	ACKNOWLEDGEMENT	-iii-
	TABLE OF CONTENTS	-iv-
	LIST OF ILLUSTRATIONS	-xi-
	LIST OF TABLES	-xx-
1	INTRODUCTION AND SUMMARY	1-1
1.1	PROGRAM OBJECTIVES AND GUIDELINES	1-2
1.2	PROGRAM TASKS	1-4
1.3	PROGRAM SUMMARY	1-5
1.4	PROGRAM RECOMMENDATIONS	1-10
2	MARTIAN ENVIRONMENTAL CHARACTERISTICS	2-1
2.1	MARTIAN SURFACE FEATURES	2-1
2.1.1	Light Areas (Continents or Deserts)	2-1
2.1.2	Dark Areas (Maria)	2-3
2.1.3	Polar Caps	2-4
2.1.4	Canals	2-5
2.1.5	Oases	2-7
2.1.6	Craters	2-7
2.1.7	Summary of Martian Surface Features	2-8

TABLE OF CONTENTS (Continued)

Section	Title	Page
2.2	SEASONAL AND SECULAR VARIATIONS	2-11
2.2.1	Wave of Darkening	2-11
2.2.2	Secular Variations	2-13
2.3	ATMOSPHERIC CHARACTERISTICS	2-14
2.3.1	Atmospheric Composition	2-14
2.3.2	Aerosols	2-14
2.3.3	Pressure	2-15
2.3.4	Surface Density	2-16
2.3.5	Temperature	2-18
2.3.6	Circulation	2-20
2.4	MARTIAN CLOUDS AND HAZE	2-22
2.4.1	Blue-White Clouds	2-22
2.4.2	Yellow Clouds	2-23
2.4.3	Blue Haze	2-23
2.4.4	Summary of Cloud Types	2-24
2.5	MARTIAN SATELLITES	2-26
2.6	MARTIAN PHOTOMETRIC CHARACTERISTICS	2-27
2.6.1	Visual Magnitude	2-27
2.6.2	Martian Spectral Reflectivity	2-27
2.6.3	Mariner IV Photography	2-30
2.6.4	Photometric Function Analysis	2-32
2.7	POLARIZATION PROPERTIES	2-33
2.8	MARTIAN RADIATION ENVIRONMENT	2-34

TABLE OF CONTENTS (Continued)

Section	Title	Page
2.9	REFERENCES	2-38
3	MISSION OBJECTIVES AND PHOTO SYSTEM REQUIREMENTS	3-1
3.1	RESOLUTION AND COVERAGE REQUIREMENTS	3-2
3.1.1	Medium Resolution Coverage Requirements	3-6
3.1.2	High Resolution Coverage Requirements	3-6
3.2	STEREO REQUIREMENTS	3-13
3.2.1	Detectable Object Height	3-13
3.2.2	Recommended Stereo Coverage	3-15
3.3	MULTISPECTRAL REQUIREMENTS	3-16
3.3.1	Advantages of Multispectral Techniques	3-16
3.3.2	Multispectral Filter Considerations	3-18
3.3.3	Recommended Multispectral Parameters	3-18
3.4	SUMMARY OF PHOTO SYSTEM REQUIREMENTS	3-20
3.5	REFERENCES	3-22
4	TRAJECTORIES AND PHOTO COVERAGE OF MARS	4-1
4.1	ORBIT SELECTION CONSIDERATIONS	4-2
4.1.1	Voyager Interplanetary Trajectory Considerations	4-6
4.1.2	Martian Orbit Considerations	4-14

TABLE OF CONTENTS (Continued)

Section	Title	Page
4.2	RECONNAISSANCE ORBITS AND COVERAGE	4-23
4.2.1	Detailed Coverage Examples	4-24
4.2.2	Satellite Subpoint Characteristics	4-41
4.2.3	Orbit Parameters and System Considerations	4-45
4.3	REFERENCES	4-58
5	OPTICAL SUBSYSTEM ASSESSMENT	
5.1	OPTICAL SUBSYSTEM INSTRUMENTATION	5-1
5.1.1	Lens System Types	5-1
5.1.2	General Optical Subsystem Parameters	5-7
5.1.3	Imaging System Thermal Considerations	5-26
5.1.4	Lens/Camera Calibration	5-29
5.2	STEREO INSTRUMENTATION	5-31
5.3	MULTISPECTRAL IMAGING INSTRUMENTATION	5-33
5.3.1	Colorimetric and Spectrometric Instrumentation Techniques	5-33
5.3.2	Multispectral Filters	5-34
5.4	REFERENCES	5-37
6	PHOTOSENSOR ASSESSMENT	6-1
6.1	ELECTRO-OPTICAL SENSORS	6-3
6.1.1	Vidicon Tubes	6-5
6.1.2	Image Orthicon Tubes	6-7

TABLE OF CONTENTS (Continued)

Section	Title	Page
6.1.3	Return Beam Vidicon Tubes	6-12
6.1.4	SEC Vidicon Tubes	6-14
6.1.5	Plumbicon Tubes	6-14
6.1.6	Comparison of Electro-Optical Sensors	6-16
6.2	SILVER HALIDES	6-19
6.2.1	Silver Halide Characteristics	6-19
6.2.2	Space Processing of Silver Halide	6-20
6.2.3	Film Radiation Shielding Requirements	6-27
6.3	TAPE SENSOR SYSTEMS	6-38
6.3.1	Dielectric Tape	6-38
6.3.2	Electrostatic Tape	6-39
6.3.3	Photoplastic Tape	6-41
6.3.4	Comparison of Tape Sensors	6-43
6.4	OTHER SENSOR MATERIALS	6-45
6.4.1	Electrophotography	6-45
6.4.2	Dry Silver	6-45
6.4.3	Frost Xerography	6-45
6.4.4	RS Process	6-46
6.4.5	Diazo	6-46
6.5	SENSOR SUMMARY	6-47
6.6	REFERENCES	6-49
7	CONVERSION SUBSYSTEM ASSESSMENT	7-1
7.1	MISSION DATA HANDLING CAPABILITY AND REQUIREMENTS	7-1

TABLE OF CONTENTS (Continued)

Section	Title	Page
7.1.1	Spacecraft Data Transmission Capability	7-2
7.1.2	Mission Data Rate Requirements	7-2
7.2	DATA STORAGE CAPABILITY	7-9
7.2.1	Magnetic Tape Recorders	7-9
7.2.2	Photographic Film Storage	7-12
7.3	DATA READOUT TECHNIQUES	7-19
7.3.1	Flying Spot Scanners	7-19
7.3.2	Electro-Mechanical Scanners	7-21
7.4	BANDWIDTH UTILIZATION	7-22
7.5	REFERENCES	7-24
8	PHOTOSYSTEM TRADEOFF ANALYSES	8-1
8.1	SYSTEMS COMPARISON: GROUND RESOLUTION	8-2
8.2	SYSTEMS COMPARISON: GROUND COVERAGE	8-15
8.3	SYSTEM COMPARISON: OVERALL CONSIDERATIONS	8-20
8.3.1	Dual Resolution Capability	8-20
8.3.2	Multi-Spectral Capability	8-20
8.3.3	Stereo Capability	8-20
8.3.4	Mensuration Capability	8-21
8.3.5	Data Readout Flexibility	8-21
8.3.6	Dual Resolution Readout	8-22
8.3.7	Repeated Readout	8-22

TABLE OF CONTENTS (Continued)

Section	Title	Page
8.3.8	Delayed Readout	8-23
8.3.9	Lifetime Limitations	8-23
8.3.10	Development Risks	8-24
8.4	SYSTEMS COMPARISON; SUMMARY	8-24
APPENDIX A:	CHARACTERISTICS OF MARTIAN ORBITS	A-1
APPENDIX B:	VIEWING GEOMETRY, COVERAGE AND LOCATION ERRORS	B-1
APPENDIX C:	OTHER ORBITAL CONSIDERATIONS	C-1
APPENDIX D:	NON-UNIFORM IMAGE MOTION ON PLATE OF CAMERA SYSTEM IN ELLIPTICAL ORBIT.	D-1
APPENDIX E:	GLOSSARY	E-1

LIST OF ILLUSTRATIONS

Figure Number	Title	Page
2-1	Planetary Seasonal Variations	2-12
2-2	Pressure Vs. Altitude Above Electris Region	2-17
2-3	Vertical Distribution of Temperature of Martian Atmosphere	2-19
2-4	Diurnal Variation of Surface Temperature	2-20
2-5	Visual Phase Curve of Mars	2-28
2-6	Spectral Variation of Magnitude and Phase Coefficient	2-29
2-7	Spectral Variation of Martian Albedo	2-31
2-8	Solar Activity	2-36
3-1	Surface Feature Resolution Requirements	3-5
3-2	High Resolution Coverage and Communication Requirements	3-8
3-3	Martian Areas of Interest	3-12
3-4	Minimum Object Height for Stereo Vision	3-14

LIST OF ILLUSTRATIONS (Continued)

Figure Number	Title	Page
4-1	Orbit Selection Process	4-3
4-2	Comparison of Photo System Parameters for Selected Orbits	4-5
4-3	Type I Trajectory Region for 1973 and 1975 Opportunities	4-12
4-4	Near Mars Approach Geometry	4-19
4-5	Mars Surface Covered by Sensor (Inclination: -60 degrees)	4-26
4-5a	After 10 Days in Orbit	4-26
4-5b	After 20 Days in Orbit	4-27
4-5c	After 30 Days in Orbit	4-28
4-5d	After 60 Days in Orbit	4-29
4-5e	After 90 Days in Orbit	4-30
4-5f	After 120 Days in Orbit	4-31
4-5g	After 180 Days in Orbit	4-32

LIST OF ILLUSTRATIONS (Continued)

Figure Number	Title	Page
4-6	Mars Surface Covered by Sensor (Inclination: -40 degrees)	4-33
4-6a	After 10 Days in Orbit	4-33
4-6b	After 20 Days in Orbit	4-34
4-6c	After 30 Days in Orbit	4-35
4-6d	After 60 Days in Orbit	4-36
4-6e	After 90 Days in Orbit	4-37
4-6f	After 120 Days in Orbit	4-38
4-6g	After 180 Days in Orbit	4-39
4-7	Percent Martian Surface Coverage Vs. Days in Orbit	4-40
4-8	Percent Surface Covered Vs. Hours in a Circular Polar Orbit	4-42
4-9	Satellite Subtrack and Constant Altitude Contours; i = -60°	4-43
4-10	Satellite Subtrack and Constant Altitude Contours; i = -40°	4-44

LIST OF ILLUSTRATIONS

Figure Number	Title	Page
4-11	Sun Angle Along the Satellite Subtrack; i = -60°	4-46
4-12	Sun Angle Along the Satellite Subtrack; i = -40°	4-47
4-13	Variation of Swath Width with Altitude for 10 Degree Field of View	4-48
4-14	Parameters for Orbit Having Periapsis Altitude of 1000 km and Eccentricity of 0.656032	4-49
4-15	Parameters for Orbit Having Periapsis Altitude of 500 km and Eccentricity of 0.548182	4-50
4-16	Parameters for Orbit Having Periapsis Altitude of 1000 km and Eccentricity of 0.783737	4-51
4-17	Geometry of Orbit Having Eccentricity of 0.656032	4-52
4-18	Geometry of Orbit Having Eccentricity of 0.548182	4-53
4-19	Geometry of Orbit Having Eccentricity of 0.783737	4-54
4-20	Approximate Relative Positions of Earth and Mars at 30 Day Intervals	4-55

LIST OF ILLUSTRATIONS

Figure Number	Title	Page
4-21	Illustration of Precession of Line of Apsides with Respect to Terminator and Earth Direction	4-56
5-1	Typical Lens System Types	5-2
5-2	Aperture Size Vs. Mass for Refractive and Catadioptric Optical Systems	5-9
5-3a	Focal Length Vs. Ground Resolution for 300 km Altitude	5-11
5-3b	Focal Length Vs. Ground Resolution for 600 km Altitude	5-12
5-3c	Focal Length Vs. Ground Resolution for 900 km Altitude	5-13
5-3d	Focal Length Vs. Ground Resolution for 1200 km Altitude	5-14
5-4	Ground Resolution Vs. Altitude for 100 lp/mm System	5-15
5-5	Basic Lens Parameters and Field of View	5-16
5-6a	Lateral Coverage Vs. Altitude for 25mm Format	5-18
5-6b	Lateral Coverage Vs. Altitude for 75mm Format	5-19

LIST OF ILLUSTRATIONS

Figure Number	Title	Page
5-7	Exposure Time Nomograph	5-22
5-8	Allowable FMC Error Vs. Exposure Time	5-23
5-9	Vehicle Stability Rate Requirements Vs. Exposure Time	5-25
5-10	Lens Nomenclature for Thermal Analysis	5-27
6-1	Electro-Optical Tube Schematics	6-6
6-2	Electro-Optical Sensor Illumination Transfer Curves	6-9
6-3	Electro-Optical Sensor Modulation Transfer Functions	6-10
6-4	Modulation Transfer Functions and Spectral Characteristics of Kodak Films	6-22
6-5	Comparison of Fairchild Fairweb with Processed SO-243 High Definition Film	6-25
6-6a	Radiation Exposure for Kodak SO-243 High Definition Aerial Film - Bimat Processed	6-29
6-6b	Radiation Exposure for Kodak SO-243 High Definition Aerial Film	6-30
6-6c	Radiation Exposure for Kodak SO-206 Special Aerial Negative Film	6-31

LIST OF ILLUSTRATIONS

Figure Number	Title	Page
6-7a	Exposure Dose Versus Aluminum Shield Thickness for a Mars Mission	6-33
6-7b	Exposure Dose Versus Polyethylene Shield Thickness for a Mars Mission	6-34
6-8	Shielding Mass Versus Film Length for 70mm SO-243 Film	6-35
7-1	Comparison of Microwave and Optical Total Communication System Mass Vs. Bit Rate	7-3
7-2	Data Transmission Requirements Vs Percent Coverage	7-4
7-3	Planetary Spacecraft Communications as a Function of Mission Life	7-6
7-4a	Percent Coverage of Mars Vs. Required 70mm Film Length for a 50 lp/mm System	7-13
7-4b	Percent Coverage of Mars Vs. Required 70mm Film Length for a 100 lp/mm System	7-14
7-4c	Percent Coverage of Mars Vs. Required 70mm Film Length for a 200 lp/mm System	7-15
7-5a	Percent Coverage of Mars Vs. Mass of Required 70mm Film and Processing Material for a 50 lp/mm System	7-16

LIST OF ILLUSTRATIONS

Figure Number	Title	Page
7-5b	Percent Coverage of Mars Vs. Mass of Required 70mm Film and Processing Material for a 100 lp/mm System	7-17
7-5c	Percent Coverage of Mars Vs. Mass of Required 70mm Film and Processing Material for a 200 lp/mm System	7-18
8-1	Typical Martian Orbiter Film Camera	8-5
8-2	Film System Mass as a Function of Ground Resolution	8-7
8-3	Return Beam Vidicon System Mass as a Function of Ground Resolution	8-8
8-4	Vidicon System Mass as a Function of Ground Resolution	8-9
8-5a	Comparison of Systems Mass Vs. Resolution: 100 Days in Orbit (10^4 bits/sec. Data Rate)	8-10
8-5b	Comparison of Systems Mass Vs. Resolution: 100 Days in Orbit (10^5 bits/sec. Data Rate)	8-11
8-6a	Comparison of Systems Mass Vs. Resolution: 200 Days in Orbit (10^4 bits/sec Data Rate)	8-12

LIST OF ILLUSTRATIONS

Figure Number	Title	Page
8-6b	Comparison of Systems Mass Vs. Resolution: 200 Days in Orbit (10^5 bits/sec Data Rate)	8-13
8-7	Comparison of Photosystem Parameters for Selected Orbits	8-16
8-8a	Percent Planet Coverage Vs. Number of Photographs Required (100 Meter Ground Resolution)	8-17
8-8b	Percent Planet Coverage Vs. Number of Photographs Required (10 Meter Ground Resolution)	8-18
8-8c	Percent Planet Coverage Vs. Number of Photographs required (1 Meter Ground Resolution)	8-19

LIST OF TABLES

Table Number	Title	Page
1-1	Program Guidelines	1-3
1-2	Outline of Program Tasks	1-4
1-3	Martian Surface and Cloud Features	1-5
1-4	Photosystem Coverage Summary	1-6
1-5	Example Systems Comparison	1-9
2-1	Characteristics of Primary Martian Surface Features	2-9
2-2	Characteristics of Secondary Martian Surface Features	2-10
2-3	Martian Atmospheric Composition Models	2-14
2-4	Martian Surface Pressure	2-16
2-5	Martian Cloud Formations	2-25
2-6	Mission Radiation Environment	2-35
3-1	Significance of Typical Terrestrial Surface Features	3-3
3-2	Martian Surface Features - Areas of Interest	3-9
3-3	Summary Multispectral Considerations	3-19
3-4	Summary of Optimum Photo System Requirements	3-21

LIST OF TABLES

Table Number	Title	Page
4-1	Summary of Constraints	4-11
4-2	Example Orbit Characteristics	4-25
5-1	Advantages and Disadvantages of Zoom Systems	5-4
5-2	Performance Comparisons of Refractive vs. Catadioptric Optical Systems	5-6
5-3	Physical Comparisons of Refracting Vs. Catadioptric Optical Systems	5-6
5-4	Long Focal Length Reiractive Lens Systems	5-8
5-5	Long Focal Length Catadioptric Lens Systems	5-8
5-6	Comparisons of Large and Small Format Sizes	5-17
5-7	Martian Thermal and Albedo Radiation on a Spherical Satellite	5-27
5-8	Advantages and Disadvantages of Various Types of Filter Supports	5-35
6-1	Photosensor Chart	6-2
6-2	Space Television Camera Systems	6-4

LIST OF TABLES

Table Number	Title	Page
6-3	Vidicon Performance and Physical Characteristics	6-8
6-4	Image Orthicon Performance and Physical Characteristics	6-11
6-5	Return Beam Vidicon and Physical Characteristics	6-13
6-6	SEC Vidicon Performance and Physical Characteristics	6-15
6-7	Plumbicon Performance and Physical Characteristics	6-17
6-8	Electro-Optical Sensor Summary Chart	6-18
6-9	Silver Halide Characteristics Chart	6-21
6-10	Silver Halide Processing Techniques for Space Applications	6-26
6-11	Meteorological Dielectric Tape Camera System Characteristics	6-40
6-12	Electrostatic Tape Camera System Characteristics	6-42
6-13	Comparison of Dielectric, Electrostatic and Photoplastic Tape Materials	6-44
6-14	Comparison of Sensors for Voyager Martian Mission Applications	6-48

LIST OF TABLES

Table Number	Title	Page
7-1	Data Transmission Parameters, 100 Days in Orbit	7-7
7-2	Data Transmission Parameters, 200 Days in Orbit	7-8
7-3	Mariner Tape Recorder Characteristics	7-11
7-4	Digital Source Bit Rate Reduction by Data Coding	7-23
8-I	Common System Parameters Assumed for Example Systems Comparisons	8-3
8-2	Individual Sensor System Characteristics Assumed for Systems Comparisons	8-6
8-3	Photosystem Comparison Summary	8-25

SECTION 1

INTRODUCTION AND SUMMARY

The planet Mars has been observed from Earth for centuries, but theories regarding its origin, composition and activity are subject to continuous debate. The early Martian orbital missions will provide a means for obtaining more information concerning the characteristics of the planet than has been obtained as a result of all previous observations from Earth.

An orbital photographic imaging system will acquire extensive data of Martian surface features and atmospheric phenomena. This photographic coverage will permit scientists in many disciplines (e.g., astronomy, biology, cartography, geology, meteorology) to examine the data and determine the history, structure and current activity of the planet.

This report describes an approximately 3,000 manhour Martian Orbital Photographic Study program conducted by Fairchild Space and Defense Systems, a Division of Fairchild Camera and Instrument Corporation, for the National Aeronautics and Space Administration – Marshall Space Flight Center. The program objectives, guidelines and specific tasks are described in this introductory section. A brief summary of program results and recommendations is presented.

1.1 PROGRAM OBJECTIVES AND GUIDELINES

This comprehensive five month study program has been aimed at achieving a more precise definition of realistic Martian orbital photographic experiment objectives and instrumentation techniques for the earlier orbital missions. The results of the study program were intended to influence the final selection of the photo system for the Voyager Orbital Package and serve as a basis for future system hardware definition programs.

The program has involved investigation of the following major areas:

- Martian orbital, environmental and photometric parameters
- orbital mission scientific objectives and photosystem requirements
- photo subsystem assessment including optical, photosensor and conversion subsystems
- photosystem tradeoffs.

Basic program guidelines were established by Marshall Space Flight Center and followed during the study. The investigations were initially directed toward the mission objectives for a 1973 Voyager mission. Mission durations of up to 14 months have been considered, covering the stated transit time of up to 8 months plus 1 to 6 months in orbit. Orbits with periapses ranging from the specified low of 300 kilometers to the high of 1200 kilometers have been examined.

Ground resolutions of about 60 meters (medium resolution) and a limiting 1-2 meters for high resolution were suggested for parametric analysis. Resolution criteria were to be established as a result of analyses of Martian surface features and atmospheric phenomena. Refractive and reflective optical subsystem capability and certain photosensor devices or materials (e.g., electro-optical, silver halide, dielectric tape, and photoplastic tape) were specified for consideration. A general limit of 80 kilograms was suggested for the photographic system.

1.3 PROGRAM SUMMARY

The program has involved the study of orbital photographic experiment objectives and instrumentation techniques for the early missions to Mars. Martian surface and environmental characteristics have been examined in order to establish these mission objectives and basic photosystem requirements for the early orbital missions to Mars.

The surface features of Mars have been analyzed in detail in terms of distribution and extent, surface configuration and material, diurnal, seasonal and secular variations and photographic characteristics. Summary charts of these factors have been prepared for both the primary and secondary surface features indicated in Table 1-3. Atmospheric characteristics such as composition, pressure, density, temperature and circulation have been considered. The distribution occurrence variations and photographic visibility of cloud and haze phenomena have been examined. Polarization and spectral characteristics and the effect of the Martian radiation environment have been investigated.

TABLE 1-3 MARTIAN SURFACE AND CLOUD FEATURES

Primary Features

Continents or Deserts
Maria
Polar Caps

Secondary Features

Canals
Oases
Craters

Cloud Phenomena

Blue-white clouds
Yellow clouds
Blue haze

The mission objectives and the photosystem requirements to satisfy these objectives have been established. Resolution requirements have been determined, based on analogies to features on Earth. Recommended coverage requirements for medium and high resolution mapping are summarized in Table 1-4. Fourteen areas have been selected for high resolution photographic coverage. Stereo and multispectral coverage requirements have been specified for the high and medium systems.

TABLE 1-4 PHOTOSYSTEM COVERAGE SUMMARY

CAMERA	MEDIUM RESOLUTION	HIGH RESOLUTION
Desirable Resolution	40 to 70 meters	5 meters
Coverage	Optimum: Complete Coverage Desirable: 40°N to 40°S Latitude Minimum: 30°N to 30°S Latitude Limited Polar Coverage	Selected Areas: Atlantis, Elysium, Hellas, Lunae Lacus, Mare Acidalium Mare Hadriaticum, Mare Sirenium, Margaritifer Sinus, Meridiani Sinus, Solis Lacus, Syrtis Major, Tharsis, Thoth-Nepenthes Trivium Charontis
Stereo and Multispectral coverage	Overlapping stereo coverage; limited multispectral coverage	Probably no stereo coverage, limited multispectral coverage

Orbit selection criteria have been investigated for Martian mission opportunities. Photosystem considerations and both orbit and interplanetary trajectory constraints have been considered. A range of acceptable orbit parameters has been established based upon these constraints. Comparisons have been made between circular and elliptical orbits and between polar and non-polar orbits. Detailed analyses of obtainable Martian surface coverage were made for selected example orbits. Satellite subpoint track plots and planet coverage plots as a function of time in orbit have been presented for example orbits.

Parametric assessments of photographic subsystem performance capabilities have been conducted. Optical, sensing, recording and conversion devices and instrumentation techniques have been evaluated.

Refractive and reflective optical system types were compared, and the advantages and disadvantages of each for the orbital photographic application have been determined. Zoom lenses were rejected because of high performance requirements. Relative aperture size versus mass relationships for refractive and catadioptric lens systems have been specified. Reflective systems offer considerable mass savings for long focal length applications, but the final lens system selection must be made after specific mission objectives and system parameters have been defined. Optical system constraints on ground resolution, coverage and image quality have been parametrically examined. System resolution, focal length, format size, exposure time, image motion compensation and vehicle stability requirements have been analyzed. Stereo and multispectral instrumentation techniques have been evaluated.

Photosensitive devices and materials have been evaluated to select sensors suitable for the Martian orbital planetary missions. Sensor physical characteristics, performance and development status have been considered. Photosensors which were considered are:

electro-optical tubes
silver halides
dielectric, electrostatic and photoplastic tapes
electrophotography
dry silver
frost xerography
diazo.

Vidicon sensors and silver halide film Type SO-243 were selected as the most suitable for Martian applications. Space processing techniques and radiation shielding requirements have been specified. The tape systems, although promising, require additional development. Relative advantages and disadvantages of the vidicon, silver halide and tape sensors have been compared and tabulated.

The communication limitations for the orbital missions have been considered. Data rate capabilities for the mid 1970's have been evaluated; both optical and r. f. system techniques have been assessed. Based on bandwidth limitations, the storage requirements for the mission are parametrically determined. The requirements for use of magnetic tape recorders for vidicon imaging systems have been examined and recorder characteristics and anticipated performance have been assessed. Silver halide films provide a dual sensing and storage capability, but require a film scanning device for readout. Based on the anticipated communication capabilities, the film length and mass requirements have been determined. The relatively small lengths of film required (i.e., only 30 meters for complete planet coverage with 100 meter ground resolution and a 100 line pair/mm system resolution) indicate that the mission is apparently communication limited. At a data rate of 10^4 bits/second for the conditions stated, over 500 days would be required to transmit the 4×10^{11} total bits stored on 30 meters of film, but only about 50 days would be required for a data rate capability of 10^5 bits/second. Suitable CRT and electro-mechanical scanning systems have been described and compared. Development of solid state mechanical scanning techniques is indicated.

Overall photosystem performance capabilities have been compared for one inch vidicon, two inch return beam vidicon and 70 mm SO-243 silver halide example systems. System parameters and mission characteristics have been specified. The three system concepts have been parametrically evaluated on the basis of coverage capability, ground resolution capability versus system mass, and compared for other system factors as well.

Table 1-5 presents an example summary comparison of the system mass and the number of photographs required for the three systems; a 4×10^{11} bit total mission communications capability is assumed for this example.

TABLE 1-5 EXAMPLE SYSTEMS COMPARISON
(10^4 bits/sec; 100 days in orbit, 4×10^{11} total bits)

	70 mm Film System	Return Beam Vidicon System	Vidicon System
High Resolution System (5 meters):			
Mass (kg)	80	120	500
Total Frames	3.5×10^2	3.5×10^3	5.5×10^4
Medium Resolution System (50 meters):			
Mass (kg)	24	27	17
Total Frames	3.5×10^2	3.5×10^3	5.5×10^4

Relative ratings of the individual systems, resulting from the system tradeoffs performed, have been prepared and tabulated. For the example systems compared and the mission characteristics assumed, the film system provides the best high resolution capability for the smallest mass penalty. The film system also requires the fewest number of photographs to satisfy the mission coverage recommendations.

1.4 PROGRAM RECOMMENDATIONS

The Martian Orbital Photographic Study performed by FSDS has been necessarily limited in scope and in the depth of analysis permitted during the approximately 3,000 manhour program. Since additional Martian surface and environmental investigations as well as extensive photosystem analyses are required, recommendations for future efforts are presented.

1.4.1 Mission Objectives and Photosystem Requirement Definition

- Detailed mission objectives and photosystem requirements must be redefined as the mission guidelines are changed or defined in greater detail for specific missions. Changes in mission date, payload and communications data rate are particularly important. For example, the quantity of stereo and/or multispectral data to be acquired must be more fully defined in terms of mission communication limitations, data handling requirements, data utilization and system instrumentation requirements.

- Non-photographic experiment requirements must be firmly established and the impact on the photosystem evaluated. The commonality of orbital parameters, mission life, data rate, mass and power requirements must be considered.

1.4.2 Martian Surface Feature and Environment Analyses

- Martian surface features should be analyzed in greater detail and an extensive terrain target model should be developed. The limited Mariner IV imagery data can be used during preparation of the model. Terrain, cloud and haze simulation should be considered. Toward this end, Martian clouds and haze phenomena should be re-evaluated in order to delineate cloud types by pattern, geographic location, seasonal variation and observed movement. The model should be used for experimental analysis with variable illumination angles, brightness, reflectivity, etc.

- For each planned mission, the anticipated propagation of the wave of darkening during the mission should be plotted. Specific maria, canal and oasis regions of interest should be identified; particular times for observation should be indicated for each region and this data should be correlated with orbit ground track data.

- An extensive evaluation of representative macro and micro terrain and ecologic feature interpretability at specific resolution levels should be conducted. Available small scale imagery, particularly satellite imagery, should be used for the investigation. This suggested effort would corroborate the Martian terrain feature resolution requirements specified in the current study.

- When more well defined guidelines are established, the criteria for selecting areas for high resolution coverage must be re-examined. Consideration should be given both to the selection of areas in advance of the mission and on the basis of results of analysis of the medium resolution coverage during the mission. In addition to the fourteen areas selected for high resolution coverage during the study, other anomalous areas should be selected for possible future high resolution observation from the Martian orbiting vehicle. The feasibility of photographing each or all of the selected regions at high resolution should be considered as a function of orbit parameters, illumination limitations, communication capability and acquisition time.

1.4.3 Orbit Selection Analyses

- Greater emphasis should be placed on the interrelationships between orbit selection criteria and photographic system requirements. Cumulative coverage overlays, such as those illustrated in this document, should be developed for all potential orbits considered to evaluate the optimum coverage obtainable. This should include the combined coverage obtained simultaneously by sensors in two different orbits.

- Plotted coverage patterns should be correlated with the

selected areas of particular interest. Altitude effects on scale and resolution should be examined in detail for selected orbits. Several values of sensor field-of-view should also be evaluated.

1.4.4 Photographic Subsystem Analyses

- The final decision regarding the use of refractive or reflective lens systems must be reserved until orbital parameters (particularly the periapsis) as well as resolution, coverage and spectral requirements are more firmly defined. Similarly, the choices of focal length, F/No. and format must be based not only on sensor selection, coverage requirements and other system tradeoffs, but also on orbit characteristics.

- Additional sensor performance analyses are required. In particular, more extensive analysis of the low contrast performance of silver halide and electro-optical sensor systems is essential. Detailed verification analyses of radiation sensitivity and shielding required for specific missions should be performed. Actual mission date, duration and transit time should be used for the analyses. Additional film radiation exposure experiments should be performed, simulating theoretically determined anticipated doses and energy levels.

- Conversion (storage and readout) requirements should be analyzed in terms of the exact data communication rates anticipated for the mission. The fall off in rate as a function of increased communication distances should be included. Considering the general bandwidth limitations, a mission profile of total data acquisition versus mission duration should be developed.

1.4.5 Photographic System Design and Analysis

- The imaging system tradeoffs in this document are preliminary only; more comprehensive design analyses are required. Preliminary imaging system designs should be prepared based on specific mission characteristics (orbits, mission duration, coverage, resolution, data rates, etc.)

- Detailed system performance analyses should be executed for the specific systems designed and system design and performance characteristics should be compared. A single overall figure of merit for comparing film and electro-optical system capability should be developed for the Martian application.

SECTION 2

MARTIAN ENVIRONMENTAL CHARACTERISTICS

The basic physical characteristics of Martian geography and environment must be examined in detail in order to properly establish mission objectives and determine system requirements for a Martian Orbital Photographic System. The subsections which follow review the results of analyses of primary and secondary Martian surface features, seasonal and secular variations, atmospheric characteristics and cloud patterns. Photometric and polarization parameters of Martian surface materials are also considered as well as the radiation environment.

Particular emphasis has been placed on the evaluation of the nominal environment and consideration of pertinent surface feature and atmospheric factors which can be established or confirmed by analyzing photographic imagery of Mars obtained by Mars orbiters. The information summarized in this section provides the basis for the determination of scientific objectives for a photographic mission and the establishment of photo system performance requirements presented in Section 3.

2.1 MARTIAN SURFACE FEATURES

The primary Martian surface markings include the light areas (continents or deserts), dark areas (maria) and polar caps. The apparent linear network of canals and the scattered circular oases are secondary markings which appear to be closely related to the primary dark areas and exhibit similar changes in color, contrast and fabric. The craters revealed by the Mariner IV photography, although never positively identified through telescopic sightings, are also considered to be secondary features. A summary of the characteristics of Martian surface features is given in Section 2.1.7.

2.1.1 Light Areas (Continents or Deserts)

The light areas, often referred to as continents or deserts, cover approximately 70 percent of the Martian surface. They are situated primarily in the Northern Hemisphere, although many large areas occur below 30°S. Particularly prominent in the Southern Hemisphere are the bright regions of Phaethontis, Argyre, Noachis, Hellas, Ausonia, Eridania and Electris.

The light areas may be either elevated plateaus with low to moderate relief, or depressed lowland planar regions of low relief. Based

primarily on meteorological evidence, Rea (Ref. 2-1) contends that the light areas are low lying dust covered deserts and that the dark areas are highlands. This assumption is based on the fact that dust storms originate in the bright areas and occasionally obscure major regions of the planet, but that many of the dark areas remain visible. Some astronomers, however, suggest that the light areas are highlands. McLaughlin (Ref. 2-2) concludes that apparent frost phenomena occuring on certain light areas, such as Hellas and Elysium, indicate that these regions are elevated plateaus.

Many theories exist concerning the composition of the desert areas of Mars. It is generally believed that the deserts are composed of some form of limonite, a hydrous iron oxide. Polarization measurements (Ref. 2-3) and brightness albedo and color - index matching (Ref. 2-4) between limonite and the desert areas of Mars substantiate this theory. Based upon infrared spectroscopy, Kuiper (Ref. 2-5) indicates that the light areas consist of reddish, brownish felsitic rhyolite (i.e., extrusive rock). Van Tassel and Salisbury (Ref. 2-6) suggest that surface materials of the light areas could be composed primarily of fine-grained silicates, or of coarse-grained silicates coated with finely divided limonite. They contend that mechanical weathering has been the major process in the production of Martian soil with windblown silicate particles (i.e., aeolian erosion) the dominant agent. Binder and Cruikshank (Ref. 2-7) suggest that the bright areas may be composed of rock outcrops and detrital fragments covered with a hard surface stain of limonite. Terrestrially, such a limonite stain is a naturally occuring substance that readily forms in a suitable environment during normal chemical weathering of igneous rocks.

The bright areas are generally orange, yellow-ocher or reddish colored, with an albedo of 0.15 to 0.20. The optical properties of the light areas are largely invariable and uniform, except for seasonal brightening of some areas presumed to be high plateaus covered with frost (e.g., Hellas). Sharonov (Ref. 2-8) has shown that the albedo of the continents increases for longer wavelengths (i.e., from 0.093 at 430 mμ to 0.263 at 730 mμ) and that the contrast ratio between light and dark areas also increases with wavelength (i.e., from 0.1 at 400 mμ to 0.52 at 730 mμ).

Telescopic observations have depicted sharp borders between the maria and the continents. Hoop (Ref. 2-9) suggests that these sharply defined borders may be indicative of abrupt vertical relief produced by faulting. For example, at the apex of Syrtis Major, the maria boundary is exactly aligned and determined by the canals extending onto the adjacent desert, suggesting that the canals are the result of faulting or crustal fracturing.

In line with this tectonic theory, Tombaugh (Ref. 2-10) suggests that the crustal readjustments produced by internal convection cells could have created horsts and grabens, thus providing the basis for the sharply defined maria borders depicted in telescopic observations.

The Mariner IV photography failed to reveal sharp borders between continent and maria regions; the apparent contrast between representative portions of the continent and maria regions was not well defined on the photographs. Opik (Ref. 2-11) contends that the difference between the maria and continents is the relative number of small dark or bright areas in the surface mosaic. For example, the maria may be almost saturated with dark elements, whereas the continents probably contain a mixture of bright and dark elements in different proportions. In any case, only gradual transitions may exist where previously sharp borders were depicted between the maria and continental regions.

2.1.2 Dark Areas (Maria)

The dark areas or maria occupy approximately 30 percent of the Martian surface. They occur primarily along a latitudinal zone extending from the equator to approximately 30°S. However, several large dark areas such as the Maria Acidalium and Boreum occur in the Northern Hemisphere. Syrtis Major, Mare Sirenium, Mare Tyrrhenum and Mare Acidalium appear to be the most consistently dark regions.

Substantial controversy exists over whether the maria are low-land depressed regions or elevated mountain ranges. Sagan and Pollack (Ref. 2-12) contend that the mean maria slopes are between 1 to 2 degrees, with ridge heights approximately 6 km above the adjacent deserts. They assert that the major dark areas attain elevations of 10 to 20 km and have exceedingly steeper slopes. They further postulate from polar cap recession data that the dark areas are highlands because they exhibit greater wind velocities and frost vaporization rates. Rea (Ref. 2-1) and Wells (Ref. 2-13) point out that the darkest of the Martian dark areas are very rarely crossed by yellow clouds implying that at least some of the dark maria are elevated. Wells states that clouds analogous to terrestrial lenticular clouds form at the borders of a dark and bright area but do not penetrate into the dark region. The W - shaped white clouds consistently forming in the Tharsis region near Phoenicis Lacus may be indicative of this topographic/meteorologic phenomena.

It is interesting to point out, however, that recent radar investigations by Pettengill (Ref. 2-14) revealed no clear correlations between height

of land and the presence of dark areas of Mars. Radar echoes from a region at 21°N. Latitude on Mars were characterized by extensive smear, indicative of high relief. On the average for the area scanned, the summits were some 14,000 meters higher than the deepest valleys. This is comparable to the elevation difference between the highest terrestrial continental summits and the deepest ocean basins.

The composition of the maria regions is also subject to great controversy. Focas (Ref. 2-15) noted that the maria are made up of patches of dark material superimposed on a lighter background. Binder and Cruikshank (Ref. 2-7) suggest that the maria consist of a normal desert surface partially covered by a dark material. They further state that the maria do not consist of fresh exposures of porous and granular black basalt or wind-driven volcanic ash, as previously suggested by the theories of Rea (Ref. 2-1), Mc Laughlin (Ref. 2-2) and Wells (Ref. 2-13). Instead, the maria may consist of organic material of lower form (i.e., microbial colonies or lower vegetation forms). Kuiper (Ref. 2-16), on the other hand, proposes that the dark areas are lava beds which are mantled by a variable dust cover and hardy vegetation. Opik (Ref. 2-11) also contends that vegetation may be concentrated in the dark area elements. However, polarization studies appear to indicate that the maria surface is covered by some kind of granular material, perhaps 10 microns in size.

The dark areas have typically been described as blue, green, red, brown and grey. However, Rea (Ref. 2-1) points out that there has been little confirmation of many of these colors, and that red is the only shade recorded spectrographically in the maria. Opik (Ref. 2-11) contends that the maria are actually of a brownish-grey shade, less reddish than the continents. Sharonov (Ref. 2-8) calculated that the maria, like the continents, tend to increase in albedo with increasing wavelength (i.e., from 0.087 at 430 $m\mu$ to 0.160 at 730 $m\mu$).

Seasonal variations in brightness have been observed in many dark areas with the retreat of the polar cap in the spring hemisphere. Seasonal and secular variations are discussed in Section 2.2.

2.1.3 Polar Caps

The northern polar cap is centered on lat. 89°N, long. 290° and extends to approximately 57°N at its maximum size. The south polar cap is centered on lat. 83.5° S, long. 30° and extends to approximately 42° S at maximum size (Ref. 2-1). The southern cap is larger at its maximum extent due to its longer, colder winter season. Correspondingly, the rapid, near complete melting of the south polar cap

is the result of the shorter, hotter summer. Michaux (Ref. 2-17) states that the shrinkage of the south cap in summer usually reduces it to below 5 degrees in arc, with possible complete melting. By comparison, the minimum north cap always remains above 6 degrees in arc. The extensive polar seasonal changes are described in Section 2.2.

The north cap is visible only during aphelic opposition; whereas the south cap is observed during perihelic opposition. However, the polar caps are not visible during the winter seasons in the respective hemispheres because they are completely obscured by a thick white mist.

The relief in the polar regions is not accurately known. However, the phenomena observed during the melting of the polar caps in the spring appear to suggest possible evidence for the existance of elevated plateaus (e.g., Hellas), mountains (e.g., Mountains of Mitchel and Thyles Mons) and rift systems (e.g., Rima Australis).

Kuiper (Ref. 2-5) and Dollfus (Ref. 2-18) contend that the polar caps are composed of fine ice crystals in the form of hoarfrost. (Hoarfrost also develops on the earth when temperatures at ground level are so low that they force water vapor in the atmosphere to sublimate directly as ice instead of condensing out as dew.) However, on the basis of recent evidence obtained from Mariner IV experiments, Leighton and Murray (Ref. 2-19) propose that the polar caps are composed primarily of deposits of frozen carbon dioxide (i.e., dry ice) and covered by a thin layer of water ice. Estimates of the thickness of the polar caps range from about 1 mm to 10 cm. De Vaucouleurs (Ref. 2-20), for example, suggests a 1 cm average cap thickness.

The polar caps are generally observed to possess a white or pale blue color, but various shades of grey have also been observed. Haines (Ref. 2-21) contends that the contrast between the polar cap and surrounding areas appears to increase as wavelength decreases. On the other hand, the dark fringe observed along the edge of the cap during its retreat is clearly visible with a red filter in the absence of clouds. Focas (Ref. 2-22) found that the average visual magnitude of the caps is 1.53 in spring and 1.31 during the winter when covered by white mist.

2.1.4 Canals

The canals are fine linear features which appear to be distributed in regular patterns across the Martian surface. These lines extend between dark areas and generally terminate in maria and/or dark oases areas. Over 400 canals have been mapped through telescopic

observation (Ref. 2-21) with lengths ranging from hundreds to thousands of km (Ref. 2-23). The determination of canal width is still in dispute; Opik (Ref. 2-11) states that the canals may be between 100 to 200 km wide. Katterfeld (Ref. 2-24) states that the canals appear to be more numerous in the southern hemisphere than in the northern hemisphere. The canals exhibit the same seasonal changes as the maria, and show predominant northeast and northwesterly linear orientation patterns.

The surface configuration of Martian canals is still in doubt. The popular theory is that the canals are depressed strips bounded by lateral escarpments. This configuration is similar to classical rift valley depressions found on earth. However, Sagan and Pollack (Ref. 2-12) contend that the classical canals are narrow linear ridges with slopes exceeding 4 degrees and heights reaching elevations of approximately 6 km above the adjacent deserts.

Many theories have been advanced to explain the nature and formation of the canals. In 1908, Lowell (Ref. 2-25) stated that the canals were artificial waterways constructed by intelligent Martian beings and used for purposes of irrigation. The major hypotheses, however, suggest either an endogenic (i.e., volcanic and tectonic) or exogenic (i.e., meteorological and asteroidal) origin as opposed to the cultural classification. McLaughlin (Ref. 2-2) states that the canals may be major fault zones in which the surface irregularities have trapped volcanic ash or igneous dikes. Tombaugh (Ref. 2-26) contends that the canals are depressions within which vegetation may flourish. Katterfeld (Ref. 2-24) concludes that the canals have a tectonic origin (i.e., faulting and fracturing), while Rea (Ref. 2-1) suggests that the canals are most likely strings of small volcanoes aligned along crustal fractures. Opik (Ref. 2-11) contends that meteoric impacts have produced cracks in the crust.

Under varied telescopic viewing conditions, the canals appear as fine linear markings, wide hazy bands or dark narrow streaks (Ref. 2-27). Occasionally, observers have reported cases of apparent doubling of the canal lineaments; i.e., the canal lineament appears as two parallel bright lines. The reality of this apparent doubling phenomenon, however, is still in doubt. Some observers, such as Burgess (Ref. 2-28) attest to the presence of linear features on Mariner IV photography. For example, in Mariner Frame No. 11, a well defined east-northeasterly trending tonal lineament (possibly a rift valley) can be identified. Consequently, the existence of a possible depression with well marked lateral escarpments can be inferred for this linear feature.

2.1.5 Oases

Oases are randomly scattered dark circular features found at the intersection of canals. Haines (Ref. 2-21) states that about 200 oases have been reported and that their mean diameter is on the order of 150 km. Trivium Charontis appears to be one of the largest oasis areas on the Martian surface. This feature is characterized by a radiating pattern of canals which trend in North, East and Westerly directions from the oasis center.

Most astronomers consider the oases to be impact craters formed by the collision of asteriods. Correspondingly, Opik (Ref. 2-11) contends that cracks in the crust (i.e., canals) would radiate from the point of impact (i.e., oasis). McLaughlin (Ref. 2-29) and Katterfeld (Ref. 2-30) suggest that the concentration of volcanic activity would be centered at the points where the ruptures (i.e., canals) intersect, namely, the oases.

The oases, like the canal and maria regions, normally undergo cyclic changes in hue. No oasis forms were discernible on Mariner IV photography; however, many of the larger craters (i.e., greater than 120 km diameter) could conceivably appear as dark oases when viewed and/or photographed from earth-based telescopes.

2.1.6 Craters

The Mariner IV photographs revealed that Mars has a heavily cratered surface. The existence of these craters came as a surprise to many astronomers who had previously observed Mars from earth-based telescopes. However, the volcanic or meteoric origin of the craters has not been determined (Ref. 2-31).

It is interesting to note that despite the extremely low resolution (2 km) of the Mariner IV photography, a large number of craters were identified. For the most part, the gross morphology of the craters was well defined, enabling investigators to make preliminary determinations relative to crater slopes, rim heights and crater depths.

Although less than 1 percent of the Martian surface was covered by the Mariner IV photography, nearly 100 craters have been identified. Crater diameters range from 2 km to 120 km, with up to 10 degree slopes. Some crater rims are 200 meters above the surrounding terrain and their interiors are depressed by more than 400 meters.

A pertinent observed phenomenon is that a number of craters near the

evening terminator in the southern hemisphere appeared to be covered with frost. The nature of this frost has not been ascertained.

2.1.7 Summary of Martian Surface Features

The primary and secondary features of the Martian surface have been analyzed relative to the following physical factors:

- distribution and extent
- surface configuration
- surface material
- seasonal variations
- photographic characteristics

The results of the analyses of the primary and secondary Martian surface features are summarized in Tables 2-1 and 2-2, respectively.

TABLE 2-1 CHARACTERISTICS OF PRIMARY MARTIAN SURFACE FEATURES

FEATURES	DISTRIBUTION AND EXTENT	SURFACE CONFIGURATION	SURFACE MATERIAL	SEASONAL VARIATIONS	PHOTO FACTORS
LIGHT AREAS ("DESERTS" OR "CONTINENTS")	Approx 70% of surface. Primarily in N. Hemisphere; scattered below 30°S.	Plateaus with low to moderate relief or lowland depressed plain regions.	Dry desert-like regions covered by fine dust, detritus and rock fragments. Possibly limonite, silicates covered with fine limonite, or rhyolite.	Seasonal brightening of such areas as Hellas attributed to frost. Border areas change with growth or retreat of dark areas.	Colors range from salmon pink to reddish, orange or yellow ochre. Albedo: 0.15 to 0.20.
DARK AREAS ("MARIA")	Approx 30% of surface. Primarily from equator to 30°S. Several large mare in N. Hemisphere.	Depressed lowland surface regions or elevated regions with gentle slopes.	Fine granular material (10μ): microbial, lower vegetation forms, porous and granular mixtures of volcanic ash, dust or hygroscopic salts.	Changes in dark areas with seasonal melting and reforming of the polar caps. Dark wave spreads from spring pole to equator.	Bluish-green or brownish-grey shades. Albedo: 0.08 to 0.12.
POLAR CAPS	Southern polar cap centered on long. 30°, lat. 83°; extends to 42°S. Northern polar cap centered at long. 290°, lat. 89°N extends to 57°N	Relief not known, polar cap thickness: 1 mm - 10 cm.	Fine ice crystals in the form of hoarfrost or frozen CO_2.	Extensive seasonal changes. Cap growth in fall and winter. Recedes in spring and summer. Wave of darkening produced in maria.	Whitish or pale blue color. Dark fringes along edges of caps. Visible with red filter in absence of clouds.

TABLE 2-2 CHARACTERISTICS OF SECONDARY MARTIAN SURFACE FEATURES

FEATURES	DISTRIBUTION AND EXTENT	SURFACE CONFIGURATION	SURFACE MATERIAL	SEASONAL VARIATIONS	PHOTO FACTORS
CANALS	Primarily in bright areas and between dark areas, terminating at maria or oases. Length: hundreds to thousands of km.	Narrow linear ridges or rift valley depressions bounded by escarpments.	Volcanic ash, dust, igneous material or vegetation. Similar to material in dark areas.	Darkens in spring. After long periods of time, some canals appear to double.	Fine linear appearance. Greenish, bluish, or dark grey hue.
OASES	Circular features in bright areas and intersections of canals. About 200 have been reported.	Dark circular areas with diameters of 150 km. May be craters.	Volcanic ash or impact fragments. Similar to material in maria areas.	Undergo seasonal changes in hue, similar to maria.	Apparently circular outline. Color similar to maria and canals.
CRATERS	Heavily cratered, similar to lunar areas. Revealed by Mariner IV. (1% surface coverage).	Crater diameters: 2 to 120 km. Rims to 100 m high, depths of 500 m. Crater walls have up to 10° slopes.	Volcanic dust, ash or impact detritus.	Crater sides in southern Hemisphere appear rimmed with frost in mid to late winter.	Crater structure well defined on Mariner IV photography.

2.2 SEASONAL AND SECULAR VARIATIONS

The primary and secondary Martian surface features have been observed to undergo seasonal variations in color and contrast. For example, certain light areas such as Hellas and Elysium become temporarily brighter during winter possibly because they are covered with a deposit of frost. Correspondingly, some craters observed on Mariner IV photography during the winter season appear to be rimmed by a whitish substance, which may be frost (Ref. 2-32).

The Martian surface features exhibiting the most dramatic and pronounced changes on a seasonal basis are the polar caps and the dark areas (Ref. 2-33). As the season in a particular hemisphere changes from winter to spring, the polar cap begins to recede, the white mist obscuring the cap dissipates and the dark areas (i.e., maria, canals and oases) adjacent to the cap undergo changes in their pattern of darkening. As the season progresses, this wave of darkening moves towards the equator and ultimately crosses it. The dark areas of that hemisphere become darker in tone and show weak color tints often described as being green, blue-green, reddish or brownish. The pattern reverses during the autumn and the cap, almost totally hidden by a thick mist, reaches its maximum extent during winter. A map defining the areal extent and distribution of the northern and southern polar cap regions for various seasons is shown in Figure 2-1 (Ref. 2-15).

The planetary arrival windows of 1973, 1975, 1977 and 1979 are also illustrated in Figure 2-1 (Ref. 2-34). It is evident from this figure, for example, that a planetary arrival in 1975 for a six month mission would permit complete observation and imaging of both the receding northern cap (during late spring and early summer) and the associated darkening phenomenon occuring in the adjacent maria, canal and oasis areas. The southern polar cap area, during this time (late autumn and early winter) would be completely obscured by clouds and the dark areas in that hemisphere would exhibit their poorest contrast.

2.2.1 Wave of Darkening

A retreating polar cap in the warming hemisphere exhibits a peripheral dark fringe. As the season progresses, an increased darkening occurs in the maria, canal and oasis areas. This wave of darkening proceeds across the equator to about 22° lat. in the opposite hemisphere. Focas (Ref. 2-15) calculates that the darkening waves are propogated at a velocity of 35 km/day.

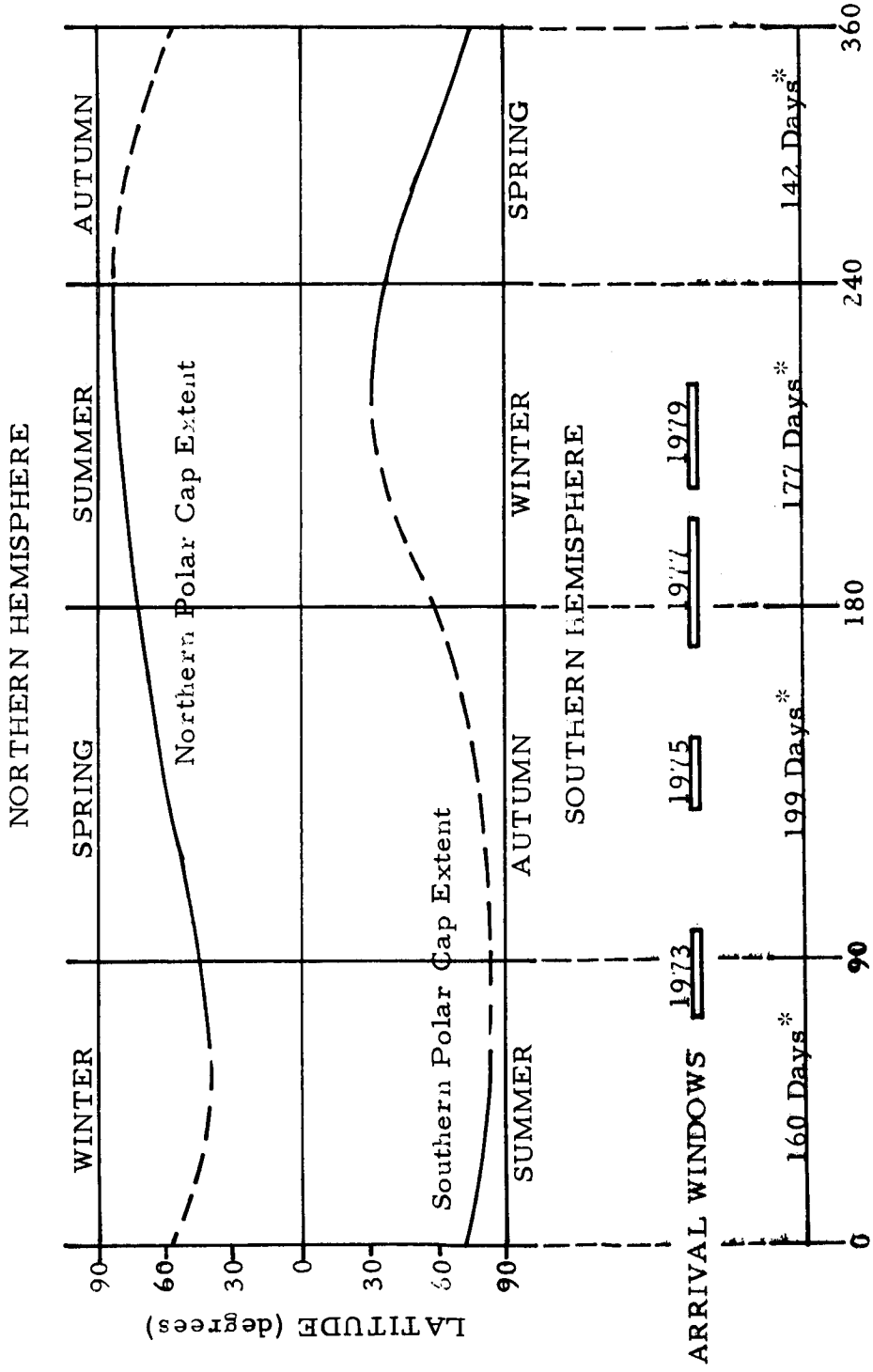

FIGURE 2-1 PLANETARY SEASONAL VARIATIONS

The wave of darkening is sometimes explained by the sublimation of moisture from one polar cap to the other polar cap. Rea (Ref. 2-1), on the other hand, suggests that the darkening wave may be due to either small particles seasonally transported on and off the dark areas, or to a seasonal darkening of a permanent surface due to a reaction with water vapor and high radiation fluxes.

Opik (Ref. 2-11), Dollfus (Ref. 2-18) and Kuiper (Ref. 2-35) contend that the wave of darkening of the maria regions represents the response of microorganisms or lower vegetation forms to water vapor in transit. McLaughlin (Ref. 2-2) suggests that the darkening wave may be due to moistening of volcanic ash. Arrhenius (Ref. 2-36) suggests that the darkening wave may be caused by hygroscopic salts which respond to small changes in atmospheric humidity.

2.2.2 Secular Variations

Various dark areas undergo secular changes in shape and darkening, in addition to seasonal changes. An example of this phenomenon is the Solis Lacus region, where changes in shape have occurred over a period of 50 years (Ref. 2-17). Opik (Ref. 2-11) states that the greatest change ever recorded involved the darkening of the continent region northeast of Syrtis Major. A vast dark region developed in 1954 and persisted through 1956 around a skeletal system of dark markings at Thoth-Nepenthes. Although changes have been observed in the shading, the boundaries of this latter region have remained essentially constant. The dark northern extension of Mare Cimmerium has also been observed to undergo secular changes in hue.

Light areas also undergo secular variations. Rea (Ref. 2-1) reports that the generally bright area of Hellas was dark during the 1954 opposition, but returned to its normal appearance in 1956. A round, dark spot which appeared in the Arcadia desert in 1956 had not been present in previous years (Ref. 2-17).

As with seasonal changes, the physical cause of secular changes remains a matter of great controversy. Both organic and inorganic hypotheses have been offered to explain the observed phenomena. Opik (Ref. 2-11) for example, contends that the secular changes may be due to some peculiar regenerative property associated with vegetation, whereas Rea (Ref. 2-1) suggests that these variations may be ascribed to changes in the wind pattern and/or to volcanic activity.

2.3 ATMOSPHERIC CHARACTERISTICS

The basic observed characteristics of the Martian atmosphere, such as its composition, pressure, density, temperature and circulation, have been examined because of their affect on the detectability of surface features photographed from orbit. Although generally important, this area was not emphasized during the study.

2.3.1 Atmospheric Composition

Nitrogen has been considered to be the most abundant element in the Martian atmosphere; however, Mariner IV data indicates that carbon dioxide constitutes about 70 to 90 percent of the total atmosphere. The remaining 10 to 30 percent consists primarily of argon, neon and nitrogen with minute amounts of oxygen, ozone and water vapor. By analogy, preliminary data obtained from recent Venus experiments indicates that the Venusian atmosphere has a dominance of carbon dioxide with small traces of oxygen and water vapor, but with no nitrogen content. Table 2-3 presents a comparison of a preliminary Mariner IV composition model to earlier atmospheric composition models of Mars.

TABLE 2-3 MARTIAN ATMOSPHERIC COMPOSITION MODELS

Atmospheric Constituents	PERCENT ATMOSPHERIC COMPOSITION			
	de Vaucouleurs Model, 1960 (Ref. 2-37)	Hess Model 1961 (Ref. 2-38)	Owen & Kuiper Model, 1964 (Ref. 2-39)	Mariner IV Model, 1965 (Ref. 2-40)
Carbon Dioxide	2.2	1.3	14.0	70. — 90.
Argon	4.0	5.6	1.0	up to 20.
Nitrogen	93.8	93.0	85.0	up to 10.
Oxygen	< 0.1	0.1	-	-
Water Vapor	-	0.04	-	-
Assumed Surface Pressure (mb)	85	85	17	≈ 5

2.3.2 Aerosols

The presence of clearings, turbidity, clouds and mists on Mars suggests that the atmosphere may contain submicron sized solid particles in suspension. Astronomers theorize that fine particles of aerosol suspensions could enter the atmosphere by either wind transport off the surface,

meteoric dust from space or sublimation from atmospheric vapors (i.e., ice or CO_2 crystals). Estimates relative to the amount of aerosol saturation in the atmosphere vary greatly. Yanovitskiy (Ref. 2-41) contends that the Martian atmosphere has a higher saturation of fine aerosol per unit of mass than that of the Earth.

Fine aerosols in permanent atmospheric suspension can produce either purely scattering or absorptive optical properties. Dollfus (Ref. 2-42) contends that the measured illuminance of the atmosphere in sunlight exceeds that of Rayleigh scattering from a pure gaseous atmosphere and that the excess scattering is attributed to fine aerosols in permanent suspension. Opik (Ref. 2-11) on the other hand, contends that the presence of aerosols indicates that the fraction of the atmospheric extinction due to scattering is about 15 percent, while 85 percent is absorbed and converted into heat.

Recent infrared absorption measurements by Barrington et al (Ref. 2-43) appear to indicate that an upper limit of scattering by particulate matter (i.e., aerosols of dust clouds or frozen CO_2 particles) is attained in the spectral region between 3.4 and 3.6 μ. Optical atmospheric scattering and absorption effects are discussed in Section 2.6.

2.3.3 Pressure

On the basis of photometric and polarimetric observations made prior to 1963, the surface pressure on Mars was generally considered to be about 85 mb (Ref. 2-37). However, recent spectroscopic observations and Mariner IV occultation measurements appear to indicate that surface pressure values may be considerably lower, i.e., in the 3 to 8 mb range. Table 2-4 summarizes surface pressure values obtained from recent spectroscopic and Mariner IV measurements for various carbon dioxide atmospheric abundance assumptions (Refs. 2-23, 2-40).

TABLE 2-4 MARTIAN SURFACE PRESSURE

Type of Measurement	Assumed Carbon Dioxide Abundance (Percent)	Surface Pressure (mb)
Mariner IV Occultation	50 80 100	5.0 to 7.0 5.2 ± 0.8 4.9 ± 0.8
Spectroscopic	60-85 90 100	7.1 ± 2.2 8.0 ± 4.0 3.1 to 7.0

The graph of pressure above the surface of the Electris region shown in Figure 2-2, was taken from Mariner IV data compiled by Fjeldbo, Fjeldbo and Eshleman (Ref. 2-40). The greatest fractional decrease of pressure/unit height occurs at an altitude of about 90 km, the mesopause level of the atmosphere, where the calculated temperature minimum may also occur (i.e., temperature ranging from 50°K to 85°K).

2.3.4 Surface Density

Data obtained from Mariner IV occulatation experiments appear to indicate that the density of the Martian atmosphere at the surface is quite low. Data compiled by Kliore, et al (Ref. 2-44) shows representative number and mass surface densities of $(1.9\pm0.1)\times10^{17}$ mol/cm^3 and $(1.43\pm0.1)\times10^{-5}$ gm/cm^3, respectively, for a 100 percent carbon dioxide atmosphere and $(2.1\pm0.1)\times10^{17}$ mol/cm^3 and $(1.55\pm0.1)\times10^{-5}$ gm/cm^3, respectively, for an 80 percent carbon dioxide atmosphere.

Fjeldbo, Fjeldbo and Eshleman (Ref. 2-40) state that the molecular number density at the Martian surface is only 0.8 percent of the Earth's surface value, equivalent to the similar value at a height of about 34 km above the Earth's surface. On the other hand, the Martian surface mass density is about 1.2 percent of that calculated for the Earth. In general, however, the overall atmospheric density for Mars was found to be less than that for the Earth at all altitudes. By contrast, preliminary data

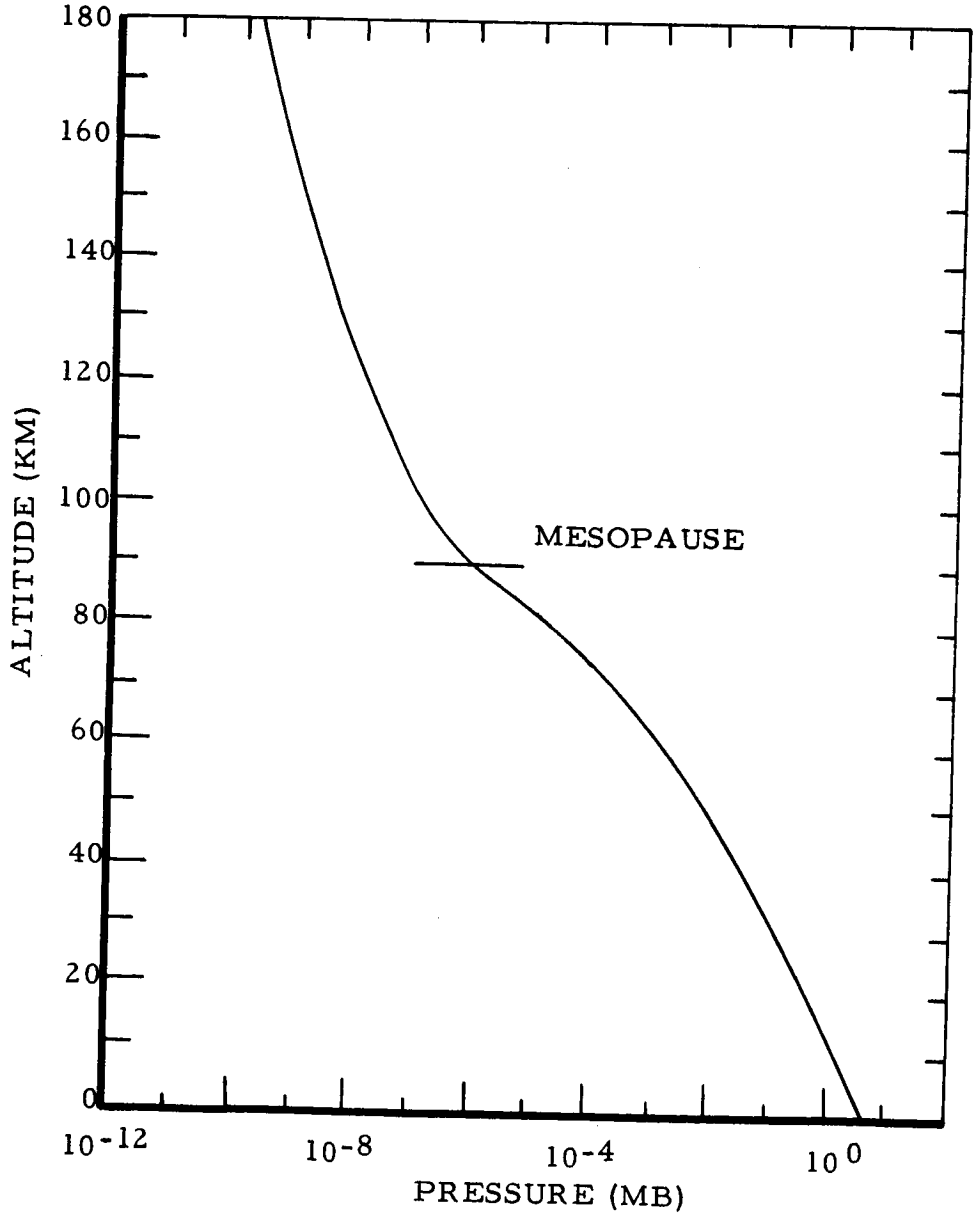

FIGURE 2-2 PRESSURE VS. ALTITUDE ABOVE ELECTRIS REGION

obtained from recent Venus 4 measurements appear to indicate that the Venusian atmospheric density is 15 times that of Earth.

2.3.5 Temperature

The results obtained from Mariner IV occultation measurements show that the Martian atmosphere is considerably colder than was previously anticipated. Representative above surface temperatures would appear to be in the order of 170°K for a 50 percent carbon dioxide atmosphere and 180°K for a 100 percent carbon dioxide atmosphere.

Recent spectroscopic and Mariner IV measurements enabled Gross, McGovern and Rasool (Ref. 2-45) to predict the representative Martian vertical temperature distribution. The results shown in Figure 2-3 indicate that the temperature at the exospheric level appears to be in the range of 400 to 700°K. By contrast, recent Venus 4 measurements appear to indicate that the temperature of the Venusian atmosphere is between 320° and 550°K.

Martian seasonal and diurnal surface temperature variations have been determined. For example, Leighton and Murray (Ref. 2-19) calculate that the minimum winter temperature could be below 100°K at the pole and below 145°K between 50° latitude and the pole. Opik (Ref. 2-11) states that a diurnal temperature range of about 100°K is possible at the equator at perihelion (refer to Figure 2-4). At an average distance from the sun, on the other hand, the near equatorial temperature would be 245°K. Leighton and Murray also predict diurnal temperature ranges varying between 100 and 150°K. Kachur (Ref. 2-46) contends that a considerable seasonal variation of mid-day temperatures occurs, ranging from 259 - 269°K at aphelion to 295 - 305°K perihelion.

Sagan and Pollack (Ref. 2-12) theorize that the highlands are only a few degrees cooler than the low bright areas because of the small Martian surface slopes and the small greenhouse effect of the atmosphere. In addition, Opik states that daytime temperatures in the maria are about 8°K higher than that of the continents. He attributes this condition to the greater absorptivity of the maria to solar radiation.

Knowledge of the distribution of temperature gradients over the Martian surface would be useful, especially for imaging in the IR portions of the electromagnetic spectrum. Terrestrial thermal patterns produced by volcanism and other non-solar emissions have been recorded by both imaging and non-imaging IR systems. Subsequent comparison of the signatures obtained on the visible photo image with IR signatures enable the image interpreter to analyze and accurately identify the inherent characteristics of specific target/background features.

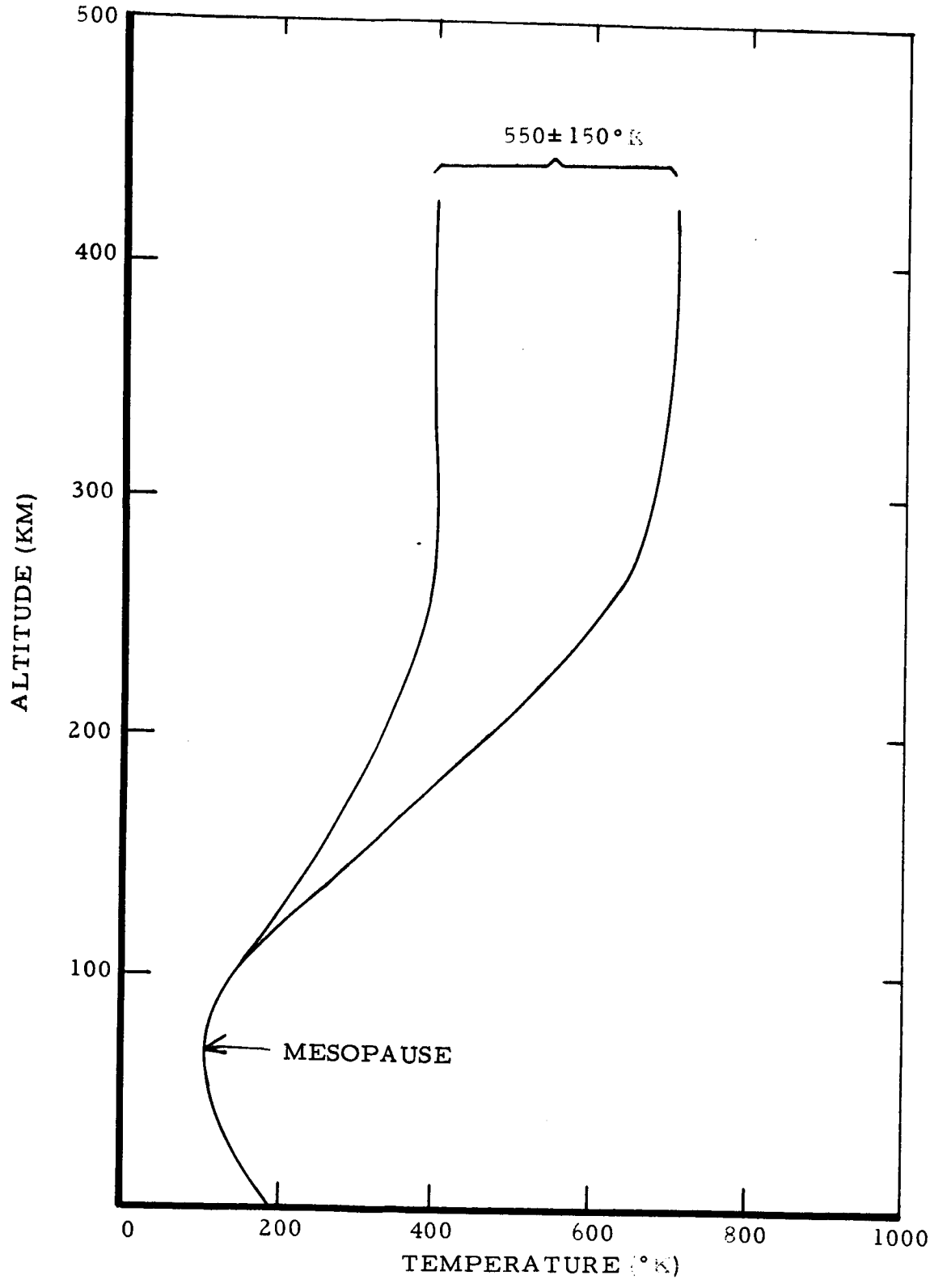

FIGURE 2-3 VERTICAL DISTRIBUTION OF TEMPERATURE OF MARTIAN ATMOSPHERE (Assuming Pure CO_2 Composition and 8 mb Surface Pressure)

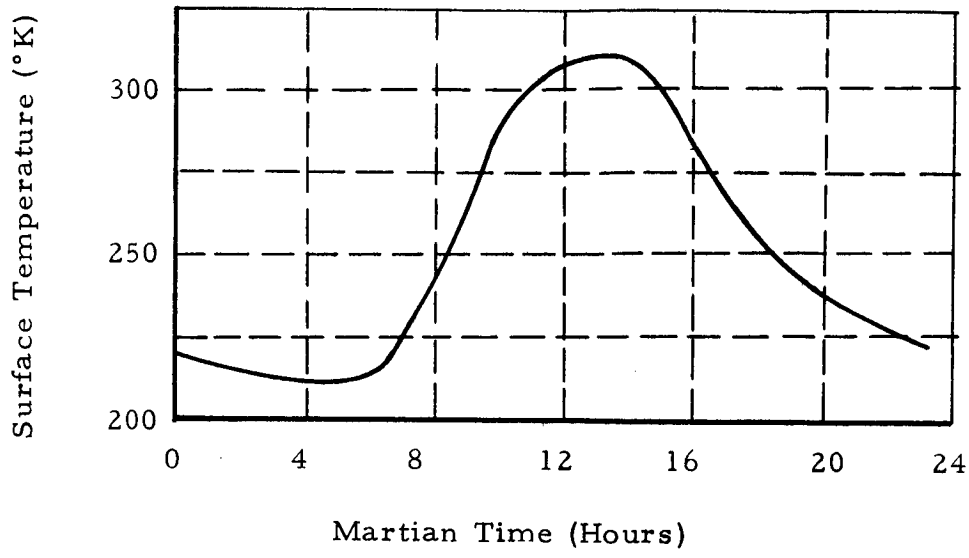

FIGURE 2-4 DIURNAL VARIATION OF SURFACE TEMPERATURE (At Equator Near Perihelion)

2.3.6 Circulation

Miyamoto (Ref. 2-47) suggests that prevailing surface wind directions at middle latitudes are westerly during most of the year, but become easterly during the Martian summer. Clouds developing locally along the dark fringe of the receding polar cap drift in prevailing easterly winds to low latitudes along NE-SW lines. They subsequently cross the equator, turn toward the east and move with the winter hemisphere westerly winds. Otterman and Bronner (Ref. 2-48) further suggest that meridional components transport moisture from the waning polar cap to lower latitudes in spring.

Considering the general circulation pattern of the Martian atmosphere, Tang (Ref. 2-49) deduces that an axially symmetric zonal circulation regime around a pole cannot remain stable. Therefore, he concludes that during the Martian year, a wave type circulation pattern (i.e., migrating system of highs and lows similar to earth) prevails in the atmosphere. Leovy and Mintz (Ref. 2-50) also suggest the development of a fluctuating wave regime in the winter hemisphere.

Opik (Ref. 2-11) contends that aeolian (wind) erosion must be a powerful agent on Mars. It is responsible for eroding landforms such as craters and canals, depositing the eroded debris on the surface and causing migration of dust drifts and storms all over the surface and in the lower atmosphere. Windspeeds required for raising dust have been calculated to range from 60 km/hr to in excess of 300 km/hr (Ref. 2-1). Opik further suggests that the presence of dust clouds may be indicative of "dust devils" or tornadoes with diameters in excess of 100 meters.

According to Tang, theoretical values of maximum surface wind speeds may exceed 360 km/hr. Pollack and Sagan (Ref. 2-12) further contend that there is a seasonal variation of wind speeds associated with the annual variation of the poleward temperature gradient and that prevailing winter winds are much stronger in intensity than those occuring during summer.

2.4 MARTIAN CLOUDS AND HAZE

The occurrence of clouds and haze in the Martian atmosphere could greatly complicate visibility and adversely affect the photographic quality of any Martian surface imagery. The basic prerequisite is to photograph through an atmosphere having acceptable levels of optical transmission, light scattering and other related optical characteristics.

It is also apparent that the direct observation of meteorological phenomena will be an important aspect of the Martian photographic mission. These observations could possibly be accomplished by the selective non-vertical pointing of the low resolution camera toward the limb of the planet. In this manner, one could obtain fairly accurate estimates of atmospheric cloud heights, at selected intervals.

The main cloud types observed in the Martian atmosphere are the blue-white clouds, yellow clouds and blue haze. Each is named for the color(s) which it predominantly reflects. The physical characteristics of the three major cloud types are presented below. A summary of the basic characteristics is given in Section 2.4.4.

2.4.1 Blue-White Clouds

It is generally difficult to distinguish between the blue and white clouds in the Martian atmosphere since the blue clouds frequently appear along with white clouds and mists. Consequently, these cloud types have been combined and classified "blue-white" for the purpose of this study.

Blue-white clouds are generally believed to consist of transparent particles of ice crystals (Ref. 2-51) and/or fine water droplets (Ref. 2-18), ranging in size from 0.1 to 2 microns in diameter. They usually appear over the winter polar regions, the equatorial regions, and over certain mid-latitude areas, such as Aeria and Elysium. In addition, blue-white clouds repeatedly appear over what are presumed to be high altitude surface areas such as Olympica, Candor and Tharsis. These clouds have also been observed to commonly appear over the terminator at sunrise and in the equatorial band at sunset (Ref. 2-17).

The blue-white clouds appear to differ in height over the polar and equatorial regions. Generally speaking, however, estimates of their elevations range from between 15 and 25 km, with a possible maximum of 100 km (Ref. 2-52).

The blue-white clouds are apparent when they are photographed in blue

or ultraviolet, but are seldom seen when photographed in red or infrared. Their albedo is reported to be about 0.2 or less (Ref. 2-21). On the basis of polarization measurements, Dollfus (Ref. 2-3) contends that the blue-white clouds (particularly the white clouds) are similar to terrestrial fogs or ice crystal cirrus type clouds.

2.4.2 Yellow Clouds

Little is known about the nature of the yellow clouds. In general, however, the yellow color of the clouds spectroscopically matches the color of limonite (Ref. 2-53), which is believed to be present on the Martian surface. This suggests that the clouds are composed of dust particles which are windswept from the surface of the bright areas. Estimates of particle size range from 2 to 100 microns in diameter. They are primarily low level phenomena, occurring most frequently between 5 and 10 km altitude.

Three large scale periodic yellow cloud movements have been identified by Gifford (Ref. 2-54). The most frequent dust storms appear to originate during late fall and winter, in the North Equatorial zone (Libya desert region) and travel across the equator to terminate in the South Temperate zone (Ausonia to Phaenthontis desert regions). A second less frequent yellow cloud movement commences during mid-summer in the North Equatorial zone (Candor - Chryse deserts) and moves to the edge of the North Temperate zone (near Mare Acidalium). Still a third major system starts in the mid-South Temperate zone (Argyre-Noachis desert) during late spring and terminates at Syrtis Major just north of the equator.

Some yellow clouds occupy local areas within light desert areas while others cover entire deserts. They usually begin as small areas and grow larger over a period of several days. A good example was the great yellow cloud of September, 1956, which gave a yellowish cloud hue to the entire planet for several days (Ref. 2-47). The yellow clouds are apparent in red, but not blue light and are observed most frequently during perihelic or near perihelic opposition. They are known to last from one to two days and are most often seen on the morning terminator (Ref. 2-21). Sporadic events, however, have been known to last for weeks (Ref. 2-11).

2.4.3 Blue Haze

A blue haze or violet layer normally exists in the atmosphere of Mars. It has been theorized that the condensate making up the blue haze could be submicron particles of either carbon dioxide crystals, water ice,

ice crystals or dust acting as Rayleigh scatterers (Ref. 2-23). The haze has also been suggested to be fine dust particles blown off the surface by seasonal winds (Ref. 2-12), meteoric dust from space or nitrogen dioxide in the atmosphere (Ref. 2-55). Regardless of the theory advanced, a great debate still exists relative to the optical effects caused by the blue haze layer. The haze appears to completely obscure the surface markings when photographed through blue or ultraviolet filters. Its opacity increases for wavelengths shorter than 0.46μ and it becomes totally opaque at about 0.45μ (Ref. 2-27). The blue haze has been observed to dissipate from time to time, particularly near oppositions. Clearings may be as small as about 1/8 of the disk or according to Slipher (Ref. 2-33), completely expose the Martian surface. The duration of such a blue clearing is quite variable with the atmosphere remaining clear for days, or even weeks. No satisfactory explanation presently exists for the clearing of the blue haze.

Morning haze occurs frequently in the northern hemisphere and degrades observations about 50 percent of the time. Conversely, evening haze occurs infrequently. Capen (Ref. 2-56) suggests that the use of a red filter to obtain topographic photo coverage would minimize the effects of haze obscuration, particularly during the morning hours.

The height of the haze layer is believed to vary with locality. For example, Kuiper (Ref. 2-35) finds the haze layer markedly higher over the equator than over the poles. The height of the haze layer is not presently known; however, it has been placed at between 6 and 200 km.

2.4.4 Summary of Cloud Types

The basic physical characteristics of the three major Martian cloud types are summarized in Table 2-5. The physical characteristics evaluated for each of these cloud types include composition, extent and distribution, seasonal and diurnal variations, height, velocities and photographic visibility.

The frequency of occurrence, optical density, and maximum distribution of these cloud or haze patterns are the pertinent factors that must be considered during the planning of orbital photographic missions. Also, selected portions of these cloud phenomena should definitely be photographed during the initial orbital photographic missions.

TABLE 2-5 MARTIAN CLOUD FORMATIONS

	BLUE-WHITE CLOUDS	YELLOW CLOUDS	BLUE HAZE (VIOLET LAYER)
COMPOSITION	Transparent particles (Ice, Water droplets) 0.1-2μ diameter	Dust particles (Limonite color) 2-100μ diameter	Submicron particles (CO_2, H_2O crystals, Dust)
EXTENT & DISTRIBUTION	Polar and Equatorial regions; Mountain ranges	Middle latitudes; Local and large area formations	Varies with locality; Morning haze in Northern Hemisphere
DIURNAL VARIATIONS	Seen at sunset and late afternoons	Duration: 1-2 days, sometimes weeks.	Coverage varies; evening haze infrequent. Forms in 5 hours
SEASONAL VARIATIONS	Occurs at winter pole and equatorial belt; Common at North Cap	Observed at perihelic opposition	Frequently dissipates, especially near oppositions
HEIGHT	Varies at poles and equator, 15-25 km	Low level phenomena, 5-10 km	High level phenomena, 6-200 km
VELOCITIES	35 km/day	35 km/hour	Seasonal wind circulation
PHOTOGRAPHIC CHARACTERISTICS	Visible in blue, UV; not in red, IR	Visible in red (extreme opacity) Not apparent in blue	Visible in blue, violet, UV (Opaque below 0.46μ)

2.5 MARTIAN SATELLITES

The two small satellites, Phobos and Deimos, revolve around Mars in nearly circular orbits.

Phobos, the closest satellite, is approximately 6000 kilometers above the surface of Mars, approximately 19 km in diameter, and has a period of 7 hours, 39 minutes and 13 seconds (about one-third that of Mars) (Ref. 2-17). Deimos, on the other hand, is approximately 20,000 kilometers above the surface of Mars, has a diameter of about 10 km and a period of 30 hours, 17 minutes and 17 seconds. These estimates of satellite diameter are based primarily on brightness data, with the satellite albedos assumed to be equal to that of Mars. Mars itself has a diameter of approximately 6750 km and a period of 24 hours, 37 minutes and 22.7 seconds.

The exact physical characteristics of the environments of Phobos and Deimos are unknown. The total lack of environmental data results primarily from the fact that the direct measurement of atmospheric and surface characteristics is entirely beyond the reach of present-day telescopes and that it is difficult to determine the photometric characteristics of such small and faintly illuminated satellites.

It is anticipated that preliminary environmental information related to Phobos and Deimos could be obtained during a Martian orbital photographic mission. The photographic observation could possibly be accomplished by pointing the medium resolution camera in the direction of each of the individual Martian moons at selected orbital intervals.

2.6 MARTIAN PHOTOMETRIC CHARACTERISTICS

Research in the area of Martian photometry has been severely restricted because direct observations of Mars from Earth are limited to phase angles up to only 47° and extrapolations must be made for larger angles. At present, photometric models of the Martian surface are based upon work by de Vaucouleurs (Ref. 2-57) and others. A preliminary photometric model currently being developed by Dr. Leighton and associates is expected to be available early in 1968 (Ref. 2-58). However, this model will be based on the limited Mariner IV photographic data and will therefore refer only to a small portion of the Martian surface. Newer data, obtained as a result of future Mariner and Voyager missions will permit major updating of current photometric models.

Basic data concerning the visual magnitude and albedo of Mars are presented in the subsections which follow. In addition, the use of the photometric function for photo interpretive analysis is described.

2.6.1 Visual Magnitude

The mean value of the visual magnitude of Mars, reduced to unit distances from Earth and Sun, and to zero phase angle is -1.52 (Ref. 2-17). This value was derived from visual, photovisual and visual photoelectric observations. Figure 2-5 represents the visual phase curve based on data obtained by Muller (Ref. 2-59) as a result of visual brightness observations from 1876 to 1889. The phase coefficient from this data is 0.01486 mag/deg. Mars appears redder at phase angles in the order of 45° and may appear bluer at larger phase angles because of increased atmospheric scattering.

The Martian visual magnitude and the phase coefficient are both spectrally dependent. The variations of each, plotted as a function of the reciprocal of wavelength, are shown in Figure 2-6 (Ref. 2-57). In general, the magnitude increases for wavelengths above 0.4 microns, and the phase coefficient decreases from 0.018 mag/deg. for wavelengths below 0.5 microns to a low of about 0.011 mag/deg. for wavelengths above 0.6 microns. The visual magnitude of Mars has also been found to vary with longitude. However, the spectral variations do not appear to be particularly longitude dependent.

2.6.2 Martian Spectral Reflectivity

The average albedo of the Martian surface is a relatively low 0.15 compared to the 0.39 value for the Earth. The spectral variation of the

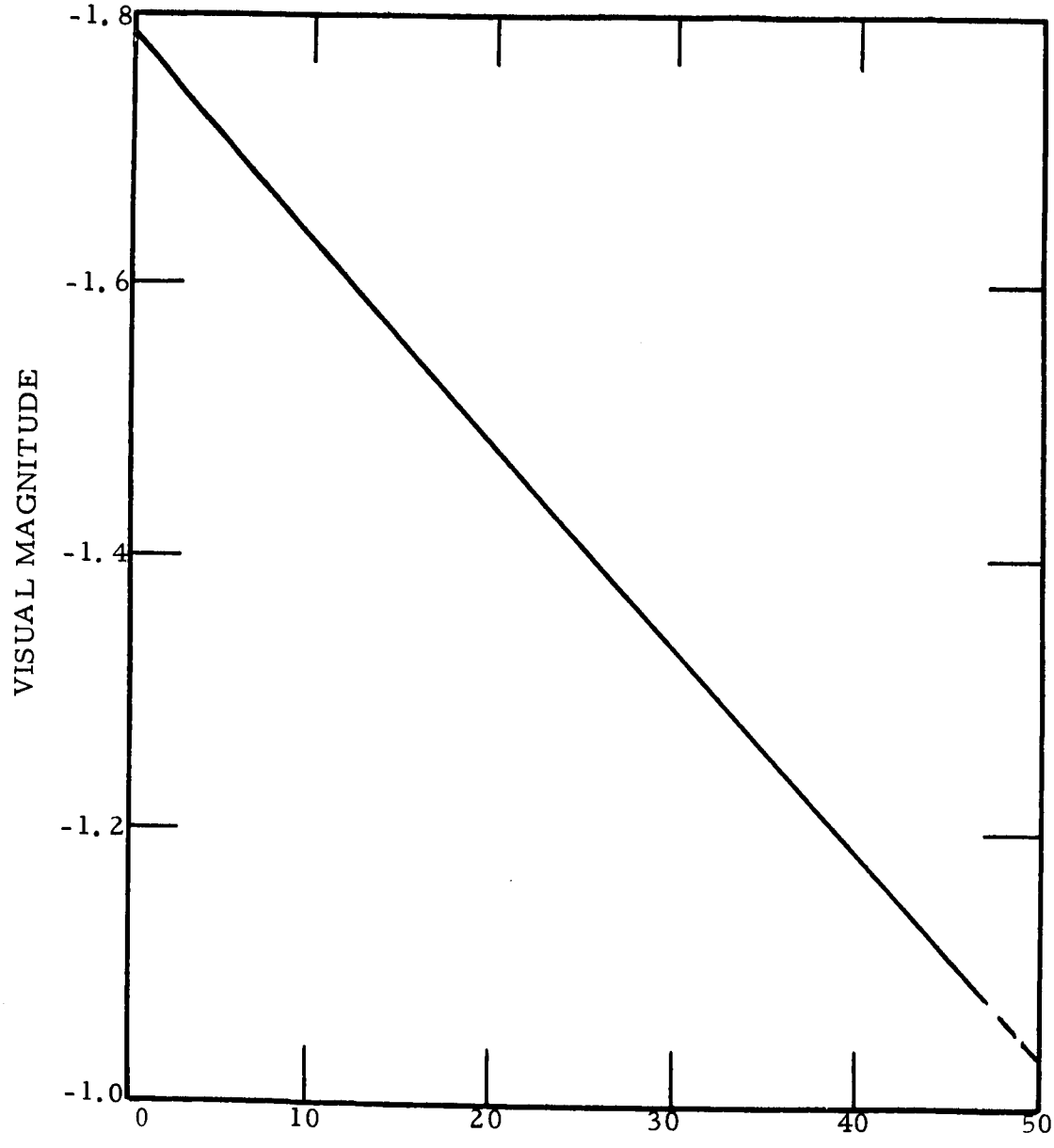

FIGURE 2-5 VISUAL PHASE CURVE OF MARS

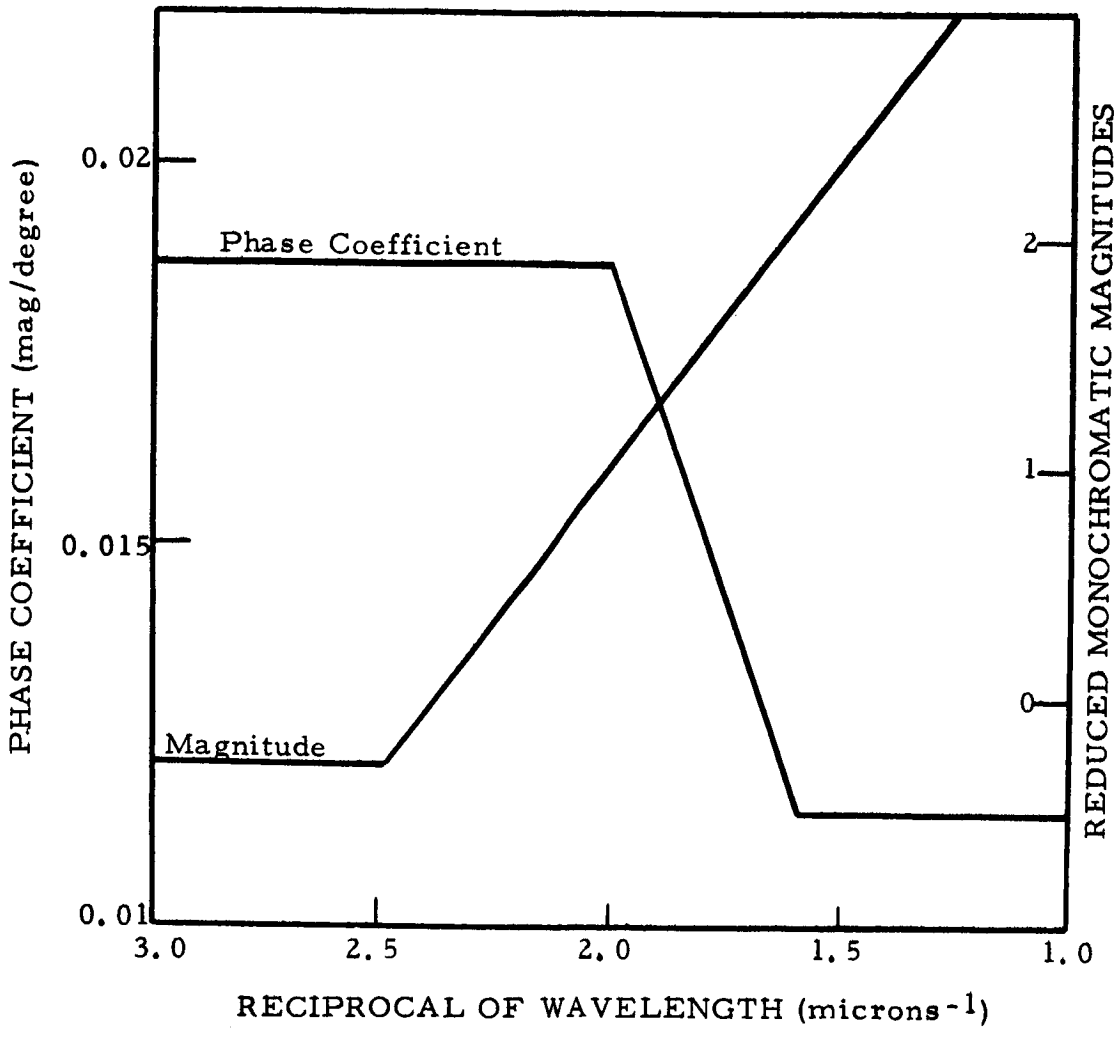

FIGURE 2-6 SPECTRAL VARIATION OF MAGNITUDE AND PHASE COEFFICIENT

Martian albedo is presented in Figure 2-7, which indicates that the albedo increases for the longer wavelength portion of the visible spectrum and remains high in the infrared region (Ref. 2-60).

Surface markings are visible through green, yellow, and red filters, with contrasts increasing for longer wavelengths (Ref. 2-11). Rea (Ref. 2-61) indicates that the lack of contrast is particularly notable in photographs taken in blue light; the maria become invisible in the blue, and remain so for the shorter wavelengths, between 0.426 and 0.458 microns. Experiments aimed primarily at the study of the Martian surface should therefore use wavelengths in the 0.65 micron region (Ref. 2-62).

The albedo of the bright areas is about twice that of dark areas for wavelengths longer than 0.55 microns, the maria being relatively dark in the near infrared. However, at shorter wavelengths, the ratio becomes less than 2 in the green, and nearly 1 in the blue (Ref. 2-53).

It is therefore evident that albedo and spectral response of surface features will be significant factors in the interpretation of major Martian physiographic features. For example, various regional physiographic and related geologic features have been identified from low-resolution TIROS photographs, particularly those of arid regions, where light toned (high albedo) alluvial and desert surfaces contrast sharply with the darker bedrock and vegetation regions (Ref. 2-63).

When viewed at longer wavelengths, Mars shows limb darkening, or a decrease of brightness toward the edge at full phase. As with the full moon, the rough and dusty solid surface of Mars should appear uniformly bright. Therefore, Opik concludes that limb darkening is an indication of an absorbing atmosphere (Ref. 2-11). On the other hand, Evans and Sharonov indicate that limb darkening at longer wavelengths could also be the result of Rayleigh scattering by the atmosphere (Refs. 2-64, 2-65).

2.6.3 Mariner IV Photography

The Mariner IV photographs of the Martian surface were acquired under a variety of viewing conditions. For example, Sun angles of individual photographic frames in the flyby sequence ranged from beyond the terminator to 76° (i.e., Sun 14° from zenith). Mariner frame No. 3, taken with a Sun angle of 76°, did not permit adequate differentiation of topographic and tonal detail (Ref. 2-66). Mariner frame No. 11, on the other hand, taken with a Sun angle of 43° (Sun 47° from the zenith), shows considerable tonal detail and surface feature differentiation. The

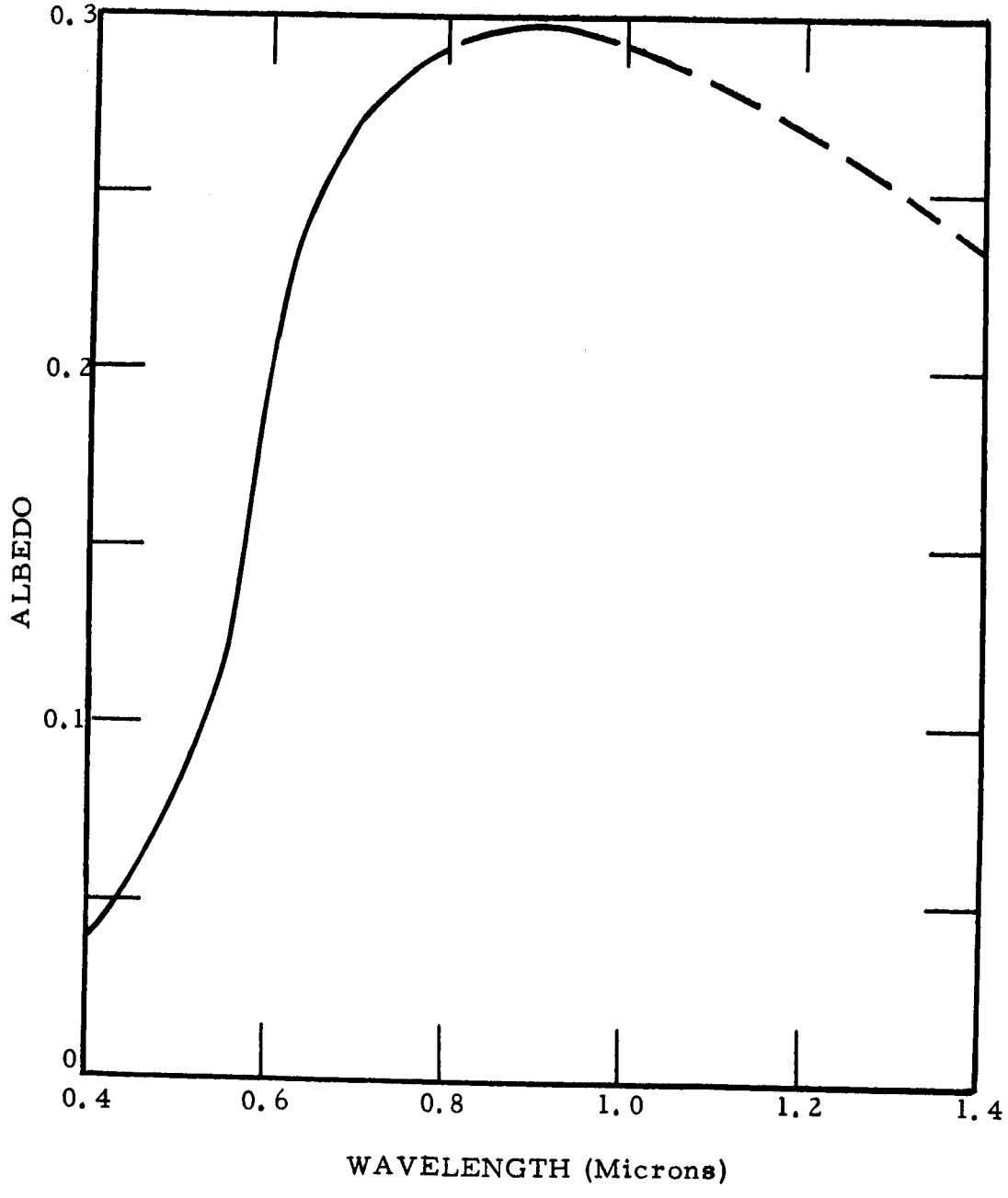

FIGURE 2-7 SPECTRAL VARIATION OF MARTIAN ALBEDO

photograph appears to have been taken under satisfactory lighting and viewing conditions. The results obtained from the Mariner IV flyby mission indicate that good image contrast, reflectivity, and surface feature differentiation can be achieved when individual photographic frames are taken at sun angles ranging from 20 to 70 degrees.

2.6.4 Photometric Function Analysis

A method has been developed for extracting topographic information about the Moon from monoscopic photographs by using photometric techniques (Ref. 2-67). This photometric method could be attractive for space applications because the need for redundant photographic coverage used in stereoscopy is eliminated. However, a detailed knowledge of the surface photometric properties is required. Then, if the illumination value, source-target-sensor geometry and surface photometric characteristics are known, the slopes in the resulting image can be determined.

Experimental studies performed on representative lunar photography have utilized known lunar photometric properties to measure lunar slopes and surface irregularities to a fairly high degree of accuracy. Previous experimental and analytical studies have shown that, unlike diffuse or specular reflectors, the reflection of incident variable radiation by the lunar surface is characterized by a peaked back-scatter in the direction of the source, a lack of specular reflection, and a uniform albedo. However, it is not well known if lunar photometric properties are common to other soils of the solar system, since little detailed photometric information is available because of poor resolution, angular variation, and atmosphere. Soils on Earth, for example, exhibit completely different photometric properties and have been subjected to different erosion processes than those of the Moon. Rindfleisch indicates (Ref. 2-68) that it is highly possible, therefore, that the techniques developed for lunar photometric analysis of topographic features will be severely limited in applicability to other planetary surfaces (i.e., the Martian surface).

2.7 POLARIZATION PROPERTIES

The polarization properties of the Martian surface have been observed by Dollfus and Focas for a number of years. Their measurements have been both visual and photoelectric, extending from the blue to the near infrared. These observations have been primarily compared to small size sample areas of terrestrial minerals which appear to simulate polarimetric characteristics of the Martian surface.

The analysis of the polarimetric properties of the Martian surface have been used to derive gross indications of surface constitution, particle size distribution, regions of increased roughness, scale of roughness and the nature of observed seasonal changes of certain maria regions. In addition, polarization measurements of Mars have been used to obtain estimates of true surface temperature, diurnal, seasonal and latitudinal temperature variations, atmospheric pressure and cloud particle composition and texture.

The interpretation of total polarization requires a knowledge of the photometric properties of the Martian surface. For this surface, the effect of the phase angle at the time of observation of the planet (i.e., latitude or viewing angle) must be considered. In addition, both the function of the wavelength and the visual magnitude of Mars (mean value of -1.52) must be included as parameters. The relative photometric effects of the soil and atmosphere (including the effects of aerosols) are then separated by an observation of the total apparent brightness at the Martian surface location. It is important to note that the analysis of astronomical polarimetric observations with combined aerosol effects is quite involved, and as indicated by Egan and Foreman (Ref. 2-69), depends on certain deductions from laboratory simulation efforts.

Because of communication limitations, extensive use of polarization filters with the imaging system is not likely for the initial orbital photographic missions of Mars. A separate polarimeter, possibly with the instrument boresighted to the camera, would provide useful polarimetric data which could be correlated with imagery data. The application of polarization techniques in Martian lander systems also requires further consideration.

2.8 MARTIAN RADIATION ENVIRONMENT

Mariner IV did not detect the existence of Martian radiation belts such as the Van Allen belts around Earth (Ref. 2-70). However, consideration must be given to the radiation incident from various sources during transit to the planet as well as during performance of the reconnaissance mission (Ref. 2-71). The normal incident radiation that such a Martian orbital spacecraft will encounter results from the following primary sources:

- The radiation belts around the Earth,
- Normal incident solar particles and large increases in the solar particles during solar flare events,
- Incident galactic radiation of extremely high energy and low dosage.

The peak intensities and distribution of these energies are shown in Table 2-6 (Ref. 2-72).

The transition time through the Earth radiation belts will be of small duration as compared to the total time of flight. If adequate shielding is given for the incident solar flare radiation, sufficient protection will be supplied by the shielding for transfer through the Earth radiation belts.

Extensive work has been performed relative to the radiation hazard from solar flares (Ref. 2-73). Solar activity appears to follow a cyclic pattern, with a cycle duration of approximately 11 years and a possible variation of from 8 to 14 years (Ref. 2-74). Figure 2-8 shows the solar activity for cycles 18, 19, and 20, with cycle 19 a probable maximum. The actual early Voyager missions will occur during solar cycles 20 and 21. Missions in 1973 and 1975 would take place during periods of relatively low solar activity, a 1977 mission during a moderate activity period, with the next solar activity maximum occurring during 1980-81.

Galactic radiation is of such high energy (billions of electron volts) that no reasonable amount of shielding to protect against it can be considered for use in a spacecraft. However, only very small dosages of galactic radiation need be considered. This radiation effect, as measured by the first Mariner Venus mission, was about 6-10 Rads of radiation for the four month mission. Therefore, a dosage of 2 Rads/month for galactic radiation can be considered as a design figure. The investigation of the radiation shielding requirements for a planetary photographic system primarily involves consideration of the use of film as a sensor.

TABLE 2-6

MISSION RADIATION ENVIRONMENT

Type	Location (All at Geometric Equator)	Peak Intensity
Inner Van Allen Belt		
Protons > 30 Mev	1.5 earth radii	$3x10^4 cm^{-2} sec^{-1}$
Electrons > 0.5 Mev	1.3 earth radii	$6x10^8 cm^{-2} sec^{-1}$
Electrons > 5 Mev	1.3 earth radii	$2x10^7 cm^{-2} sec^{-1}$
Outer Van Allen Belt		
Protons < 4.5 Mev	3.5 earth radii	$6x10^7 cm^{-2} sec^{-1} sterad^{-1}$
Protons 40-110 Mev	3.5 earth radii	$4x10^3 cm^{-2} sec^{-1}$
Electrons < 40 Kev	4.2-4.8 earth radii	$3x10^8 cm^{-2} sec^{-1}$
Electrons > 230 Kev	4.8 earth radii	$1x10^7 cm^{-2} sec^{-1}$
Electrons > 1.6 Kev	4.2 earth radii	$1x10^6 cm^{-2} sec^{-1}$
Solar Flares		
"Typical"		
Protons 1-15 Mev	Outside geomagnetic field 10-15 earth-radii	$3x10^4 cm^{-2} sec^{-1} sterad^{-1}$
Protons > 40 Mev		$1x10^3 cm^{-2} sec^{-1}$
"Intense"		
Protons 90-500 Mev		$6x10^6 cm^{-2} sec^{-1}$
Cosmic Rays		
Greater than 1.5 Gev/nucleon	1 A.U. from sun	$8\ m^{-2} sec^{-1} sterad^{-1}$

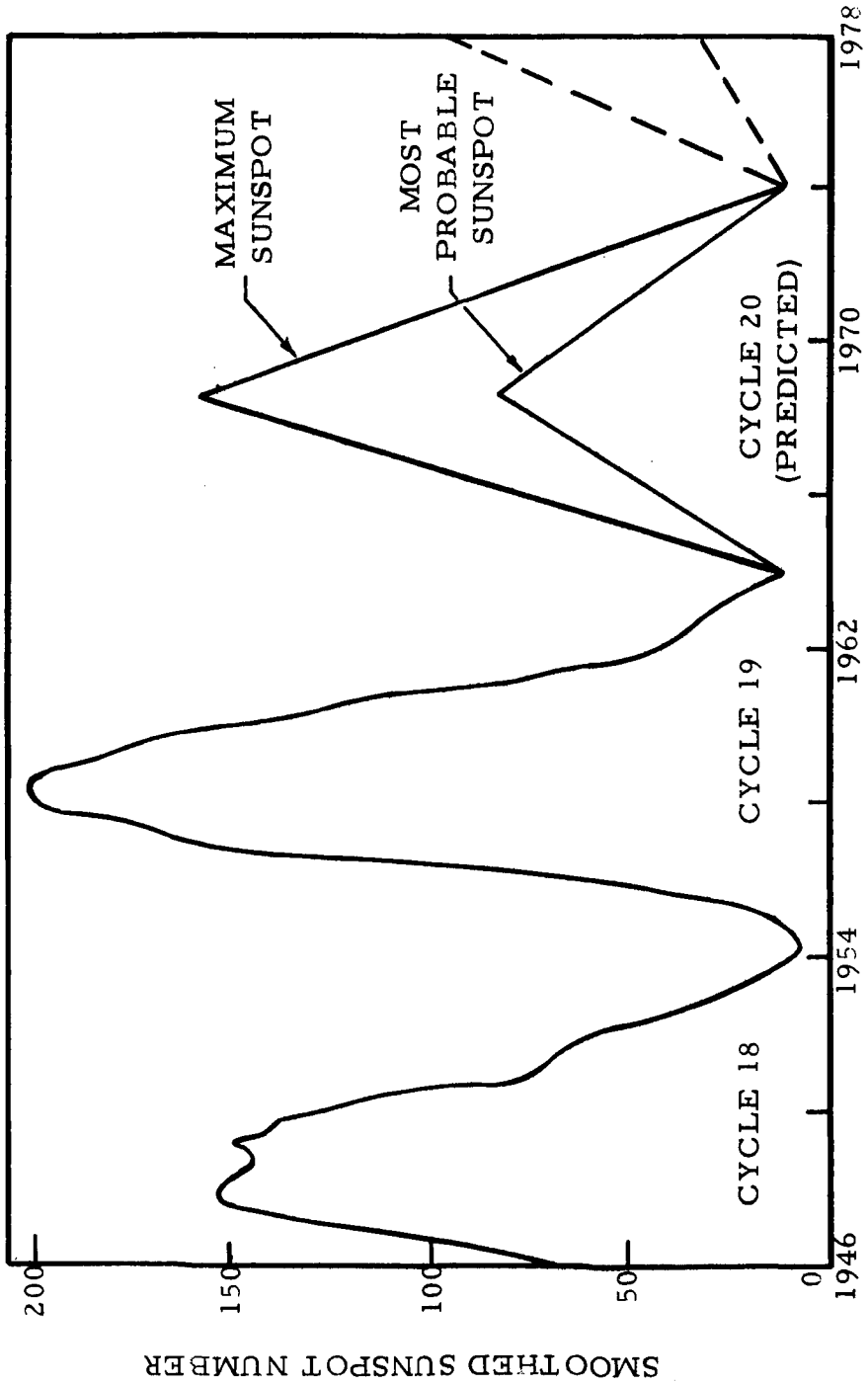

FIGURE 2-8 SOLAR ACTIVITY

The effects of radiation on film and the resulting shielding requirements to contend with the probable radiation dosages expected are described in Section 6.2 of this report.

2.9 REFERENCES

2-1 REA, D. G., "Some Comments on the Composition of the Martian Surface," Icarus, Vol. 4, No. 1, April 1965

2-2 MC LAUGHLIN, D. B., "Interpretation of Some Martian Features," Publ. Astron. Soc. Pacific, Vol. 66, 1954

2-3 DOLLFUS, A., "Planetary Studies," Proc. Lunar and Planetary Exploration Colloquium, Vol. 2, No. 3, North American Aviation, Inc., August 1961

2-4 SHARONOV, V. V., "A Lithological Interpretation of the Photometric and Colorimetric Studies of Mars," Astron. Zh., Vol. 38, No. 2, 1961, or Soviet Astronomy-AJ, Vol. 5, 1961

2-5 KUIPER, G. P., "Planetary Atmospheres and Their Origin," The Atmospheres of the Earth and Planets, Ch. 12, 2nd Ed., University of Chicago Press, 1952, (1st Ed., 1949)

2-6 VAN TASSEL, R. A. and SALISBURY, J. W., "The Composition of the Martian Surface," Icarus, Vol. 2, No. 3, September 1964

2-7 BINDER, A. B. and CRUIKSHANK, D. P., "Comparison of the Infrared Spectrum of Mars With the Spectra of Selected Terrestrial Rocks and Minerals," Commun. Lunar and Planetary Lab., Vol. 2, No. 37, 1965

2-8 SHARONOV, V. V., "The Brightness Contrasts Observed on the Surface of Mars," Poulkovo Obs. Circular, No. 32, 1941

2-9 HOOP, H. H., "Mars Surface Formation, Surface Materials, and Terrain," Redstone Sci. Info. Center, Doc. RSIC-592, September 1966.

2-10 TOMBAUGH, C. W., "Evidence of Faulting on the Crust of Mars," Part I: Grabens. NASA Report No. CR-51174, July 1963

2.9 REFERENCES (continued)

2-11 OPIK, E. J., "The Martian Surface," Science, Vol. 153, July 15, 1966

2-12 SAGAN, C. and POLLACK, J. B., "Elevation Differences on Mars," SAO Spec. Report No. 24, 1966

2-13 WELLS, R. A., "Evidence That the Dark Areas on Mars Are Elevated Mountain Ranges," Nature, Vol. 207, No. 4998, August 14, 1965

2-14 PETTENGILL, G. H., "Paper Delivered at International Astronomical Union, Prague," New York Times Article, August 30, 1967

2-15 FOCAS, J. H., "Observations of Mars Made in 1961 at the Pic du Midi Observatory," JPL Tech. Rpt. No. 32-151, January 30, 1962

2-16 KUIPER, G. P., "Visual Observations of Mars, 1956," Astrophys. J., Vol. 125, 1957

2-17 MICHAUX, C. M., "Handbook of the Physical Properties of the Planet Mars," NASA SP-3030, 1967

2-18 DOLLFUS, A., "Etude des Planetes par la Polarixation de leur Lumiere," Ann. Astrophys., Supplement, No. 4, 1957

2-19 LEIGHTON, R. B. and MURRAY, B. C., "The Behavior of Carbon Dioxide and Other Volatiles on Mars," Science, Vol. 153, July 8, 1966

2-20 DE VAUCOULEURS, G., "Reconnaissance of the Nearer Planets," Air Force Office of Scientific Res. Tech. Rpt. AFOSR/DRA-61-1, November 1961

2-21 HAINES, R. F., "A Review of the Expected Environment of Mars and a Discussion of Some Questions Related to Visual, Photographic, and Radiometric Experiments," AIAA/AAS, Stepping Stones to Mars Symposium Proc., March 1966

2.9 REFERENCES (continued)

2-22 FOCAS, J. H., "Seasonal evolution of the Fine Structure of the Dark Areas of Mars," Planetary and Space Science, Vol. 9, 1962

2-23 BROOKS, E. M., "Comprehensive Summary of Available Knowledge of the Meteorology of Mars and Venus," NASA Report No. CR-786, May 1967

2-24 KATTERFELD, G. N., "On the Question of the Tectonic Origin of the Linear Formations on Mars," Vsesoiuznoe Geograficheskoe Obshchestvo (Leningrad), Izvestiya, Vol. 91, No. 3, 1959

2-25 LOWELL, P. H., "Mars and Its Canals," The Macmillian Company, 1908

2-26 TOMBAUGH, C. W., "Mars - A World for Exploration," Astronautics, Vol. 4, 1959; and "Comparison of Lunar and Martian Features," Proc. Lunar and Planetary Exploration Colloquium, North American Aviation, Inc., Vol. 1, No. 4, January 1959

2-27 DOLLFUS, A., "Etude Visuelle de la Surface de la Planete Mars Avec Un Pouvoir Separateur," L'Astronomie, Vol. 67, 1953

2-28 BURGESS, E., "There Are Canals on Mars," Spaceflight, Vol. 8, No. 2, February 1966

2-29 MC LAUGHLIN, D. B., "The Volcanic-Aeolian Hypothesis of Martian Features," Publ. Astron. Soc. Pacific, Vol. 68, 1956

2-30 KATTERFELD, G. N., "Volcanic Activity on Mars," NASA TT F-410, 1966

2-31 NICKS, O. W., "A Review of the Mariner IV Results," NASA SP-130, 1967

2-32 MOLLOY, M. W. and LIDDEL, U., "Significant Achievements in Space Science," NASA SP-136, 1965

2.9 REFERENCES (continued)

2-33 SLIPHER, E. C., "The Photographic Story of Mars," Sky Publishing Co. (Cambridge, Mass.), 1962

2-34 "Imagery Experiment Value Function," Boeing Company, Boeing Rpt. D2-113581-2, Appendix S1, 1967

2-35 KUIPER, G. P., "Planetary Atmospheres and Their Origin," The Atmospheres of the Earth and Planets, Ch. 12, 2nd Ed., G. P. Kuiper, Ed., University of Chicago Press, 1952

2-36 ARRHENIUS, S., "The Planet Mars," The Destinies of the Stars, G. P. Putnam and Sons (New York), 1918

2-37 DE VAUCOULEURS, G., "The Physical Environment on Mars," Physics and Medicine of the Atmosphere and Space, Ch. 39, O. Benson and H. Strughold, Eds., John Wiley & Sons, Inc., 1960

2-38 HESS, S. L., "Mars as an Astronautical Objective," Advan. Space Sci. and Tech., Vol. III, F. I. Ordway III, Ed., Academic Press (New York), 1961

2-39 OWEN, T. C., and KUIPER, G. P., "A Determination of the Composition and Surface Pressure of the Martian Atmosphere," Commun. Lunar and Planetary Lab., Vol. 2, No. 32, 1964

2-40 FJELDBO, G., FJELDBO, W. and ESHLEMAN, V. R., "Models for the Atmosphere of Mars Based on the Mariner IV Occultation Experiment," Scientific Reports No. 's 2 and 15, January 1966

2-41 YANOVITSKIY, E. G., "On the Aerosol Component of the Martian Atmosphere," In Investigation of the Atmospheres of Venus and Mars. NASA TT F-394, January 1967

2-42 DOLLFUS, A., "Determination of the Luminance of the Martian Atmosphere," Acadene des Sciences, Comptes Rendus, 262, 1966

2.9 REFERENCES (continued)

2-43 BARRINGTON, A. E., and others, "Flyby Measurements of the Profiles of Water Vapor, Particulate Matter, and Carbon Dioxide in the Martian Atmosphere," NASA TN D-4115, August 1967

2-44 KLIORE, A., and others, "Radio Occultation Measurement of the Martian Atmosphere over 2 Regions by the Mariner IV Space Probe," COSPAR, Internat. Space Science Symposium, Vienna, May 10-19, 1966

2-45 GROSS, S. H. and others, "Mars: Upper Atmosphere," Science, Vol. 151, March 11, 1966

2-46 KACHUR V., "Thermology of the Martian Surface," AIAA Aerospace Sciences Meeting, Los Angeles, June 27-29, 1966

2-47 MIYAMOTO, S., "Martian Atmosphere and Crust," Icarus, Vol. 5, 1966, also in "Meteorological Observations of Mars During the 1965 Opposition," Contrib. No. 125, 1965

2-48 OTTERMAN, J. and BRONNER, F. E., "Martian Wave of Darkening: A Frost Phenomenon?," Science, Vol. 153, 1966

2-49 TANG, W., "On the Steady Symmetrical Regime of the General Circulation of the Martian Atmosphere," Contributions to Planetary Meteorology by G. Ohring, W. Tang, F. B. House, and J. Mariano. Geophysical Corp. of Am., Tech. Rpt. No. 66-8-N, March 1966

2-50 LEOVY, C. and MINTZ, Y., "A Numerical General Circulation Experiment for the Atmosphere of Mars," Memorandum RM-5110-NASA, December 1966

2-51 GOODY, R. M., "The Atmosphere of Mars," J. Brit. Interplanetary Soc., Vol. 16, 1957, or Weather, Vol. 12, January 1957

2.9 REFERENCES (continued)

2-52 WILSON, A.G., "The Problems of the Martian Blue Haze," Proc. Lunar and Planetary Exploration Colloq., Vol. 1, No. 4, North American Aviation, January 12, 1959

2-53 LOOMIS, A.A., "Some Geologic Problems of Mars," Geol. Soc. American Bull. 76, 1965

2-54 GIFFORD, F.A., "A Study of Martian Yellow Clouds that Display Movement," Monthly Weather Rev., Vol. 92, No. 10 October 10, 1964

2-55 KIESS, C.C., KARRER, S.; and KIESS, H.K., "A New Interpretation of Martian Phenomena," Publ. Astron. Soc. Pacific, Vol. 72, 1960

2-56 CAPEN, C.F., "The Mars 1964-65 Apparition," JPL Technical Report No. 32-990, 1965

2-57 DE VAUCOULEURS, G., "Geometric and Photometric Parameters of the Terrestrial Planets," Memorandum RM-4000-NASA, 1964

2-58 CAMPEN, C.F., "Personal Communication," ASP/ACSM Convention, St. Louis, October 3, 1967

2-59 MULLER, G., "Helligkeitmessungen der bei Planetenbeobachtungen Benutzen Vergleichsterne," Publ. Astrophys. Obs. Potsdam, Vol. 8, No. 4, 1893

2-60 MOROZHENKO, V.A. and YANOVITSKIY, E.G., "Surface Characteristics of the Moon, Mars, and Venus," ATD Report 66-53, May 16, 1966

2-61 REA, D.C., "The Atmosphere and Surface of Mars, A Selective Review," Presented at Lunar and Planetary Seminar, CIT, September 17, 1965

2-62 KOVAL, I.K., "Surface Characteristics of the Moon, Mars and Venus," ATD Report 66-53, May 16, 1966

2.9 REFERENCES (continued)

2-63 DANIELSON, E., "Personal Communication," Jet Propulsion Laboratory, November 9, 1967

2-64 EVANS, D. C., "Ultraviolet Reflectivity of Mars," Science, Vol. 149, August 27, 1965

2-65 SHARONOV, V. V., "A Model of the Martian Atmosphere and Planetary Surface," NASA TTF-394, January 1967

2-66 SLOAN, R. K., "Scientific Results of Mariner Missions to Mars and Venus," NASA Sci. & Tech. Doc. N66-31495, 1966

2-67 RINDFLEISCH, T., "Photometric Method for Lunar Topography," Photogram., Eng., Vol. 27, No. 2, March 1966

2-68 RINDFLEISCH, T., "A Range of Applicability for the Photometric Method of Topographic Mapping," Jet Propulsion Laboratory Space Programs Summary 37-44, Vol. 4, N67-29156, 1967

2-69 EGAN, W. G. and FOREMAN, K. M., "A New Perspective on Martian Photometric Measurements," AAS 67-329, June 11-14, 1967

2-70 VANALLEN, J. A., FRANK, L. A., KRIMIGIS, S. M. and HILLS, H. K., "Absence of Martian Radiation Belts and Implications Thereof," Science, Vol. 149, 1965

2-71 WEIDNER, D. K. and HASSELTINE, C. L., "Natural Environment Design Criteria Guidelines for MSFC Voyager Spacecraft for Mars 1973 Mission," NASA TMX-53616, June 8, 1967

2-72 LEACH, E. R., FAIRAND, B. P. and BETTENHAUSEN, L. H., "The Space Radiation Environment and Its Interactions with Matter," Battelle Memorial Institute, REIC Report No. 37, January 15, 1965

2.9 REFERENCES (continued)

2-73 "An Evaluation of the Radiation Hazard Due to Solar Particle Events," Boeing Company, Report No. D2-90469

2-74 HILL, C. W., RITCHIE, W. B. and SIMPSON, K. M. Jr., "Radiation Hazards in Space," Lockheed Nuclear Products Report ER 7777, April 1966

SECTION 3

MISSION OBJECTIVES AND PHOTO SYSTEM REQUIREMENTS

Considerable controversy exists regarding the origin, history, composition, atmosphere and geophysical and biological activity of Mars. The primary objective of the earlier Voyager Martian missions is to obtain information concerning these planetary characteristics by means of orbital reconnaissance and possibly surface laboratory measurements. Specifically, high priority should be given to obtaining data which will permit:

- identification and classification of Martian continents and maria
- determination of the nature of the polar caps
- specification of the origin of the canals, oases and craters
- explanation of the wave of darkening as well as other seasonal and secular changes
- identification of the extent and composition of Martian cloud and dust phenomena
- description of the nature of atmospheric circulation
- determination of the possible existence of organic activity
- location of potential landing sites.

Orbital photography provides an excellent means for obtaining much of the required information. Large portions of the planet surfaces can be mapped to permit interpretation of surface and atmospheric features and subsequent determination of the fundamental structure and activity of the planet. The success of the recently completed Lunar Orbiter program has demonstrated the application of the orbiting technique for acquiring considerable photographic coverage of lunar or planetary bodies. The photographs obtained from

each of the five Lunar Orbiter missions have helped to narrow the choice of potential manned Apollo landing sites on the moon from thirty to eight candidate areas. In addition, the Lunar Orbiter photographs have provided scientists with a wealth of topographic and geologic information from which the nature and composition of the lunar surface is currently being evaluated (Ref. 3-1).

Orbital photography can provide an excellent map data base for determination of the regional significance of specific topographic and geologic information. The geologic significance of some typical terrestrial surface features normally interpreted on aerial photographs is summarized in Table 3-1 (Ref. 3-2). Features such as those listed may be of great importance with respect to determining the fundamental structure and state of activity of Mars. However, surficial processes of Mars must be carefully analyzed, since they may not be directly analogous to the geologic processes occurring on Earth. Tectonic processes on Earth, for example, depend to a large extent on the accumulation of sediments in basins or areas of subsidence. In the same manner, factors that effect the composition of the atmosphere indirectly influence the course of tectonic processes. However, because of basic differences in Martian atmospheric composition and density (e.g., low water content, rare atmosphere), the structural history of Mars may not have followed the same path of development as the Earth.

The subsections which follow describe the photo imaging system requirements for the Mars Voyager orbital mission. Included are the results of the evaluation and recommendations of resolution and coverage requirements, typical areas for high resolution photography, stereo requirements, and multispectral requirements. A summary of photo system requirements, specified as a result of the study, is presented in Section 3.4.

3.1 RESOLUTION AND COVERAGE REQUIREMENTS

The greater the effective ground coverage per frame of imagery, the greater the capability for delineating regional topographic and structural information. However, a higher resolution imaging system permits the image interpreter to extract a greater amount of data, particularly with regard to detailed engineering evaluations of selected local areas. Resolution requirements must be analyzed in terms of specific mission objectives and realistic sensor system capabilities.

TABLE 3-1

SIGNIFICANCE OF TYPICAL TERRESTRIAL SURFACE FEATURES

SURFACE FEATURES	SIGNIFICANCE
Physiographic provinces	Normally indicate specific regions which are characterized by distinctive environments and/or distinctive rock types.
Constructional and Erosional Landforms	Indicate past and present processes of deposition and erosion.
Impact Phenomena	Features such as impact craters and splatter areas indicate extent and nature of extraterrestrial (meteoric) activity.
Igneous Phenomena	Features such as dikes, sills, eroded necks, volcanic cones, craters, calderas and lava flows indicate current and past history of internal igneous activity.
Folded and Fractured (Faulted) Areas	Indicate tectonic activity.
Polar Ice Caps, Deserts	Indicate specific climatic environments and processes.

Prior image interpretive analyses of space photography indicate that regional interpretation and delineation of most geologic, geomorphic and surficial features on Earth can best be accomplished at ground resolutions ranging from 40 to 70 meters. Figure 3-1 shows the various ground resolution requirements for identifying the basic physical characteristics of typical macro terrain, meteorological and gross biological/ecological features (Ref. 3-3).

Ground resolutions in the order of 100 to 500 meters or worse can be employed for purposes of synoptic meteorological observation and gross landform detection. This has been demonstrated with some small-scale TIROS photography (Ref. 3-4), whereby major physiographic and geologic features in highly contrasted arid regions have been identified with relative ease. A 100 meter resolution requirement may be adequate for performing basic meteorological investigations of imaged cloud phenomena, but would have to be considered an absolute minimum requirement for preliminary analysis of regional landforms, gross rock types, gross structure, topography and surface configuration. A medium resolution of from 40 to 70 meters would be desirable for analysis of these features.

Recent communication with Jet Propulsion Laboratory personnel (Ref. 3-5) appear to indicate that the high resolution imaging system capability for the Mariner 1969 photo mission will be approximately 200 meters, at best. This represents an order of magnitude improvement over the low Mariner IV, 2 km ground resolution capability, but will not provide imagery of sufficient resolution to satisfy the Voyager mission objectives.

It is evident from Figure 3-1 that the detailed interpretation and analysis of landforms, basic rock types and structures require resolutions of about 5 meters. However, even higher resolutions are required for the delineation of detailed engineering characteristics and biological/ecological phenomena. For the evaluation of organic life characteristics on Mars, it appears that ground resolutions of 1 meter or better should be provided to enable biologists to obtain the detailed information required.

It can be concluded that for purposes of detailed geologic, geomorphic, topographic and biological/ecological evaluations, ground resolutions of 5 meters or better should be provided for the Voyager high resolution imaging system. This value is consistent with the optimum high resolution imaging requirements established by both U.S. Geological Survey

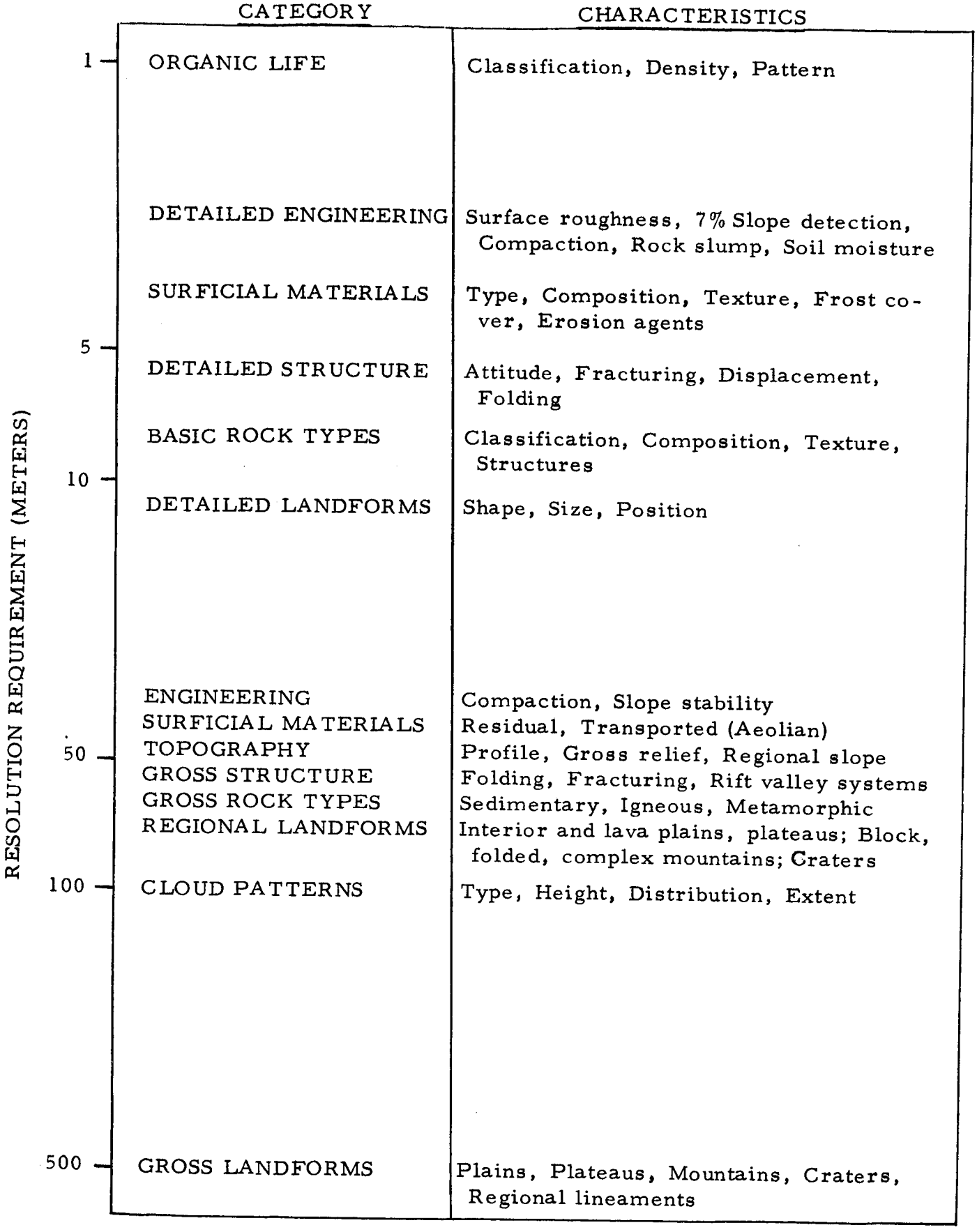

FIGURE 3-1 SURFACE FEATURE RESOLUTION REQUIREMENTS

and Environmental Science Services Administration for space photography of the Earth. Recent IBM studies (Ref. 3-6) also appear to indicate that ground resolutions of approximately 2 meters or better would be required for detailed experiments in the areas of geology, geography and ecology.

3.1.1 Medium Resolution Coverage Requirements

The review of Martian environmental phenomena in Section 2 indicates that great controversy still exists related to the pertinent physical characteristics of the observed primary and secondary surface features, the wave of darkening, and meteorological features, such as clouds and haze. This almost total lack of definitive environmental data for Mars makes it essential that as complete an areal portion of the Martian surface as possible be covered at the desired medium resolution of 40 to 70 m.

The importance of providing complete photo coverage of the Martian surface scarcely needs emphasis. The greater the effective ground coverage capability of the medium resolution imaging system, the greater the capability for delineating gross (regional) topographic and structural grain over a large portion of the Martian surface. Hence, it is evident that the broad, apparently featureless, expanses of light colored areas in the mid-latitude regions should be mapped primarily at the medium resolution level. The delineation of local anomalous features within these regions would dictate the need for possible high resolution photo coverage of selected areas during succeeding orbital passes.

Optimally, the medium resolution imaging system should provide complete coverage of the surface. If this coverage cannot be obtained because of orbital or communication restrictions, a median coverage pattern ranging from 40°N latitude to 40°S latitude (approximately 65% coverage) would be desirable. The minimum acceptable surface coverage pattern should extend from 30°N latitude to 30°S latitude (approximately 50% coverage). This minimum coverage requirement will still permit effective area imaging of the primary maria - desert regions in the equatorial zone. Some limited polar coverage should also be obtained, if possible.

3.1.2 High Resolution Coverage Requirements

The main purpose of the high resolution imaging system will be to

provide pertinent large-scale coverage of locally selected areas on the Martian surface. The resultant imagery will be of great value for detailed identification and analysis of specific terrain and ecological conditions. High resolution imagery will also be a basic prerequisite for performing detailed engineering and potential landing site evaluations of selected portions of the Martian surface. In addition, this imagery will further enhance the interpretive results obtained from the medium resolution (i. e., 40 to 70 meter) photographic data.

It is currently estimated that the high resolution imaging system will cover approximately 1 to 5% of the medium resolution coverage of the Martian surface. The relative utilization of the total communications capability must be considered in determining the amount of high resolution coverage to be obtained. Figure 3-2 illustrates the percent of the total communications capability required for transmission of the high resolution data as a function of the percentage of high resolution to medium resolution coverage, assuming a 10 to 1 ratio between medium and high resolution (e. g., 50 meter and 5 meter resolution). A high resolution total coverage representing one percent of the medium resolution coverage would require half of the total communication capability for transmission of the high resolution data. Transmission of five percent high resolution coverage would require approximately 83 percent of the total communication capability.

Table 3-2 shows representative Martian terrain features which have been classified "anomalous" because of their basic physical characteristics. These features represent preliminary selections of areas which should be examined in greater detail in the high resolution imaging mode. It is anticipated that detailed analysis of high resolution imagery for each of these typical areas of interest will provide significant data relative to determining specific physiographic units, erosional and depositional processes, meteoric activity, igneous volcanic activity, tectonic activity and climatic processes. There will undoubtedly be other localized potentially anomalous areas which will be recommended for possible high resolution coverage. Many such areas will be selected after preliminary evaluation of the medium resolution photographic data.

Figure 3-3 illustrates the relative positions of the fourteen selected areas of interest. Please note that this figure is to be used in conjunction with the transparent overlay map of Mars (Ref. 3-7) contained in the folder at the back of this report.

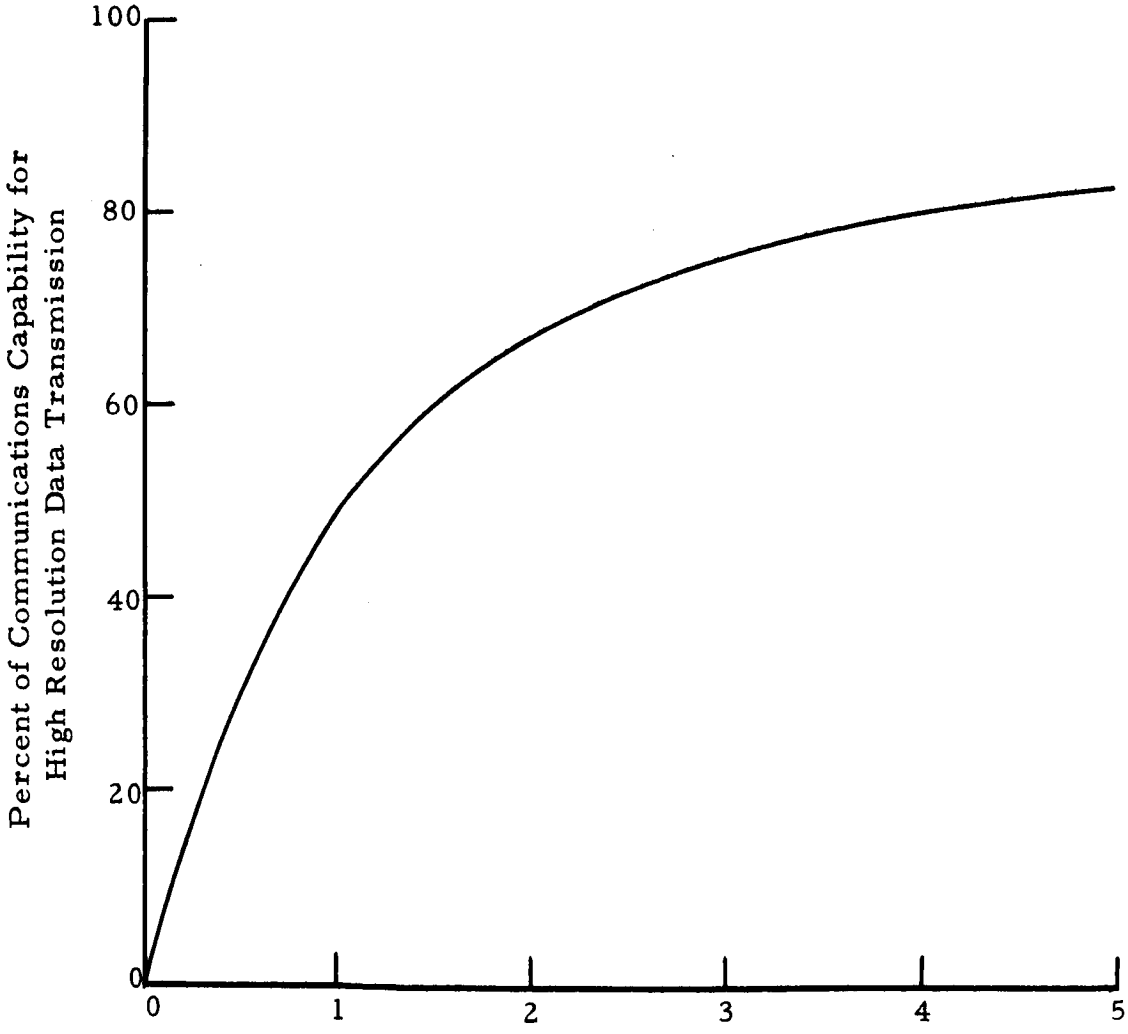

FIGURE 3-2 HIGH RESOLUTION COVERAGE AND COMMUNICATION REQUIREMENTS (Ratio of Medium to High Resolution 10:1)

TABLE 3-2 MARTIAN SURFACE FEATURES - AREAS OF INTEREST

REFERENCE NUMBER	SURFACE AREA DESIGNATION	APPROX. LOCATION	OBSERVED CHARACTERISTICS
1	Mare Sirenium	Lat: 10°S Long: 195°	Very dark and sharply defined small triangles along northern contact with Memnonia desert regions. May be indicative of faulting. Configuration may be determined by the angles of canals converging at the contact with the adjacent desert regions.
2	Atlantis	Lat: 25°S Long: 195°	Inter-mare continental platform region. (Area covered by Mariner IV, Frame 11.) Preliminary analysis indicates presence of large craters and possible tectonic activity.
3	Tharsis	Lat: 10°S Long: 255°	Dark circular pattern (oasis?). Mountainous relief suggested by recurrence of orographically produced W-shaped clouds in fixed locales of this region.
4	Solis Lacus	Lat: 25°S Long: 285°	Region characterized by long term secular variations which produce new patterns of darkening. Changes in the shape of Solis Lacus have been observed from 1877 to 1939.

TABLE 3-2 MARTIAN SURFACE FEATURES - AREAS OF INTEREST

REFERENCE NUMBER	SURFACE AREA DESIGNATION	APPROX. LOCATION	OBSERVED CHARACTERISTICS
5	Lunae Lacus	Lat: 20°N Long: 295°	Well defined, dark circular pattern situated in primary desert region. Classified as isolated oasis. Possible structural implications.
6	Mare Acidalium	Lat: 50°N Long: 330°	Largest maria region in northern hemisphere. Consistently dark and subjected to seasonal darkening color changes.
7	Margaritifer Sinus	Lat: 10°S Long: 330°	Continental region situated between two maria regions. Evidence of tectonic activity suggested.
8	Meridiani Sinus	Lat: 5°N Long: 5°	Characterized by dark triangular patterns with apices trending NNE. Suggests evidence of tectonic activity.
9	Hellas	Lat: 40°S Long: 60°;	Considered to be brightest areas on Martian surface. Areas periodically brighten (may be temporarily covered with frost) and are both considered to be elevated plateaus or summits (or depressions).
9A	Elysium	Lat: 25°N Long: 145°	

TABLE 3-2 MARTIAN SURFACE FEATURES - AREAS OF INTEREST

REFERENCE NUMBER	SURFACE AREA DESIGNATION	APPROX. LOCATION	OBSERVED CHARACTERISTICS
10	Syrtis Major	Lat: 15°N Long: 80°	North-northeast extension of Mare Tyrrhenum. Characterized by NNE-trending apex boundary indicative of faulting. Considered to be darkest uniform area on Martian surface.
11	Thoth-Nepenthes	Lat: 10°N Long: 95°	Region characterized by long-term secular variation and development of darkening pattern (observed since 1907). Skeletal framework of dark markings (i.e., canal system) has virtually converted into a mare. A vast dark region developed fully in 1954 and has persisted.
12	Trivium Charontis	Lat: 15°N Long: 165°	Well defined, dark triangular area (large oasis) characterized by canals radiating outward. Evidence of linear tectonic activity extending into surrounding region.
13	Mare Hadriaticum	Lat: 30°S Long: 85°	Southern portion of Mare Tyrrhenum. Characterized by well-defined southern contact with light desert area. Elongated triangular outline exhibited by Mare Hadriaticum appears to be controlled by intricate canal structure. Strong possibility of tectonic influence (faulting?).

FIGURE 3-3 MARTIAN AREAS OF INTEREST

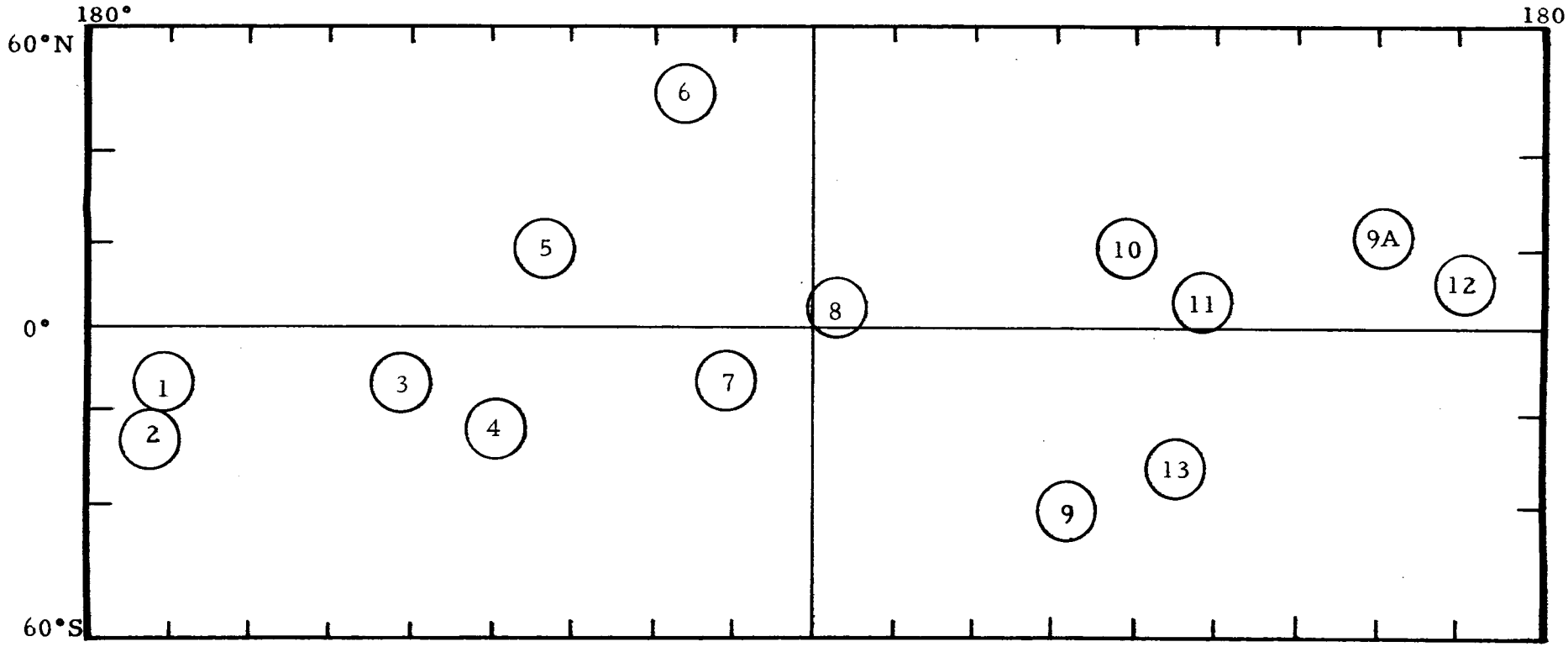

Ref. No.	Surface Area	Ref. No.	Surface Area
1	Mare Sirenium	8	Meridiani Sinus
2	Atlantis	9	Hellas
3	Tharsis	9A	Elysium
4	Solis Lacus	10	Syrtis Major
5	Lunae Lacus	11	Thoth-Nepenthes
6	Mare Acidalium	12	Trivium Charontis
7	Margaritifer Sinus	13	Mare Hadriaticum

3.2 STEREO REQUIREMENTS

Stereo viewing enables the image interpreter to identify many object surface slope conditions that cannot be identified or detected in single photographs alone. Stereoscopic imaging utilizes two images of the same scene taken from different camera stations. The difference in position of the recorded scene, as presented in the two conjugate images, provides data relative to elevations of representative points in the scene. The displacement differences are clearly visible in the fused stereoscopic model (Ref. 3-8). Techniques for stereo implementation are described in Section 5.2.

3.2.1 Detectable Object Height

In general, high altitude stereoscopic imagery does not provide maximum vertical resolution (i.e., optimum three-dimensional perception) because of the minimal differences in measurable parallax between successive conjugate image frames. The smallest differential of object height detectable by measurements of stereoscopic parallax is related to altitude and system resolution. Representative curves defining the minimum height requirements of objects discernible for stereo viewing 35 and 70 mm image formats are shown in Figure 3-4. It can be seen from this figure that the minimum object height decreases as the altitude decreases or the format increases. Consequently, representative stereo imagery obtained with a 100 lp/mm, 70 mm format system from an altitude of 500 km, would permit a minimum object height determination of approximately 100 meters. Measurements of object height to the nearest 100 meters minimum would be barely acceptable for performing regional geologic and geomorphic interpretation and evaluation of representative macroterrain features. However, this minimum object height would be of no practical value when measuring or estimating local differences in topographic detail (i.e.; microrelief elements) and vegetation height. In order to properly evaluate these conditions in stereo, measurements of object height within ±2 meters would be acceptable.

There does not seem to be a practical way to obtain photography from space on which heights of small objects, such as those of forest stands can be reliably estimated (Ref. 3-9). Convergent photography offers a possibility for increasing the parallax base without increasing the size of the photo format; however, this technique would not constitute a significant improvement for measuring local differences of

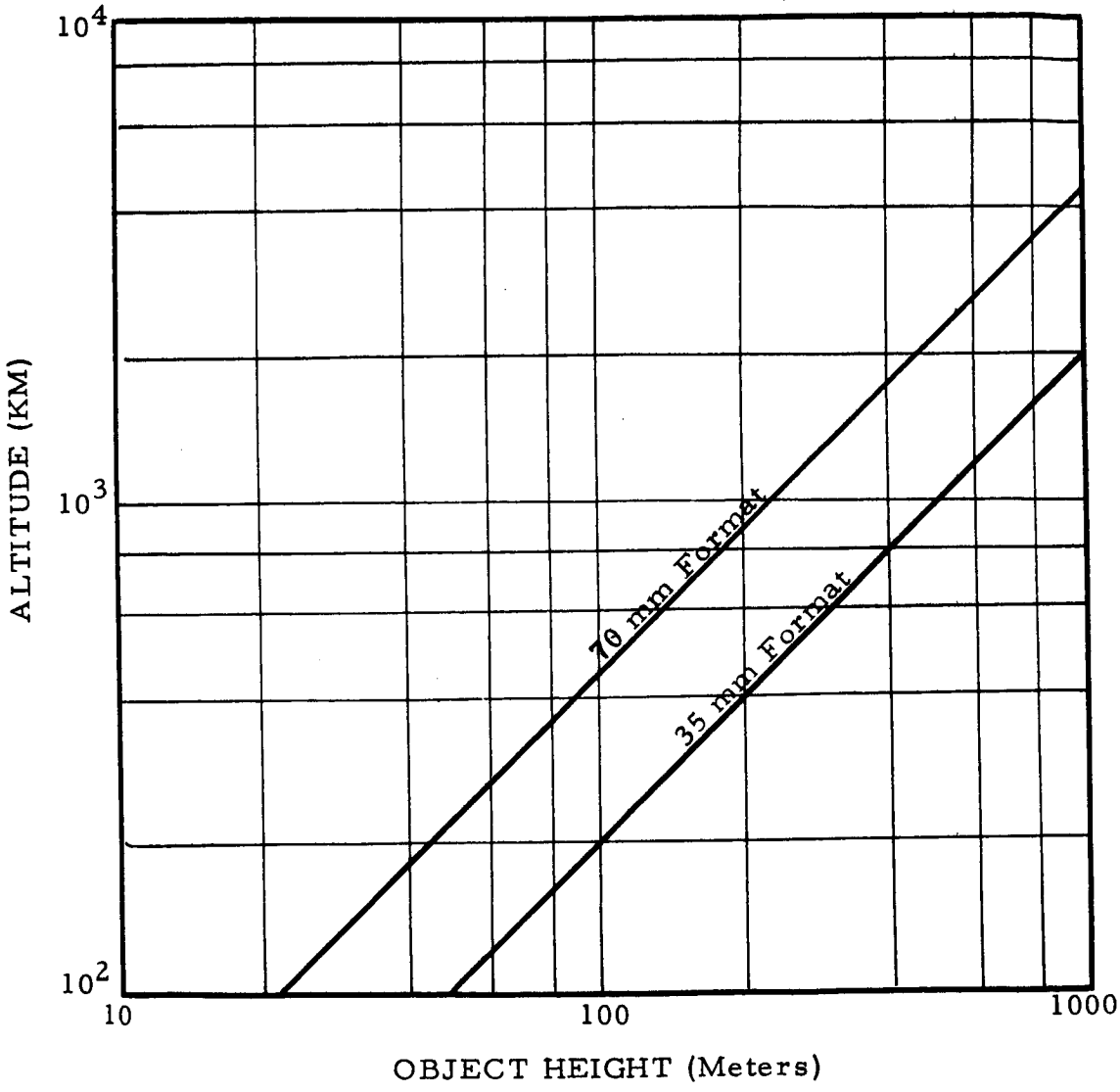

FIGURE 3-4 MINIMUM OBJECT HEIGHT FOR STEREO VISION (100 lp/mm System, 60% Overlap)

topographic relief on photography from orbital altitudes. Perhaps the ultimate solution may be to exploit the known photometric properties of a portion of the surface and utilize the resultant data in conjunction with optimum stereoscopic images of that surface. This may result in the establishment of a relative degree of surface control and, in turn, may provide accurate estimates regarding representative object height.

3.2.2 Recommended Stereo Coverage

The medium resolution imaging system should provide at least 10 percent stereo coverage of selected portions of the Martian surface, ideally with 60% overlap. Selected stereo coverage should be primarily limited to imaging typical areas of interest (such as those described previously) and to the imaging of anomalous areas selected on the basis of previous monoscopic analyses.

Effective vertical stereo coverage cannot be acquired during the high resolution imaging mode due to severe limitations in both the base/height ratio and percentage overlap (see Section 5.2). Use of a twin convergent camera would permit acquisition of high resolution stereo coverage of selected areas of the Martian surface, but would impose an additional weight penalty (primarily due to the lens). It is conceivable, therefore, that the high resolution imaging system will employ only a single frame camera. If this is the case, there probably will be no consecutive stereo coverage of selected areas by the high resolution imaging system.

3.3 MULTISPECTRAL REQUIREMENTS

The interpretation of aerial photographs is normally based upon principles of size, shape, pattern, shadow, tone, texture, and association. However, shadow and texture become less important with increased altitude and decreased resolution and association is useful only in the gross geographic sense. Tone, on the other hand, is considered to be the primary factor for image interpretation using multispectral sensing because it varies with wavelength and is dependent upon the spectral reflectance of the object being viewed.

Numerous studies of multispectral tone signatures have been conducted in the fields of forestry, agriculture, geology and glaciology.

In current agricultural experiments, for example, it is anticipated that comparisons of the response of the various crop types and conditions by using several spectral bands may yield a characteristic multispectral response signature for each crop type or crop condition studied (Ref. 3-10). Recent studies have concluded that multispectral satellite photography may provide useful information for analysis of glaciers and other snow or ice masses, where the use of visible light imagery is limited due to the few color or tonal contrasts exhibited by snow (Ref. 3-11).

Multispectral imaging techniques have been used previously for planetary photographic sensing systems. The previously acquired Mariner IV photographs, for example, were taken with alternating green and orange filters (Ref. 3-12), to provide good photographic contrast and data on color differences on Mars. Similarly, the Mariner '69 medium resolution imaging system will use green and red filters to photograph Martian surface markings.

The relative advantages of the multispectral and/or colorimetric approaches over the use of standard black and white techniques are considered in the following subsections. The factors involved in selection of specific filters for a Martian mission are also presented. The implementation of multispectral instrumentation, however, is described in Section 5.3.

3.3.1 Advantages of Multispectral Techniques

In any photographic system, the ground scene recorded on the sensor surface represents the contrast difference which exists between

objects. In black and white systems this contrast is seen as a density difference which corresponds to the difference in brightness. If, for example, colored panels of the same brightness value were photographed adjacent to each other, no differentiation between them would be possible with a black and white sensor. Multispectral systems, however, have the capability to record color as well as brightness differences (Ref. 3-13). In addition, multispectral systems permit differentiation of objects which may be spectrally close in color.

Another distinct advantage of multispectral over black and white systems is that an object,which reflects in a certain spectral region, lying in achromatic shadow is usually detectable. This ability to see into shadow areas should be of value in interpretation of Martian surface imagery.

Consideration must be given to the acquisition of some multispectral data even at the expense of additional high resolution data. Experience has proved that objects in the ground scene, although completely unresolved, have been readily detected by multispectral systems, because of their distinct color. This has been especially true in complex scenes with no large contrast changes, or in cases where the terrain exhibits a gradual shift in the type of geological phenomenon (e. g., dry to moist soil, sand to stone, or change in soil types from one area to another).

Multispectral techniques can also be used to obtain true color imagery of the Martian surface. This requires that the same area be recorded separately, but preferably simultaneously, in the red, green and blue spectral regions. The additive synthesis process is used to obtain color presentations from the three individual black and white records. This process requires that the individual records be presented in exact registration to permit viewing without significant degradation. The use of the multispectral technique permits the variation of the values of hue, brightness and saturation. Thus, in addition to the display of true color, false color renditions can be used to exaggerate small spectral differences between objects.

Although the use of color improves the ability of the interpreter to identify objects, such a technique is difficult to implement. As a result, limited multispectral instrumentation is more likely to be utilized for planetary missions.

3.3.2 Multispectral Filter Considerations

Mars exhibits a range of colors which cover the entire visible spectrum. According to Yost (Ref. 3-13), if the complete spectrum is to be investigated, then wide band filters must be employed for multispectral use. Since red and green taken additively in color synthesis yield yellow, and since pure reds and greens exist themselves in the scene, these two filters at least are necessary.

The Martian terrain apparently is composed primarily of red hues so that it might even be advisable to break the 0.6 to 0.7 micron (micrometer) spectral region into several intervals. The use of an infrared filter may also be desirable because Mars appears to be very bright in the near infrared. On the other hand, since green is not the prominent color on Mars, the green filter could have a peak at approximately 0.55 microns with a range from 0.47 to 0.6 microns.

A wide band blue filter could also be employed at times when the Martian atmosphere is clear of blue haze. Blue filters characteristically exhibit low transmission so that the wavelength range should be approximately 0.1 microns to cover the entire blue spectral region. However, if the haze layer is thick at the time of exposure, it will completely obscure the surface for wavelengths less than 0.47 microns.

3.3.3 Recommended Multispectral Parameters

Limited multispectral imaging of selected portions of the Martian surface and atmosphere by the medium and high resolution camera systems would provide additional pertinent correlative data for investigation of the:

- composition and texture of surficial materials comprising selected maria and desert regions.
- secular variations in regions such as Solis Lacus.
- composition and texture of possible frost covered regions such as Hellas and the polar caps.

- probable soil moisture content and the existence of vegetation.

- major cloud, haze and atmosphere phenomena.

On the basis of results obtained thus far in various geoscientific disciplines, spectrally filtered multispectral imagery is useful for providing pertinent scientific data relative to determining reflective values of surficial and atmospheric materials, texture, composition, morphology and structural fabric of terrain. In addition, the major advantage is the greater differentiation of target signatures which results with multispectral photography.

The multispectral parameters established for the Martian orbital photographic system are summarized in Table 3-3. Included is a review of recommended multispectral requirements relative to wavelength, filters, and selective medium and high resolution surface coverage.

TABLE 3-3 SUMMARY MULTISPECTRAL CONSIDERATIONS

ITEM	REMARKS
Wavelengths	0.3 to 0.5 microns - Limited attenuation; excellent for imaging atmospheric effects such as blue haze and blue-white clouds. 0.5 to 0.7 microns - Good visibility; useful for study of yellow dust clouds. Upper limits of this range (i.e., above 0.64 microns) recommended for viewing surface feature detail. 0.7 to 1.0 microns - Better visibility; recommended for minimum haze obscuration, higher reflectivity of surficial materials.
Filters	Blue, Green, Red, IR.
Coverage	Very selective; approximately 5% of coverage of both medium and high resolution camera systems. Recommended for imaging specific areas of interest.
Advantage	Greater differentiation of target signatures.

3.4 SUMMARY OF PHOTO SYSTEM REQUIREMENTS

The primary objectives of the Voyager mission to Mars are to obtain information relative to the nature of possible extraterrestrial life, and the atmospheric, surface, and environmental characteristics of Mars, by performing experiments in orbit about the planet. It is anticipated that the exploratory investigations to be conducted by the planned Mariner 1969 flyby photo missions to Mars, will set the basis for future photographic experiments of the Voyager orbiter, particularly those relevant to determining the nature of the representative Martian surface and the existence of extraterrestrial life.

The requirements established for the Martian orbital photographic system are summarized in Table 3-4. Included is a review of the pertinent medium and high resolution camera system parameters relative to gross scientific objectives, monoscopic surface coverage, stereo surface coverage, multispectral response coverage and recommended user applications.

TABLE 3-4 SUMMARY OF OPTIMUM PHOTO SYSTEM REQUIREMENTS

CAMERA	PRIMARY OBJECTIVES	PLANETARY COVERAGE	STEREO COVERAGE	MULTISPECTRAL RESPONSE	USERS
Medium Resolution (40 to 70m) (Vertical Frame Camera)*	Determine size, shape and position of Martian features. Identify morphology of individual surface features. Examine cloud and dust formations.	Optimum: Complete coverage Desirable: 40°N Lat. to 40°S Lat. complete Acceptable Min: 30°N Lat. to 30°S Lat. complete Overlapping Coverage Preferred Limited Polar Coverage	Selected items of interest; approximately 10% of total medium resolution coverage at 60% overlap.	Limited spectrometric coverage: approximately 5% of total medium resolution coverage. Possibly some color coverage.	Astronomers Geologists Meteorologists Photogrammetrists Cartographers
High Resolution (5m) (Vertical Frame Camera)*	Identification and discrimination of selected items of interest.	1 to 5% of Medium Resolution Coverage	Probably none; unless twin convergent camera system is considered.	Limited and selective; up to 5% of total high resolution coverage.	Biologists Astronomers Geologists Cartographers Photogrammetrists Vehicle Designers

*NOTE: For imaging of the planet's limb or meteorological phenomena, a high angle oblique view with camera pointing toward horizon should be considered.

3.5 REFERENCES

3-1 "The Lunar Orbiter, A Radio Controlled Camera," Boeing Company, 1967

3-2 "Space Research-Directions for the Future," Space Science Board, National Academy of Science Publication 1403, Washington, 1966

3-3 BECCASIO, A. D. and SIMONS, J. H., "Regional Interpretation from Side Looking Airborne Radar," ASP/ACSM Convention, March 1965

3-4 MERRIFIELD, P. M. and RAMMELKAMP, J., "Terrain Seen from TIROS," Photogram. Eng., Vol. 17, No. 1, January 1966

3-5 DANIELSON, E., Personal Communication, Jet Propulsion Laboratory, November 9, 1967

3-6 WOODRICK, N. W., Personal Communication, International Business Machines, April 1967

3-7 "Mars Exploration," General Electric Company, PIB D-39, 1966

3-8 TATOR, B. A., "Photointerpretation in Geology," Manual of Photographic Interpretation, Amer. Soc. Photogrammetry, Banta Publ. Co., 1960

3-9 WILSON, R. C., "Space Photography for Forestry," Photogram. Eng., Vol. 18, No. 5, May 1967

3-10 HOFFER, R. M., et al, "Vegetative, Soil, and Photographic Factors Affecting Tone in Agricultural Remote Multispectral Sensing," University of Michigan, Sci. and Technology, 4th Symposium on Remote Sensing, April 1966

3-11 MEIER, M. F., et al, "Multispectral Sensing Tests at South Cascade Glacier, Washington," University of Michigan, Sci. and Technology, 4th Symposium on Remote Sensing, April 1966

3.5 REFERENCES (continued)

3-12 SLOAN, R. K., "Scientific Results of Mariner Missions to Mars and Venus," NASA Sci. and Tech. Doc. N66-31495, 1965

3-13 YOST, E., Personal Communications, C. W. Post College, Long Island University, November 6-17, 1967

SECTION 4

TRAJECTORIES AND PHOTO COVERAGE OF MARS

The primary objective of the Voyager program, the most ambitious unmanned post-Apollo space mission, is to carry out scientific investigations of the solar system through instrumented vehicles which will orbit and land on the planets. The Voyager mission profile (Ref. 4-1) consists of launching two identical spacecraft on separate interplanetary trajectories to Mars. Upon arrival, each spacecraft will be inserted into orbit around Mars. A flight capsule from each spacecraft then will be separated and will descend to the surface and land. After landing, a surface laboratory will operate on the surface of Mars while the spacecraft continues to operate in orbit around Mars. Furthermore, the basic Voyager guideline requires that essentially all of the equipment be standardized for four opportunities to Mars, 1973, 1975, 1977 and 1979. This standardization will include the launch vehicle, its shroud, spacecraft bus, spacecraft propulsion system, and capsule system. The orbiter, entry, and post-landing science payloads, however, are expected to vary from opportunity to opportunity. The introduction of such a standardization requirement introduces new and unique features in the selection and design of the interplanetary trajectories; these features are discussed in this section as they affect the photo-sensor mission objective.

Because of the radio transmission delays and lower data rates associated with the large planetary communication distances, the space vehicles utilized must be highly automated and contain a well selected complement of scientific experiments to provide maximum mission return. Therefore, the satellite orbits selected for these missions must permit an efficient investigation of the planet environment and, at the same time, simplify spacecraft configuration and system design requirements.

This section presents a discussion of factors considered in selecting Martian photo-imaging orbits and the results of a coverage analysis for example orbits.

4.1 ORBIT SELECTION CONSIDERATIONS

Factors which must be considered in selecting particular orbits about Mars are illustrated in Figure 4-1. Primary constraints and considerations fall into the following categories:

- Overall program considerations (Mars opportunities in '73, '75, '77 and '79).
- Engineering constraints on heliocentric and Martian orbits.
- Multiple scientific objectives.

All of these factors are discussed in detail in the following paragraphs but, since the primary concern of the present study pertains to the photc imaging experiment, preliminary comments on orbit considerations from the reconnaissance viewpoint are presented initially.

In photographing a planet by an orbiting camera, the requirements upon the camera as well as the type of data obtainable are strongly influenced by (1) the orbit, and (2) the viewing geometry, especially as a consequence of the curvature of the planet away from the sub-satellite point. To be more specific, the orbit influences the Martian orbital photographic experiment objectives and consideration of scientific instrumentation concepts for achievement of these objectives in the following manner:

- The height above the area of interest on the planet surface fixes the focal length of the system for a given ground resolution.
- The available light from the scene as viewed from the spacecraft dictates the lens system f-number and the shutter speed for a given response of the sensor.
- The ground velocity to altitude ratio (i.e., V/H, maximum at periapsis) dictates the image motion compensation requirement.

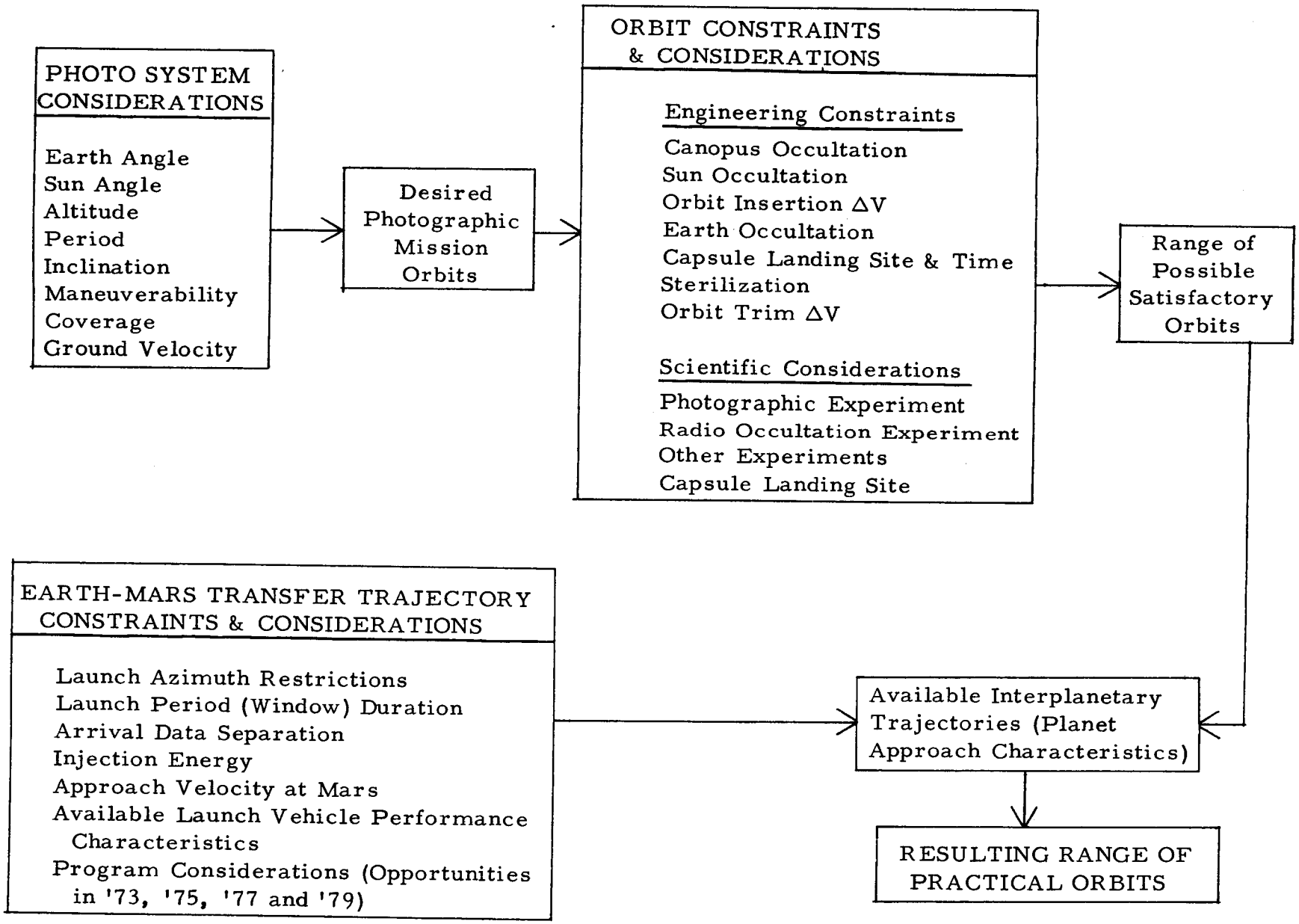

FIGURE 4-1
ORBIT SELECTION PROCESS

- The orbital period in conjunction with the period of planet rotation, influences the required camera field of view perpendicular to the orbital path necessary to achieve the desired coverage of the planet within a specified time period.

- The inclination of the orbit dictates the latitudes that can be viewed along the spacecraft nadir (the camera can look off the nadir but resolution degrades because of the increased slant range).

- The orbit should avoid or minimize the conditions of zero sun angle so that shadowing detail can be obtained providing useful reconnaissance information.

- Errors in the location of sensor data affect the accuracy of maps resulting from the photography, location errors arise primarily from errors in satellite subpoint position, satellite altitude, and satellite or sensor orientation.

- The orientation and period of the orbit must be considered in terms of both providing for coverage over the illuminated portion of the planet and compatibility with data processing and transmission to Earth constraints.

Some of the above interactions of orbit characteristics and photo-system performance are illustrated in Figure 4-2 for a specific sensor system having a 150 mm focal length lens, a 70 mm format and an overall system resolution of 100 lp/mm. As can be seen, the system ground resolution is twice as good for a 500 km circular orbit as for the 1,000 km case although the lateral coverage for the lower altitude is 1/2 that of the higher. These are rather obvious effects; however, the comparison in ground resolution obtainable with elliptic orbits having periapsis altitudes equal to that of the two circular orbits is quite illustrative. As can be seen, the smallest resolvable ground element has increased by 50% by the time the sensor in an elliptical orbit has traveled less than 40 degrees from periapsis. The lateral coverage, on the other hand, has increased by 50%, resulting in a surface area covered having an hourglass shape. The variation in resolution and width of swath covered causes difficulty in constructing mosaics of the planet surface.

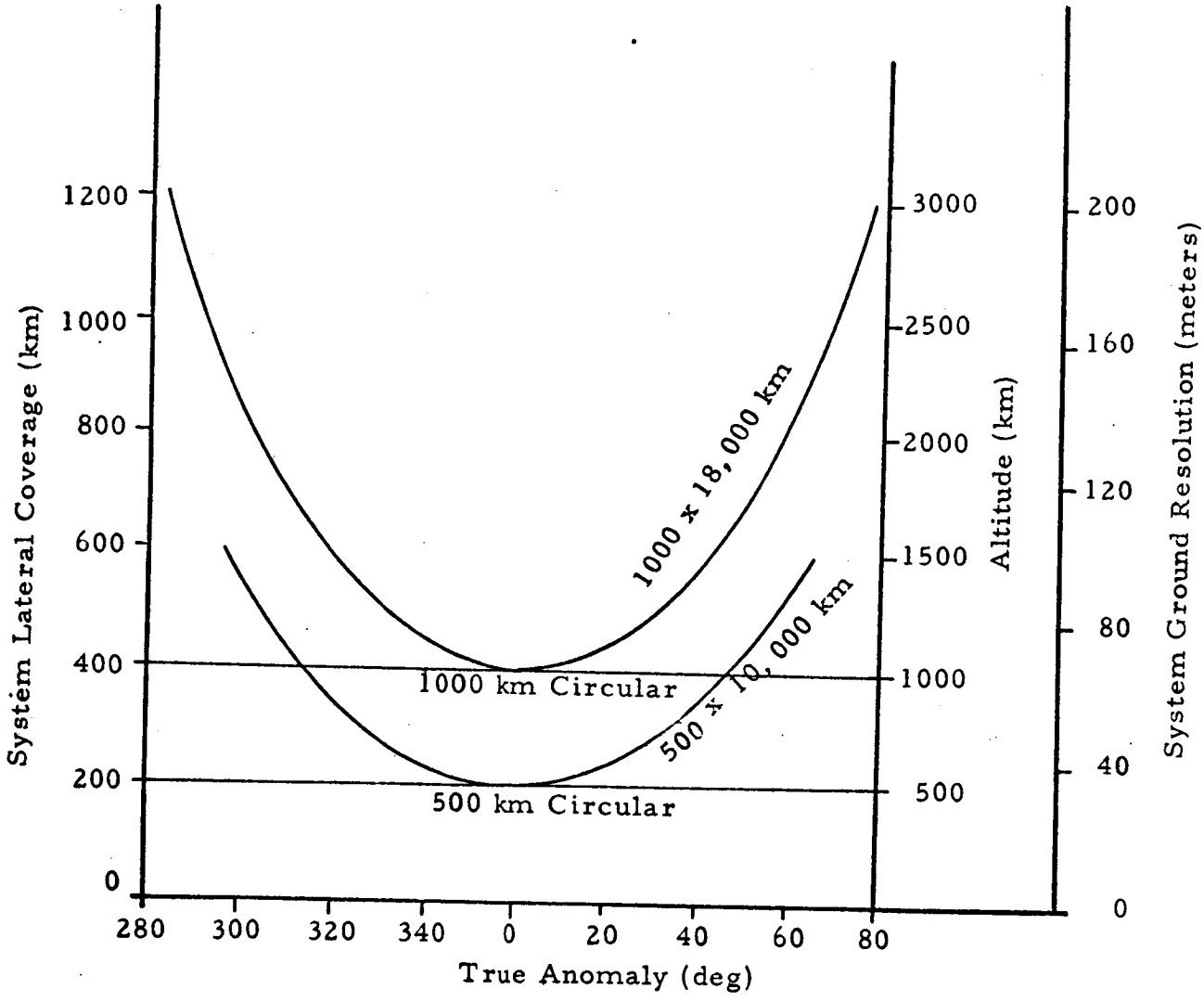

COMPARISON OF PHOTO-SYSTEM PARAMETERS FOR SELECTED ORBITS
(150 mm focal length, 100 lp/mm system resolution, 70 mm format)

Figure 4-2

The interplay between orbital parameters and sensor system performance will be discussed in more detail in the latter portion of this section.

4.1.1 Voyager Interplanetary Trajectory Considerations

Preliminary studies (Ref. 4-2, 4-3, 4-4, 4-5, 4-6) have led to consideration of the following general guidelines and typical constraints for the interplanetary trajectory design of the Voyager missions:

- The out-of-orbit capsule delivery mode will be used. Essentially, this means that both capsule and bus will be inserted into an orbit about the planet. Separation of capsule and bus, and the final descent of the capsule (de-orbit process) will be performed after the orbit has been established. To perform this maneuver, orbit trim capabilities must be considered, and velocity increment capability allocated.

- The Voyager guidelines call for two identical planetary vehicles to be launched on one Saturn V. After injection into the interplanetary phase of the trajectory, an arrival date separation maneuver will be performed to separate the arrival of the planetary vehicles at Mars by a preset number of days. The velocity increment (ΔV) required to perform this maneuver is a variable which is a function of launch date and arrival date of the trajectory.

- In a system design of this type, it was determined best (Ref. 4-9) to assume initially that the propulsion system is constrained to have fixed propellant loading during any opportunity. However, the possibility of off-loading in different opportunities is present.

- For purposes of spacecraft design, it is desirable to maintain essentially the same arrival geometry at the planet throughout the launch period. This arrival geometry is impossible to achieve exactly; however, changes are usually small if the arrival date at the planet is held fixed. For planning purposes, constant arrival date trajectories are used.

- Both Type I and Type II trajectories are considered. Type I trajectories are characterized by a heliocentric transfer angle, θ, of less than 180 degrees from launch to encounter; for Type II trajectories, the total transfer angle lies between 180 and 360 degrees.

- The intent of preliminary trajectory selection calculations is to put a 2,500-lb. (1,132 kg) spacecraft and a 5,000-lb. (2,264 kg) capsule into orbit about Mars (useful weight in orbit of 7.5 klb), and provide as much interplanetary trajectory selection flexibility as possible to accommodate any satellite orbit or science requirements.

4.1.1.1 Interplanetary Trajectory Design Aspects - The interplanetary trajectory selection may be constrained by a number of factors related to the near-Earth mission design, the interplanetary transfer phase, and the Mars approach conditions.

Launch Azimuth - One of the major constraints on the launch period is determined by the range of launch azimuths available from Cape Kennedy. The launch azimuth range basically constrains the declination of the outgoing asymptote of the hyperbolic trajectory near Earth. For the Type I trajectories, the constraint on declination usually determines the beginning of the launch period, whereas, for the Type II trajectories, it may determine the end of the launch period (Ref. 4-2, 4-3).

Launch Period - The launch period must be of sufficient duration to ensure approximately 99% probability that the space vehicle will be launched. This constraint usually determines the latest arrival date trajectories that can be flown for Type I trajectories and the earliest arrival date trajectories for Type II trajectories.

Arrival Date Separation - For the 2-on-1 launch mode innovated by the Voyager missions, both planetary vehicles are essentially injected on the same transfer trajectory to Mars. For operational reasons, it is required to separate the arrival date of the two planetary vehicles. This arrival date separation is achieved by performing a maneuver with each planetary vehicle several days after launch. It is usually possible to allocate enough velocity increment to this maneuver so that it does

not constrain the launch period selection; however, for certain opportunities, the velocity increment requirements are high, and the arrival date separation maneuver determines the opening of the launch period for Type I trajectories and the end of the launch period for Type II trajectories (Ref. 4-3).

Orbit Redetermination Capability During Interplanetary Transfer - To determine accurately the trajectory of the spacecraft when it is near encounter, it is desirable that the declination of the probe in Earth equatorial coordinates be sufficiently different from zero. This constraint eliminates a small range of arrival dates for certain opportunities (Ref. 4-2, 4-3).

Injection Energy - Departure energy required for the Mars mission is a function of launch and arrival dates. For the Type I trajectories, the close of the launch period is usually determined by the performance of the launch vehicle. For the Type II trajectories, the opening of the launch period is usually determined by the injection energy constraint (Ref. 4-2, 4-3, 4-7).

Approach Velocity at Mars - The approach velocity at the planet (hyperbolic excess velocity) determines the velocity increment required to inject the vehicle into the desired satellite orbit. The approach velocity in each opportunity is constrained so that the "tightest" orbit considered can be achieved within the available ΔV for orbit insertion. For the Type I trajectories, this approach velocity constraint usually determines the earliest arrival date which can be flown, whereas, for the Type II trajectories, it usually determines the latest arrival date which can be flown (Ref. 4-2, 4-3, 4-7, 4-8, 4-9).

Standard Launch Vehicle Performance - The gross payload capability of the Saturn V, which will be the Voyager launch vehicle, is a function of injection energy C_3, launch azimuth, and Earth parking orbit altitude. An orbit altitude of 100 nmi will be used for Voyager launches. The relationship between injection energy and injected weight is an inverse one; the higher the energy required, the lower the gross payload becomes. Gross-injected weight is related to launch azimuth in a different manner. A maximum payload is achieved for a launch azimuth of 90 degrees. This payload decreases as the launch azimuth varies

from that value. The variation is symmetric; therefore, the payload for a launch azimuth of 120 degrees is the same as that for a launch azimuth of 60 degrees when the injection energy is held constant (Ref. 4-3).

4.1.1.2 Establishment of Martian Spacecraft Orbits - In the interplanetary trajectory studies performed for the Voyager missions presented in Ref. 4-3, two Martian orbits were considered. The first orbit had a periapsis altitude of 1,100 km and an apoapsis altitude of 10,000 km, and the second had a periapsis altitude of 1,000 km and an apoapsis altitude of 20,000 km. The tight orbit (1,100 x 10,000 km) is more constraining and, therefore, was used in the interplanetary trajectory constraint considerations. The constraint had a built-in capability to rotate the line of apsides 20 degrees in the plane of the orbit. This 1,100 x 10,000 km altitude orbit with a 20-degree rotation capability was used for performance purposes only, since specific orbit requirements must be identified for specified arrival geometries. A trade-off can be performed between orbit size and rotation; for example, the orbit can be loosened to provide more rotation capability without changing the booster performance characteristics.

4.1.1.3 Available Interplanetary Trajectories - The above mentioned guidelines, requirements, and constraints allows definition of a specific region of possible interplanetary trajectories. To obtain a standardized propulsion system for the four Voyager opportunities, the year which requires the highest total velocity increment was chosen, and the inert and propellant masses which yield this total velocity increment was fixed and then applied to the other three opportunities (Ref. 4-3). The useful weight in orbit (weight of capsule and spacecraft without the propulsion system weight) also was fixed for the four opportunities. These standardized weight allocations were then used to determine the total injected weight and, therefore, a limiting value of injection energy.

The final selection of a range of trajectories is, therefore, dictated by the following constraints: the declination of the outgoing asymptote, the injection energy, the hyperbolic excess velocity at Mars, the arrival date separation velocity increment, and the length of the launch period. The preliminary studies presented in Ref. 4-3 determined

that the 1979 opportunity was the most critical year in terms of total velocity increment requirements (primarily because of a high arrival date separation velocity increment requirement with high hyperbolic excess velocities at Mars). This total velocity increment requirement was approximately 2.12 km/sec for Type I trajectories. Therefore, this value was standardized for the other three opportunities and the velocity increment allocated. It should be noted that 40 m/sec were allocated for the gravity losses velocity increment; a conservative allocation.

From the gross injected weight (55.3 klb), the limiting injection energy obtained from the Saturn V performance data was 32.5 km^2/sec^2 for a launch azimuth of 45 degrees.

The amount of velocity increment allocated for orbit insertion gives the limiting values of the hyperbolic excess velocity. Therefore, a summary of constraints on the interplanetary trajectory regions can be formed and is presented in Table 4-1.

These constraints, together with a launch period duration constraint (say 20 days), can then be plotted on a launch date vs. arrival date chart (Figure 4-3) to define an interplanetary selection region. It should be noted that the propulsion system is constrained to fixed propellant loading during an opportunity. It is possible that off-loading propellant for an opportunity may be performed to extend the launch period duration.

All the parameters considered, however, are interdependent. Numerous trade-offs may be made to redefine mission requirements. In other words, certain constraints may be relaxed if others are tightened. It is desirable to determine which constraints could be tightened to increase the capsule weight.

A study was performed (Ref. 4-3) using a parametric variation scheme that considers the main trade-off between launch period duration and useful weight in Mars orbit. Figure 4-3 shows contours of constant useful weight in orbit. The following refinements were taken into consideration:

TABLE 4-1

SUMMARY OF CONSTRAINTS

Year	Max. Injection Energy (km^2/sec^2)	Max. Hyperbolic Excess Velocity (km/sec)	Max. Declination of Outgoing Asymptote	Arrival Date Separation Velocity Increment (km/sec)
1973	32.5	3.24	+36°	0.200
1975	32.5	3.53	+51°	0.065
1977	32.5	3.53	+51°	0.065
1979	32.5	3.50	+36°	0.100

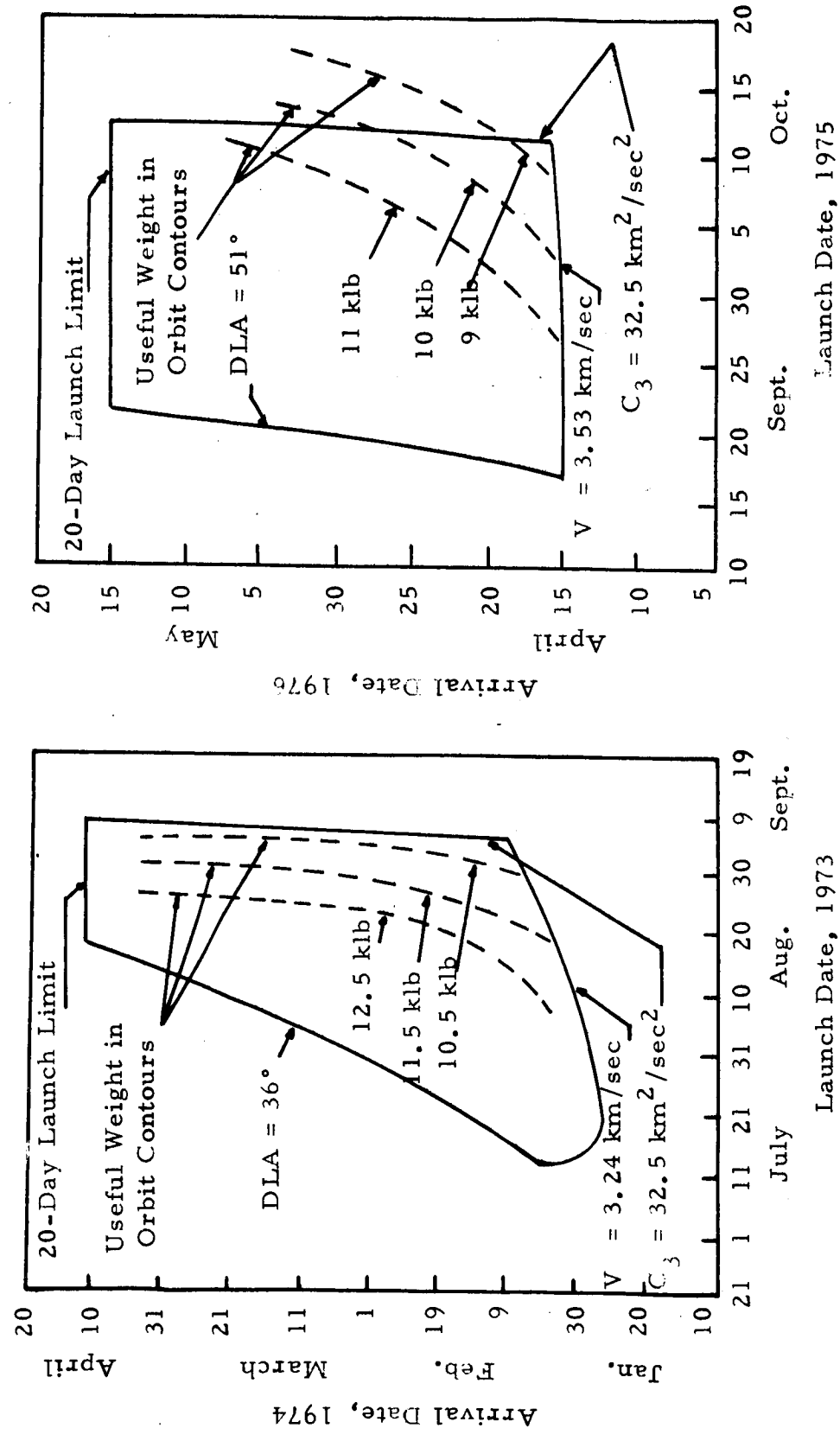

TYPE I TRAJECTORY REGION FOR 1973 AND 1975 OPPORTUNITIES

Figure 4-3

- Variation of arrival date separation velocity increment with launch date.
- Variation of azimuth limits with launch date.
- Variation of orbit insertion velocity increment as a function of launch and arrival dates.
- Gravity loss velocity increment allocation of 5 m/sec.
- The assumptions of constant arrival date trajectories and fixed propellant loading were maintained.

It should be noted that these refinements increase the value of the useful weight in orbit.

The graphs of Figure 4-3 may be used as follows: given an arrival date, the opening of the launch period is given by the azimuth (or DLA) constraint. The end of the launch period for the specified arrival date is then dictated by the useful weight in orbit desired. In other words, the intersection of a constant arrival date line with a useful weight in orbit contour gives the limiting injection energy and hyperbolic excess velocity for that case, thus also giving the maximum launch period. It should be noted that a fixed limiting injection energy may not be exceeded because of standardization.

Because of relatively short launch period durations for the 1975 and 1977 opportunities, and a short arrival date selection for the 1979 opportunity, determination of the trajectory selection regions for these three opportunities was desirable for Type II trajectories.

The angle at Earth between the departure asymptote and the Sun-Earth vector is called ZAL. This parameter is equivalent to the Earth-Probe-Sun angle a few days after launch. If this angle is over 90 degrees, this would imply that the Earth is initially in the rear hemisphere of the spacecraft. Therefore, to ensure coverage during the time ZAL is greater than 90 degrees, an omnidirectional antenna must be provided for Type II trajectories.

To alleviate the arrival date separation velocity increment constraint, while keeping the total velocity increment constant (standardized), certain trade-offs of velocity increments can be performed. For example, if the maximum hyperbolic excess velocity at Mars is reduced, the velocity increment required for orbit insertion will be reduced, thus allocating higher velocity increment capability for arrival date separation.

The main advantage of Type II trajectories is either more useful weight in orbit or longer launch periods. The main disadvantages are longer flight times and communication distances, which will tend to reduce mission reliability and data transmission rate. However, the direction of the hyperbolic approach asymptote (possible directions are different for Type I and Type II) is an important consideration in establishing a Martian reconnaissance orbit and will be discussed in the following paragraphs.

4.1.2 Martian Orbit Considerations

This subsection presents the engineering constraints and scientific requirements that pertain to the selection of Martian satellite orbits for the Voyager missions. A series of parametric representations useful for relating these criteria to key orbital characteristics is given in Appendix A.

4.1.2.1 Engineering Constraints - Because of interactions between the engineering design of the spacecraft and the selection of suitable satellite orbits, it is necessary to define a series of constraints affecting the Voyager orbit design (Ref. 4-9).

Canopus Occultation - Because the star Canopus will be used as a reference body for attitude stabilization, it is desirable that it not be occulted by Mars while the spacecraft is in orbit about the planet. *

---

* According to Ref. 4-10, Canopus and the Sun can be occulted for as much as two hours after the orbit is established, without significantly affecting attitude stabilization or the generation of the required electrical power from solar energy.

It is also important to avoid stray light reflected from the planet's surface falling within the field of view of a sensor, the rectangular dimensions of which are 40 by 60 degrees. Because the lander is dependent upon successful orbiter operation before capsule release, it is more important to avoid Canopus occultation during the time period immediately following orbit insertion (prior to capsule release).

Sun Occultation - Because the Sun will be used both as a reference body for the attitude control system and as a power source, it is desirable to avoid occultation by Mars while the spacecraft is in orbit about the planet. For the reason given for avoiding Canopus occultation, it is more important to avoid Sun occultation during the time period immediately following orbit establishment. If occultation does occur, it should not exceed some specified time duration and percentage of the orbital period.*

Orbit Insertion Velocity Increment - Because of the requirement to place a specified payload weight in Mars orbit, there is a limitation on the velocity increment (ΔV) that can be allocated for the orbit insertion maneuver. For a given spacecraft weight and propulsion system, the orbit insertion ΔV will vary with the arrival date separation and interplanetary trajectory.

Earth Occultation During Maneuvers - To obtain telemetry during the orbit insertion and capsule deorbit maneuvers, it is important that the Earth not be occulted by Mars during a specified time interval immediately preceding and following the motor burn.

Capsule Landing in View of Earth - Because of the longer post-landing communication interval possible with direct-link communication, it is desirable to have the surface laboratory remain in view of Earth for a specified time period following landing. Because the landing site for the out-of-orbit mode of capsule descent lies near periapsis, a landing in full view of Earth implies the use of an orbit with periapsis located near the morning terminator (Ref. 4-9).

* Ibid.

4.1.2.2 Scientific Considerations - The scientific considerations that pertain to the selection of a satellite orbit fall in two categories: (1) observations conducted from Mars orbit, and (2) surface observations performed by the lander. Among the experiments from orbit are: photography at both high and medium resolution (of prime concern during this study), observation of atmospheric composition and temperature, radiometric observation of Mars surface temperature at low spatial resolution, physical and dynamical parameters of Mars, and radio occultation. The scientific experiment categories, with requirements specifically related to satellite orbit size and orientation are discussed below.

Photographic Experiment - For the purpose of obtaining high resolution photographic coverage of Mars, it is desirable that the solar illumination angle (measured from the local horizontal near the subperiapsis point) be between 20 and 70 degrees. Because of the scientific interest in the dark areas located in the southern hemisphere of Mars, and other features described in Section 2 and 3, it is desirable to locate periapsis in the southern hemisphere. It also would be desirable to observe the northern hemisphere dark areas undergoing seasonal contrast variations associated with the wave of darkening (see Section 2). Tc obtain the desired planet coverage, it is necessary to have the subsatellite track near periapsis vary over a wide range of latitudes.

The Voyager baseline orbit is near the morning terminator - but here there are problems of mists and clouds leading to much less time favorable for photo imaging than at the evening terminator. The earlier in the mission that good photo imaging can be achieved, the better, for there is a factor of several fold involved in bit rates to Earth capability due to the increasing distance between Earth and Mars as the mission progresses (see Section 7). Therefore, the earlier data is obtained, the more that can be obtained (this is quite valid from the reliability, or lifetime standpoint, also), again, indicating the desirability for reconnaissance orbits being initially located near the evening terminator.

Since the morning terminator orbit has been recommended by consideration of present constraints on capsule/lander visibility after landing, at least the second spacecraft should be placed in an evening terminator

orbit thereby obtaining data at both terminators early in the mission. The periapsis of one orbit could be in the northern hemisphere for coverage of the wave of darkening (perhaps best near evening terminator) with that of the other in the southern hemisphere for studies of the more varied Martian topography there.

Radio Occultation Experiment - This experiment requires that the orbit be oriented such that the Earth be occulted by Mars while the spacecraft is in orbit about the planet. This causes the spacecraft radio signal to pass through the Mars atmosphere, thus permitting measurement of its scale height and density. It is desirable that the radio signal be occulted over a wide range of latitudes to establish the figure of Mars and the equator-to-pole variation of the atmospheric parameters. It is important that the total number of occultations be large either by using orbits with small periods or by maintaining Earth occultation over several months.

Capsule Landing Site - The satellite orbit must be selected to allow the capsule to land over a range of latitudes. This will enable the surface laboratory to reach a particular surface feature that might be of scientific interest.

4.1.2.3 Parameters Affecting Orbit Shape and Orientation - Before an attempt is made to study the implications of the engineering constraints and scientific requirements on the availability of orbits, it is necessary to define a set of parameters that were found to be the most convenient for parametric analysis. To uniquely define the orbit size and orientation, five independent variables are required. The size of the ellipse (eccentricity and semi-major axis) is specified in terms of periapsis and apoapsis altitudes. Altitudes are used because considerations such as satellite lifetime, instrument height above the surface, and photographic resolution make it a more useful parameter. The orbital orientation is specified by inclination to the Mars equator, orientation of apsidal line with respect to the approach asymptote, and hyperbolic approach asymptote vector.

Periapsis Altitude - To satisfy the planetary quarantine constraint, it is necessary to select a periapsis altitude that provides a satellite orbital lifetime of at least 50 years (Ref. 4-9). (However, Ref. 4-11

and 4-12 indicate that this constraint is being changed to 12 years rather than 50 and Ref. 4-10 suggests 20 years as reasonable.) The altitude should be large enough to account for third-body influences and non-gravitational perturbations due to solar pressure and attitude control gas leaks as well as atmospheric drag. (The effects of the above perturbations on periapsis altitude are described in some detail in Appendix A.) The periapsis altitude also determines the best photographic resolution that can be obtained from a given imaging system.

Apoapsis Altitude - The choice of apoapsis altitude is important because of its effect on orbital period. Low apoapsis altitudes result in short periods of revolution that make mission operations more difficult and result in occultations that represent a large fraction of the orbital period. However, lower altitudes permit acquisition of higher resolution imagery for a particular sensor. Large apoapsis altitudes yield orbits that are more vulnerable to third-body influences on orbital lifetime. Large altitudes also provide orbital periods that result in long-time intervals between picture recordings. The choice of apoapsis altitude also affects the orbit insertion ΔV requirement with larger values requiring smaller velocity increments.

Approach Asymptote - The hyperbolic approach asymptote vector $\vec{S}_I$ is an important factor in determining the orbital geometry available for reasonable orbit insertion ΔV's. This vector is the difference between heliocentric velocities of Mars and the spacecraft when the spacecraft enters the gravitational influence of the planet. The relationships between $\vec{S}_I$ and the Sun and Earth directions are shown in Figure 4-4 for Type I and Type II trajectories.

The particular location of the approach asymptote within the ranges shown is specified by the launch and arrival date defining the interplanetary transfer trajectory. The declination (ϕ_S) of $\vec{S}_I$ with respect to the Mars equator determines the minimum orbital inclination that can be achieved without performing an out-of-plane orbit insertion maneuver.

Apsidal Orientation - The apsidal orientation angle (Ψ) is used to locate the orbital line of apsides with respect to the approach asymptote, $\vec{S}_I$. It is defined as the angle between the negative approach asymptote

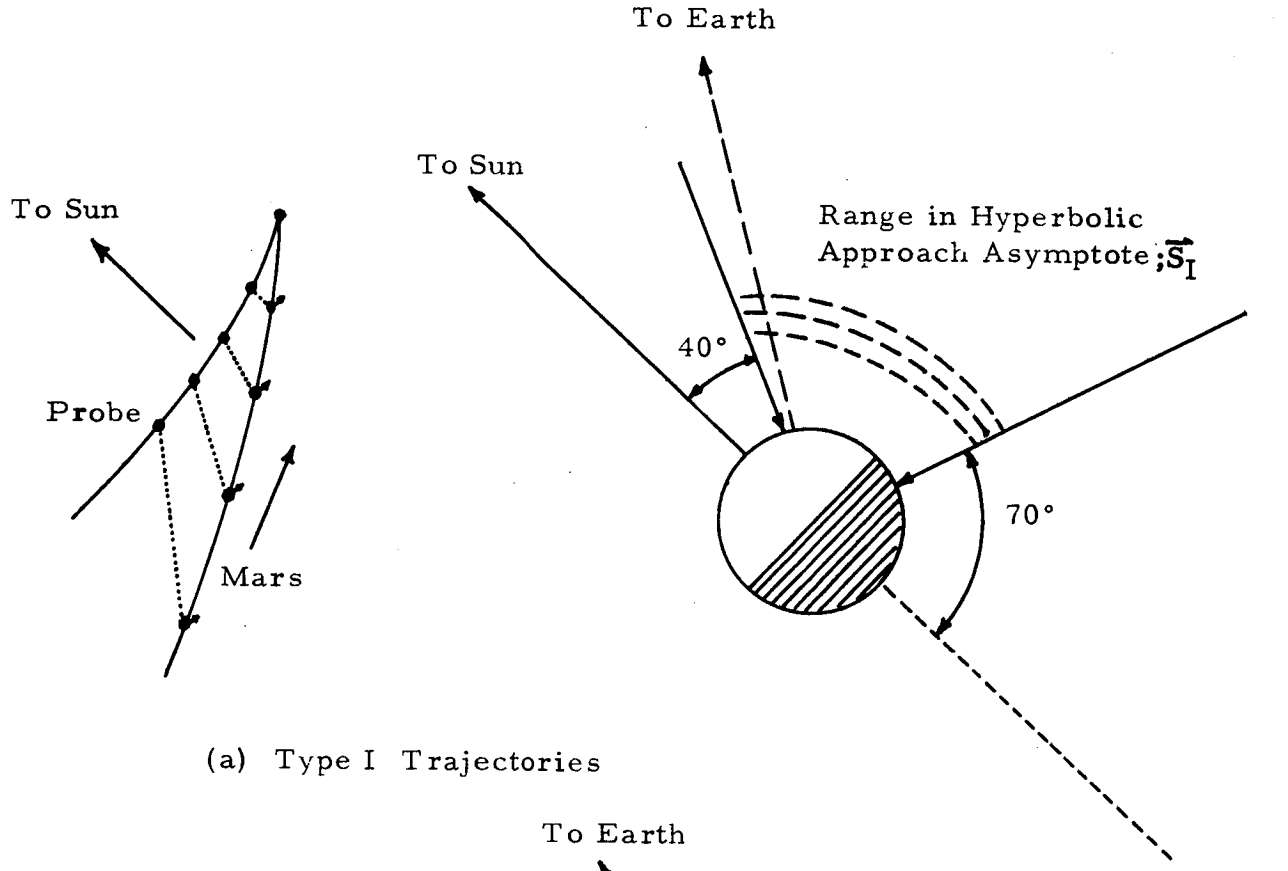

(a) Type I Trajectories

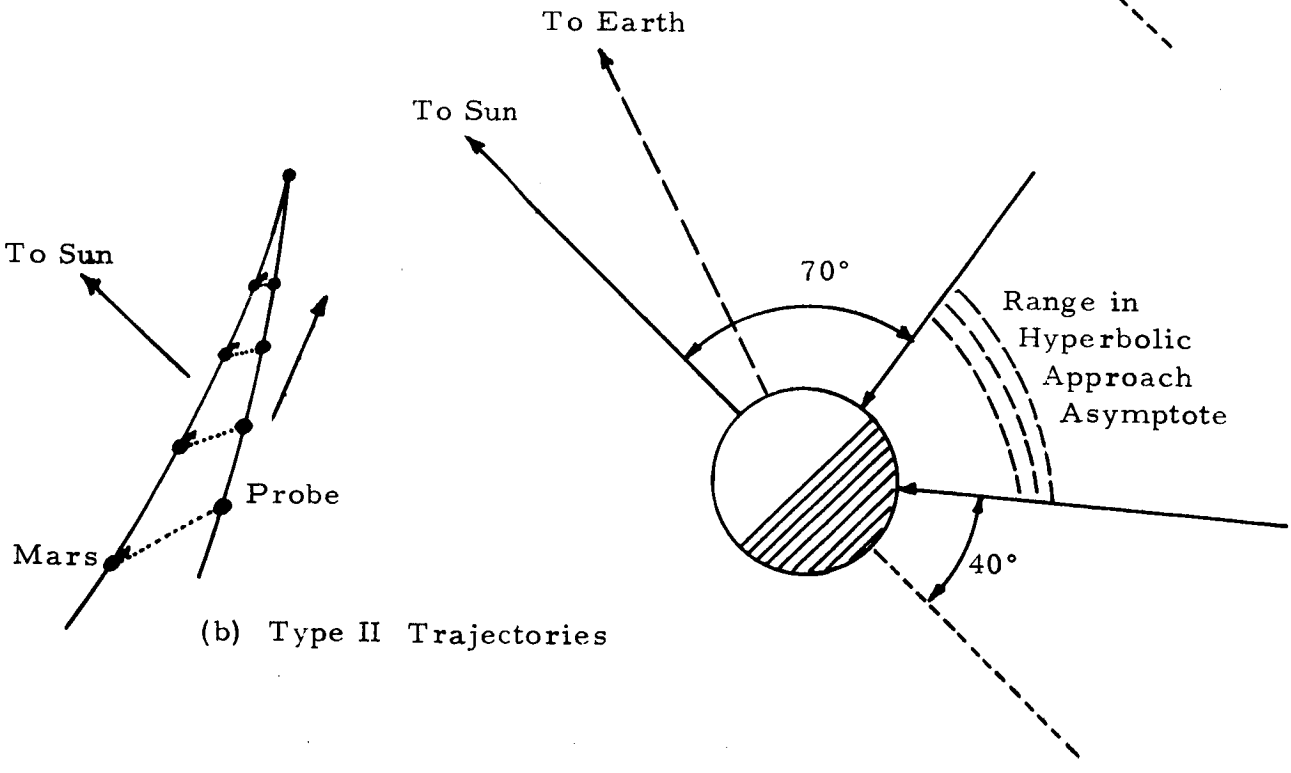

(b) Type II Trajectories

NEAR MARS APPROACH GEOMETRY

Figure 4-4

vector and ellipse periapsis radius vector, and is measured in the direction of orbital motion. The apsidal orientation angle determines the orbit insertion ΔV for a given approach speed and orbit size.

4.1.2.4 Implications of Engineering Constraints - The implications of various engineering constraints are discussed in the following paragraphs.

A complete evaluation of the effects of engineering constraints on the five orbital parameters would be the next logical step in the orbit selection process. It was observed, however, that the orbit constraints were rather insensitive to the range of orbital sizes being considered for Voyager. For this reason, several typical orbital sizes were selected and held constant throughout the parametric study presented in Ref. 4-9. A particular orbit chosen to illustrate the engineering constraints in some detail had periapsis and apoapsis altitudes of 1,000 km and 20,000 km, respectively, providing an orbital period of 13.7 hours.

A parametric display of satellite orbit constraints is given in Ref. 4-9. The results of the analysis shows the constraint regions as a function of the apsidal orientation angle ψ, and orbital inclination i, for a fixed launch and arrival date, using a Type I trajectory. Launch date was found to have little influence on the approach geometry.

Canopus Occultation - The major implication of this restraint is its restriction on orbital inclination (Ref. 4-9). Also, the Canopus constraint does not permit low apsidal orientation angles. The implications of this restriction will be discussed along with scientific considerations.

Sun Occultation - Fortunately, the "Sun Occultation" constraint region is not as restrictive as the Canopus region. The Sun occultation region, which is fairly large for early arrival dates, sets an upper limit on apsidal orientation angle and a lower limit on inclination. Also, the large inclinations are necessary to avoid Sun occultation in conjunction with retrograde orbits. When the Sun and Canopus constraints are considered simultaneously, large restrictions on orbital orientations become evident, especially for early arrival dates (Ref. 4-9).

Orbit Insertion Velocity Increment - The effect of the orbit insertion ΔV required for a tangential transfer from the approach hyperbola to the elliptical orbit is given in Ref. 4-9. The minimum value is, of course, the ΔV required for a periapsis-to-periapsis transfer. The orbit insertion ΔV allocation for the 1973 opportunity is 1.72 km/sec. A parametric presentation of ΔV requirements for establishing various orbits about Mars is given in Appendix B.

Earth Occultation During Maneuvers - Retrograde orbits have a greater likelihood of violating this constraint; the analysis of Ref. 4-9 shows that for orbits simultaneously satisfying Sun and Canopus constraints, Earth occultation occurs less than 45 minutes after orbit insertion.

Capsule Landing in View of Earth - To locate the orbital sub-periapsis point in view of Earth, the apsidal orientation angle must be less than 150 degrees for direct orbits, and substantially smaller for retrograde orbits (Ref. 4-9) and, then because it is possible to land the capsule up to 30 degrees before periapsis, locating periapsis along the 0 degree Earth elevation contour would provide a 30 degree elevation angle at the landing site. This would result in a 2-hour direct link communication period (Mars rotates at approximately 15 deg/hr).

4.1.2.5 Implications of Scientific Considerations - The requirements imposed by the various scientific experiments further restrict the orbital parameters.

Photographic Experiment - The effect of the lighting angle requirement on the availability of orbits was presented in Ref. 4-9, which showed that the periapsis for orbits exhibiting no Sun or Canopus occultation was located near the evening terminator and was characterized by good lighting angles. For direct orbits, acceptable lighting was also found near low values of apsidal orientation angle. This is the morning terminator region that provides desirable Earth elevation angles. This region is undesirable, however, because Canopus constraint violation cannot be avoided. Acceptable lighting angles were also found to exist for retrograde orbits with large apsidal orientations.

The analysis of Ref. 4-9 showed that the evening terminator region consistent with engineering requirements provides accessibility to southern latitudes. Coverage of northern latitudes immediately after establishment of the orbit involves violation of Sun and Canopus constraints.

Radio Occultation Experiment - This restriction does not severely limit the availability of orbits except for late arrival dates.

Capsule Landing Site - The desire to land the capsule over a wide range of latitudes requires an orbit that exhibits wide latitude variation near periapsis. This characteristic can be achieved by avoiding azimuth angles at periapsis that are nearly equal to 90 or 270 degrees. The orbital parameters necessary for obtaining desirable azimuth angles were discussed previously. The desire for low illumination angles near the landing site can be achieved by locating periapsis near the terminator. Because the low illumination angle region near the evening terminator does not satisfy the Earth elevation angle requirement, it is necessary to locate periapsis near the morning terminator. The inability to achieve Earth occultation with morning terminator orbits, and the orbit insertion ΔV restriction on apsidal orientation angle precludes the use of morning terminator orbits in conjunction with early arrival dates.

4.1.2.6 Conclusions of Overall Orbital Considerations - Parametric studies of 1973 Mars satellite orbits reveals that only a small range of acceptable orbital parameters exists that meet all the selected constraints. The Canopus constraint, in particular, was found to severely limit orbital inclination and also preclude the use of morning terminator orbits. The Sun occultation constraint, however, was not as restrictive, except for the early arrival date/evening terminator orbits. Morning terminator orbits were found to be unobtainable with early arrival dates because of orbit insertion velocity increment limitations. To provide maximum Earth viewing time for the lander and to provide the desired lighting angles for site photography, morning terminator orbits are necessary. Morning terminator orbits, however, do not provide for an Earth occultation experiment until several months following orbit insertion. Evening terminator orbits with capsule landing locations 30 degrees before periapsis yield a 2 hour Earth viewing period, but do not provide desired landing site flexibility.

4.2 RECONNAISSANCE ORBITS AND COVERAGE

The analyses described in the preceding paragraphs pointed out the fact that there is no orbit possible which satisfies all mission scientific objectives and constraints. The Voyager baseline incorporates an elliptical polar orbit whose selection is convincingly documented (Ref. 4-11). However, the decision on the actual orbit or orbits (and there are great advantages in having the two spacecraft in different orbits) cannot be made at this time. Consistent with quarantine restrictions, the actual photographic mission orbit should have a periapsis altitude as near as possible to the range from 400 to 500 km. There is at present a not generally accepted concern about planetary contamination by meteoric spallation from the spacecraft; this effect could conceivably limit periapsis altitude to being in excess of 800 km. However, according to Ref. 4-10, current thinking is that the spacecraft should be able to be in orbit for almost twenty years prior to impacting the planet with unsterilized elements and Ref. 4-12 indicates that the constraint is being changed to twelve years. Orbits having periapsis altitudes of 200 km to 1,000 km satisfies the fifty year constraint depending on the atmospheric model used in the orbit decay analysis (Ref. 4-13). Periapsis altitude dispersion errors due to guidance on the order of 500 km must be considered (Ref. 4-10)*, therefore, a minimum of 700 km would have to be planned for to avoid violation of the 200 km minimum. Once the orbit was established, however, there will be enough ΔV capability to trim the orbit to a desired periapsis such as 200 km (Ref. 4-10). Also, by that time the occultation experiment will have provided a much better understanding of what is the appropriate Martian atmospheric model to be used in orbit decay analyses and hence, the minimum periapsis altitude.

The Voyager baseline orbit is near the morning terminator - but here there are problems of mists and clouds leading to much less time favorable for photo imaging than at the evening terminator. As noted previously, good photo imaging should be achieved, early in the mission, since communication rates are higher at that time.

---

* Ref. 4-14, 4-15 indicate that altitude errors upon establishment of the Martian orbit should be no greater than 200 to 250 km.

The morning terminator orbit has been recommended by consideration of present constraints on capsule/lander visibility after landing. Therefore, at least the second spacecraft should be placed in an evening terminator orbit thereby obtaining data at both terminators early in the mission. The periapsis of one orbit could be in the northern hemisphere for coverage of the wave of darkening (perhaps best near evening terminator) with that of the other in the southern hemisphere for studies of the more possibly varied Martian topography there.

There is a range of possible orbits which are attractive relative to the more important mission criteria although not responding to all the factors termed most desirable. The results of an analysis of these orbits, described in Table 4-2, will now be presented in terms of performing the photo reconnaissance portion of the Voyager mission. Certain characteristics of other orbits which are of interest for the reconnaissance mission, are also discussed.

4.2.1 Detailed Coverage Examples

Detailed analyses of Martian surface coverage obtainable with some of the orbits listed in Table 4-2 have been made (i.e., two orbits having a periapsis altitude of 1,000 km and a period of 12.26 hours and the circular polar orbit). Calculations were made utilizing the GE "Planetary Area Scan by a Satellite " (PASS) computer program. Mars encounter at Julian Date = 2442106.0 was selected for the initiation of the orbit about Mars. As listed in the table, the orbits have different inclinations with respect to the equator and different periapsis subpoints. The initial periapsis is near the evening terminator for both elliptical cases, allowing for maximum acquisition of imagery during the duration of the mission as the periapsis subpoint moves toward high noon and on to the morning terminator. The following constraints applied to a hypothetical imaging system: (1) field-of-view of 10 degrees and (2) data acquired only when over the sunlit portion of the planet and at altitudes less than 3,000 km.

A series of seven illustrations are presented as Figure 4-5 which show the area on the planet completely covered for the orbit having i = -60° at the following time intervals (days): 10, 20, 30, 60, 90, 120, and 180. A transparent mercator map of Mars located in the pocket in the inside of the back cover of this document can be overlaid on these graphs to illustrate the actual Martian regions covered. Similar coverage data are presented in Figure 4-6 for the orbit having i = -40°. The percent of surface area covered as a function of time is presented in Figure 4-7 for both of these orbital cases.

TABLE 4-2 EXAMPLE ORBIT CHARACTERISTICS

Periapsis Altitude, km	Apoapsis Altitude, km	Inclination, Degrees	Period, Hours	Initial Periapsis Subpoint, Deg.	
				Long.,	Lat.
1000	17,841	-40°	12.26	150.0°	-23.53°
1000	17,841	-60°	12.26	159.64°	-32.54°
500	10,000	-40°	6.8	150.0°	-23.53°
500	10,000	-60°	6.8	159.64°	-32.54°
1284	1,284	-90°	-	-	-
500	500	-40°	2.06	150.0°	-23.53°
500	500	-60°	2.06	159.64°	-32.54°
500	500	-90°	2.06	-178.74°	-38.4°
1000	1,000	-40°	2.47	150.0°	-23.53°
1000	1,000	-60°	2.47	159.64°	-32.54°
1000	1,000	-90°	2.47	-178.74°	-38.4°
1000	33,000	-60°	24.38	-	-

Julian Date of Arrival: 2442106.0

Orbit Period = 12.26 hours
Periapsis Altitude = 1000 km
Apoapsis Altitude = 17,841 km
Inclination = -60 degrees

Julian Date of Arrival; 2442106.0
Sensor Field of View = 10 degrees
Data Acquisition Altitude = 3,000 km
Data Acquisition; Sunlit Areas Only

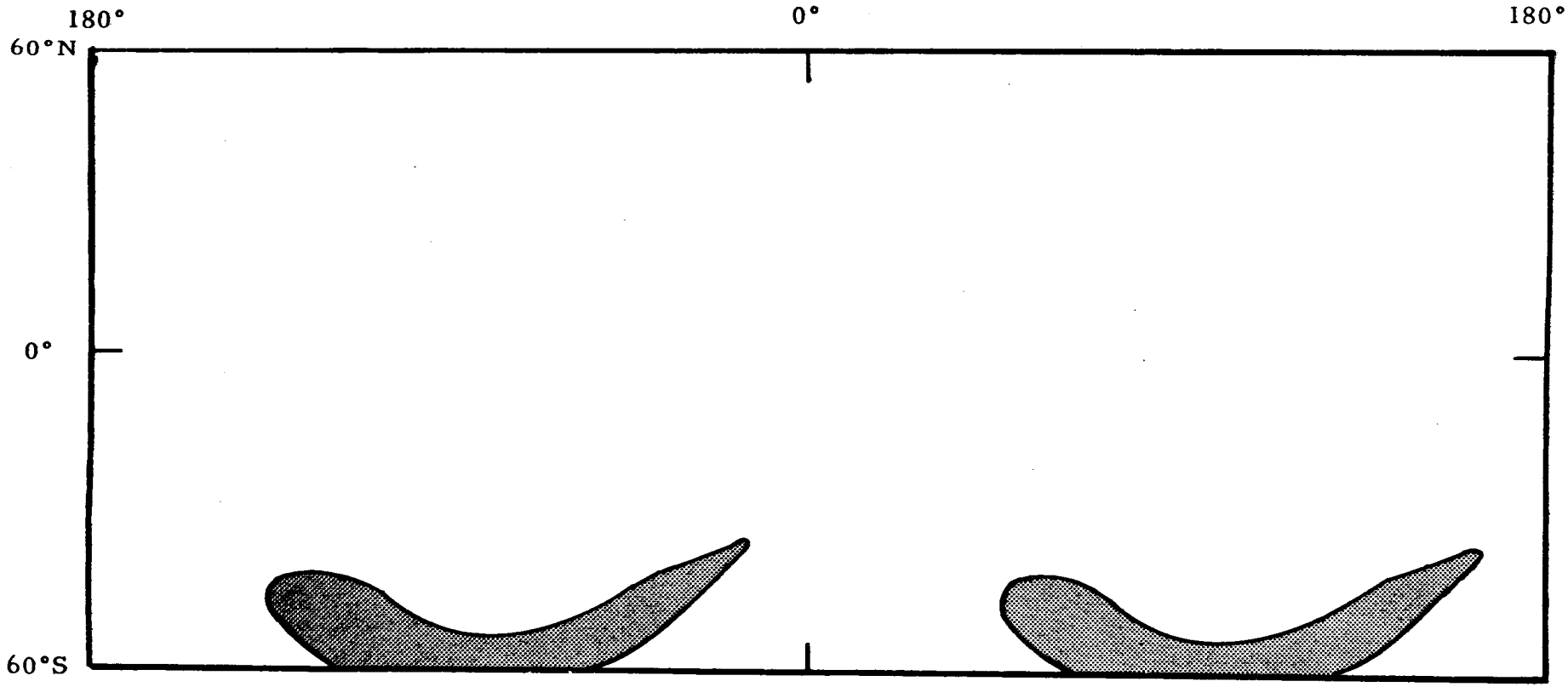

MARS SURFACE COVERED BY SENSOR
AFTER 10 DAYS IN ORBIT

(Inclination: -60 degrees)

Figure 4-5a

Orbit Period = 12.26 hours
Periapsis Altitude = 1000 km
Apoapsis Altitude = 17,841 km
Inclination =-60 degrees

Julian Date of Arrival; 2442106.0
Sensor Field of View = 10 degrees
Data Acquisition Altitude ≤ 3,000 km
Data Acquisition; Sunlit Areas Only

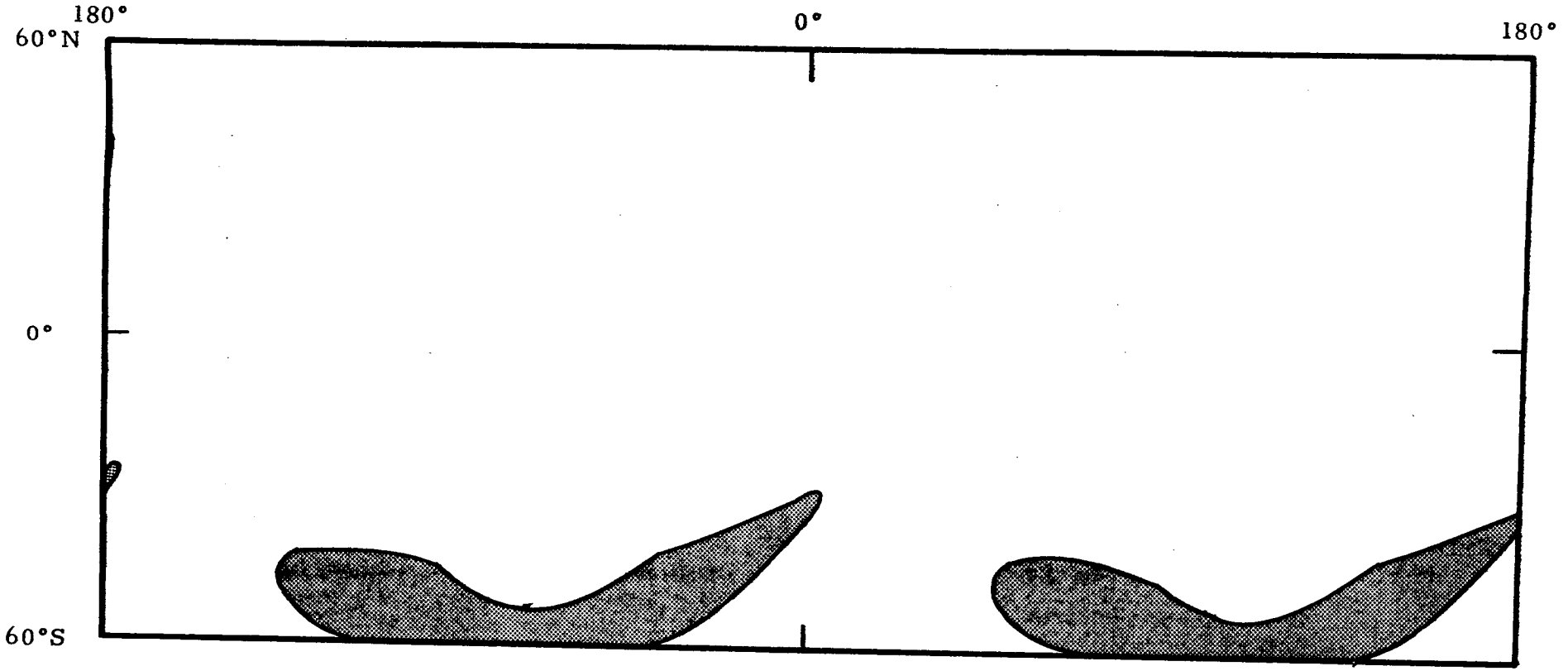

MARS SURFACE COVERED BY SENSOR
AFTER 20 DAYS IN ORBIT

(Inclination: -60 degrees)

Figure 4-5b

Orbit Period = 12.26 hours
Periapsis Altitude = 1000 km
Apoapsis Altitude = 17,841 km
Inclination =-60 degrees

Julian Date of Arrival; 2442106.0
Sensor Field of View = 10 degrees
Data Acquisition Altitude ≤ 3,000 km
Data Acquisition; Sunlit Areas Only

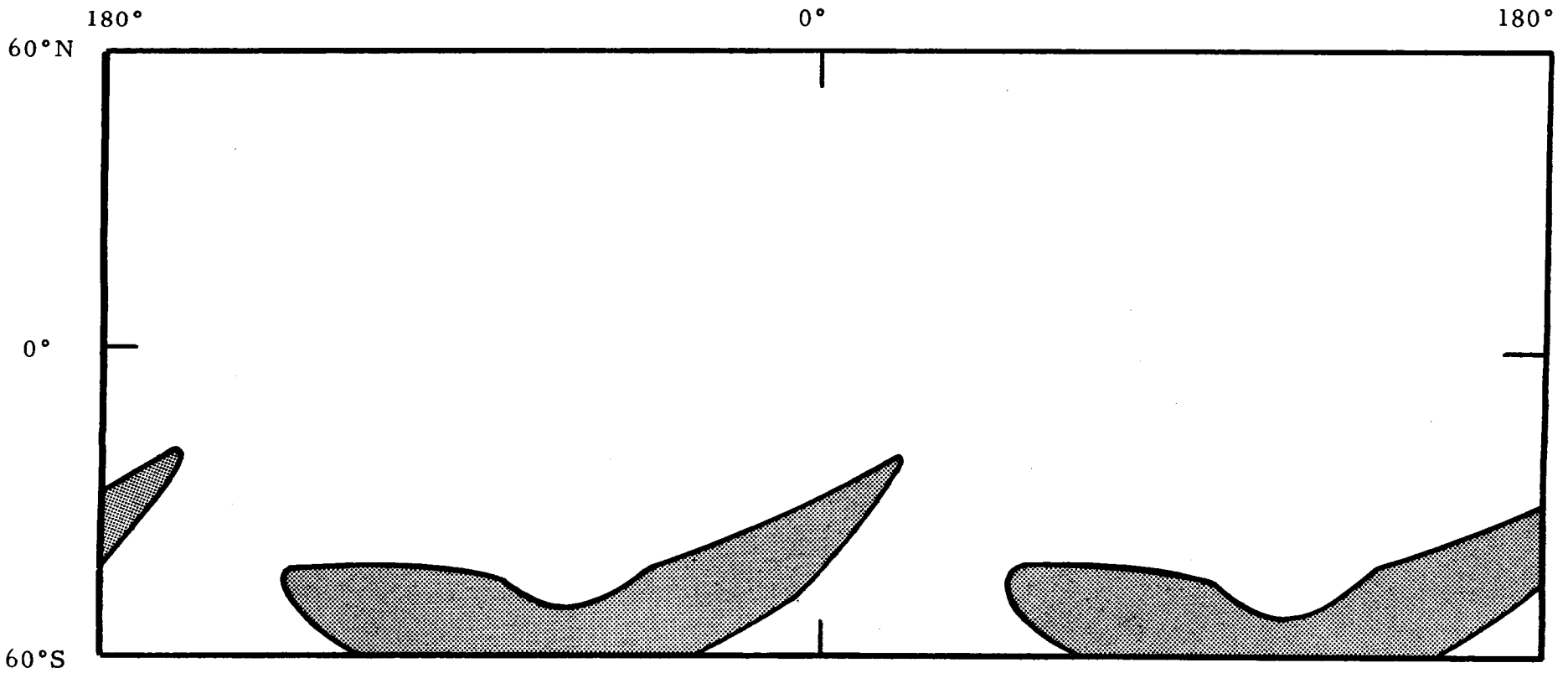

MARS SURFACE COVERED BY SENSOR
AFTER 30 DAYS IN ORBIT

(Inclination: -60 degrees)

Figure 4-5c

Orbit Period = 12.26 hours
Periapsis Altitude = 1000 km
Apoapsis Altitude = 17,841 km
Inclination =-60 degrees

Julian Date of Arrival; 2442106.0
Sensor Field of View = 10 degrees
Data Acquisition Altitude = 3,000 km
Data Acquisition; Sunlit Areas Only

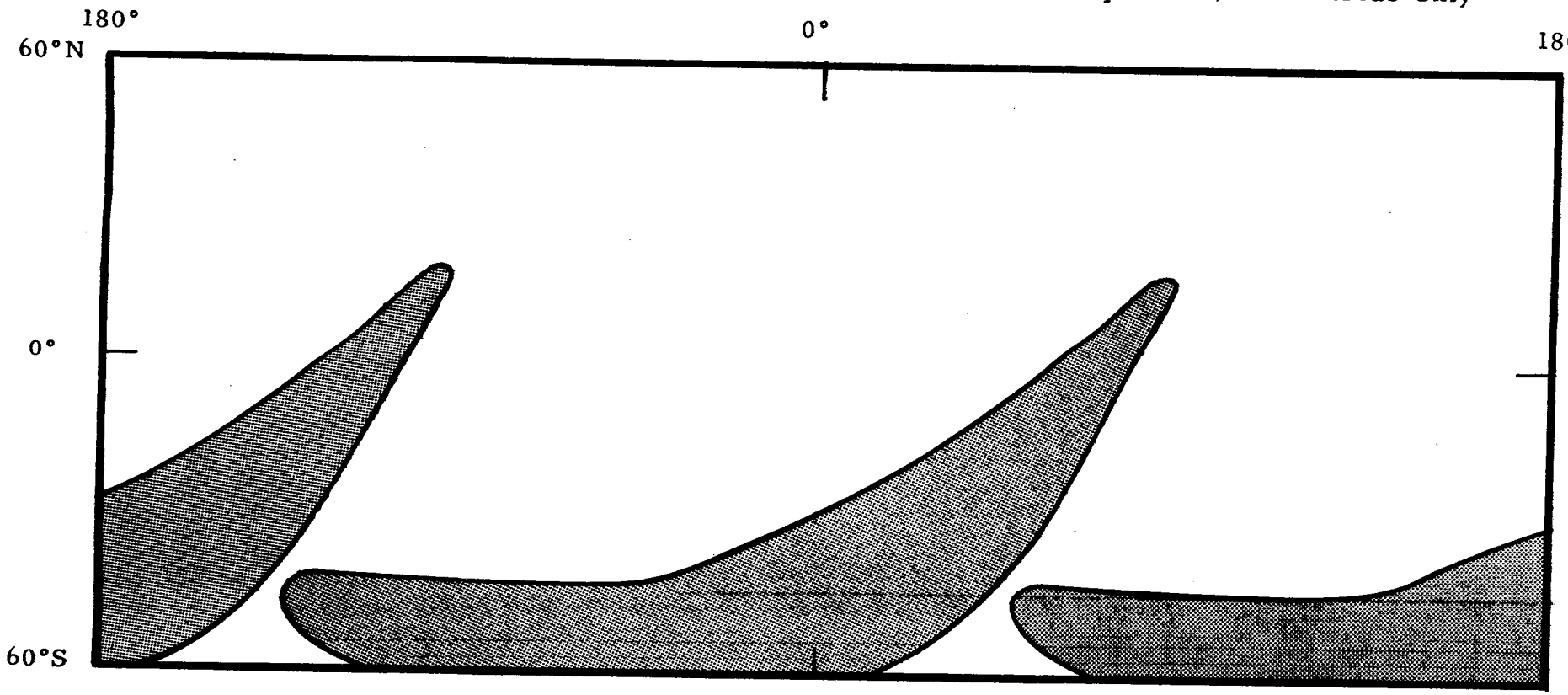

MARS SURFACE COVERED BY SENSOR
AFTER 60 DAYS IN ORBIT
(Inclination: -60 degrees)

Figure 4-5d

Orbit Period = 12.26 hours
Periapsis Altitude = 1000 km
Apoapsis Altitude = 17,841 km
Inclination =-60 degrees

Julian Date of Arrival; 2442106.0
Sensor Field of View = 10 degrees
Data Acquisition Altitude = 3,000 km
Data Acquisition; Sunlit Areas Only

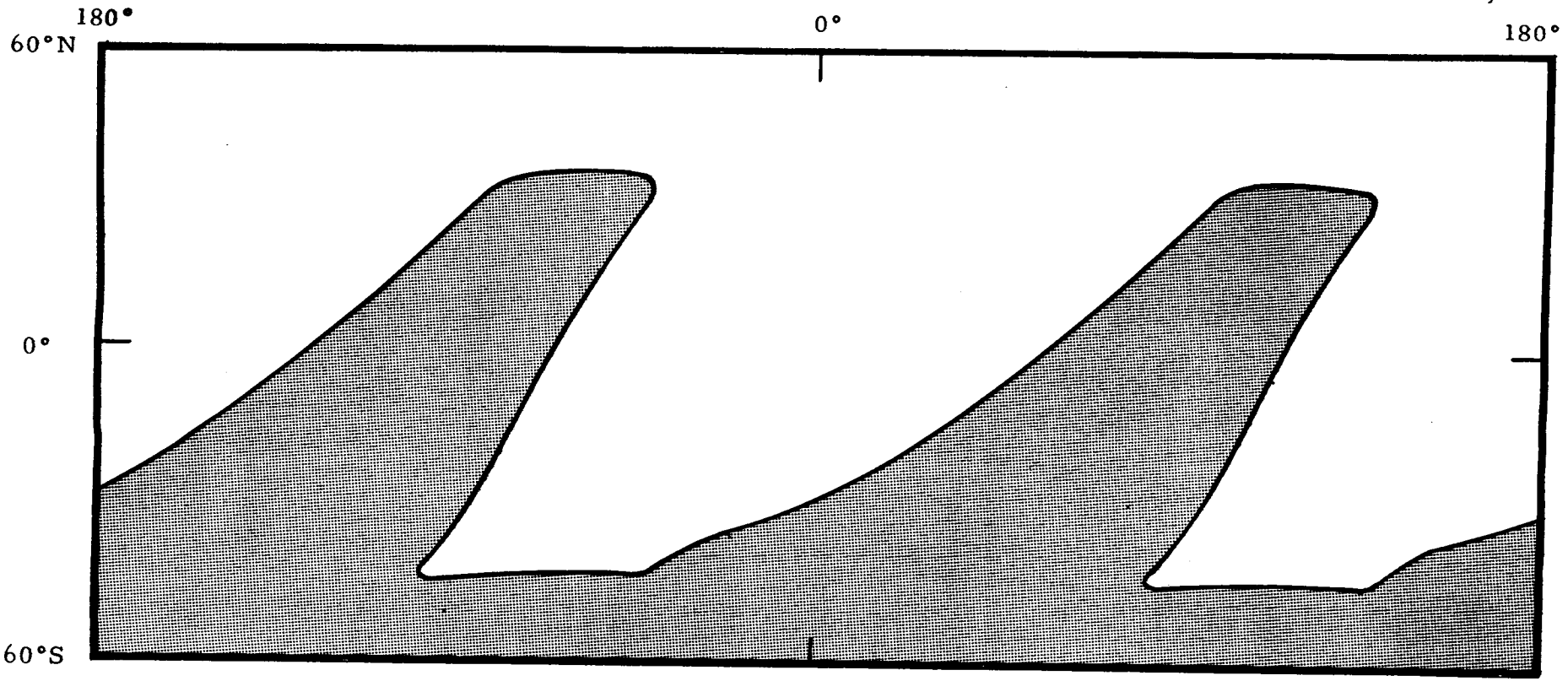

MARS SURFACE COVERED BY SENSOR
AFTER 90 DAYS IN ORBIT
(Inclination: -60 degrees)

Figure 4-5e

Orbit Period = 12.26 hours
Periapsis Altitude = 1000 km
Apoapsis Altitude = 17,841 km
Inclination = -60 degrees

Julian Date of Arrival; 2442106.0
Sensor Field of View = 10 degrees
Data Acquisition Altitude = 3,000 km
Data Acquisition; Sunlit Areas Only

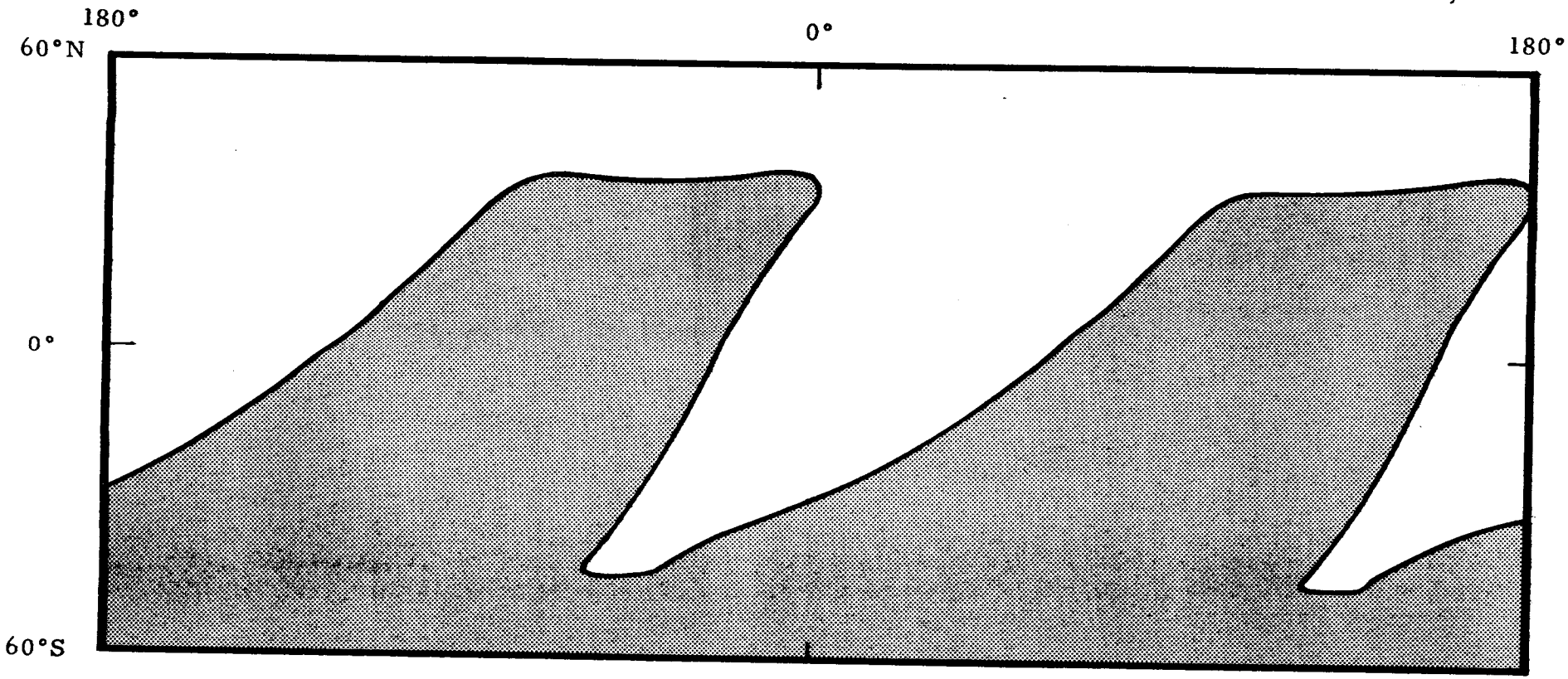

MARS SURFACE COVERED BY SENSOR
AFTER 120 DAYS IN ORBIT
(Inclination: -60 degrees)

Figure 4-5f

Orbit Period = 12.26 hours
Periapsis Altitude = 1000 km
Apoapsis Altitude = 17,841 km
Inclination =-60 degrees

Julian Date of Arrival; 2442106.0
Sensor Field of View = 10 degrees
Data Acquisition Altitude ≤ 3,000 km
Data Acquisition; Sunlit Areas Only

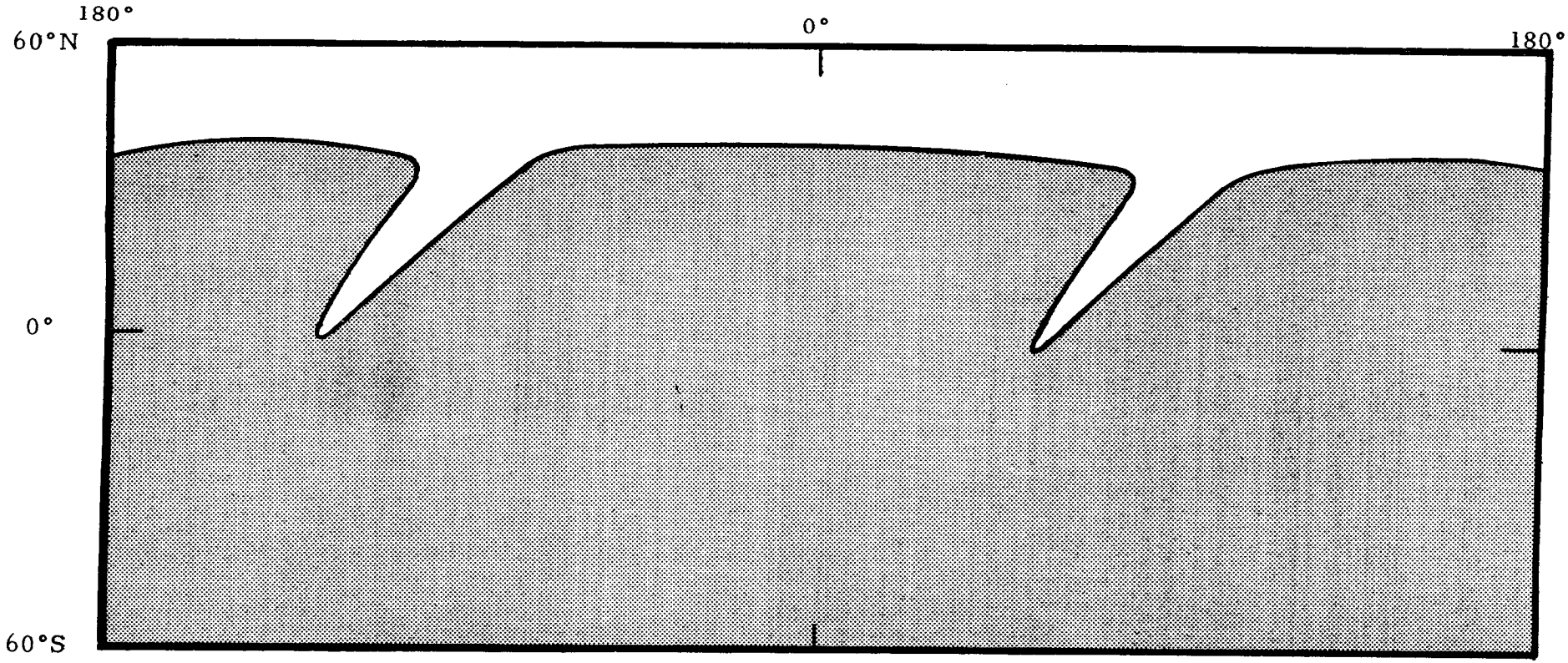

MARS SURFACE COVERED BY SENSOR
AFTER 180 DAYS IN ORBIT
(Inclination: -60 degrees)

Figure 4-5g

Orbit Period = 12.26 hours
Periapsis Altitude = 1000 km
Apoapsis Altitude = 17,841 km
Inclination =-40 degrees

Julian Date of Arrival; 2442106.0
Sensor Field of View = 10 degrees
Data Acquisition Altitude ≤ 3,000 km
Data Acquisition; Sunlit Areas Only

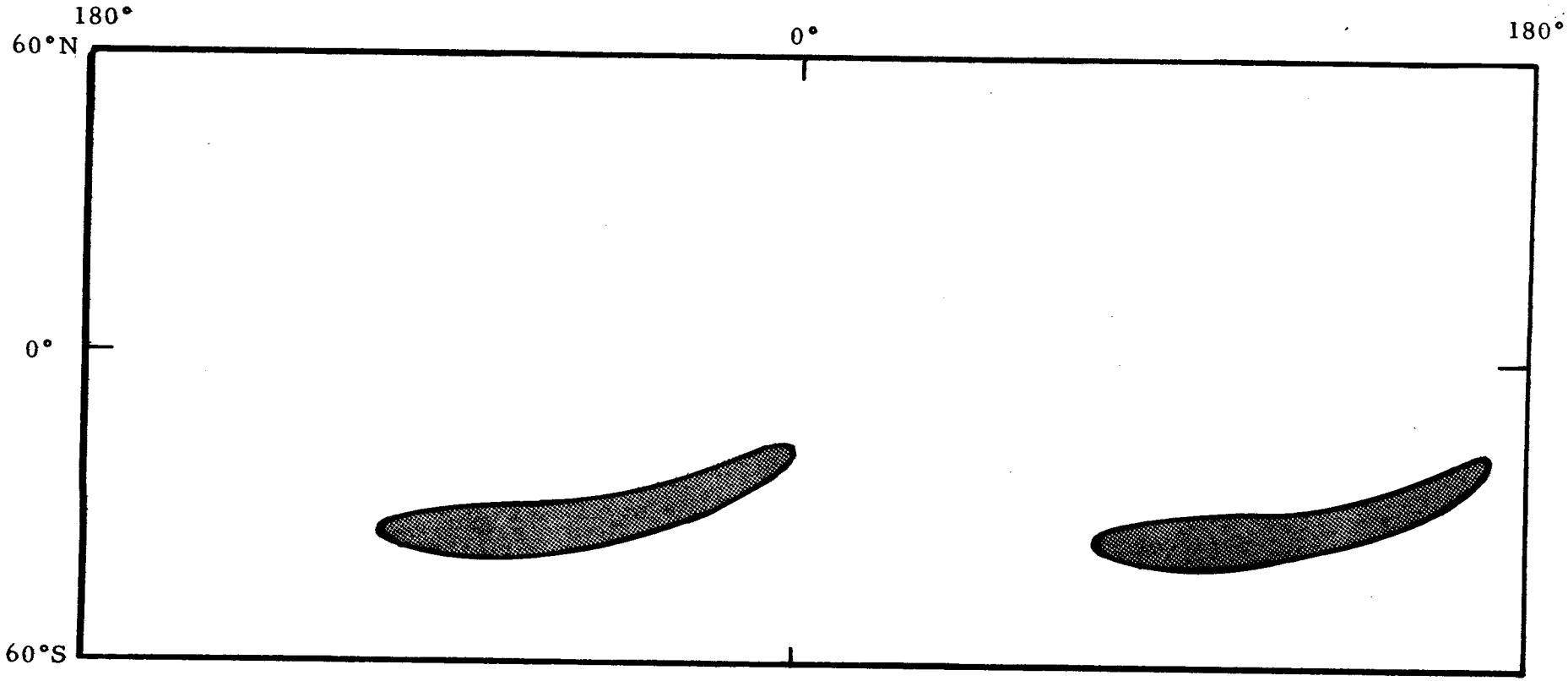

MARS SURFACE COVERED BY SENSOR
AFTER 10 DAYS IN ORBIT
(Inclination: -40 degrees)

Figure 4-6a

Orbit Period = 12.26 hours
Periapsis Altitude = 1000 km
Apoapsis Altitude = 17,841 km
Inclination =-40 degrees

Julian Date of Arrival; 2442106.0
Sensor Field of View = 10 degrees
Data Acquisition Altitude ≤ 3,000 km
Data Acquisition; Sunlit Areas Only

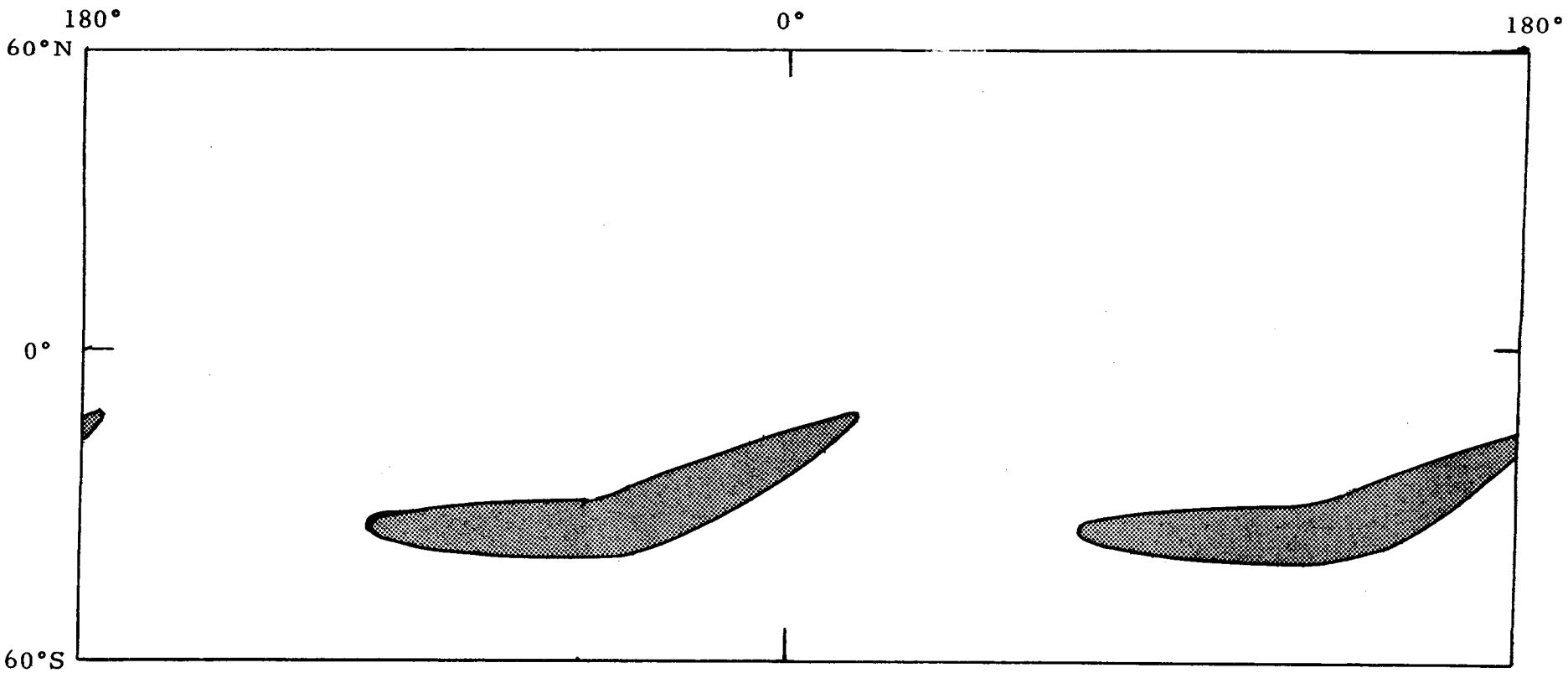

MARS SURFACE COVERED BY SENSOR
AFTER 20 DAYS IN ORBIT
(Inclination: -40 degrees)

Figure 4-6b

Orbit Period = 12.26 hours
Periapsis Altitude = 1000 km
Apoapsis Altitude = 17,841 km
Inclination =-40 degrees

Julian Date of Arrival; 2442106.0
Sensor Field of View = 10 degrees
Data Acquisition Altitude ≤ 3,000 km
Data Acquisition; Sunlit Areas Only

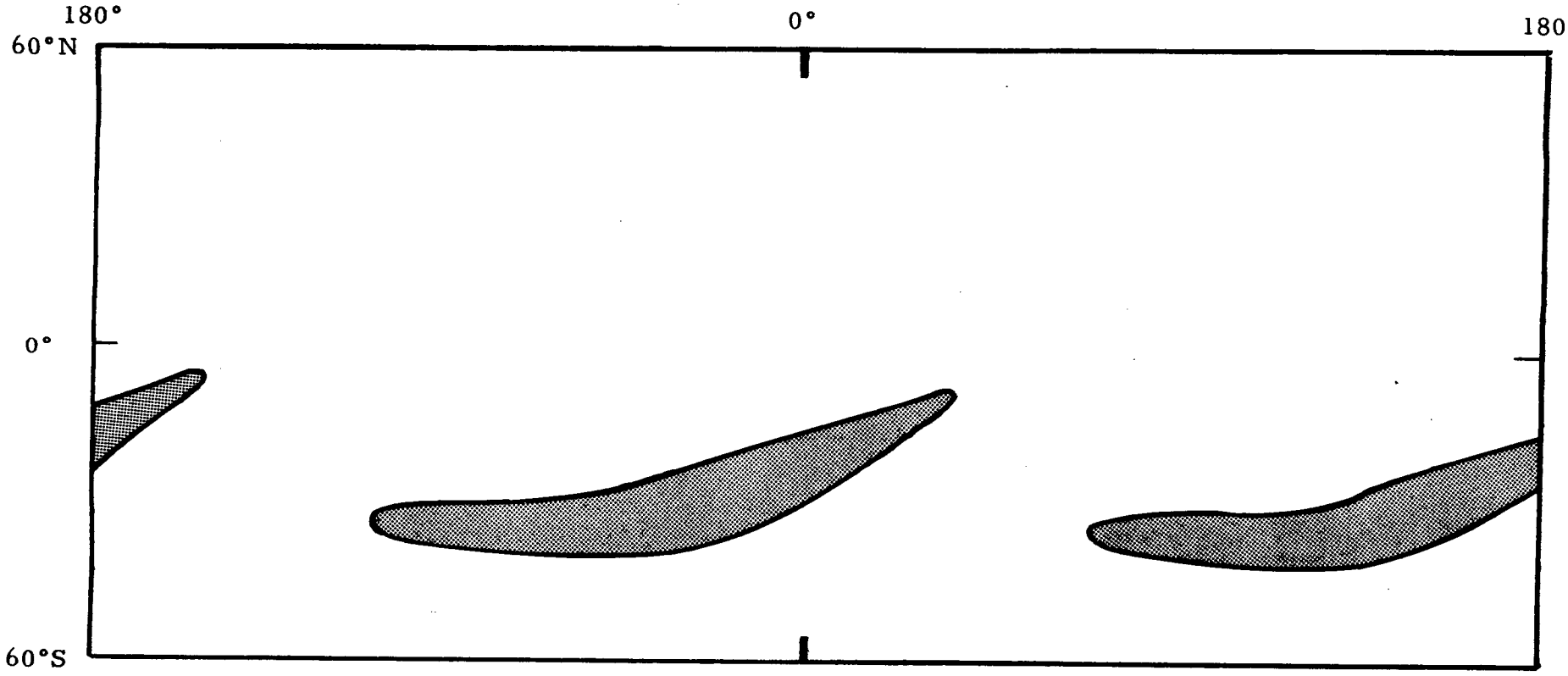

MARS SURFACE COVERED BY SENSOR
AFTER 30 DAYS IN ORBIT
(Inclination: -40 degrees)

Figure 4-6c

Orbit Period = 12.26 hours
Periapsis Altitude = 1000 km
Apoapsis Altitude = 17,841 km
Inclination =-40 degrees

Julian Date of Arrival; 2442106.0
Sensor Field of View = 10 degrees
Data Acquisition Altitude ≤ 3,000 km
Data Acquisition; Sunlit Areas Only

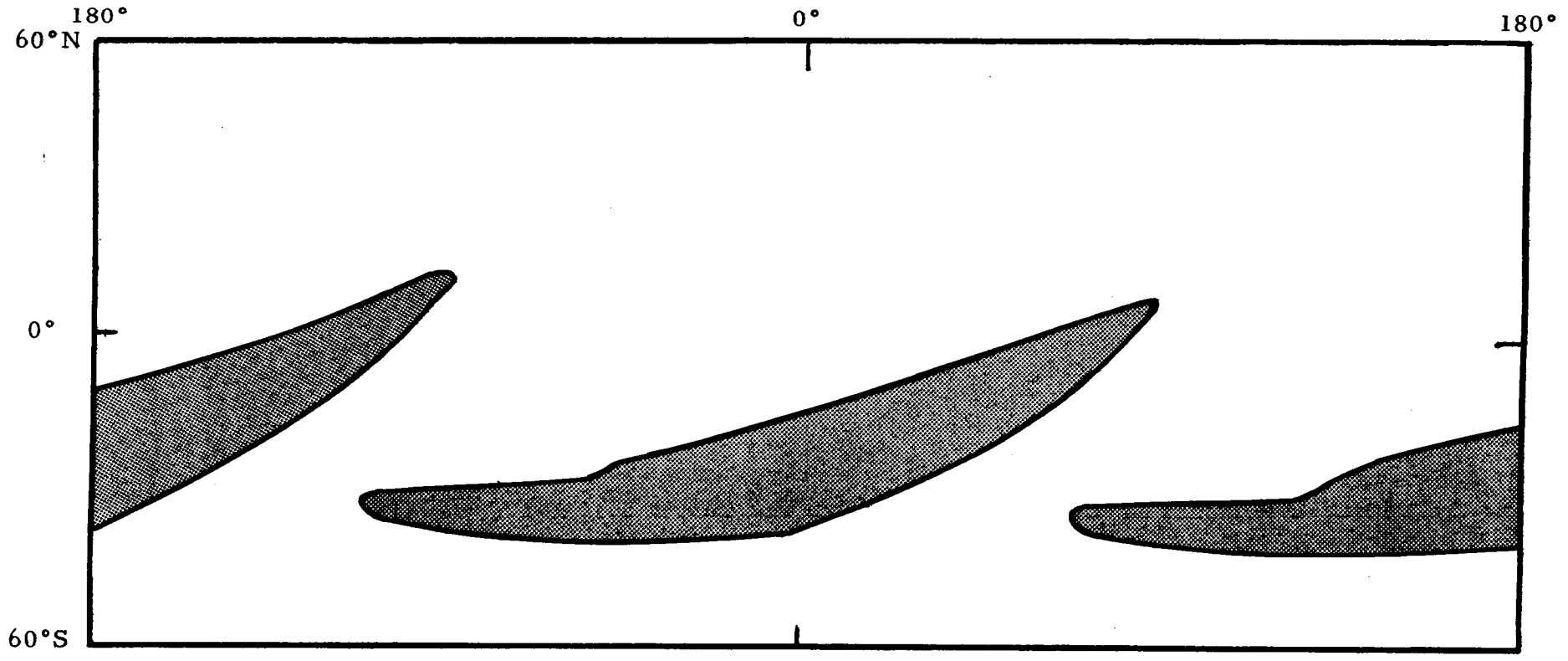

MARS SURFACE COVERED BY SENSOR
AFTER 60 DAYS IN ORBIT
(Inclination: -40 degrees)

Figure 4-6d

Orbit Period = 12.26
Periapsis Altitude = 1000 km
Apoapsis Altitude = 17,841 km
Inclination =-40 degrees

Julian Date of Arrival; 2442106.0
Sensor Field of View = 10 degrees
Data Acquisition Altitude ≤ 3,000 km
Data Acquisition; Sunlit Areas Only

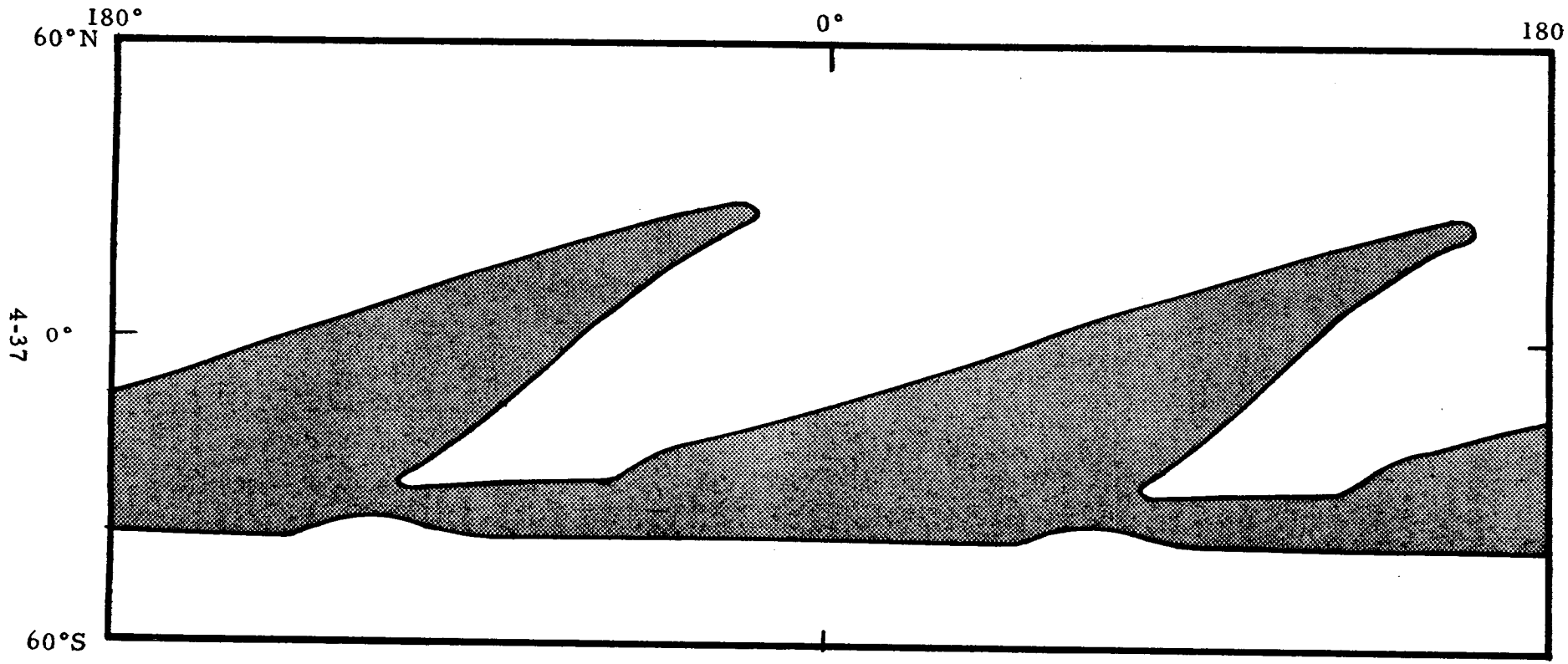

MARS SURFACE COVERED BY SENSOR
AFTER 90 DAYS IN ORBIT
(Inclination: -40 degrees)

Figure 4-6e

Orbit Period = 12.26 hours
Periapsis Altitude = 1000 km
Apoapsis Altitude = 17,841 km
Inclination =-40 degrees

Julian Date of Arrival; 2442106.0
Sensor Field of View = 10 degrees
Data Acquisition Altitude ≤ 3,000 km
Data Acquisition; Sunlit Areas Only

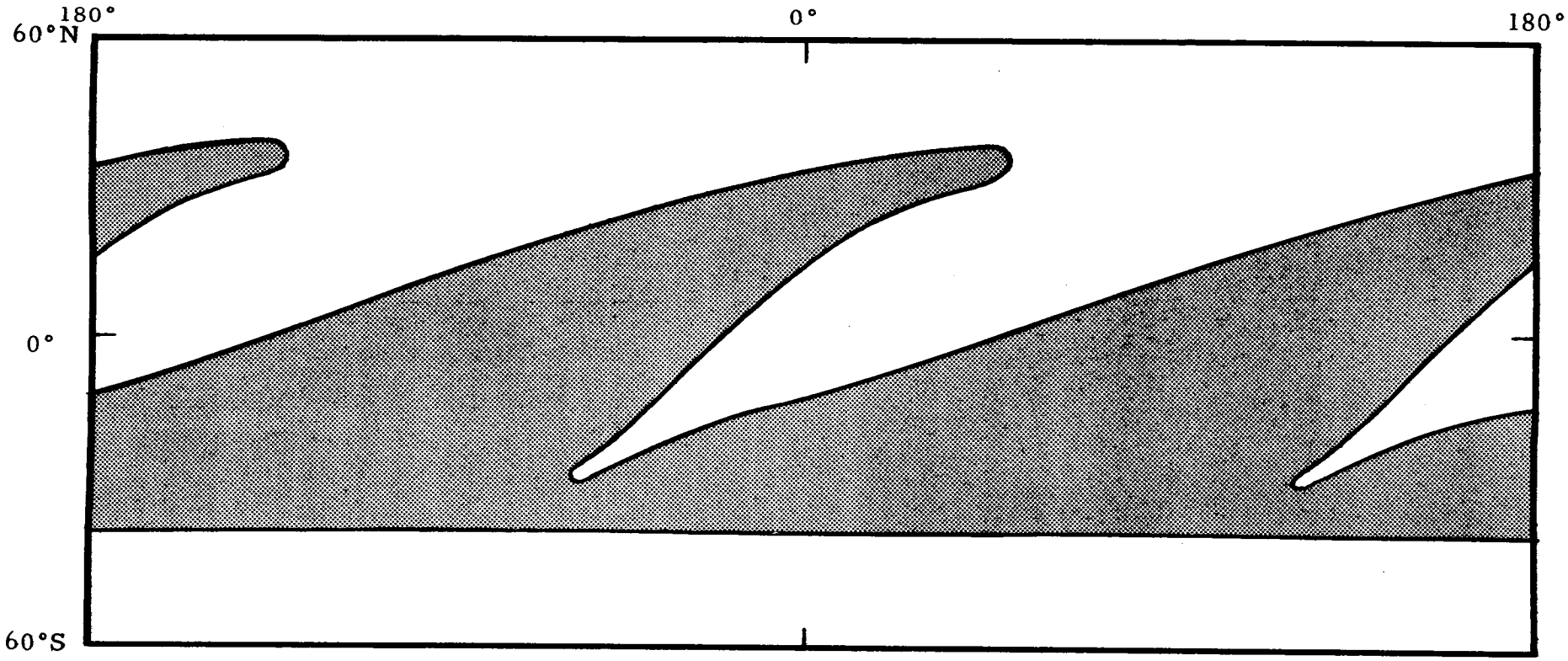

MARS SURFACE COVERED BY SENSOR
AFTER 120 DAYS IN ORBIT
(Inclination: -40 degrees)

Figure 4-6f

Orbit Period = 12.26 hours
Periapsis Altitude = 1000 km
Apoapsis Altitude = 17,841 km
Inclination =-40 degrees

Julian Date of Arrival; 2442106.0
Sensor Field of View = 10 degrees
Data Acquisition Altitude ≤ 3,000 km
Data Acquisition; Sunlit Areas Only

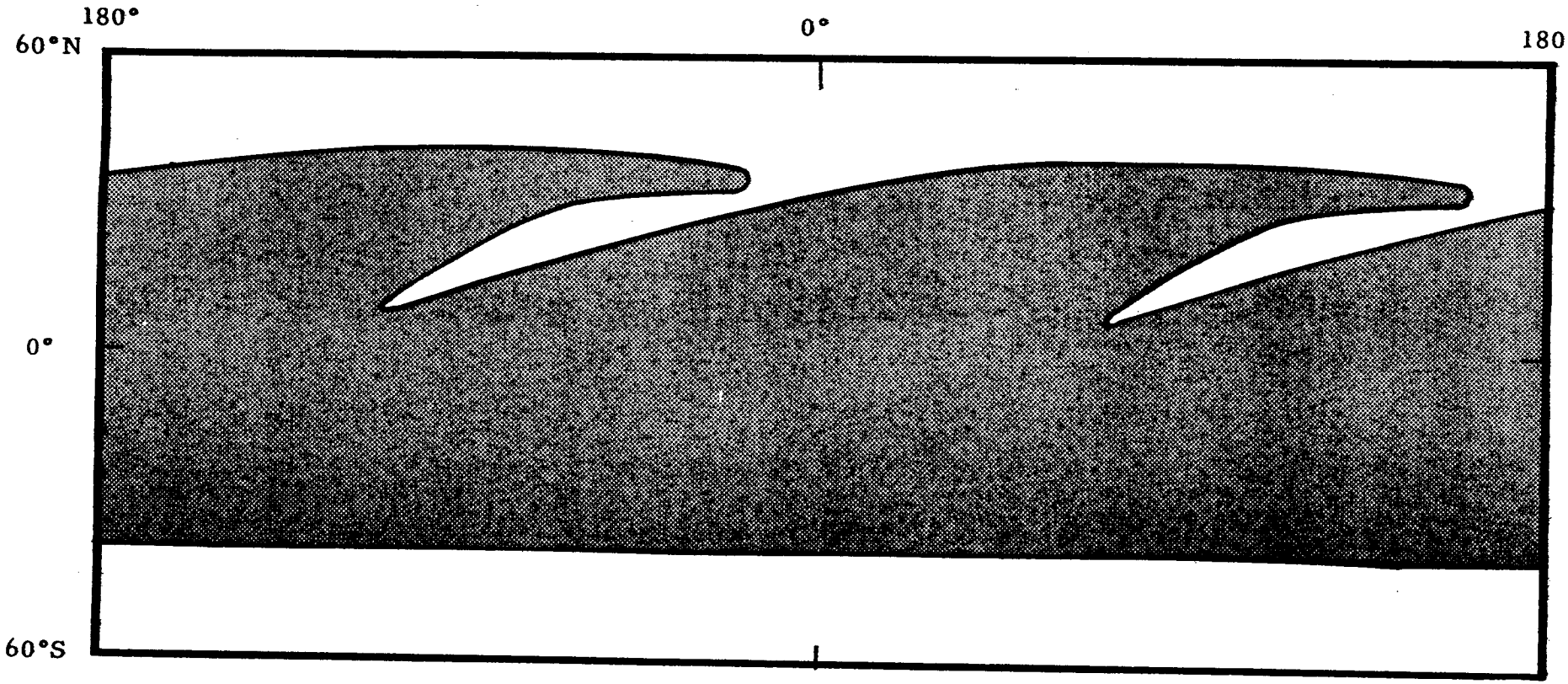

MARS SURFACE COVERED BY SENSOR
AFTER 180 DAYS IN ORBIT
(Inclination: -40 degrees)

Figure 4-6g

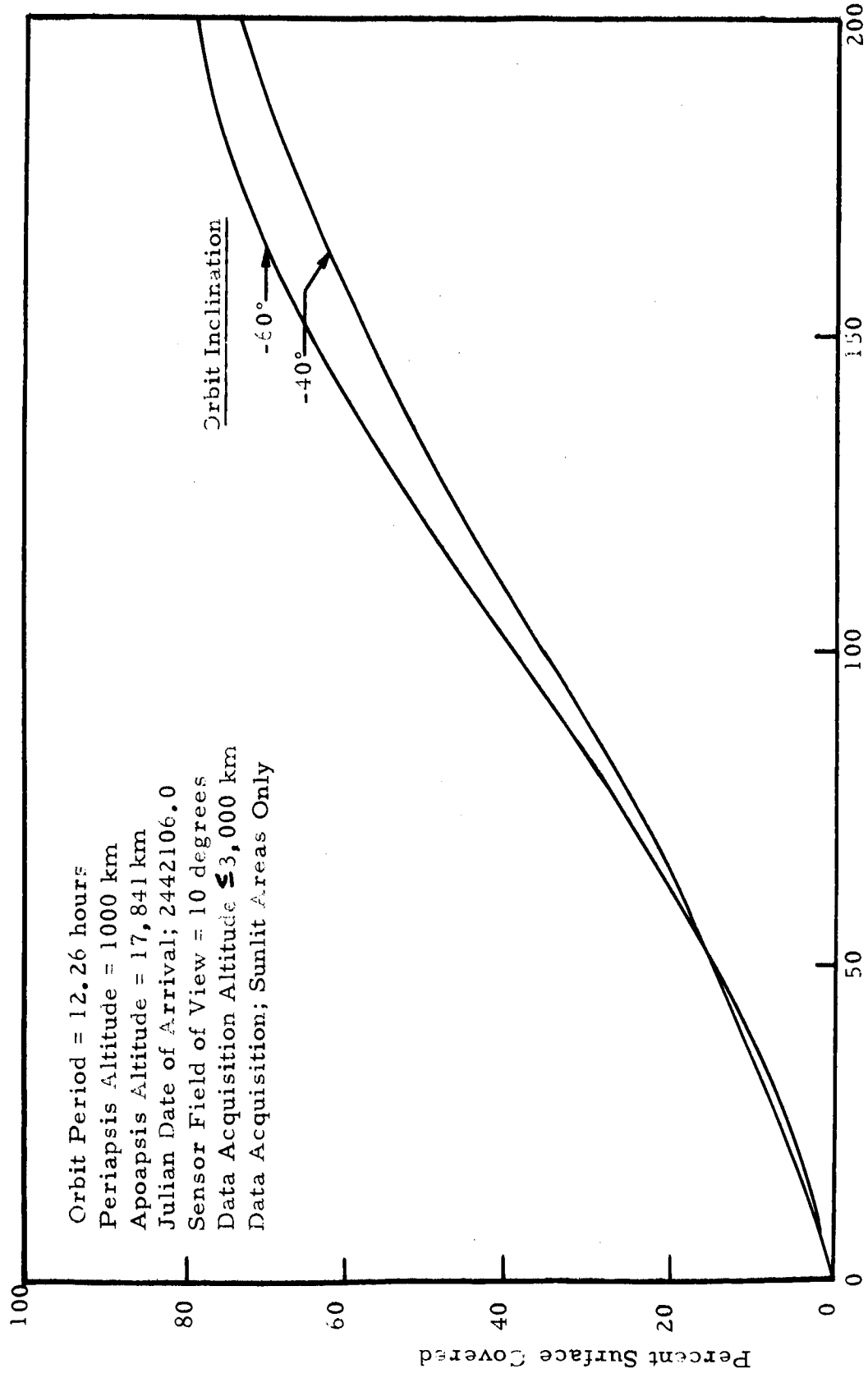

PERCENT MARTIAN SURFACE COVERAGE VS DAYS IN ORBIT

Figure 4-7

Considering the fourteen areas selected for coverage in Section 3 (Table 3-2), it is interesting to note that for the-60° inclination example orbit only one of the areas is covered during the first 30 days in orbit, two in 60 days, eight in 90 days, ten in 120 days and thirteen in 180 days. Approximately the same rate of coverage is obtained for the-40° inclination. The area of Mare Sirenium at 50°N latitude is not covered at all in either case. The rate of acquisition is slow except during the third month, however, a small orbit correction, e.g., change in arrival time, would of course change the rate of acquisition for these selected areas.

Wood (Refs. 4-16, 4-17, 4-18), Ehricke (Ref. 4-7) and others have pointed out the effectiveness of a circular polar orbit for reconnaissance missions. This is illustrated quite drastically by comparing the percent surface coverage versus time presented in Figure 4-8 for a circular polar orbit with the data presented in Figure 4-7 for the elliptic orbits having inclinations of -40 and -60 degrees. Additional cumulative coverage analyses should be performed for potential orbit parameters to determine the optimum coverage conditions. Consideration should be given to the simultaneous coverage obtained if two systems are in different orbits.

4.2.2 Satellite Subpoint Characteristics

The satellite subpoint tracks for the above two elliptical orbits are shown in Figures 4-9 and 4-10, for i = -60 and -40 degrees, respectively. The tracks are plotted for 30 day intervals up to 180 days. It should be noted that the subtrack for only that portion of the orbit during which imagery is obtained is presented (i.e., sunlit surface and $h \leq 3{,}000$ km). Again, the transparent map overlay is to be used with these subtrack plots to visualize the planet regions traversed.

To illustrate the variation in altitude during the portion of the orbit when imagery is obtained, points of equal altitude are connected by dashed lines for several specific values in Figures 4-9 and 4-10. The effect of planet oblateness on movement of the line of apsides (discussed in Appendix A) is illustrated in Figures 4-9 and 4-10. As can be seen in Figure 4-10 for the orbit having an inclination of -40 degrees, the periapsis subpoint (h = 1,000 km) moves from 23 degrees south to approximately 23 degrees north in a period of 180 days. Figure 4-9 shows that for the-60 degree inclination orbit there is very little rotation of the line of apsides.

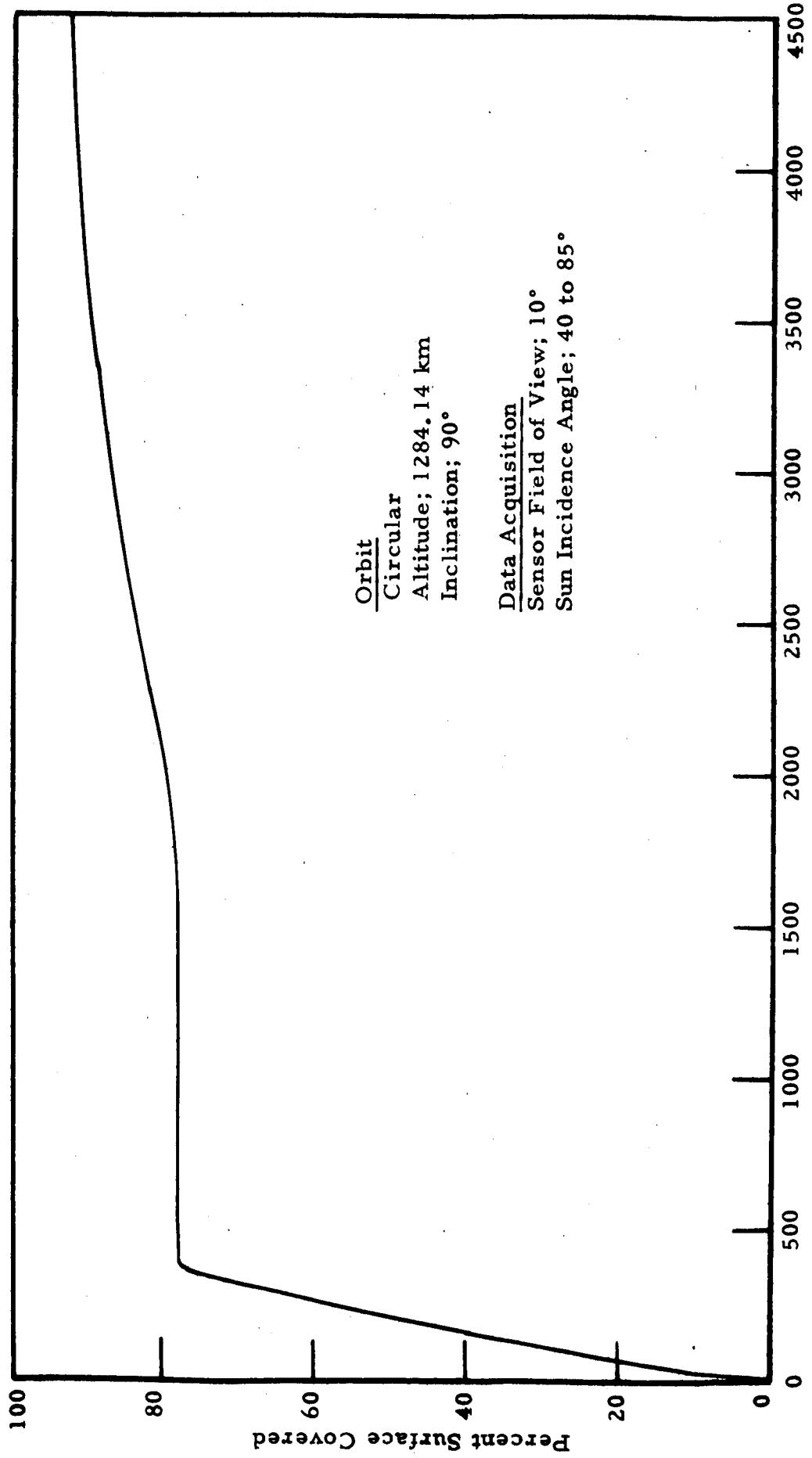

PERCENT SURFACE COVERED VS HOURS IN A CIRCULAR POLAR ORBIT

Figure 4-8

Orbit Period = 12.26 hours
Periapsis Altitude = 1000 km
Apoapsis Altitude = 17,841 km
Inclination = -60 degrees

Julian Date of Arrival; 2442106.0
Sensor Field of View = 10 degrees
Data Acquisition Altitude ≤3,000 km
Data Acquisition; Sunlit Areas Only

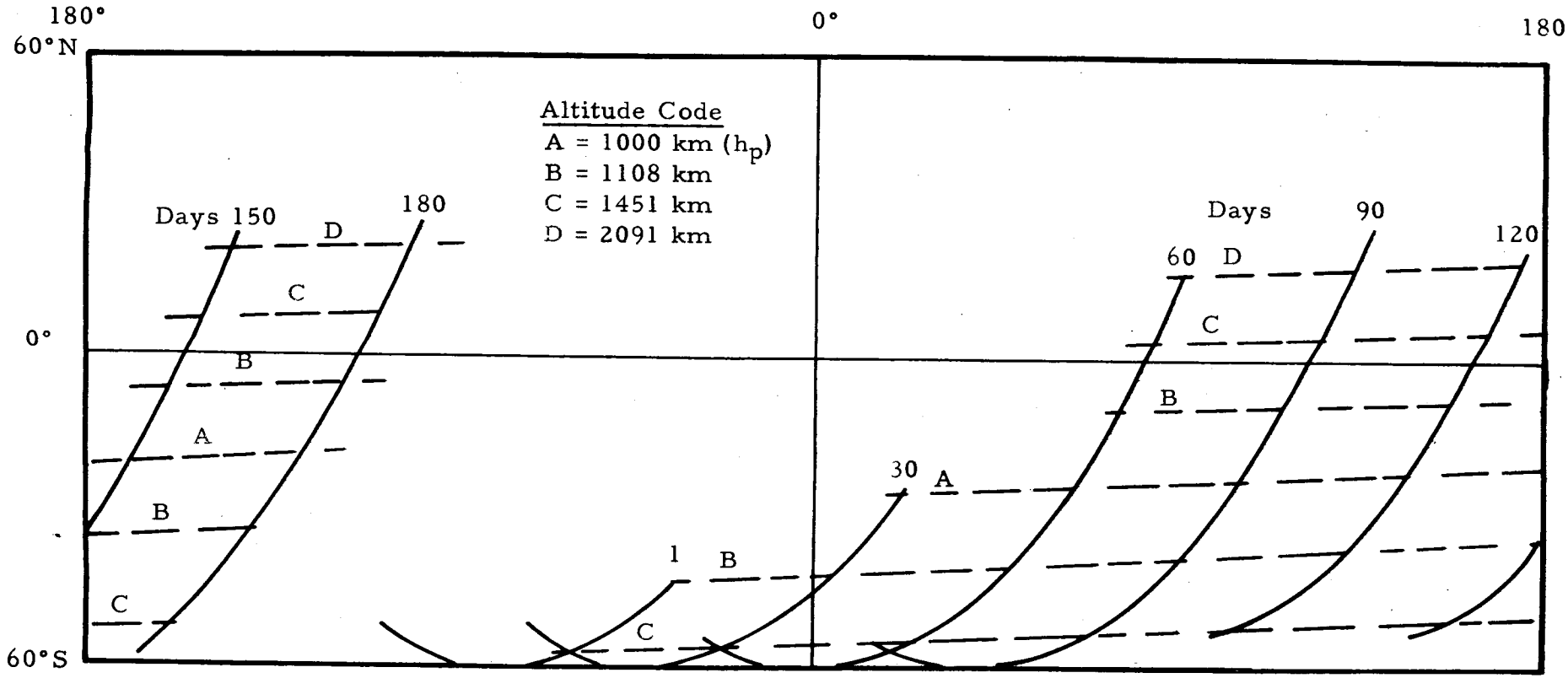

SATELLITE SUB-TRACK AND CONSTANT ALTITUDE CONTOURS; i = 60°

Figure 4-9

Orbit Period = 12.26 hours
Periapsis Altitude = 1000 km
Apoapsis Altitude = 17,841 km
Inclination = -40 degrees

Julian Date of Arrival; 2442106.0
Sensor Field of View = 10 degrees
Data Acquisition Altitude ≤3,000 km
Data Acquisition; Sunlit Areas Only

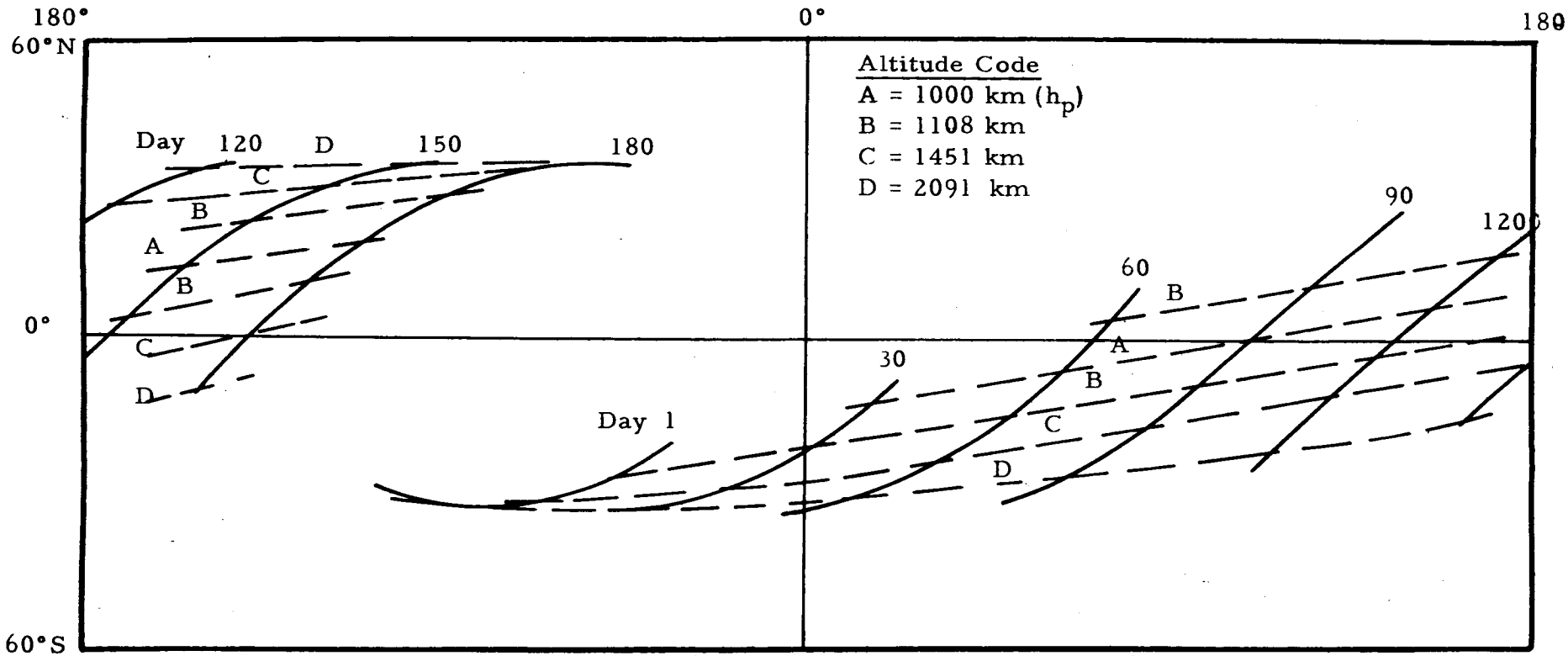

SATELLITE SUB-TRACK AND CONSTANT ALTITUDE CONTOURS; i = 40°

Figure 4-10

The variation of illumination angle with latitude for these orbital subtracks is shown graphically in Figures 4-11 and 4-12, for i = -60 and -40 degrees, respectively. As described in Appendix B, the angle of incidence is measured from the local vertical to the planet-Sun line.

To aid in visualizing the area covered during each orbit, Figure 4-13 presents the width of the orbit swath on the planet's surface as a function of altitude for the example 10 degree field-of-view of a sensor.

4.2.3 Orbit Parameters and System Considerations

Various orbital parameters (satellite velocity, altitude, ground velocity-to-height ratio and elapsed time) are given in Figures 4-14 through 4-16, as a function of angular displacement from periapsis. The data given by Figure 4-14 are for the example orbits discussed above (i.e., h_p = 1,000 km, h_a = 17,841 km). Figure 4-15 is for an orbit having h_p = 500 km and h_a = 10,000 km and Figure 4-16 is for an h_p = 1,000 km and h_a = 33,000 km. These data are necessary for selection of camera cycling rates, amount of image motion compensation required, etc. For example, the cycling rate to provide a desired overlap from frame to frame at periapsis is greater than that required for the same overlap at other points on an elliptical orbit since the V/H ratio is at a maximum. IMC requirements likewise vary since the satellite velocity is decreasing and the height is increasing as the platform moves away from periapsis. It should be noted that the V/H values are for the velocity of the subpoint track on the planet's surface and do not consider the velocity increment due to planet rotation, since it is shown in Appendix A to be negligible.

Figures 4-17 through 4-19 show the orbit geometry graphically; the 3,000 km altitude point is indicated. The variation in orbit altitude is, of course, important since for a fixed focal length and field-of-view imaging system, the surface feature resolution will decrease and the area covered (swath width) will increase, as the altitude increases. These data can be useful in determining duration of data acquisition period, Sun occultation and Earth occultation, depending upon a specific day analyzed (i.e., relative positions of Sun-Earth-Mars). Figure 4-20, for example, shows the approximate relative positions of Earth and Mars at 30 day intervals following an arrival date at Mars of 28 February 1974. Figure 4-21 illustrates the precession of the line-of-apsides with respect to the terminator and the Mars-Earth line at 60 day intervals.

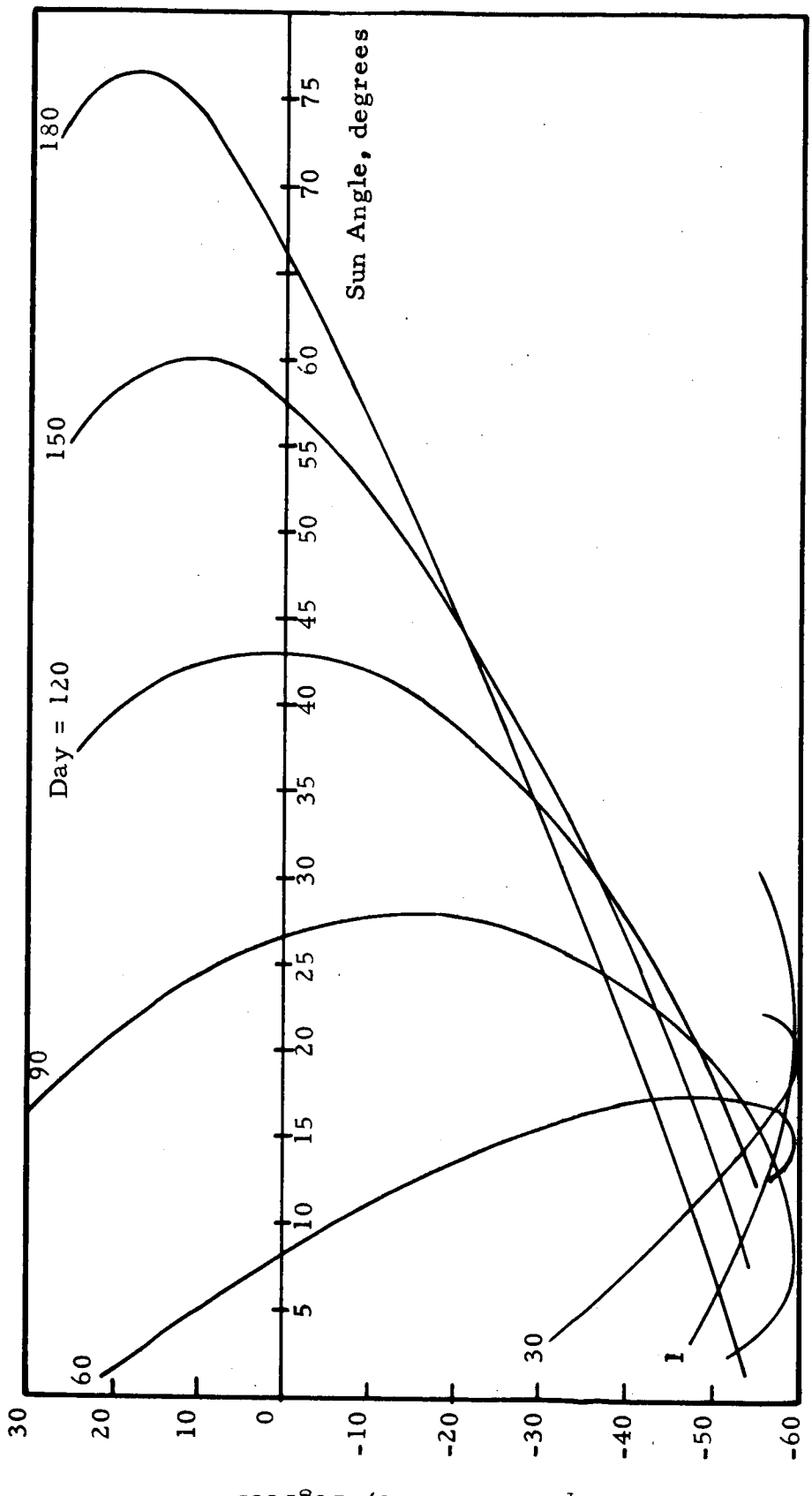

SUN ANGLE ALONG THE SATELLITE SUBTRACK, i = -60°

Figure 4-11

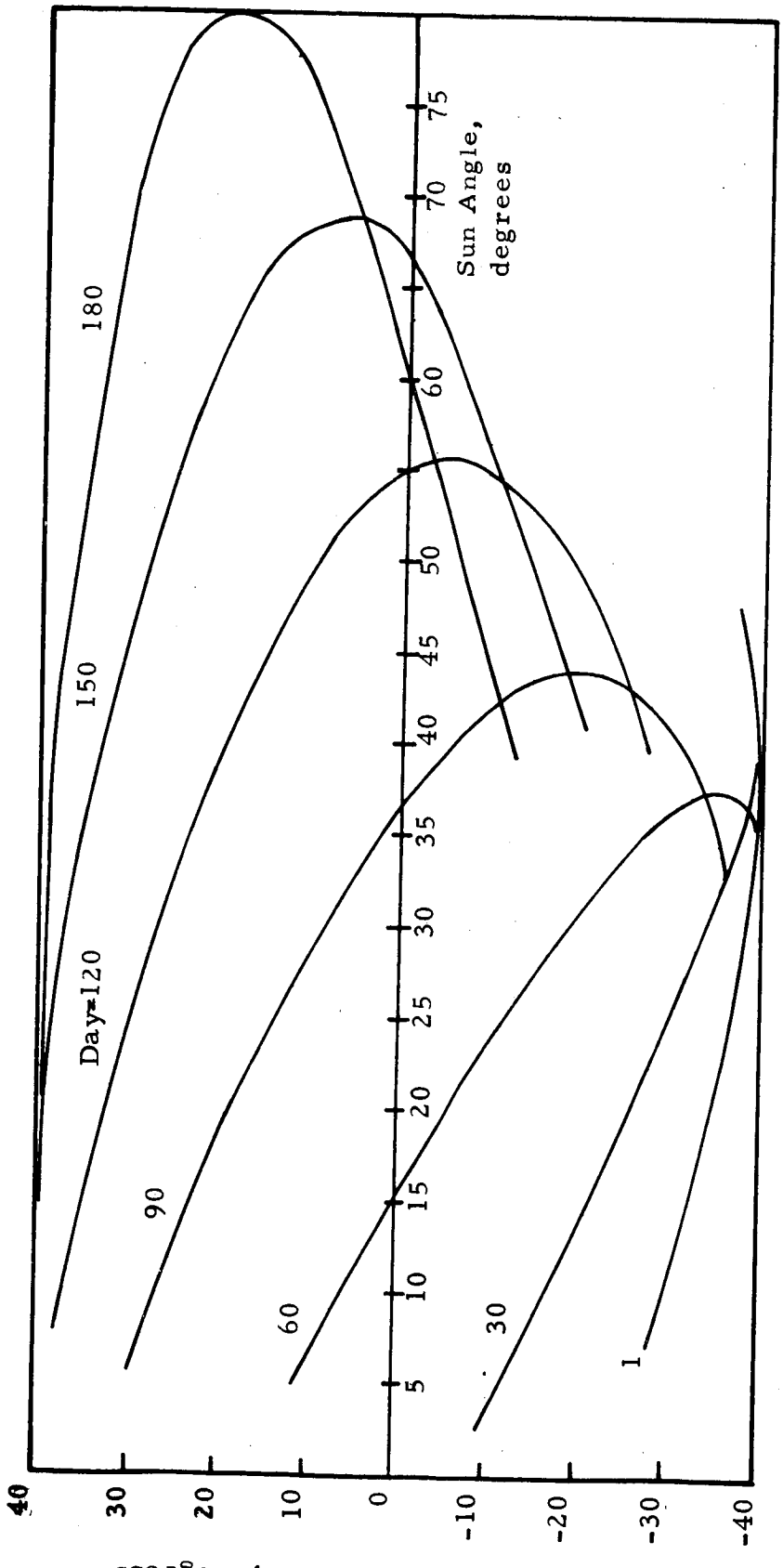

SUN ANGLE ALONG THE SATELLITE SUBTRACK, i = -40°

Figure 4-12

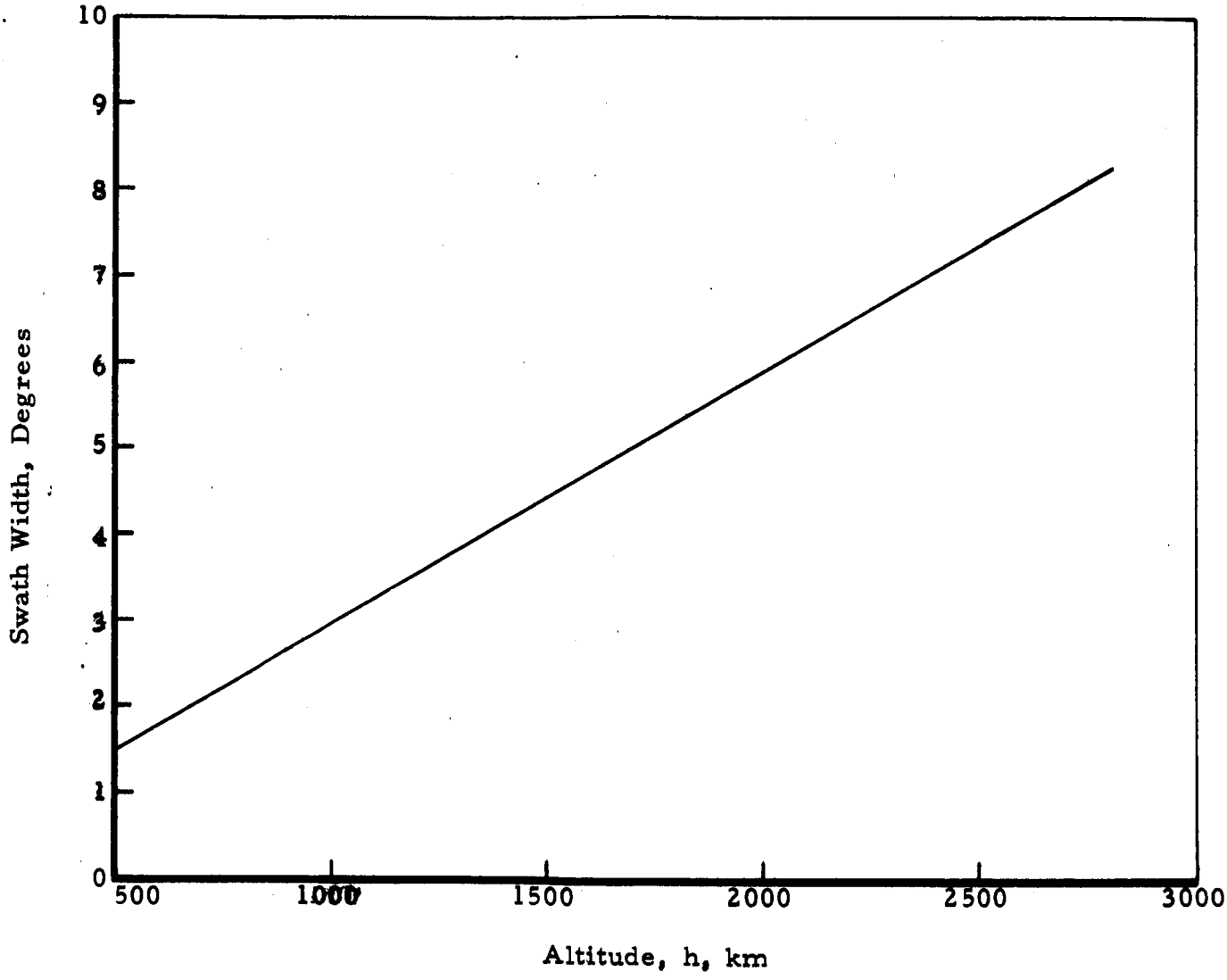

VARIATION OF SWATH WIDTH WITH
ALTITUDE FOR 10 DEGREE FIELD OF VIEW

Figure 4-13

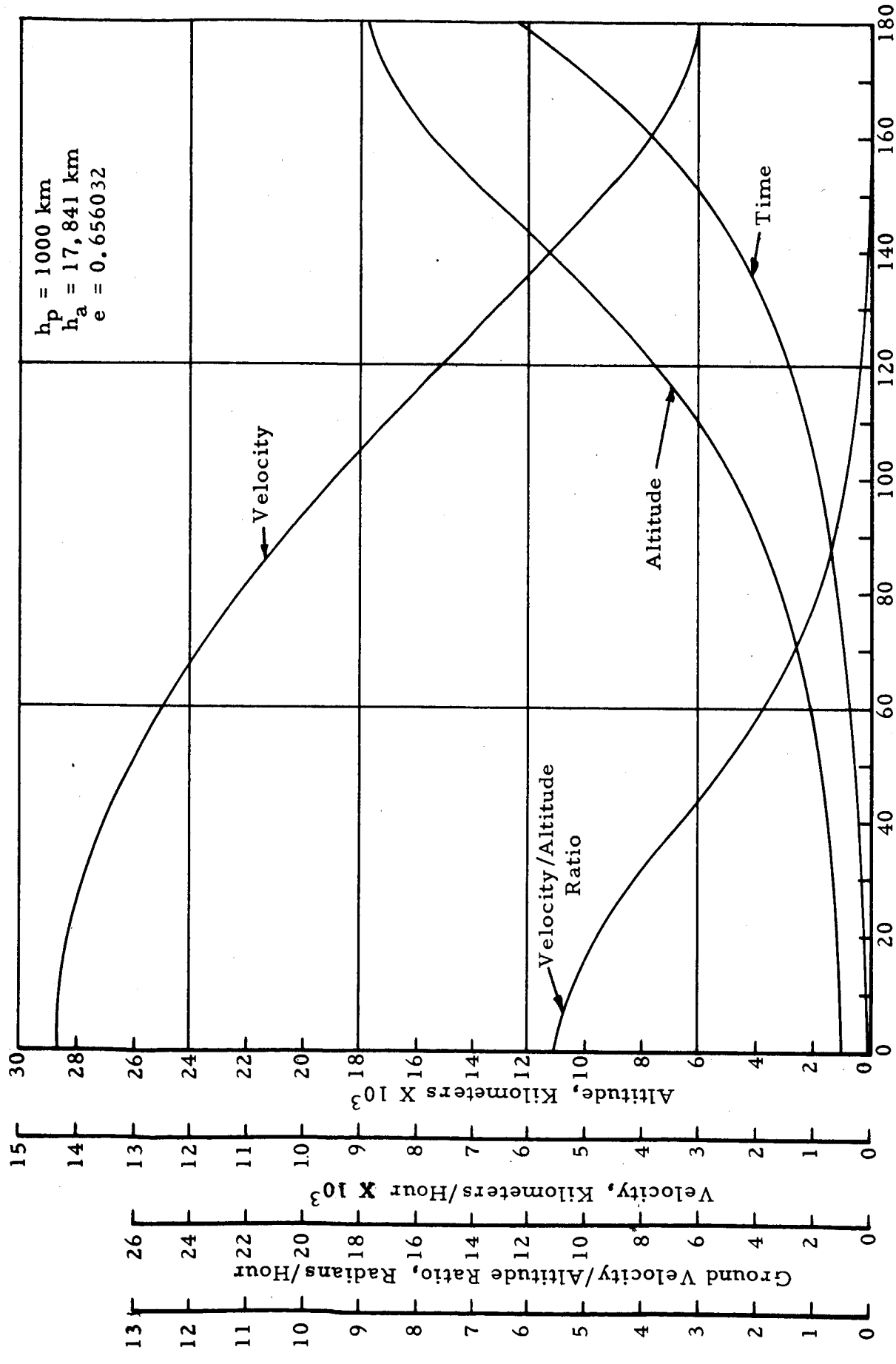

PARAMETERS FOR ORBIT HAVING PERIAPSIS ALTITUDE OF 1000 km AND ECCENTRICITY OF 0.656032

Figure 4-14

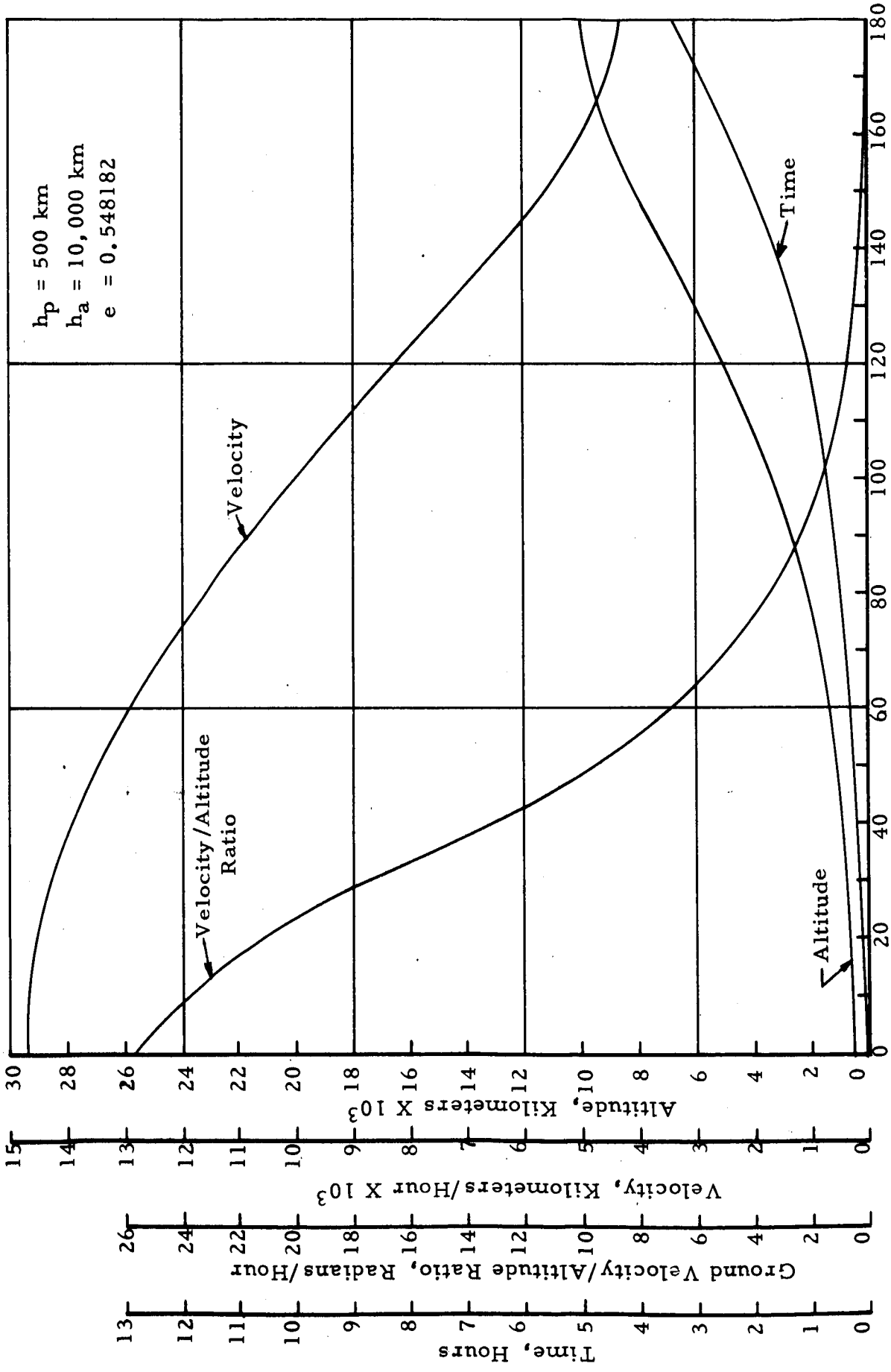

PARAMETERS FOR ORBIT HAVING PERIAPSIS ALTITUDE OF 500 km AND ECCENTRICITY OF 0.548182

Figure 4-15

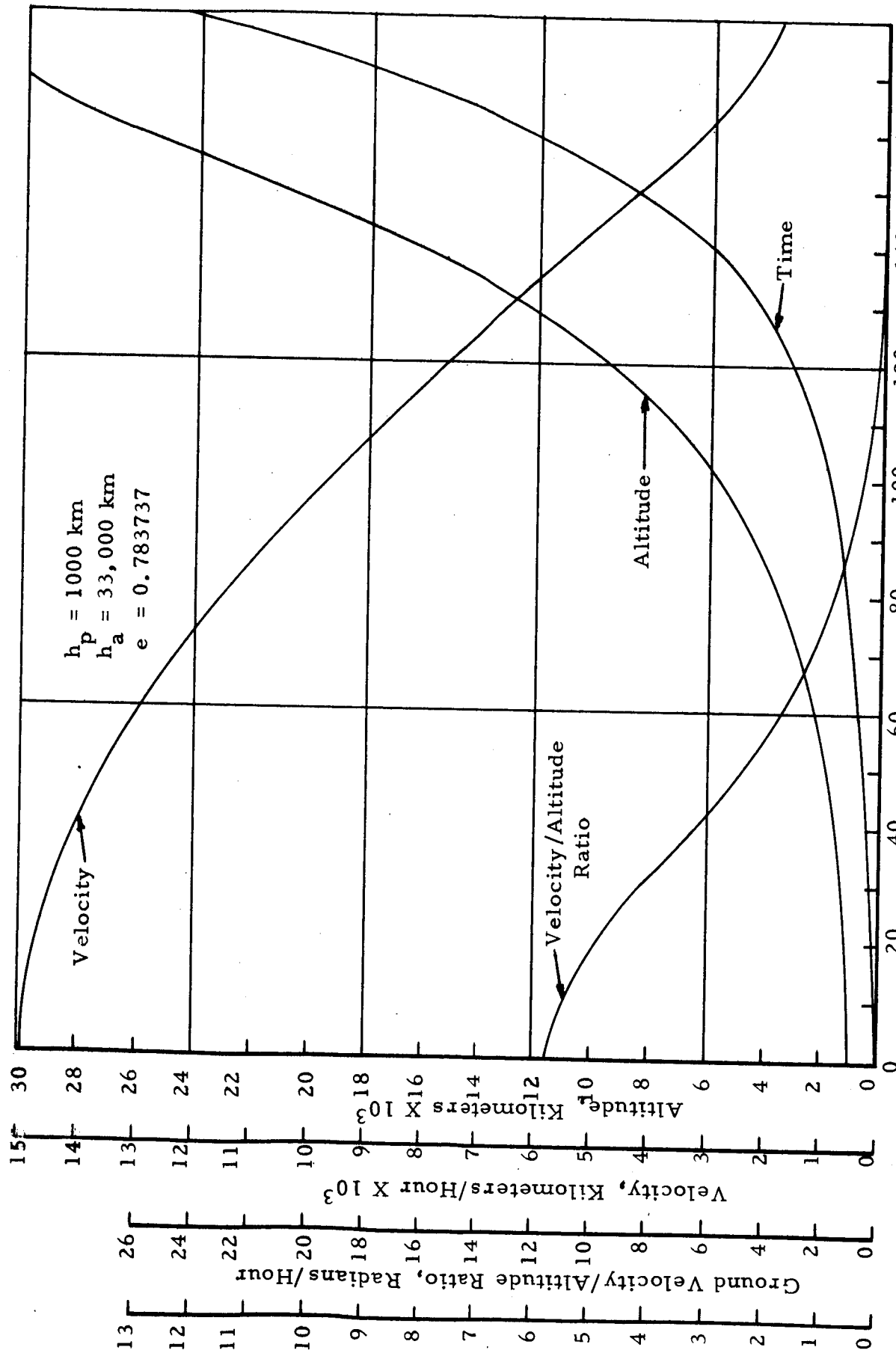

PARAMETERS FOR ORBIT HAVING PERIAPSIS ALTITUDE OF 1000 km AND ECCENTRICITY OF 0.783737

Figure 4-16

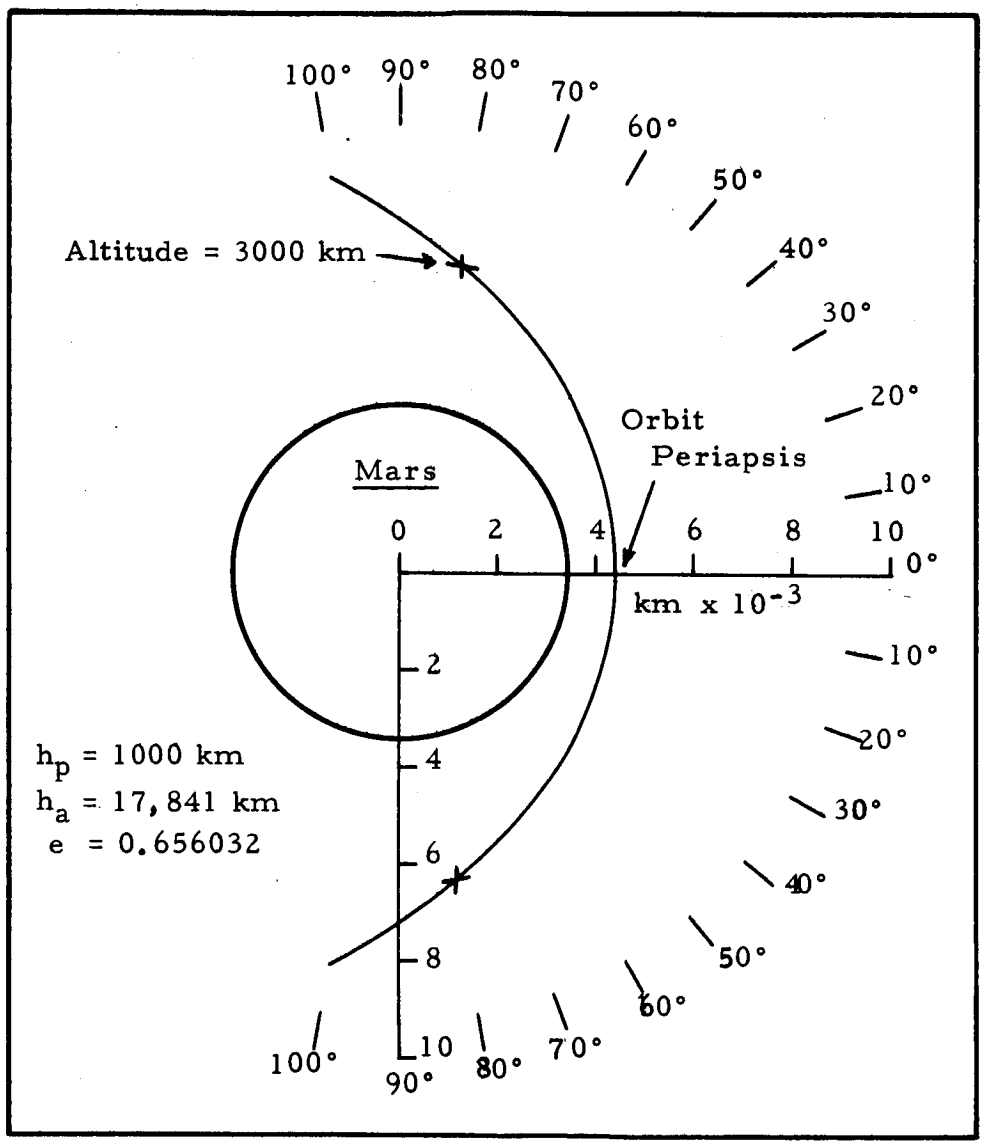

GEOMETRY OF ORBIT HAVING AN ECCENTRICITY OF 0.656032

Figure 4-17

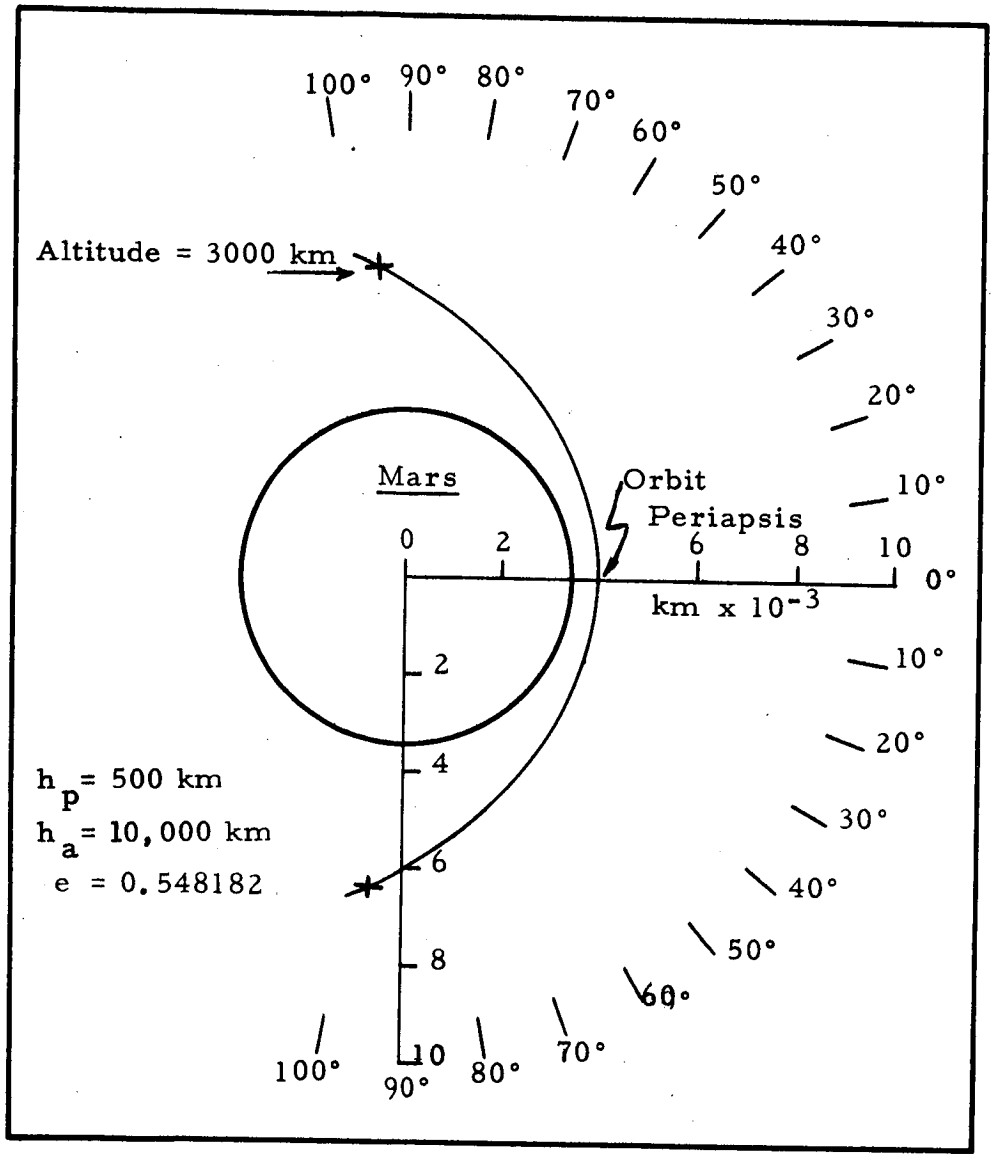

GEOMETRY OF ORBIT HAVING AN ECCENTRICITY OF 0.548182

Figure 4-18

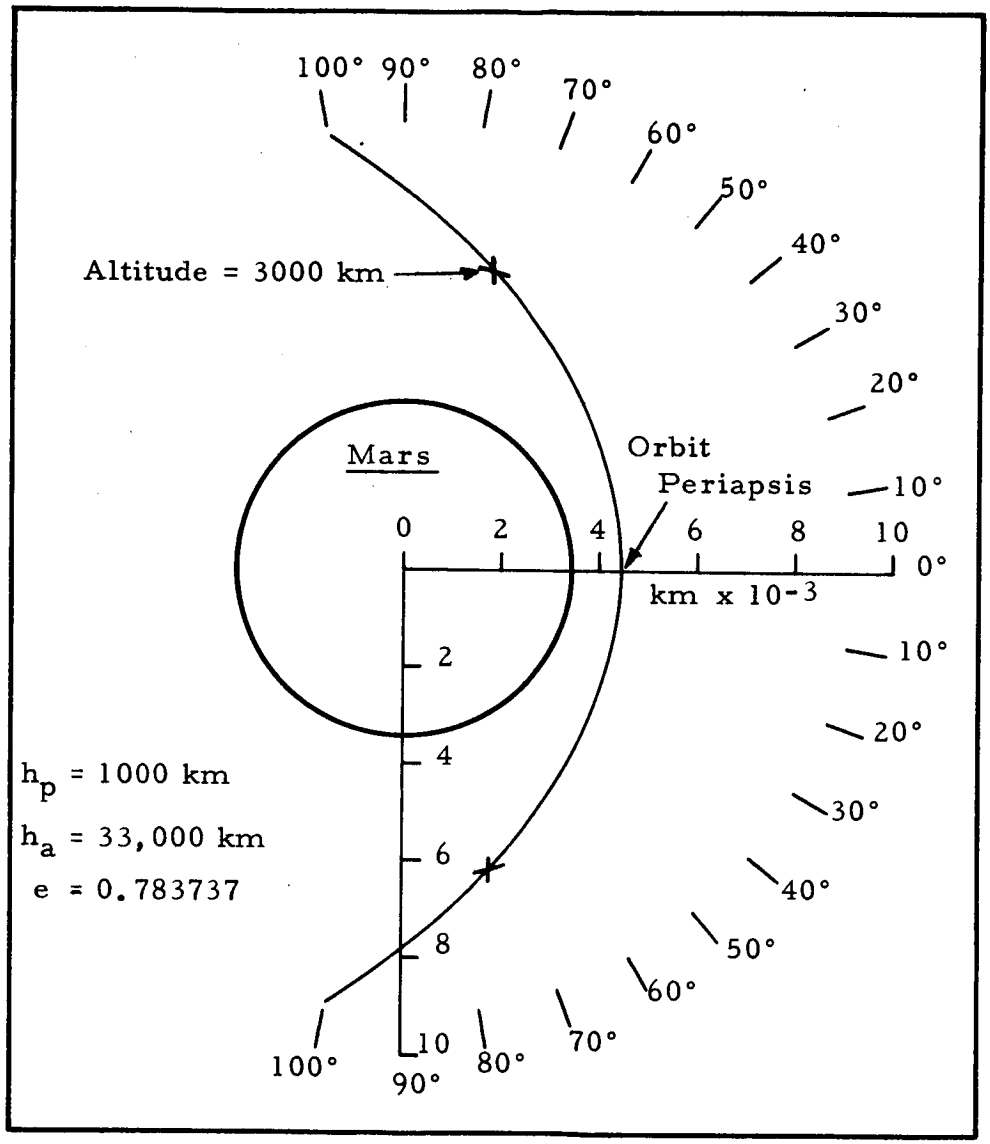

GEOMETRY OF ORBIT HAVING AN ECCENTRICITY OF 0.783737

Figure 4-19

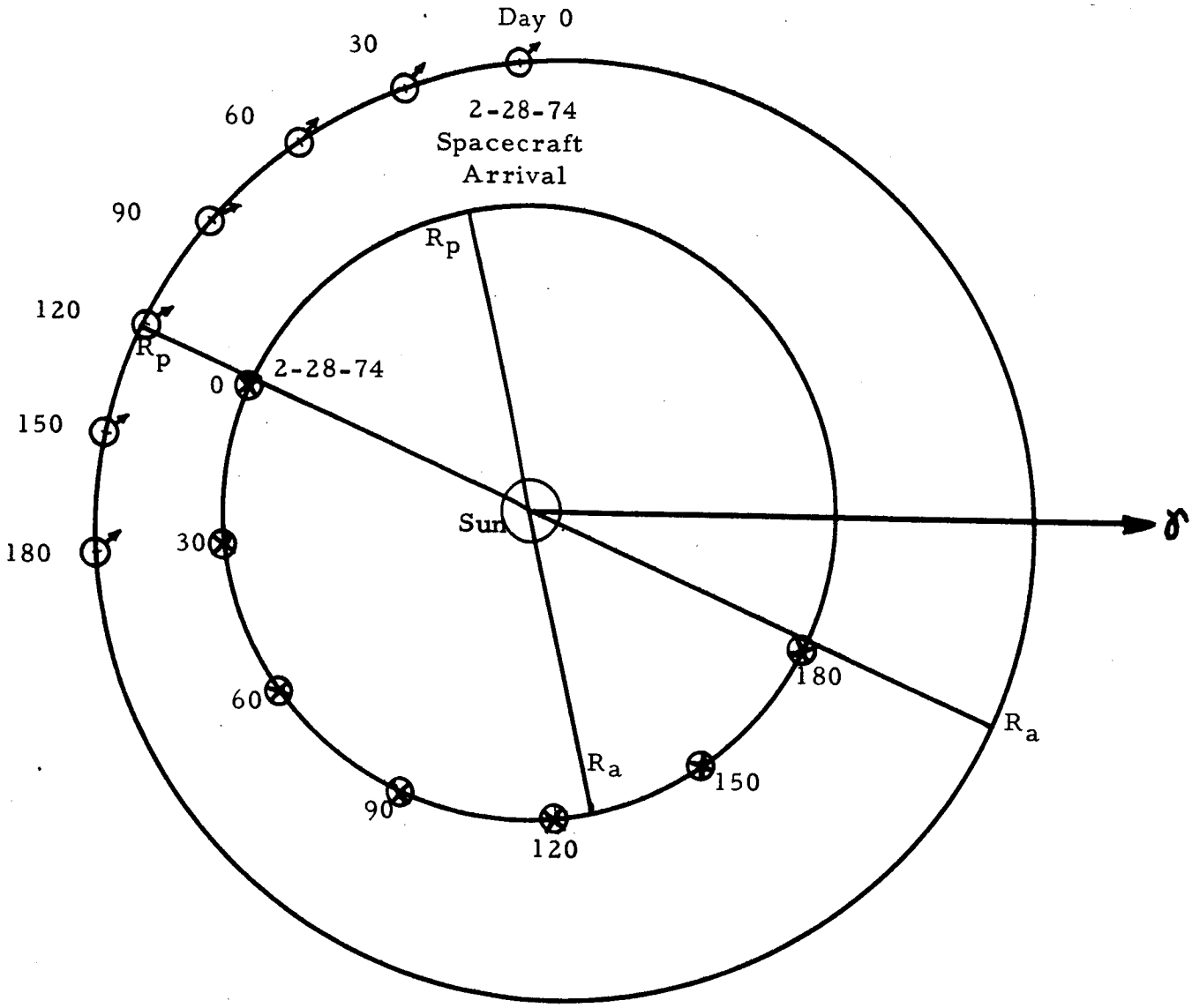

APPROXIMATE RELATIVE POSITIONS OF EARTH AND MARS AT 30 DAY INTERVALS FOLLOWING AN ARRIVAL DATE AT MARS OF 28 FEBRUARY 1974 (JULIAN = 2442106.0)

Figure 4-20

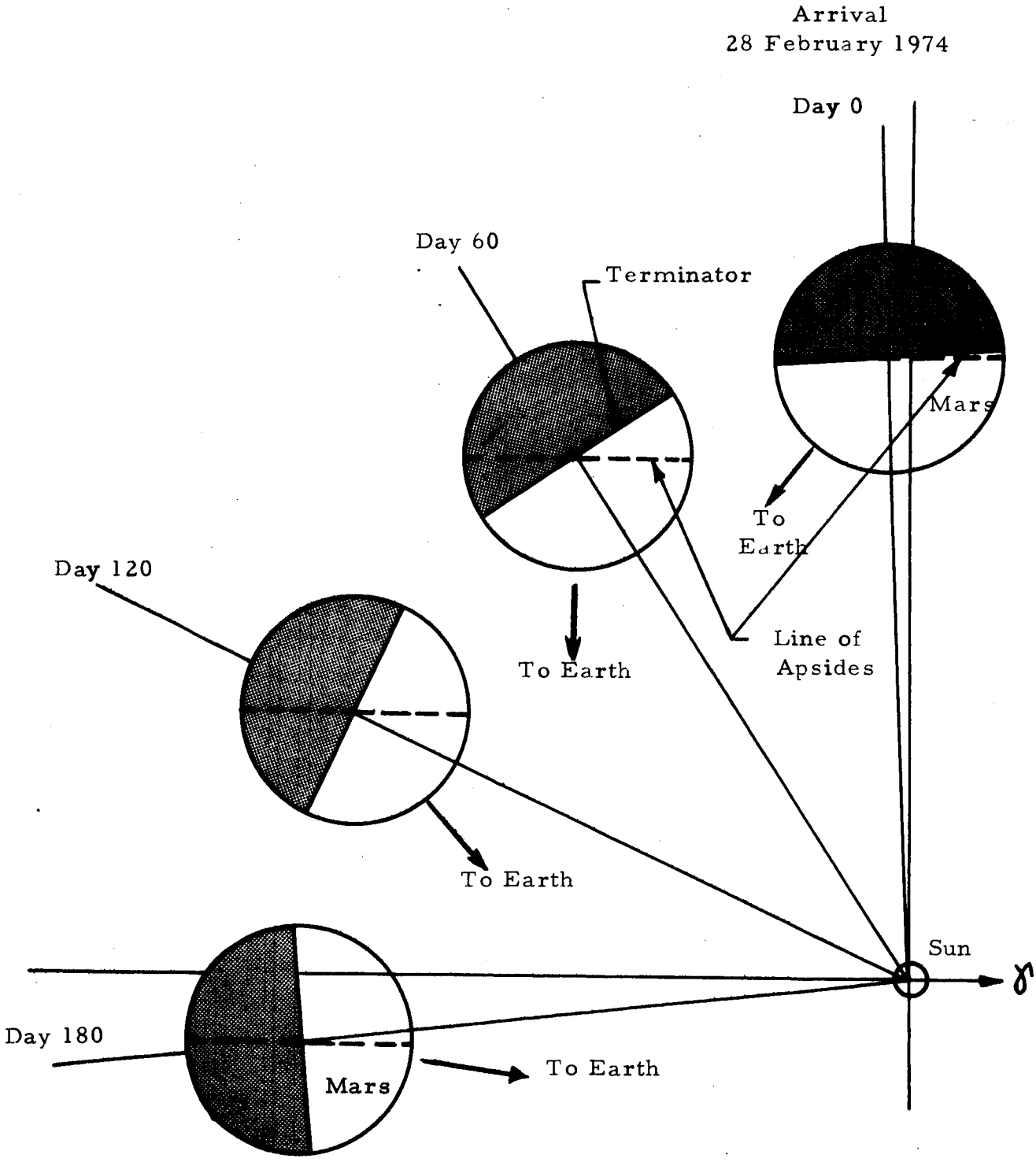

ILLUSTRATION OF PRECESSION OF LINE-OF-APSIDES WITH RESPECT TO TERMINATOR AND EARTH DIRECTION

Figure 4-21

The relationships between orbit parameters discussed in this section and photographic requirements must be emphasized in formulating the Voyager mission orbit conditions. Data useful in overall system considerations, such as Earth-Mars transfer time, maximum occultation times for various orbits, communication distances, Earth cone angle, etc., are presented in Appendix C.

4.3 REFERENCES

4-1 "Summary of the Voyager Program", NASA Office of Space Science and Applications, Jan. 1967.

4-2 LEE, V. A. and WILSON, JR., S. W., "A Survey of Mars Mission Trajectory Characteristics," Proceedings of the AIAA/AAS Stepping Stones to Mars Meeting, March 28-30, 1966.

4-3 STAVRO, W., "Inter-Planetary Trajectory Selection Criteria for Voyager Mars Missions," presented at the American Astronautical Society 1967 National Symposium, Saturan V/Apollo and Beyond, Paper No. AAS67-386 (MAM-26), June 1967.

4-4 SAGERMAN, G. and KREITER, T., "Payload Capabilities of Saturn 1B-Centaur for Launch Opportunities to Mars in 1971, 1973 and 1975 and to Venus in 1972 and 1973," Lewis Research Center, NASA TM X-1327.

4-5 KNIP, JR., G. and ZOLA, C., "Three-Dimensional Sphere-of-Influence Analysis of Interplanetary Trajectories to Mars," NASA TN D-1199, 1962.

4-6 WAGNER, C. A., "Payload to Mars Reconnaissance Orbit Using Present and Future Booster Systems," NASA TMX-1334, February 1967.

4-7 EHRICKE, K. A., "A Study of Early Manned Interplanetary Missions," General Dynamics/Astronautics Report AOK 63-0001, 31 January 1963.

4-8 HONEYWELL, E. E., "Soft Landers for Venus and Mars," General Dynamics/Pomona TM-6-341-185, April 1963.

REFERENCES (continued)

4-17 WOOD, L. H., et al, "Planetary Photographic Exploration with Solar-Electric Propulsion," presented at the AIAA Electric Propulsion and Plasamadynamics Specialists Conference, Sept. 1967.

4-18 WOOD, L. H., VACHON, R. I. and PRASTHOFER, W. P., "Photographic Exploration of Mars with Solar-Electric Propulsion," presented at the AIAA 5th Aerospace Sciences Meeting, January 1967.

REFERENCES (continued)

4-9 TITO, D. A., "Satellite Orbit Selection Criteria for Voyager Mars Missions," presented at the American Astronautical Society 1967 National Symposium, Saturn V/Apollo and Beyond, Paper No. AAS67-387 (MAM-27), June 1967.

4-10 CAMPEN, C., Personal Communications, Voyager Interim Project Office, 22 August 1967.

4-11 HALE, D., Personal Communications, MSFC, July 26, 1967.

4-12 NEWELL, H. E., "Opportunities for Participation in Space Flight Investigations - Voyager 1973 Mars Mission," NASA Memo. Ch. 2 to NHB 8030.1A, 28 July 1967.

4-13 MOLL, R., and KROP, M., "Long Lifetime Orbits About Mars," AIAA Paper No. 66-35, Presented at the 3rd Aerospace Sciences Meeting, January 24-26, 1966.

4-14 DICKSON, W. J., "Guidance and Control of a Mars Orbiter-Lander Mission," Proceedings of the AIAA/AAS Stepping Stones to Mars Meeting, March 28-30, 1966.

4-15 SEAMAN, L. T. and BROWN, H. W., "Planetary Approach Guidance for a Martian Mission," presented at the American Astronautical Society Symposium, Paper No. AAS67-453 (GC-3), 1967.

4-16 WOOD, L. H., STONE, N. H. and FLECK, H. A., "An Application of Solar Electric Power to a Sophisticated Planetary Surface Observation System", presented at the American Astronautical Society, Paper No. AAS67-432 (PS-22), June 1967.

SECTION 5

OPTICAL SUBSYSTEM ASSESSMENT

Optical subsystem parameters, lens capability and instrumentation techniques have been evaluated as a function of the basic system requirements for a Martian orbital photographic imaging system. Proper selection of optical components and specification of optical parameters is essential to satisfy the proposed Voyager mission objectives.

The study has included an assessment of lens system instrumentation consisting of a comparison of optical system types and parametric analyses of optical subsystem characteristics. Instrumentation techniques for stereo and multispectral applications have also been considered. The final instrumentation specification (including selection of lens types) must be reserved until more detailed design analyses can be performed after orbital parameters, resolution, coverage and spectral requirements are more firmly established.

5.1 OPTICAL SUBSYSTEM INSTRUMENTATION

A major task in assessment of optical subsystems for orbital planetary surveillance is the evaluation of suitable lens configurations. The use of reflective, refractive and catadioptric lens systems for the Martian orbital photo imaging missions has been considered, and the advantages and disadvantages of each have been compared.

The optical subsystem investigation has included analysis of both resolution and coverage capability and requirements. Exposure time parameters and the requirements for image motion compensation and vehicle stability have also been evaluated and results are presented. In addition, the requirements for thermal stability and lens/camera calibration are described.

5.1.1 Lens System Types

An optical system may be either refractive, reflective or catadioptric (i.e., an optical system containing both refractive and reflective elements). Each of these systems offer advantages for specific applications, but geometrical and physical system limitations must be evaluated on the basis of appropriate design goals and requirements. Typical lens designs of each type are illustrated in Figure 5-1. A zoom lens system is also shown.

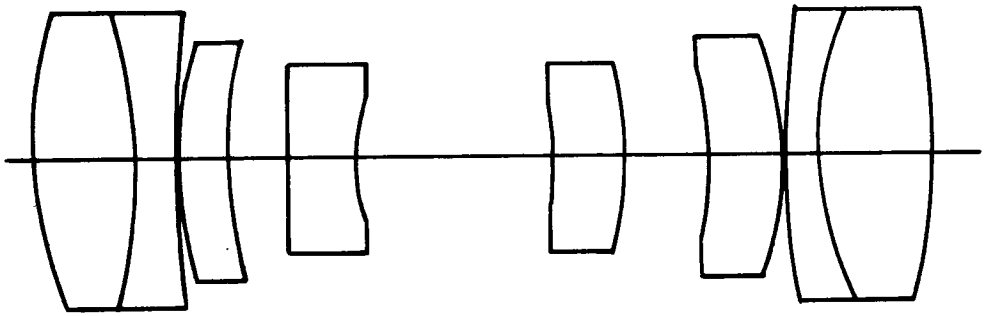

a) Refractive System

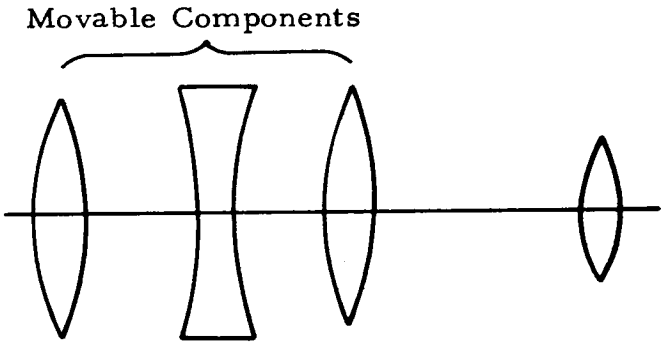

b) Zoom System

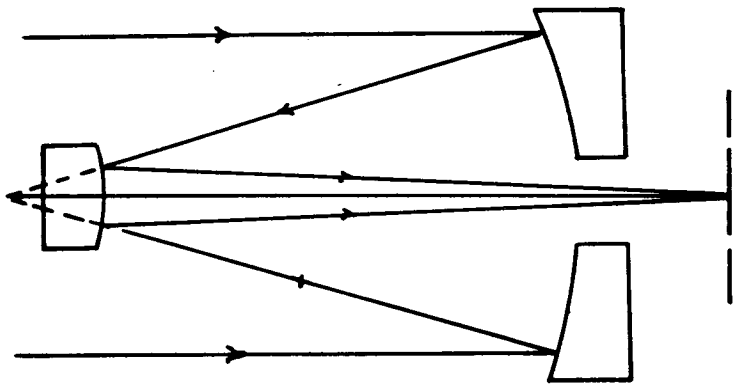

c) Reflective (Catoptric) System

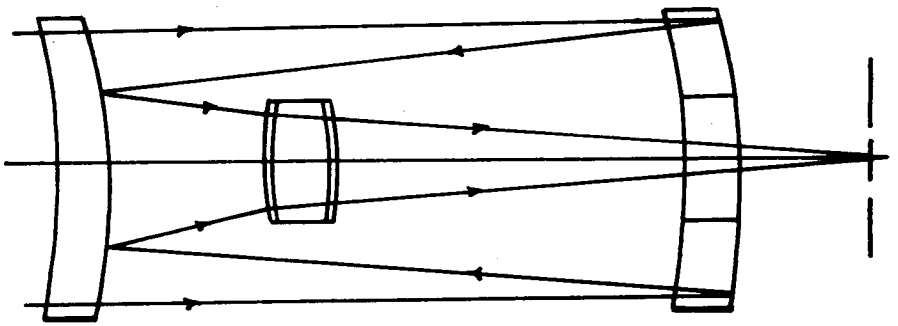

d) Catadioptric System

FIGURE 5-1 TYPICAL LENS SYSTEM TYPES

5.1.1.1 Refractive Lens Systems - Refractive (dioptric) lens systems are most commonly employed for applications requiring relatively short focal lengths and wide fields of view. However, despite excellent performance capability, especially in terms of resolution, speed and overall simplicity, refractive systems have limited application for long focal length systems because of their relatively large size and mass. Prime consideration must, of course, be given to both the size and mass requirements for the optical subsystem of a planetary imaging system.

A zoom lens is a refractive lens with a variable focal length and a zoom range equal to the ratio of the longest to the shortest focal length. Zoom lenses are generally classified according to the number of movable components the zoom system contains.

Primarily because of inherent focus problems, the definition and resolving power of zoom lenses are usually poorer than for equivalent non-zoom lenses. Greater spherical and chromatic abberations in zoom systems contribute to generally poorer performance. Pin cushion and barrel distortions are also evident at the extreme focal lengths of a zoom system. Therefore, despite the variable focal length advantage, zoom lenses are seldom selected for high performance photographic missions. Table 5-1 summarizes the relative advantages and disadvantages of zoom lens systems for the planetary imaging system application.

5.1.1.2 Reflective and Catadioptric Lens Systems - Reflective (catoptric) and catadioptric lens systems are primarily employed to satisfy long focal length, small field of view requirements. A purely reflective system usually uses a folded light path to provide an extremely long focal length (see Figure 5-1). The significant advantages of entirely reflective systems are the almost complete absence of chromatic abberation and the very uniform spectral response. Disadvantages include the curved field inherent on the image plane, the presence of central obscuration, more critical alignment requirements and the previously mentioned narrow field of view.

Catadioptric systems use a spherical mirror and an aspheric refractive corrector plate. The spherical mirror has a focal length and field curvature equal to one-half the mirror radius. The corrector is the aperture stop of the system. Its surface corrects the spherical abberation and its position is used to correct for coma. This type of system is often modified by the use of spherical corrector plates instead of the aspheric corrector plate to further reduce spherical abberation. The

TABLE 5-1 ADVANTAGES AND DISADVANTAGES OF ZOOM SYSTEMS

ADVANTAGES

- Requires less space than several lenses of different focal lengths
- Lighter than several lenses of different focal lengths
- Needs less support equipment than several lenses of different focal lengths
- Can provide constant surface coverage and scale for a varying altitude system
- Needs only one set of filters for multispectral imaging, whereas a multi-lens system would require several sets

DISADVANTAGES

- Requires critical focusing
- Yields poorer resolution than comparable fixed focal length system
- Yields more image distortion than comparable fixed focal length system
- More complex design

spherical abberation and coma correction capabilities of catadioptric systems provide significant advantages over purely reflecting systems.

Catadioptric systems are also folded systems. These systems have the advantage of usually being physically smaller and lighter than a comparable purely refractive system, especially for long focal lengths. On the other hand, the disadvantages of catadioptric systems include central obscuration, curvature of field, operation at a constant f/stop and the difficulty involved in placing filters.

Central obscuration degrades the lens performance and speed of a catadioptric system, particularly for f/numbers higher than about f/5. For equivalent f/stops, a catadioptric system would be approximately 25% slower than a comparable refractive system.

5.1.1.3 Comparison of Refractive and Catadioptric Lens Systems - The relative performance comparisons of refractive and catadioptric systems are presented in Table 5-2. Comparisons of the basic physical characteristics of these optical systems are presented in Table 5-3.

Relatively long focal length, fast lenses are required to obtain high ground resolution capability from orbital altitudes. However, in addition to these requirements, it is essential for the lens to exhibit near-zero aberrations over the usable field of view. Spherical aberration, coma, astigmation, and chromatic variations of these aberrations must be minimized. A long focal length, large aperture lens implies optics of considerable size and weight. These factors lead to a strong interest in reflective systems, where a chromatic focus is independent of wavelength, and small, light-weight mirrors are used. Broad optical system spectral response is desirable since ultraviolet, visible or infrared portions of the spectrum may be used.

Mass becomes a prime consideration whenever the relative merits of refractive and catadioptric optical systems are compared. This is especially true for space applications, since optical systems for such missions must have the lightest possible weight commensurate with adequate resolution performance and structural soundness.

Optical systems of the same type, aperture size and focal length may have significantly different masses. The mass of a particular optical system is directly related to the number of glass elements and mirrors required, the material used for the lenses and mirrors, and the barrel design and material. These, in turn, are a function of the spectral

TABLE 5-2 PERFORMANCE COMPARISONS OF REFRACTIVE VS. CATADIOPTRIC OPTICAL SYSTEMS

Parameters	Refractive System	Catadioptric or Reflective Systems
Resolution	X	
Speed	X	
Uniform Spectral Response		X
Alignment Tolerance	X	
Chromatic Aberration		X
Central Obscuration	X	
Contrast Rendition	X	

X indicates better relative performance

TABLE 5-3 PHYSICAL COMPARISONS OF REFRACTING VS. CATADIOPTRIC OPTICAL SYSTEMS

Parameters	Refractive System	Catadioptric or Reflective Systems
Size	Greater than catadioptric systems for relatively long focal lengths	Smaller than refracting systems for relatively long focal lengths
Mass	Greater mass for long focal length large aperture systems	Smaller mass for long focal length large aperture systems
Filter Mechanization	Easier to employ filters	More difficult to employ filters (because of relatively large outside diameter)
Reliability	Greater reliability since refractive system is less complex	Less reliability because of additional complexity
Lifetime	Probably longer since complexity is less and no dielectric mirror coatings are involved	Probably shorter due to complexity, critical alignment tolerances, and nature of coated surfaces

region of operation and the field of view, resolution and structural support requirements.

Materials available for optical systems are limited, but mass ratios between materials can still be high. Reflective and catadioptric systems employ glass lenses and aluminum or beryllium mirrors, whereas refractive systems employ only the higher density glass for the required lens elements. Aluminum or beryllium are generally used for lens barrels.

The characteristics of various representative long focal length refractive lens systems are presented in Table 5-4. Similarly, the characteristics of catadioptric systems are presented in Table 5-5. The lenses listed in the two tables are either currently available or designed. The characteristics of some other lenses have not been presented either because the data is proprietary or classified. (Note: The basic relationship between the F/number, aperture size and focal length of a lens is discussed in Section 5.1.2.)

The data in Figure 5-2 illustrates the relative aperture size versus mass relationships for the refractive and catadioptric lenses listed in Tables 5-4 and 5-5, respectively. The lines shown for the two optical system types were drawn using the plotted data points as guides, but were biased slightly in the optimistic direction to account for optical system mass reduction capabilities anticipated for the future.

5.1.2 General Optical Subsystem Parameters

Optical subsystem parameters must be established in order to specify system performance. In particular, the optical subsystem constraints on ground resolution, total ground coverage and image quality, which must be considered, are discussed in the following subsections.

5.1.2.1 Focal Length and Resolution Considerations - The ground resolution obtainable from a planetary orbiting vehicle is a function of the vehicle altitude above the planet surface, the imaging system resolution and the focal length of the optical subsystem. This relationship can be expressed as:

$$G = \frac{h}{f \cdot R} \qquad (5-1)$$

TABLE 5-4 LONG FOCAL LENGTH REFRACTIVE LENS SYSTEMS

Manufacturer	Aperture Size (mm)	Focal Lenth (mm)	F/Number	Mass (kg)
Itek Corp.	94	330	f/3.5	2.7
Pacific Opt. Corp.*	105	610	f/5.6	6.0
Bausch & Lomb	125	510	f/5.6	4.0
Itek Corp.	174	610	f/3.5	8.6
Bausch & Lomb	178	1020	f/7.0	6.8
Fairchild Space & Defense Systems	260	915	f/3.5	27.6
Bausch & Lomb	282	2000	f/7.2	63.0
Fairchild Space & Defense Systems	305	1220	f/4.0	51.5
Contraves	414	2400	f/5.8	195.0
Perkin-Elmer Corp.	457	1830	f/4.0	675.0

* (Lunar Orbiter Lens)

TABLE 5-5 LONG FOCAL LENGTH CATADIOPTRIC LENS SYSTEMS

Manufacturer	Aperture Size (mm)	Focal Length (mm)	F/Number	Mass (kg)
Celestron Pacific	89	800	f/9	1.6
Zoomar Inc.	91	510	f/5.6	1.4
Wollensak Optical	104	510	f/6.3	3.0
Wollensak Optical	145	1020	f/8.0	5.7
Zoomar Inc.	159	510 & 1020	f/4.0, f/8.0	3.1
Fairchild Space & Defense Systems	174	610	f/3.5	8.2
Fairchild Space & Defense Systems	203	508	f/2.5	9.5
Celestron Pacific	255	510	f/2.0	29.4
Fairchild Space & Defense Systems	305	1220	f/4.0	45.4
Nortronics	510	5100	f/10	155.0

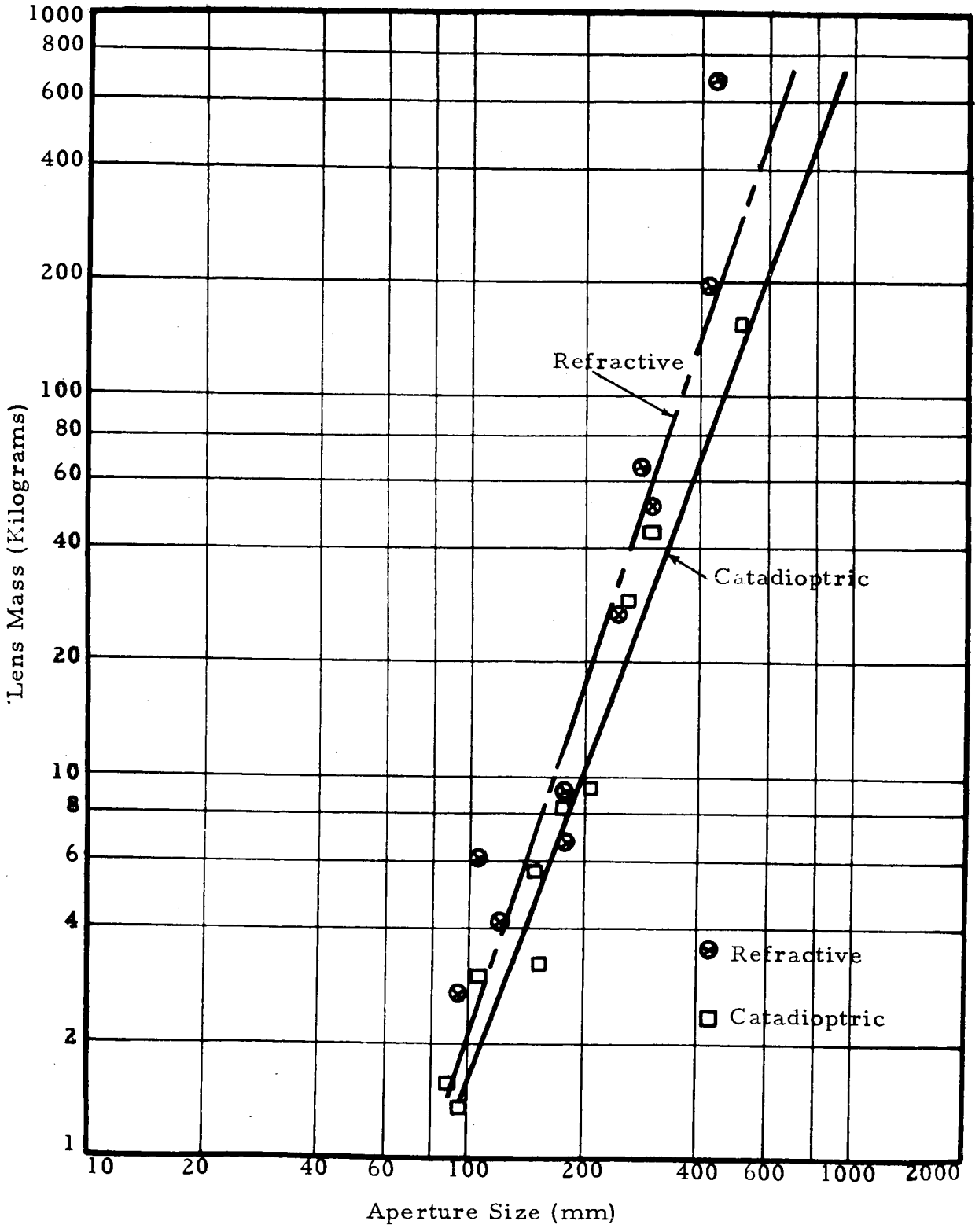

FIGURE 5-2 APERTURE SIZE VS. MASS FOR REFRACTIVE AND CATADIOPTRIC OPTICAL SYSTEMS

where G = ground resolution (meters)
h = altitude above surface (kilometers)
f = focal length (meters)
R = imaging system resolution (line pair/mm)

Figure 5-3 illustrates this relationship for altitudes of 300, 600, 900 and 1200 km. System resolutions of 50, 100 and 200 line pair/mm are considered. Figure 5-4 presents the same relationship with ground resolution as a function of altitude for various focal lengths and a fixed system resolution of 100 line pair/mm.

Assuming a 100 line pair/mm system resolution capability, a 2 meter lens focal length would be needed to satisfy a 5 meter ground resolution requirement for a nominal 1000 km altitude. This same system would provide a ground resolution capability of 2.5 to 7.5 meters for altitudes varying from 500 to 1500 km and a capability of 5 to 15 meters for altitudes varying from 1000 to 3000 km. Even longer focal length lenses would be required for poorer system resolution capabilities.

For a medium ground resolution requirement, say in the order of 50 meters, a 100 line pair/mm system would require a lens focal length of 0.2 meter from the nominal altitude of 1000 km. Similarly, a 0.4 meter focal length lens would be required if the system resolution capability was reduced to 50 line pair/mm. Assuming a 50 line pair/mm system resolution, the 0.4 meter focal length lens would provide a ground resolution of 25 to 75 meters for altitudes varying from 500 to 1500 km and a capability of 50 to 150 meters for altitudes varying from 1000 to 3000 km.

The shorter focal length requirements indicate the possible use of a small, light refractive optical subsystem for a medium resolution system.

5.1.2.2 Format and Coverage Considerations - The choice of sensor format size is a function of the lens focal length and the desired ground coverage. Figure 5-5 relates the basic lens parameters of F/number, aperture size and focal length. In addition, the achievable system lateral field of view is given for format sizes of 25 and 57 mm. (Note: As indicated in Section 6, the standard useful format size for 35 mm film and 2-inch vidicon and return beam vidicon tubes is 25 mm; the standard for 70 mm film is 57 mm.) The lateral field of view is given by:

$$\theta = 2 \tan^{-1} \frac{\ell}{2f} \qquad (5\text{-}2)$$

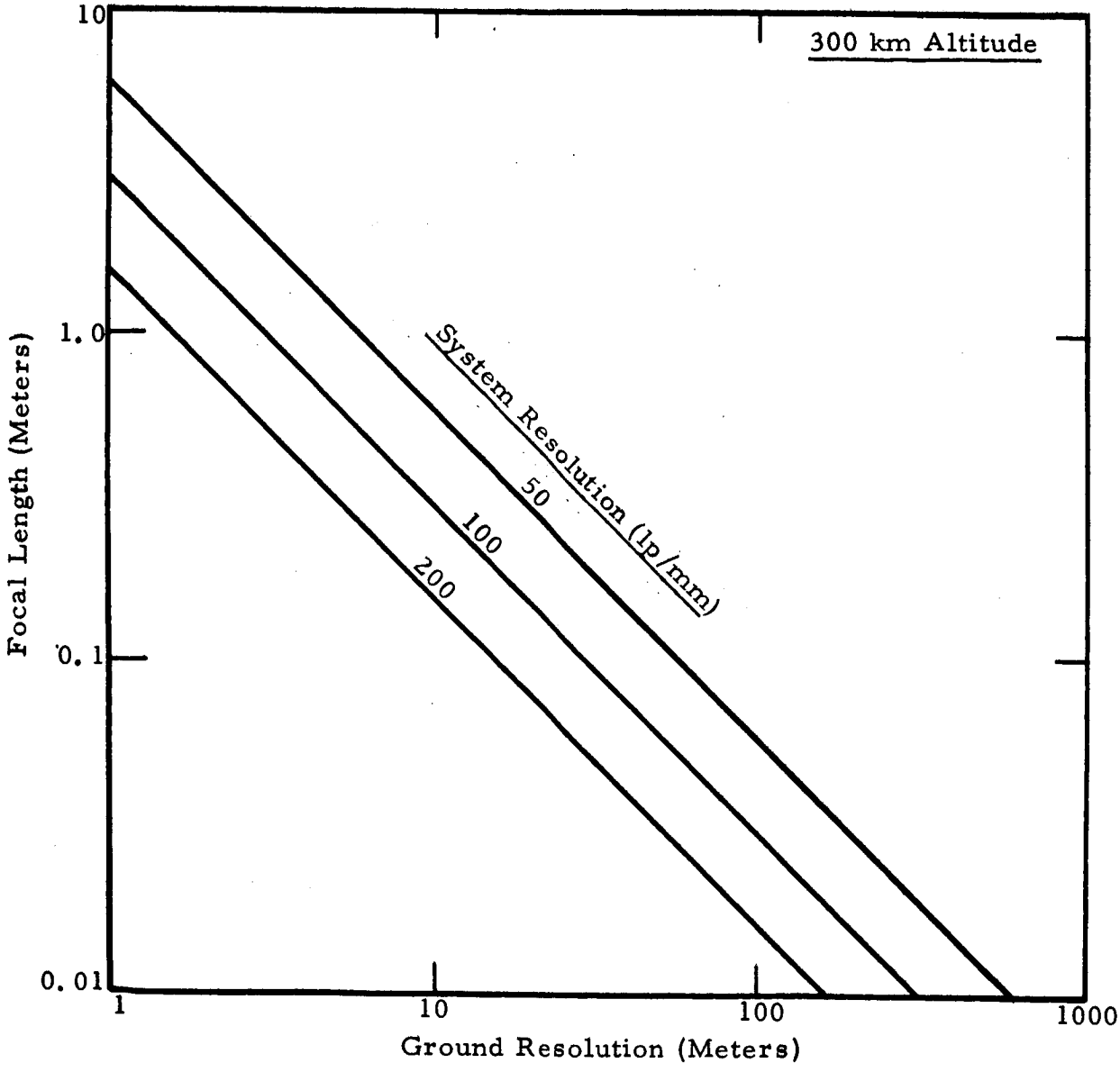

FIGURE 5-3a FOCAL LENGTH VS. GROUND RESOLUTION FOR 300 KM ALTITUDE

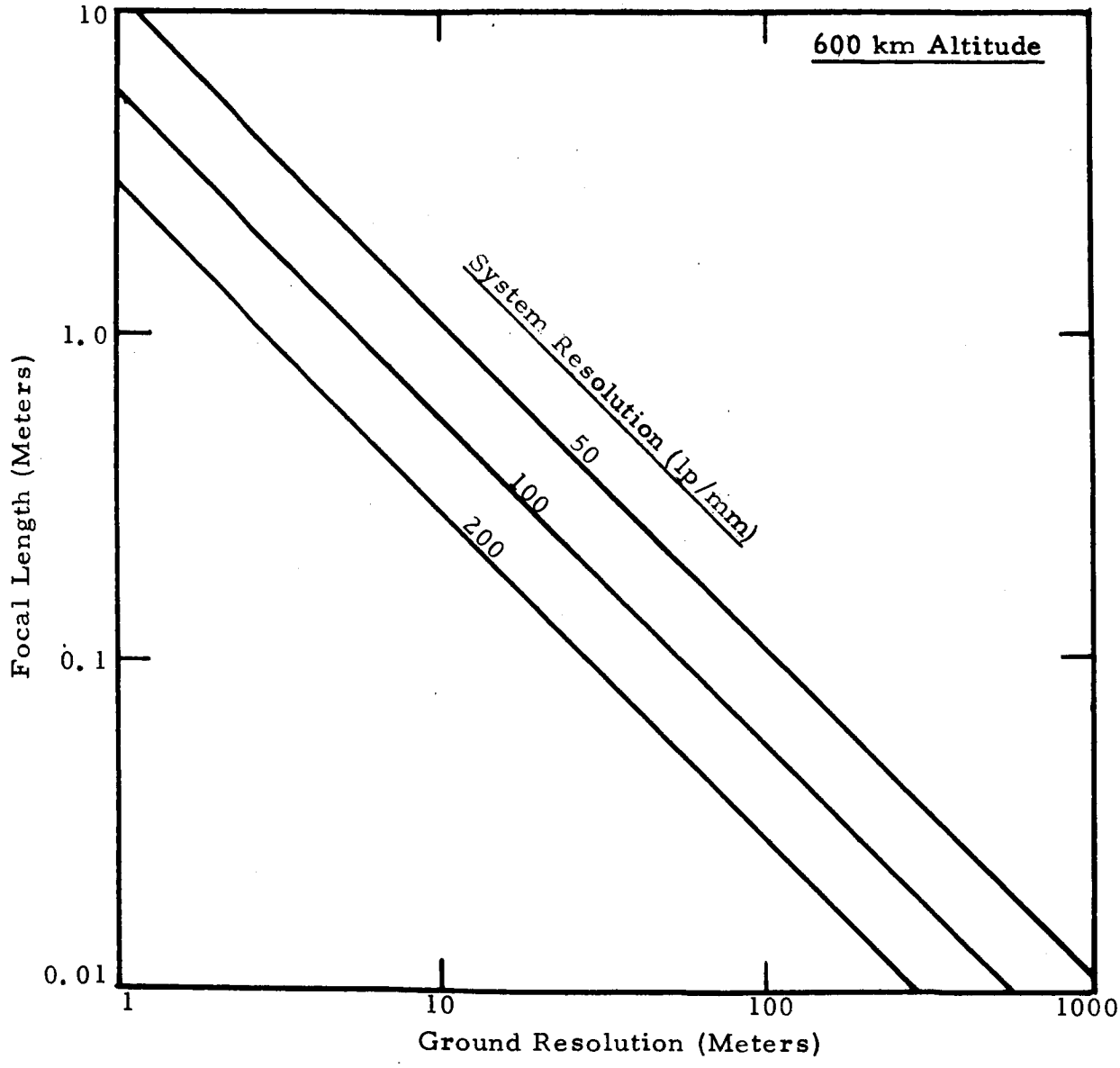

FIGURE 5-3b FOCAL LENGTH VS. GROUND RESOLUTION FOR 600 KM ALTITUDE

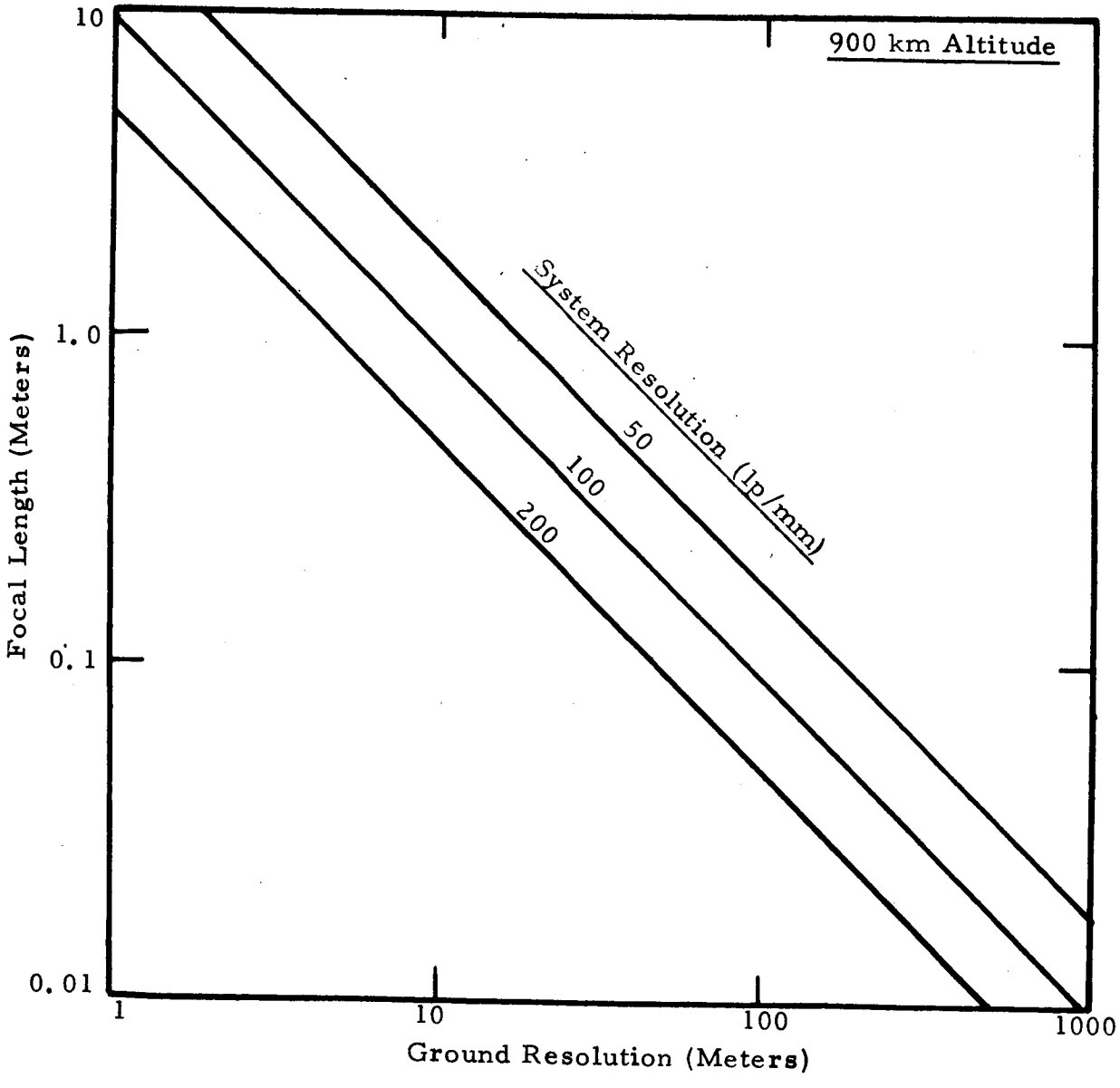

FIGURE 5-3c FOCAL LENGTH VS. GROUND RESOLUTION FOR 900 KM ALTITUDE

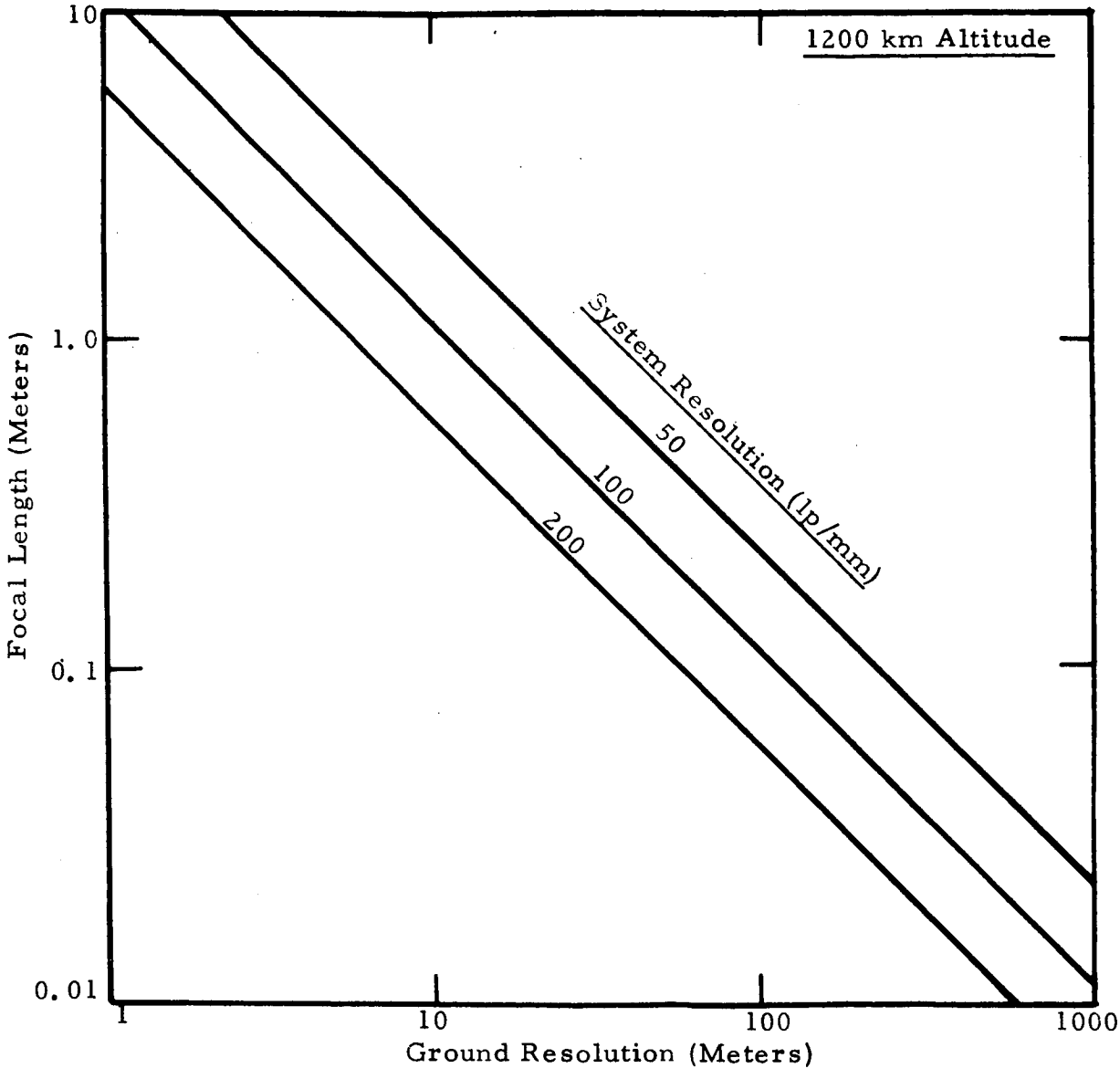

FIGURE 5-3d FOCAL LENGTH VS. GROUND RESOLUTION FOR 1200 KM ALTITUDE

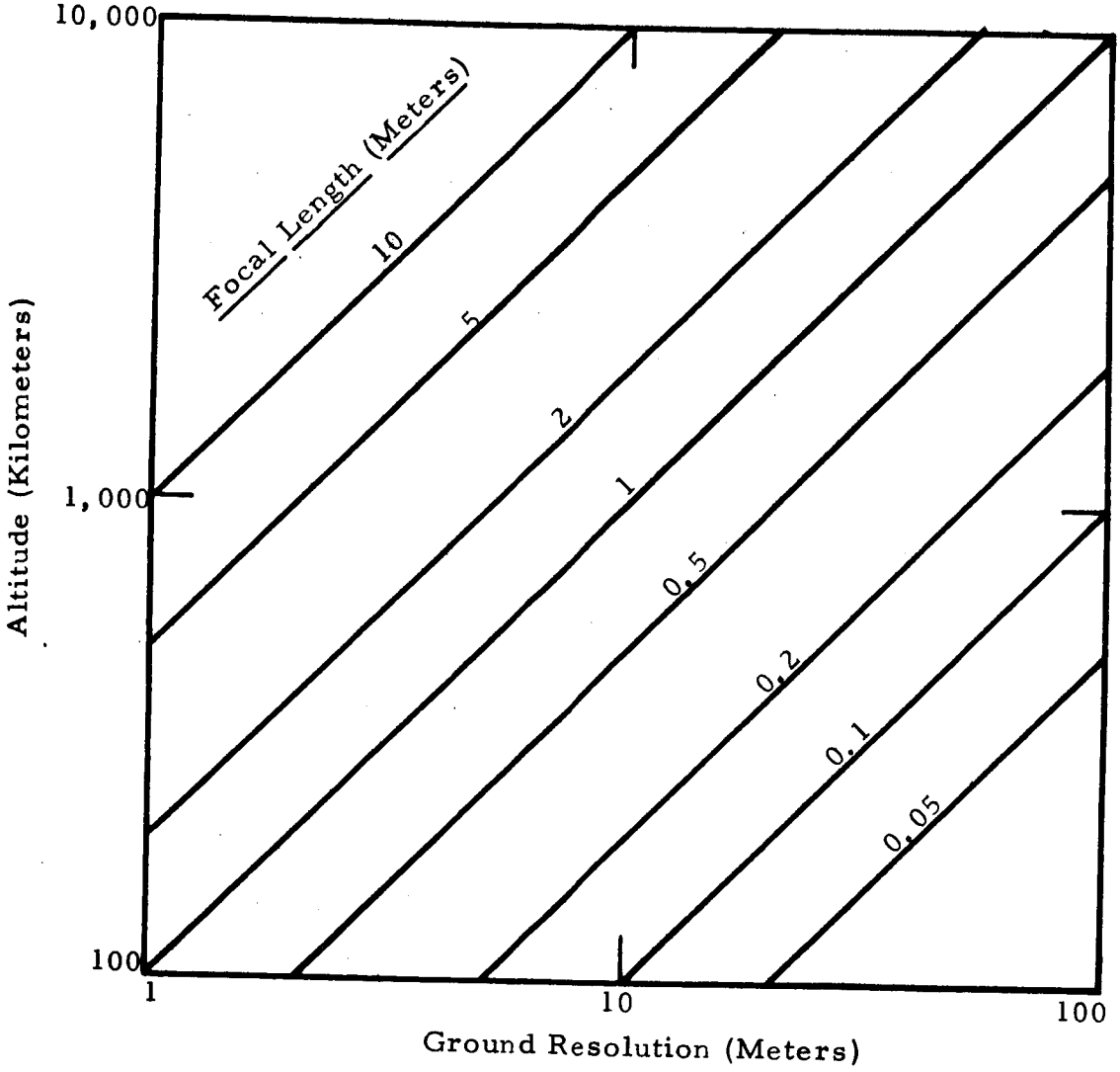

FIGURE 5-4 GROUND RESOLUTION VS. ALTITUDE FOR 100 LP/MM SYSTEM

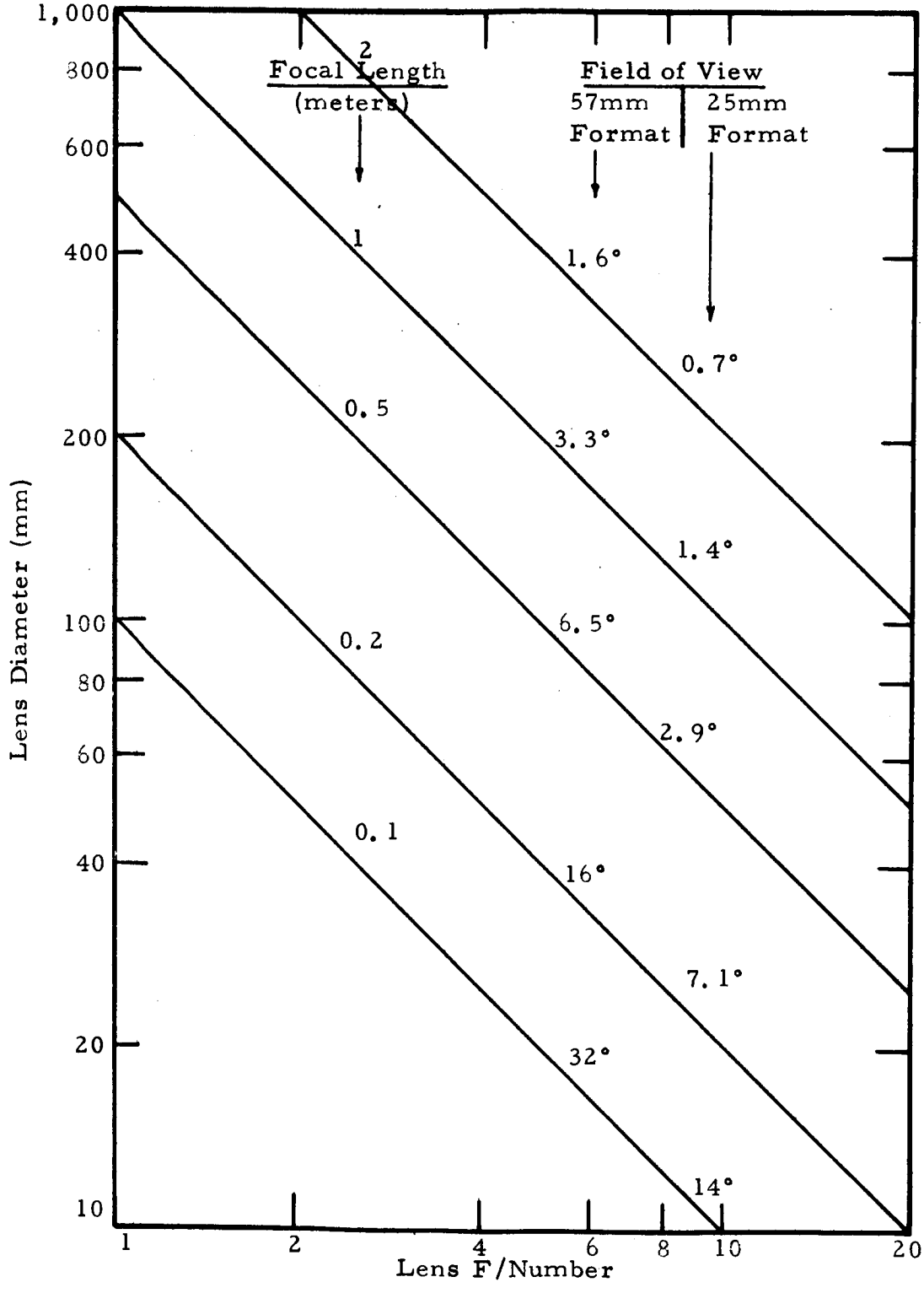

FIGURE 5-5 BASIC LENS PARAMETERS AND FIELD OF VIEW

where θ = field of view (degrees)

ℓ = format size (meters)

The lateral ground coverage of an optical imaging system, L, is given by:

$$L = \frac{\ell \cdot h}{f} \text{ (kilometers)} \qquad (5\text{-}3)$$

The lateral ground coverage as a function of altitude and focal length is illustrated in Figures 5-6a and 5-6b for 25 and 57 mm formats, respectively. The planet surface area covered per circular orbit is presented in Appendix B as a function of sensor field of view and orbit altitude.

A series of factors must be considered in selecting the format size for an imaging system. Comparisons showing the relative advantages of large versus small format sizes are presented in Table 5-6. The actual format size selection must be determined as a result of trade-offs, wherein mission requirements and sensor capabilities are carefully analyzed.

TABLE 5-6 COMPARISONS OF LARGE AND SMALL FORMAT SIZES

Factor	Larger Format Size	Smaller Format Size
Ground coverage (same lens focal length and altitude)	X	
Exposure accuracy (using automatic exposure control)		X
Number of exposures required	X	
Cycling rate requirements	X	
Image Motion Compensation		X
Mosaic making suitability	X	
Metric mapping use	X	
Stereo suitability	X	

X indicates preferred format size for each factor listed

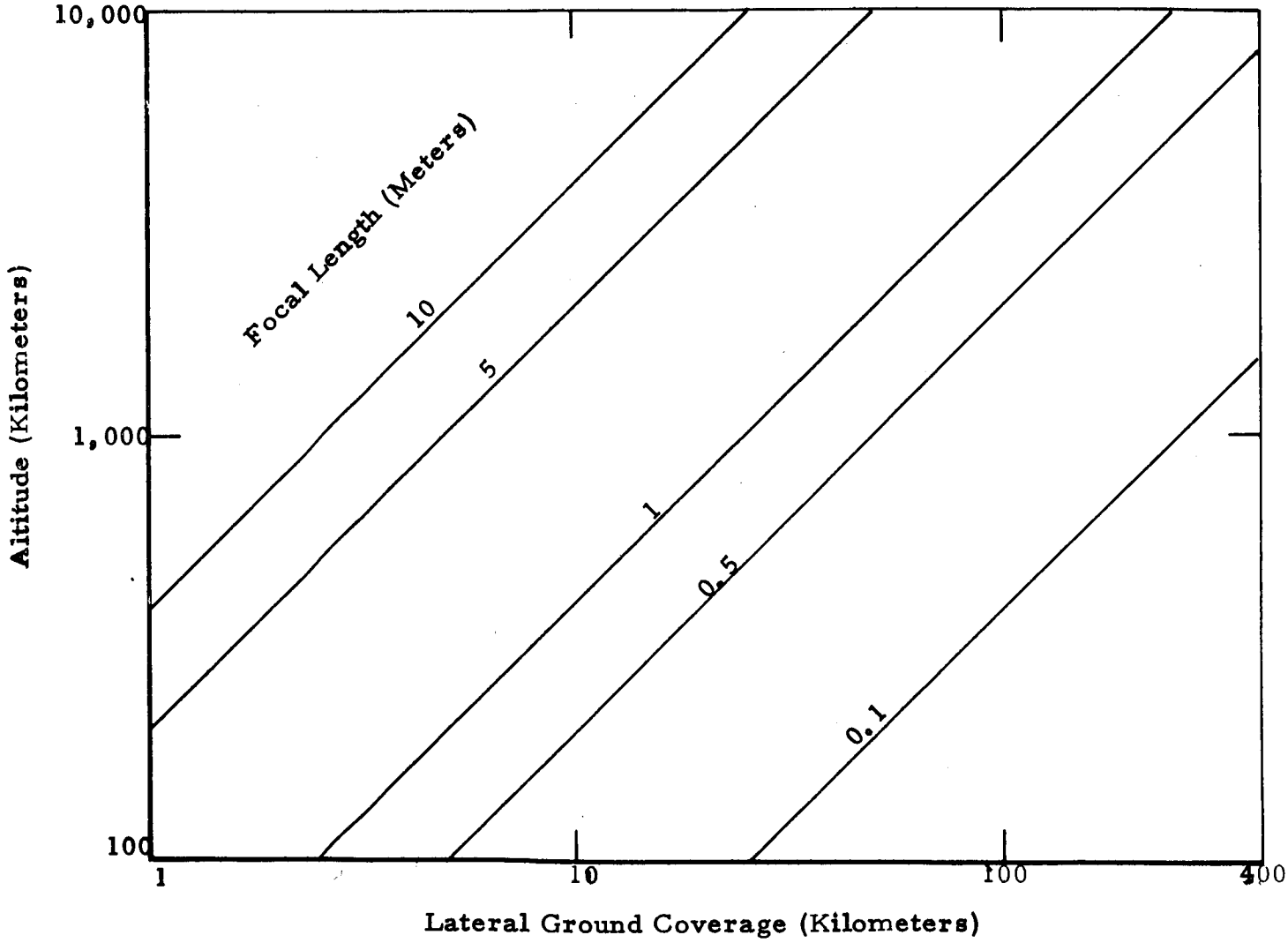

FIGURE 5-6a LATERAL COVERAGE VS. ALTITUDE (25 mm Format)

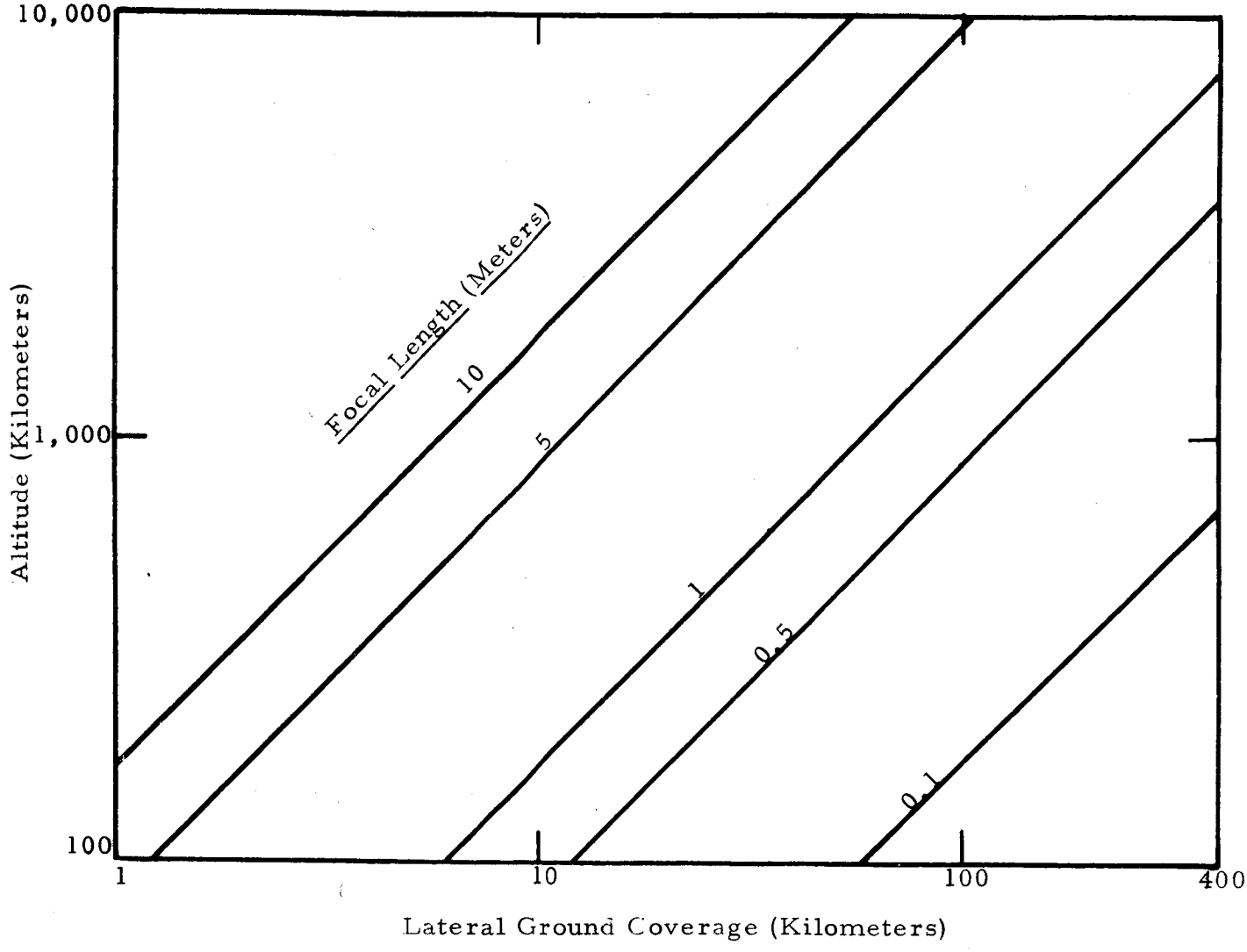

FIGURE 5-6b LATERAL COVERAGE VS. ALTITUDE (57 mm Format)

5.1.2.3 Exposure Time and Image Blurring Considerations - The primary causes of image blurring or smear in photography are atmospheric turbulence and vehicle velocity, rotation and vibration. Atmospheric turbulence is not a significant problem for Martian orbital imaging missions because of the tenuous atmosphere of Mars (Ref. 5-1). For many spacecraft applications, vibration is not a significant factor when compared with other causes of image blur. Because of this, and due to its dependency on photosystem mounting and other considerations peculiar to the particular spacecraft configuration involved, vibration is not considered further in this report. Exposure time, image motion compensation and vehicle stability are factors which must be considered.

Exposure time, a function of photosensor sensitivity, lens T/number and scene brightness, is expressed by:

$$t_e = \frac{4ET^2}{\pi B} \tag{5-4}$$

where

t_e = exposure time (seconds)

E = sensitivity (meter-candle-seconds)

T = lens T/number

B = scene brightness (candela/meters^2)

In the case of silver halide films, the sensitivity is generally expressed in terms of the Aerial Exposure Index (AEI). The exposure time in terms of the AEI can be approximated by:

$$t_e \cong \frac{3.2T^2}{\pi B(AEI)} \tag{5-5}$$

The nomograph in Figure 5-7 can be used to quickly determine the approximate exposure time if the sensor sensitivity, lens T/number and scene brightness are known. For purposes of illustration, assume a scene brightness of 700 candela/meter^2, lens T/number of 7 and an AEI of 3 for film (equivalent by Equation 5-6 to 0.269 meter-candle-seconds). A vertical line is drawn from the top scale of scene brightness until it intersects with the appropriate T/number line. From this intersection, a line is drawn horizontally until it intersects with the chosen sensor sensitivity line. From this intersection, a vertical line is drawn to the bottom scale of exposure time. The intersection of this line on the exposure time scale gives 0.025 second or 1/40 second as the correct value of exposure time.

The forward movement of the vehicle causes motion of the image which can be compensated by translational movement of the lens or photosensor. The amount of forward motion compensation (FMC) necessary is:

$$FMC = \frac{V_g \cdot f \cdot \cos \phi}{h} \qquad (5\text{-}6)$$

where

FMC = true rate of forward motion compensation (meters/second)

V_g = true ground velocity (meters/second)

f = focal length (meters)

ϕ = oblique angle between vertical and sensor line of sight

h = altitude above surface (meters)

The degree to which forward vehicle motion can be compensated depends upon the accuracy of the FMC device and the velocity/altitude sensor, as well as variations in the ground topography. For oblique systems, image motion compensation cannot be totally achieved with one directional FMC, since the image velocity is variable over the format.

The graph in Figure 5-8 is useful as an approximation of the allowable FMC error to obtain typical ground resolutions. The criterion

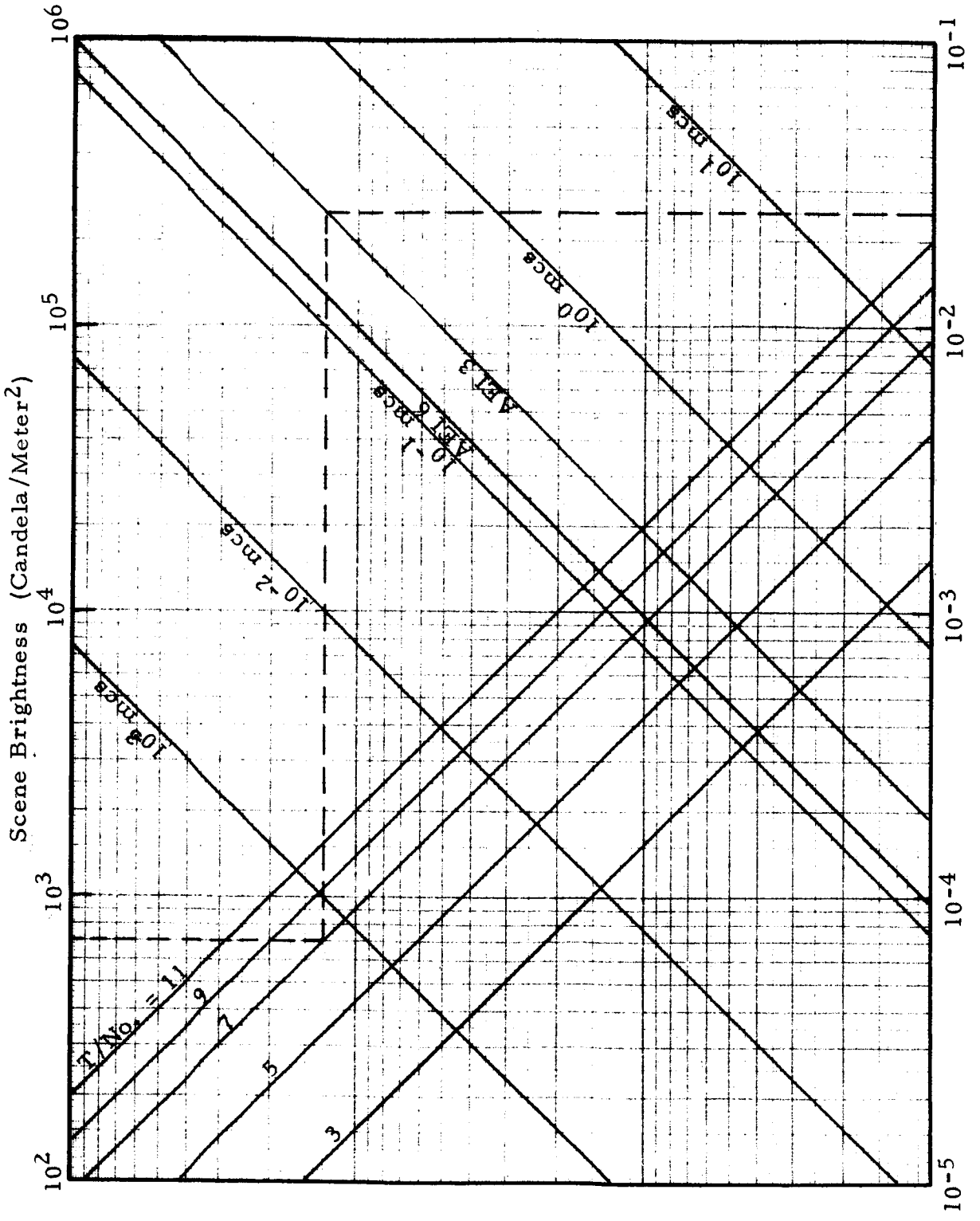

FIGURE 5-7 EXPOSURE TIME NOMOGRAPH

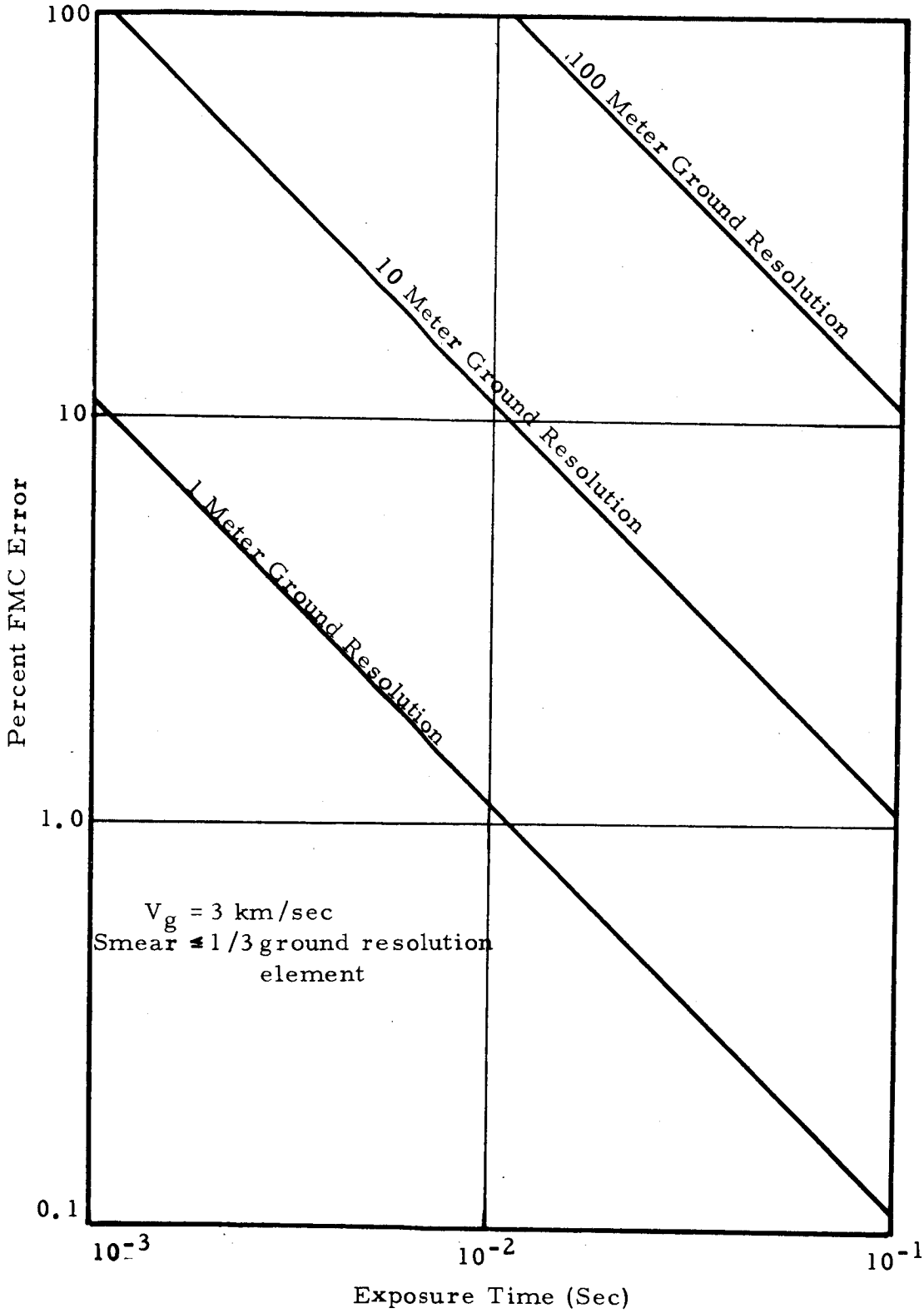

FIGURE 5-8 ALLOWABLE FMC ERROR VS. EXPOSURE TIME

assumed is that motion in the object plane can be no greater than one-third of the desired object resolution on the ground; for the graph, a 3 km/sec ground velocity is assumed, since this is a typical value for the anticipated missions (see Section 4). The limitation on FMC error allowed, F_e, is expressed as:

$$F_e \leq \frac{G}{3 V_g \cdot t_e} \tag{5-7}$$

The compensation techniques generally used to provide one-dimensional IMC (or FMC) for film systems are to move the platen or optical subsystem. Two dimensional IMC, if required can also be provided in the same manner. The state-of-the-art of FMC for film cameras is currently about 0.1% (Ref. 5-2, 5-3), however significant degradation results from slant range and elevation differences within the scene.

Electronic IMC for image amplifier cameras has been demonstrated by Fairchild Camera under contract to the Air Force (Ref. 5-4). The report on the study points out however, that to realize the advantages of the simplicity of electronic as opposed to opto-mechanical IMC, the image tube should not contain any magnetic materials.

An analysis of the non-uniform image motion on the sensor of an orbital camera system is presented in Appendix D.

Random vehicle motion also causes blurring of the image and loss of resolution. However, only the rotational component of the motions has a serious effect on the resolution. The translational components of random motion are negligible since they are reduced by a factor equal to the focal length/attitude ratio. A knowledge of the estimated rotational velocities allows for computation of the loss of resolution in the direction of blur.

Considering vehicle stability in the form of rotational motions, an estimate of the requirement to limit smear is shown graphically in Figure 5-9. A requirement for an object smear due to the RMS stability rate of the vehicle, $\dot{\phi}$, of less than one-third the desired ground resolution has been assumed. This limitation is:

$$\dot{\phi} \leq \frac{G}{3 h t_e} \text{ (radians/second)} \tag{5-8}$$

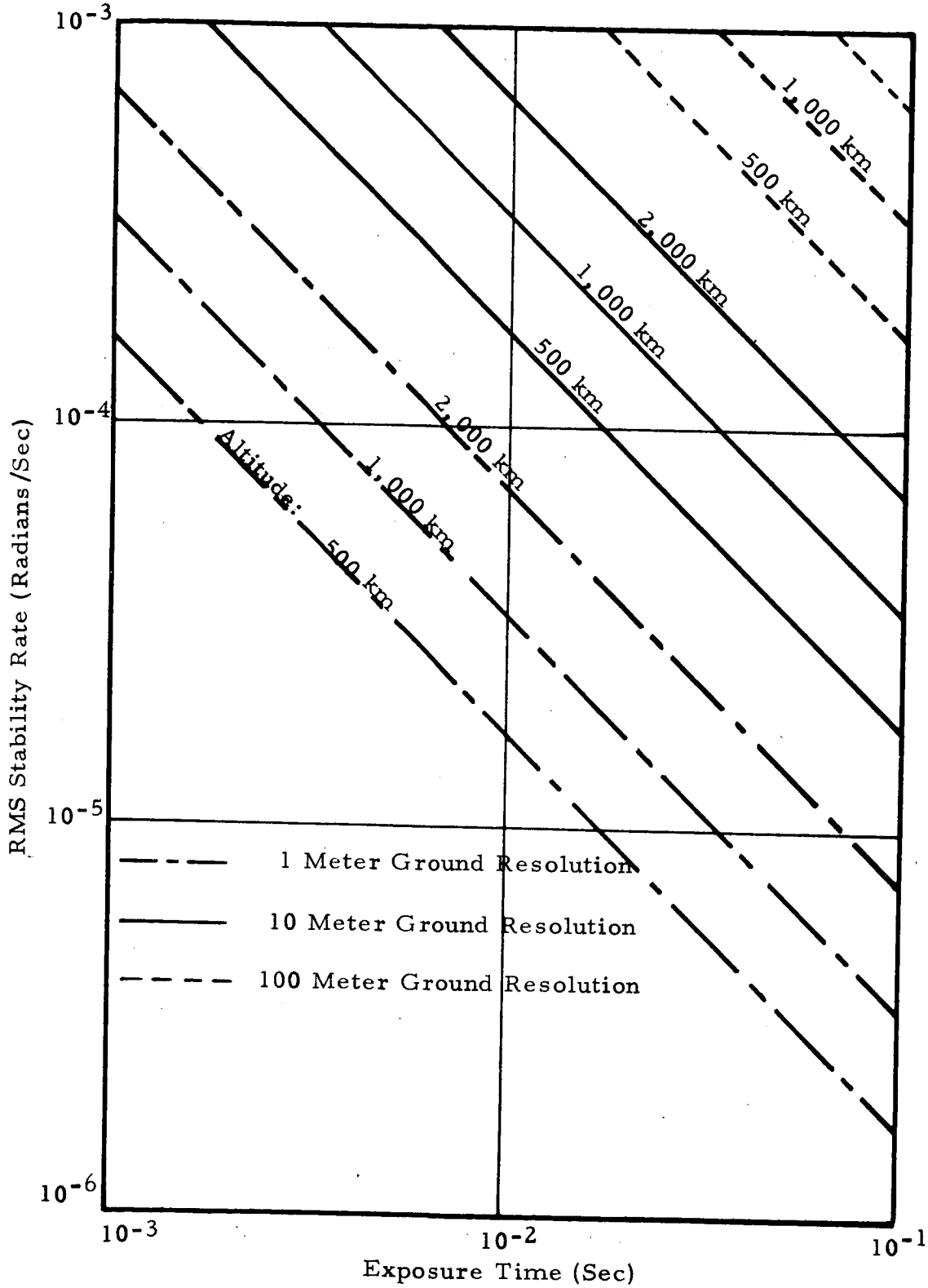

FIGURE 5-9 VEHICLE STABILITY RATE REQUIREMENTS VS. EXPOSURE TIME

5.1.3 Imaging System Thermal Considerations

Thermal environmental control is anticipated in order to satisfy the requirements of the Martian orbiting photographic system.

5.1.3.1 Thermal Environment - Environmental control is necessary during the Earth to Mars transfer phase of the mission and during the reconnaissance portion of the mission when the vehicle is in orbit about Mars. During the initial planetary transfer phase of the mission, the heat load will probably be primarily due to solar radiation. The control level is a function of this exposure and the physical construction of the vehicle.

While in orbit about Mars, the environmental control system must contend with varying heat fluxes which could otherwise produce stability problems in the optical assembly, and possibly effect the method of film processing, if any (see Section 6.2). For instance, due to the variation of the Mars to Sun distance, from approximately 1.38 AU to 1.67 AU, solar radiation on the vehicle is expected to vary from 735 to 500 watts per square meter. In addition, as shown in Table 5-7, the heat flux due to thermal radiation and albedo from Mars for a non-circular orbit is a function of altitude (Ref. 5-5).

It is important to note that a significant temperature-height profile exists for the Martian atmosphere (see Figure 2-3). However, since the pressure at the surface of the planet is extremely low (approximately 3 to 8 millibars), it is expected that little or no convection effect will be experienced by the spacecraft at the orbital altitudes of interest for the imaging mission.

Consideration must also be given to the change in thermal load created by the passage of the vehicle into the shadow of the planet. If the chosen orbit dictates that such a condition is likely, the thermal control system must have the reserve to offset this effect, so that only acceptable temperature shifts and gradients are impressed upon the system.

5.1.3.2 Lens Thermal Gradients - Temperature changes produce two basic geometrical alterations which are detrimental to the performance of an optical system, (Ref. 5-6). The shape of individual lens elements changes, and the position and attitude of individual elements change with respect to each other.

TABLE 5-7 MARTIAN THERMAL RADIATION AND ALBEDO ON A SPHERICAL SATELLITE

(Albedo = 1.5; Solar Radiation = 600 watts/m^2; Thermal Radiation Flux = 128 watts/m^2)

Altitude (km)	Thermal (watts/m^2)	Albedo (watts/m^2)
200	168	122
400	140	99
600	120	84
1,000	93	63
4,000	29	24
8,000	11	7
20,000	3	2

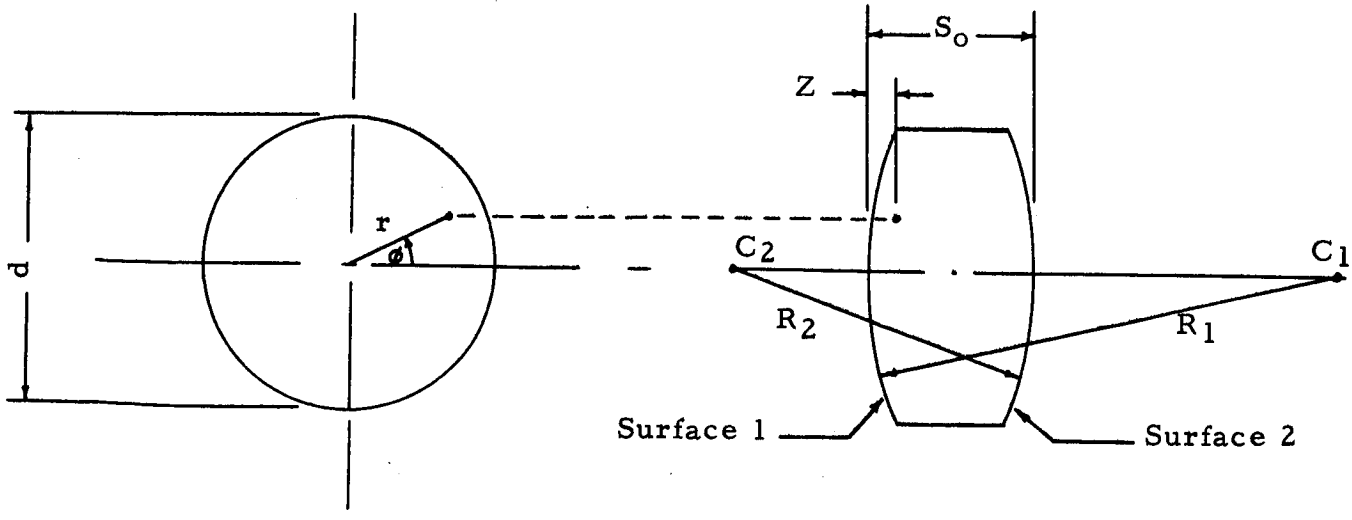

FIGURE 5-10 LENS NOMENCLATURE FOR THERMAL ANALYSIS

A thermal gradient within an element, in its most general form, can be expressed as some function of the semiaperture distance (r), the angular position in the plane of the element (∅), and the axial station along the optical centerline (Z). Hence, the temperature gradient is represented in mathematical cylindrical coordinate notation as $T = T(r, \emptyset, Z)$.

For the gradient condition indicated and the element configuration shown in Figure 5-10, the result, geometrically speaking, is the formulation of two aspheric surfaces with no axis of symmetry. This highly complex geometrical configuration should be avoided.

In contrast, if the thermal gradient is dependent on axial and angular position such that $T = T(r)$, the resulting surfaces are aspheric, but symmetrical about the optical axis. This condition can be readily addressed analytically (Ref. 5-6) and the solution for the optical performance of any assembly of this type of aspheric falls within present computer program capability.

As previously mentioned, the presence of thermal gradients in the barrel of a lens assembly relates directly to interelement geometry. Again in the most general sense, if the thermal gradient is expressed in cylindrical coordinates, the magnitude and character of the gradients produce a state of stress which ultimately results in linear and rotational displacements of the elements.

The most desirable thermal map one can achieve is a state of uniform temperature, independent of time. Realistically, however, this condition is unattainable due to the space, weight, and power limitations imposed upon the thermal control system, which must operate in the face of varying thermal loads. The best compromise is the system which controls the temperature within specified workable limits.

5.1.3.3 Thermal Design Considerations - An optical system design should reflect an awareness for minimizing dimensional changes as a result of thermal stimulation. This can be best accomplished by:

- Selection of surface finishes which have the desired heat absorption properties.

- Construction of thermal conduction barriers to isolate elements which are sensitive to temperature variation from external heat sources and internal power dissipators.

- Creation of highly conductive thermal shunts to divert heat from critical areas and establish efficient paths to prechosen sinks.

- Matching of linear coefficients of thermal expansion of interfacing materials to minimize thermal stresses and distortions.

- Establishment of the assembly configuration in a symmetrical pattern with respect to the thermal loads and sinks, thus avoiding complex temperature gradients.

The general approach to the problem of thermal control is closely related to the anticipated environment and the particular system configuration. The design of the environmental control system should take place after an examination of the thermal map obtained by simulating the assembly with a nodal network and impressing it with idealized thermal loads created by the environment and internal dissipators. The optical performance of this system can then be examined in an attempt to identify the thermal problem areas, the most sensitive components, and the degree and location in which control must be exercised in order to obtain acceptable system performance.

5.1.4 Lens/Camera Calibration

Lens/camera calibration is an essential procedure especially for a mapping camera system. The imaging system characteristics determined during calibration include geometric constants and the image quality as recorded on a specified sensor. Image quality is generally presented in terms of resolution obtained from standard bar type resolving power targets or in terms of frequency response to sine wave or square wave targets (modulation transfer function).

Geometric data provides significant information with regard to the relationship of the lens to the focal plane and fiducial markers. Flatness of the image platen (in the case of film) must be determined, as well as the proper focal length for optimum distribution of radial distortion. Calibration constants are thus established for a specific camera combination so that measurements on images produced with that combination may reliably be used to accurately determine the size, shape, and position of imaged ground objects.

Two standard testing techniques are used for calibration. An array of targets at known angles can be imaged at the image plane of the

camera system and measured to provide calibration data. Alternatively, a calibrated grid can be placed in the focal plane of the system and projected through the lens for measurement in the object space.

Standard lens/camera characteristics that should be determined during calibration are:

- equivalent and calibrated focal lengths
- average radial distortion
- indicated principal point
- distance between opposite fiducials
- angle between lines drawn from opposite fiducials
- principal point of autocollimation
- average resolution (reporting resolution on radial and tangential lines separately) at specified lens field angles
- magnitude of the bent axis or prism effect.

In addition, the asymmetric characteristics of the lens/camera should be determined. These include the location of the principal point and point of symmetry, tangential distortion, radial distortion referenced to the format area, platen contour and fiducial positions referenced to a rectangular coordinate system.

Standard equipment needed for lens/camera calibration includes a photogoniometer (an angle-measuring device of first-order accuracy) or a multiple-collimator calibrator. A precision comparator is required along with these calibration instruments. A calibrated bank of collimators is used by Fairchild Space and Defense Systems to test imaging lens/camera systems in its Space Environments Laboratory.

5.2 STEREO INSTRUMENTATION

The two major stereo instrumentation criteria involve the percentage of forward overlap and the base/height ratio between the two stereo photographs (i.e., ratio of baseline distance between successive exposure stations to the flight height above the ground). The overlap percentage is simply a function of the pertinent cycling rate and various camera parameters (Ref. 5-7).

The factors influencing the choice of the most suitable base/height ratio include securing maximum parallax (i.e., the apparent displacement of the position of a body with respect to a reference point caused by the shift in the point of observation), reducing the camera lens distortion effect to a minimum, and assuring ample stereoscopic coverage and maximum area coverage within the stereoscope model. The most accurate stereo data is acquired under conditions of greatest parallax, normally obtained by making the air base as long as possible. However, the amount by which the base is lengthened is limited by the corresponding loss of stereo coverage.

Stereoscopic perception is best when the base/height ratio is between 0.33 and 1.2(i.e., convergence angles between 18 and 60 degrees). Consequently, acquisition systems programmed to collect stereo coverage generally operate within this range. However, a base/height ratio of 0.65 is commonly considered to be optimum.

There are two basic methods employed to acquire stereo data: simultaneous or consecutive. The simultaneous method requires two individual camera stations (possibly in separate vehicles) with enough separation to properly acquire corresponding images of the surface area at the same instant. In general, the simultaneous method is not considered suitable, not only because of the requirement for two vehicles, but also because it involves attendant complications in both synchronization and coordination. That is, a means must be provided to insure that the individual cameras are viewing the same surface area at the time of exposure.

The consecutive method involves taking overlapping images from a single moving station, with the required separation of observation points determined by the velocity of the vehicle and the time between exposures. Optimum stereoscopic viewing is achieved when each photograph overlaps the next by 50 to 60% in the direction of flight. This overlap makes the corresponding images suitable for

stereoscopic study, wherein the terrain can be viewed in relief perspective.

Several different techniques can be employed for obtaining stereoscopic information by the consecutive method. Three of the most common make use of the vertical frame, panoramic or twin convergent camera configurations. The proven vertical frame camera is recommended for obtaining the required medium resolution stereo coverage because the resulting image scale is fairly uniform and geometric distortions are at a minimum. The panoramic camera, on the other hand, may not be well suited for obtaining medium resolution stereo images because of inherent problems in geometric distortion, scale variation and excessive corresponding image overlapping at the format edges.

The use of a vertical frame camera to obtain stereo coverage is limited in a high resolution mode when a relatively long focal length lens is used. In such a long focal length system, for a fixed format and specified overlap, the ground coverage, base length and consequently the parallax are substantially reduced.

The twin convergent camera configuration makes use of two frame cameras, one pointing down and to the front of the vehicle and the other pointing down and to the rear. Both cameras photograph the area of interest, thereby achieving maximum overlap and sufficient parallax. A convergent twin camera system can be considered for this application only if high resolution stereo imagery of specific areas is required and if the additional weight imposed by a second camera can be tolerated.

5.3 MULTISPECTRAL IMAGING INSTRUMENTATION

The use of multispectral filters to obtain spectral response data of the Martian terrain and atmosphere can contribute significantly to knowledge of the planet (see Section 3.3). Colorimetric information has the advantage of ease of interpretability, but limited spectrometric imagery (i.e., imagery that cannot be used to construct a true color representation of the object photographed) is also of great value (Ref. 5-8). The instrumentation required to obtain multispectral imagery is discussed here.

5.3.1 Colorimetric and Spectrometric Instrumentation Techniques

The two methods commonly employed in aerial and/or space photography to obtain multispectral imagery make use of either a filter wheel or slides. Use of a filter wheel is the most common method. Surveyor I employed a rotatable filter wheel with red, green, blue and clear filters, and Surveyor III used a filter wheel with polarizing filters. The Mariner IV Martian mission employed a filter wheel with only green and red filters because of the blue haze characteristics of Mars. Mariner 1969 will also use green and red filters.

Individual photographs can be used to obtain spectrometric data, but simultaneous photography is virtually essential to satisfy the stringent registration and perspective requirements necessary to obtain good true color imagery. A repetitive imaging single lens camera is not adequate to obtain good colorimetric imagery since an orbiting camera can almost never photograph an area more than once under identical conditions.

Two methods can be used to obtain imagery suitable for colorimetric reproduction. A multi-lens camera can be used with appropriate filters placed over each lens. The lenses would have to be aligned and matched and exposure times would have to be properly selected for each lens, since the sensitivity of the sensors is a function of wavelength (Ref. 5-9). Additionally, a multi-lens camera would have to be both small and light enough to be compatible with spacecraft payload requirements.

A second method for obtaining simultaneous color imagery is to use a single lens camera equipped with appropriate beam splitters and filters. The beam splitters divide the light from the subject onto three focal planes (three sensors), each of which has the appropriate filter in front of it. The result of the imaging process is three separate images, each of which has a record of the amount of either red, green or blue that the subject reflects. These images can then be reconstructed in such a way as to produce a full color reproduction of the subject on the ground.

In summary, spectrometric information can be obtained with relatively simple instrumentation (e.g., a filter wheel). Obtaining colorimetric imagery, on the other hand, requires the use of a multi-channel simultaneous imaging technique. The additional value of the colorimetric data must be weighed against the necessary increase in instrumentation complexity as well as the increased bandwidth requirements.

5.3.2 Multispectral Filters

Since multispectral imaging techniques require the addition of filters to the optical system, some of the pertinent filter characterisitcs such as filter material type, affect on resolving power of the optical system, and filter factors must be examined.

All filters, except for interference filters, are made up of two prime elements: a dye which determines the spectral characterisitcs of the filter and a support for the dye. Interference filters consist of two highly reflecting but partially transmitting metallic films, separated by a spacer film of non-absorbing material. This combination is vacuum deposited on a glass plate with a cover plate cemented on for protection. The separation of the metal films governs the wavelength position of the pass band and therefore, the color of the transmitted light. Light which is not transmitted is for the most part reflected.

Conventional photographic filters can be specfied either by the dye type or the support type (e.g., gelatin, glass, plastic, liquid). The medium in which the dye is supported plays an important role in the transmission and optical characterisitcs of the filter. The filter supports and the advantages of each are outlined in Table 5-8 (Ref. 5-10).

Glass or gelatin filters are most suitable for satellite photographic applications. They exhibit good transmission characteristics and high optical quality. For any particular mission, tradeoffs must be made to determine which of these filter materials offers advantages that are more compatible with specific mission goals and requirements.

For optimum optical quality, the gelatin filter surpasses all others, including the highest quality glass filters. Because gelatin filter thickness is only 0.1 mm, these filters do not significantly affect definition or focus. Gelatin filters, however, require careful handling, are difficult to clean and are quite susceptible to temperature and humidity variations. Severe heat and humidity conditions can alter the shape of the filter and considerably change its optical qualities.

TABLE 5-8 ADVANTAGES AND DISADVANTAGES OF VARIOUS TYPES OF FILTER SUPPORTS

Filter Support	Advantages	Disadvantages
Gelatin	Very thin; no significant effect on focusing regardless of where placed; excellent optical qualities; inexpensive.	Requires careful handling; difficult to clean; poor resistance to severe environmental conditions.
Glass	Easily handled and cleaned; good dimensional stability; highly resistant to most severe environmental conditions; excellent fading resistance.	Difficult to control spectral absorption and transmittance characteristics during manufacture; thickness can present focusing problem; may shatter or crack when mechanical shock is applied.
Cemented Gelatin In Glass	Easily handled and cleaned; good dimensional stability.	Can present focusing problem; tendency to come apart in severe environmental conditions.
Plastic	Inexpensive; adequate for use in non-image forming areas.	Poor optical qualities due to surface striations.
Liquid	Offers very precise spectral absorption and transmittance qualities.	Thick, bulky and messy; not suitable for aerospace photographic applications.

In general, glass filters offer excellent resistance to extreme environmenal conditions. However, mechanical or thermal shock can shatter or crack the filter and large doses of radiation can alter the transmission and optical characteristics of the glass. Focus shifts can occur when glass filters are used since thickness ranges between 1 and 10 mm. A filter with an index of refraction of 1.5 will have a focus shift of approximately 1/3 the filter thickness. The optical system may therefore require a means of compensating for focus when glass filters are employed. For a mission of the Voyager type, however, the displacement is less of a problem since distant objects are being photographed and nearly parallel rays of light are striking the filter.

Since filters absorb part of the energy incident on the optical system, their use requires an increase in exposure corresponding to the proportion of effective energy absorbed. The amount by which the exposure must be increased for a given filter and sensor combination is the filter factor. This factor depends on the filter, sensor and the energy source. A blue filter, for instance, may require an increase in exposure of thousands of times with a sensor having very little blue sensitivity, and an exposure increase of only two or three times for a very blue sensitive sensor. Obviously, the same considerations apply to the use of different combinations of filters, energy sources, and sensors.

The proper procedure to establish the required exposure time is as follows. When the approximate wavelength intervals for the sensor have been established, a spectrophotometric signature of the multispectral lens(es) must be made and multiplied (wavelength by wavelength) with the candidate filters to be used. The indicated total transmission of each lens and filter combination must be taken together with the spectrometric sensitivity of the sensor to indicate the level of scene brightness required for good exposure. Unfortunately, the scarcity of spectrometric data concerning the Martian terrain features limits the multispectral system design analysis which can be performed at this time.

5.4 REFERENCES

5-1 HULETT, H. R., "Turbulence Limitations in Photographic Resolution of Planet Surfaces," Journal of the Optical Society of America, Vol. 57, No. 11, Nov. 1967.

5-2 KAWACHI, D. A., "Image Motion and Its Compensation for the Oblique Frame Camera," Photogrammetric Engineering, Jan. 1965.

5-3 MAGILL, A. A., "Still Cameras," Chapter 4, Applied Optics and Optical Engineering, Academic Press, 1967.

5-4 DOVIAK, J. V., "A Study of Electronic Image Motion Compensation Control for Image Amplifier Cameras," Du Mont Electronic Div., Fairchild Camera and Instrument Corporation, Report AFAL-TR-65-103, May 1965.

5-5 WEIDNER, D. K. and HASSELTINE, C. L., "Natural Environment Design Criteria Guidelines for MSFC Voyager Spacecraft for Mars 1973 Mission," NASA Technical Memorandum TMX-53616, June 1967.

5-6 BENNARDO, J.A. "Optical Performance Subject to Thermal Influence," Fairchild Space and Defense Systems, To be published.

5-7 Manual of Photogrammetry, Third Edition, American Society of Photogrammetry, 1966.

5-8 MOLINEUX, C. E., "Aerial Reconnaissance of Surface Features with the Multiband Spectral System," Air Force Cambridge Research Laboratory, Proceedings of the 3rd Symposium of the Remote Sensing of the Environment, University of Michigan, 1965.

5-9 YOST, E. F. and WENDEROTH, S., "Multispectral Color Aerial Photography," Photogrammetric Engineering, Vol. XXXIII, No. 9, Sept. 1967.

5-10 ZAKIA, R. D., "Photographic Filters," Chapter 3, Photography-Its Materials and Processes, Sixth Edition, Lancaster Press, Lancaster, Pennsylvania, 1962.

SECTION 6

PHOTOSENSOR ASSESSMENT

Photosensitive devices or material provide a means for recording the amount of light incident from a target scene. Electro-optical, chemical or thermal techniques can be employed. Electro-optical sensors convert incident light into measurable currents or voltages, chemical procedures transform the imaged scene into a representative density pattern on the photographic emulsion, and thermal techniques permit recording of the scene on a photosensitive heat deformable material.

Numerous photosensing techniques have been evaluated to select suitable sensors for Martian orbital planetary reconnaissance missions. The study has included the determination of sensor physical characteristics and development status as well as the assessment of sensor sensitivity, resolution, spectral response and dynamic range.

It should be noted that an equitable comparison of sensor characteristics is sometimes difficult because of a lack of standardization both in testing and in specification of performance parameters. For example, sensitivity is generally expressed in meter-candle-seconds (or its equivalent) for electro-optical devices and in AEI (Aerial Exposure Index) for aerial reconnaissance film. The AEI number represents a specific point on the film's "D-log E" curve (film density as a function of the log of exposure).

A summary list of the photosensors considered during the program is presented in Table 6-1. The relative sensitivity and resolution capabilities are indicated for each type of sensor. Some of the sensors considered require external storage capability; other devices or materials provide a combined sensor and storage capability. Additional photosensor performance analyses are, of course, required when the mission parameters are more firmly established.

TABLE 6-1 PHOTOSENSOR CHART

Sensor	Relative Sensitivity Capability	Relative Resolution Capability	General Characteristics
Electro-Optical Tubes	High	Medium	Separate storage required, small format, light weight.
Silver Halides	High	High	Self contained storage, large format, wet processing, radiation sensitive.
Dielectric Tape	Medium	Low	Electronic processing, reusable, complex.
Electrostatic Tape	Medium	Low	Electronic processing, reusable, complex, developmental.
Photoplastic Tape	Medium	Medium	Thermal processing, reusable, requires Schlieren optics, complex.
Electrophotography	Medium	Medium	Powder processing copying material, poor tonal quality.
Dry Silver	Low	High	Thermal processing, radiation sensitive, slow speed copying material.
Frost Xerography	Medium	Medium	Like photoplastic, but requires liquid for charge transfer.
RS	Low	High	Fast chemical processing, copy material speed, stable to heat and radiation.
Diazo	Low	High	Gaseous or wet processing. UV sensitive, slow speed copying material.

6.1 ELECTRO-OPTICAL SENSORS

The suitability of various electro-optical sensors for use in planetary orbital photo imaging systems has been investigated during the study program. Video tube devices which have received particular consideration include vidicons, image orthicons, return beam vidicons, SEC vidicons and plumbicons. Additional electro-optical devices, such as image intensifier vidicons and intensifier image orthicons, have been considered. However, these devices are primarily used for low light level applications. The characteristics of several of the above-listed video sensors which have been used or designed for space applications are presented in Table 6-2 (Ref. 6-1).

Electro-optical systems utilize photosensitive materials to convert incident light to an electrical signal. Either photoemissive or photoconductive surfaces can be used. In the photoemissive process, electrons are released from the surface of the photoemissive material when sufficient energy is transferred from incident photons. In the photoconductive process, the electrical conductivity of the material increases when exposed to incident illumination. Photoconductive materials generally offer wider spectral response properties, but are limited in sensitivity by dark current noise.

Resolution data for electro-optical devices is generally given by manufacturers for operation comparable to that used for commercial television, i. e., open shutter imaging of a fixed target at 30 frames/second. In determining resolution, approximately six frames are integrated over a one-sixth of a second period. The result is a measure of resolution which is improved over the single exposure type of operation of interest in this study by perhaps more than 10%. The resolution data presented in this report is based upon manufacturers specifications without correction for single exposure operation.

TABLE 6-2 SPACE TELEVISION CAMERA SYSTEMS

TUBE TYPE	1/2" Vidicon	1" Vidicon		3" Image Orthicon		Return Beam Vidicon	
						2"	4 1/2"
Space System	TIROS	Nimbus	ESSA	Stratoscope	Tigris	EROS Design	Sync. Sat Design
Image Format (mm)	6.3x6.3	11.2x11.2	12.2x12.2	30.5x30.5	35.5x35.5	25.4x25.4	50.8x50.8
Resolution:							
TV Lines	400H 350V	800H 600V	800H 600V	400	200 to 600	5000 to 6000	6000 to 7000
Line Pair/mm	28	27	25	6.6	2.8 to 8.5	98 to 118	59 to 69
Sensitivity (meter-candle-seconds)	1	$4x10^{-2}$	$4x10^{-2}$	-	-	10^{-3}	10^{-3}
Dynamic Range	10:1	100:1	100:1	-	-	100:1	100:1
Optics:							
F/No.	f/1.5	f/4	f/1.8	Tele-scope f/2.8	f/2.8	f/4	f/2.8
Foc. Length (mm)	5	17	5.7	215	25	125	150
Field of View (deg)	105	50	108	10	80	10 to 15	19
Camera Physical Characteristics:							
Mass (kg)	6.48	8.25	8.53	27.2	18.2	14	23 to 34
Size (cm^3)	5520	8110	8110	24,500	23,300	16,000 to 24,000	40,000
Power (watts)	11.6	21.0	16.0	50	50	22 to 30	50 to 75

Initial investigations of the effect of radiation on video tubes have shown that radiation survivability does not appear to be a significant problem for electro-optical sensors. Vidicon tubes exhibit significant transient effects, but little permanent damage when exposed to pulses of radiation. Recovery is rapid, with loss of video information limited to a period less than one-half second (Ref. 6-2).

The physical characteristics and performance features of electro-optical sensors have been evaluated. Sensor operation, performance and physical dimensions are described in the following subsections. For convenience, brief descriptions of the operation of each of the tubes are provided.

6.1.1 Vidicon Tubes

The vidicon is an operationally simple photoconductive tube which offers relatively high resolution, small size and mass and has small power requirements. Transistorized vidicon deflection circuitry has been used to provide additional size, mass and reliability benefits. In addition, vidicons are suitable for slow scan operation with the resulting advantage of reduced recorder input data rates and power dissipation. The construction of a typical vidicon tube designed for electromagnetic focus and deflection is shown in Figure 6-1a. The inside surface of the vidicon faceplate is coated with a transparent and conductive coating over which is deposited a layer of photoconductive material. In operation, wherever light from the image scene falls on the photoconductor, the conductivity of the material is substantially increased. The resulting leakage of the charge leaves a "hole" in the pattern of negative charge at the illuminated points into which the scanning beam deposits electrons. Thus, during scanning, there is a current flow in the transparent conductive coating; the resulting voltage across the load resistor provides the video output signal.

The application of slow scan techniques can be considered when it is desirable to limit the bandwidth of the video signal output. Reduction of the bandwidth improves the systems signal-to-noise ratio. For open shutter operation, slow scan techniques are especially useful where the image or vehicle motions are small. However, since smear due to image motion can occur, consideration must be given to limiting exposure time.

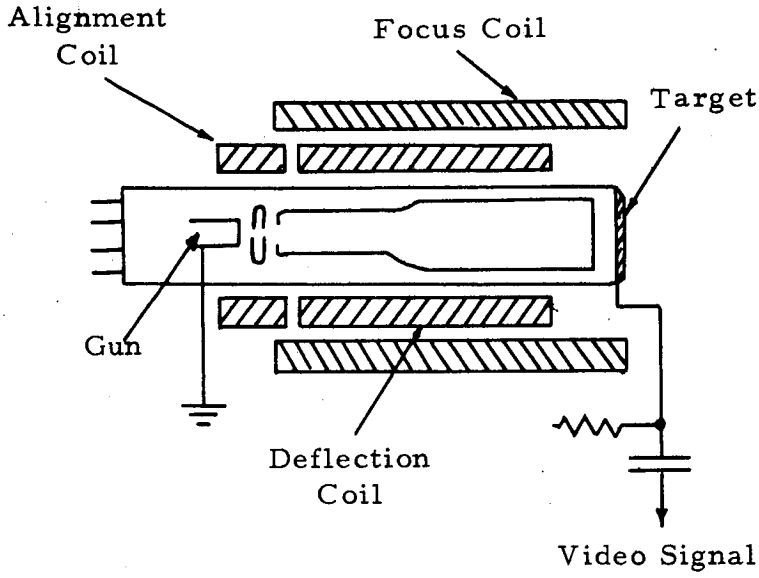

a) Vidicon Tube Schematic

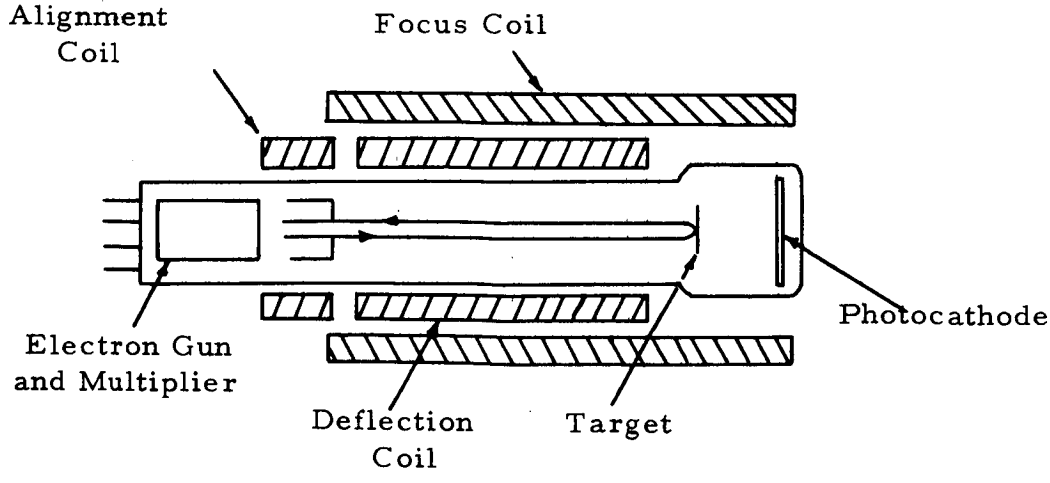

b) Image Orthicon Tube Schematic

FIGURE 6-1 ELECTRO-OPTICAL TUBE SCHEMATICS

Exposure time must be selected as a function of incident illumination, image motion and vehicle stability.

Many variants of the standard vidicon have been developed for special applications. The "hybrid" vidicon uses electrostatic focus and magnetic-deflection. It offers moderate resolution capability and can provide compact lightweight camera units. The electrostatic-focus and electrostatic-deflection vidicon provides low resolution capability, has very low power requirements and is used when extremely compact lightweight cameras are needed. Vidicon tubes are available in 0.5, 1.0, 1.5, 2.0 and 4.5 inch diameter sizes. Several space camera systems have employed the smaller vidicon tubes. The performance and physical characteristics of these tubes are presented in Table 6-3 (Ref. 6-3). Potential tube capabilities are presented in parentheses.

Current resolution capability of the 0.5 inch tube is 400 TV lines (31 lp/mm) as compared to 1000 TV lines (44 lp/mm) for the one inch tube. The 2 inch and 4.5 inch tubes have been developed to provide greater resolution capability. These larger tubes are available as vidicons or return beam vidicons. The illumination transfer function and modulation transfer function curves are shown in Figures 6-2 and 6-3, respectively, for vidicon and other typical electro-optical tubes (Ref. 6-4 through 6-7).

6.1.2 Image Orthicon Tubes

The image orthicon tube provides relatively high sensitivity, but is far more complex, larger and heavier than a vidicon tube. Typically, the image orthicon is used for low light level applications.

The image orthicon tube is comprised of a photoemissive cathode to convert an incident optical image to a photoelectron image, a target to accept the focused photo-electron image, a scanning electron beam which deposits electrons on the storage target in correspondence to scene brightness, and an electron signal multiplier operating on the reflected target modulated return beam. Figure 6-1b shows a schematic of an image orthicon and associated focus, deflection, and alignment coils.

The performance and physical characteristics of the image orthicon are presented in Table 6-4 (Ref. 6-3). The illumination and modulation transfer function data are illustrated in Figures 6-2 and 6-3, respectively.

TABLE 6-3 VIDICON PERFORMANCE AND PHYSICAL CHARACTERISTICS

Sensor	1/2" Vidicon	1" Vidicon	1-1/2" Vidicon
Sensitivity, at 10:1 S/N: (meter-candle-seconds)	6.7×10^{-2}	3.3×10^{-2}	1.3×10^{-2}
Resolution:** TV lines, limiting Line Pair/mm	400* (500) 31* (39)	1000* (1400) 44* (62)	1100* (1400) 31* (39)
Image Format (mm)	6.35 x 6.35	11.2 x 11.2	17.8 x 17.8
Dynamic Range (without adjustment)	100:1	100:1	100:1
Storage	80% at 10 sec.* (80% at 120 sec.)	80% at 10 sec.* (80% at 120 sec.)	80% at 10 sec.* (80% at 120 sec.)
Ruggedized	Yes	Yes	No
Length (cm) Mass including Yoke (kg)	8.1 0.45	12.7 1.4	26.0 1.4
Deflection and Focus	All Mag.	All Mag.	Mag. Deflection Electrostatic-Focus

NOTES

* Potential capabilities shown in parentheses.

**Resolution based on open shutter operation; degradation results for operation in a shuttered mode.

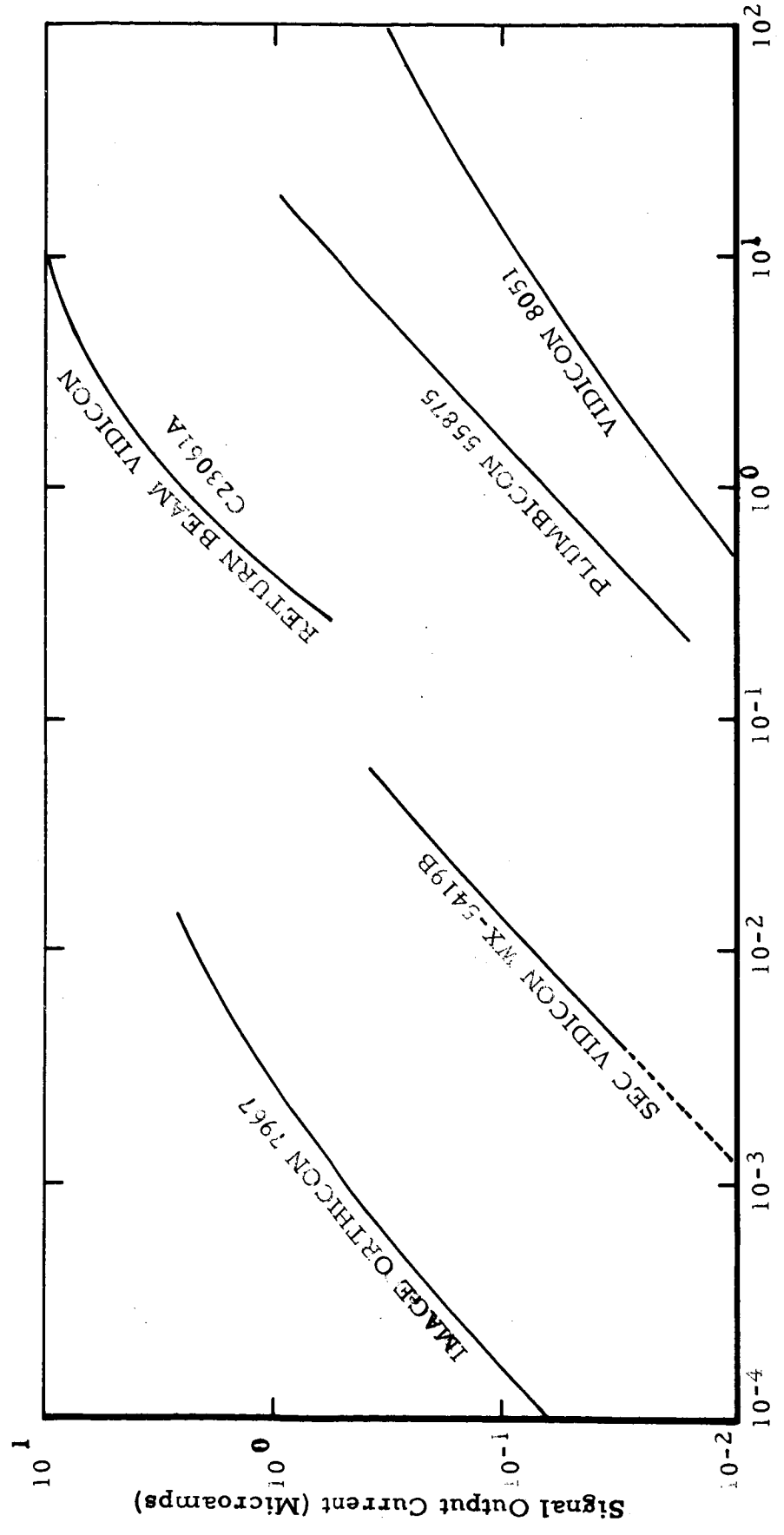

FIGURE 6-2 ELECTRO-OPTICAL SENSOR ILLUMINATION TRANSFER CURVES

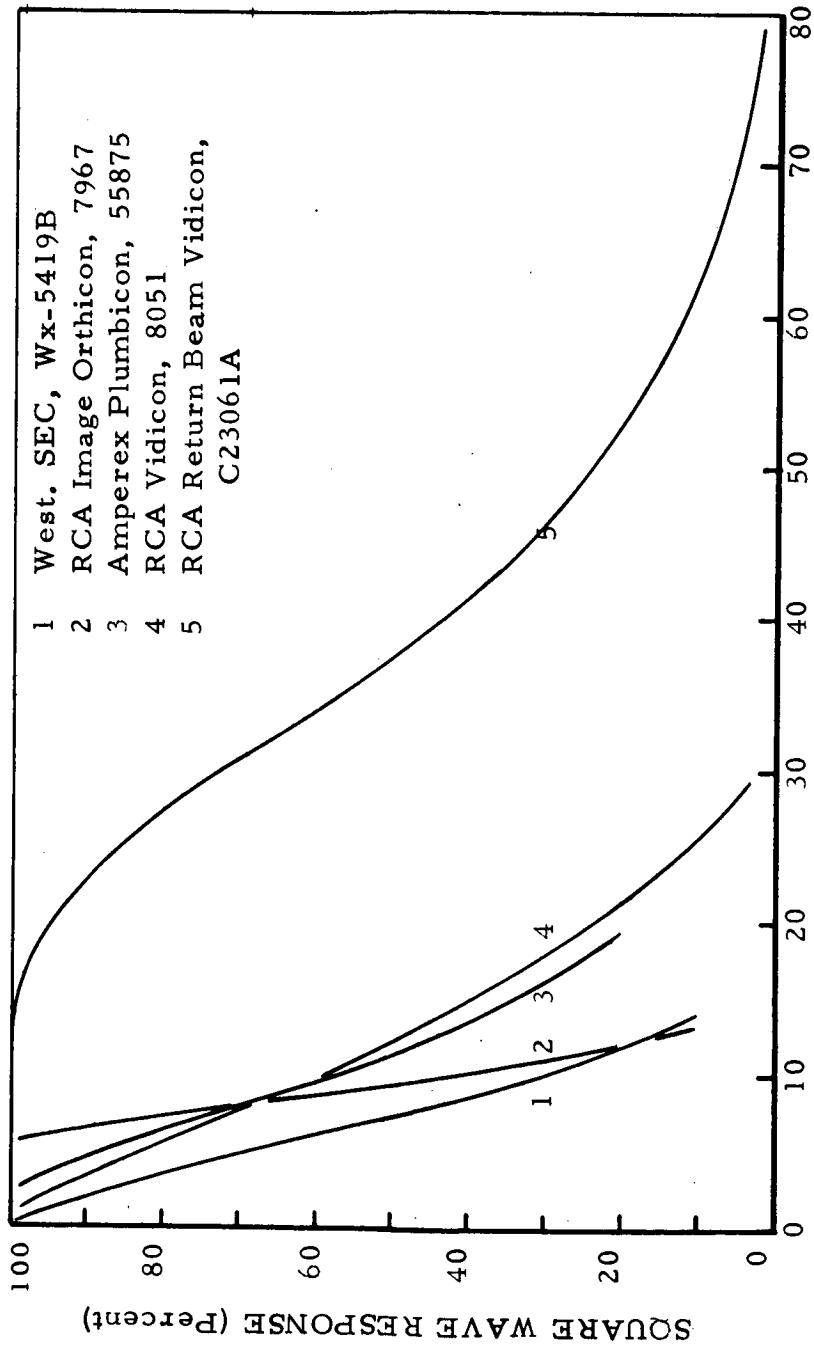

FIGURE 6-3 ELECTRO-OPTICAL SENSOR MODULATION TRANSFER FUNCTIONS

TABLE 6-4 IMAGE ORTHICON PERFORMANCE AND PHYSICAL CHARACTERISTICS

SENSOR	2" IMAGE ORTHICON
Sensitivity, at 10:1 S/N: (meter-candle-seconds)	2.3×10^{-5}* (6.7×10^{-6})
Resolution: ** TV lines, limiting Line Pair/mm	650 15
Image Format (mm)	21.6 x 21.6
Dynamic Range (without adjustment)	15:1* (100:1)
Storage	80% at 3 min.
Ruggedized	Yes
Length (cm)	24.1
Mass including yoke, (kg)	2.3
Deflection and Focus	All Mag.

NOTES

*Potential capability in parentheses.

**Resolution based on open shutter operation; degradation results for operation in a shuttered mode.

If high sensitivity is critical, serious consideration must be given to use of an image orthicon. However, a vidicon camera is superior in terms of resolution capability, size, mass, power, complexity, ruggedness and reliability.

6.1.3 Return Beam Vidicon Tubes

The return beam vidicon tube developed by RCA combines the conventional vidicon and image orthicon operating techniques. The tube uses a vidicon type target. The readout operation is similar to that of the image orthicon. A low velocity electron beam scans the reverse side of the photoconductive target, depositing electrons in correspondence to scene brightness. Operation is achieved by returning the modulated portion of the scanning beam which fails to be deposited on the target back to an electron multiplier located in the gun region. This modulated beam is referred to as the return beam. The return beam vidicon tube schematic is similar to that shown in Figure 6-1b for the image orthicon.

The two-inch return beam vidicon has both magnetic-focus and magnetic-deflection and incorporates a five stage electron multiplier. This combination provides the highest center and corner resolution of any vidicon but requires the most electrical power and mass. Presently, the 4000 TV line tube has a mass of about 4.5 kg and dissipates about 80 watts of power; in addition, cooling must be incorporated to maintain the faceplate temperature below 313°K (Ref. 6-5).

The present and potential performance parameters and physical characteristics are presented in Table 6-5 for the return beam vidicons (Ref. 6-3). The illumination and modulation transfer function data for a 2 inch tube are presented in Figures 6-2 and 6-3 respectively. The principal advantage of the return beam vidicon over other electro-optical sensors is its high resolution.

The 2-inch return beam vidicon currently has a 4000 TV line (79 lp/mm) resolution capability. The next development by RCA is expected to be a 5000 TV line tube (Ref. 6-8). The potential development, during the 1970's of an 8000 TV line (158 lp/mm) 2-inch return beam vidicon holds promise for future planetary orbital mission applications. However, the availability of such a tube in a ruggedized form in time for the early Voyager missions must be carefully considered.

TABLE 6-5 RETURN BEAM VIDICON PERFORMANCE AND PHYSICAL CHARACTERISTICS

SENSOR	2" Return Beam Vidicon	4-1/2" Return Beam Vidicon
Sensitivity, at 10:1 S/N: (meter-candle-seconds)	3.3×10^{-2} to 6.7×10^{-3}* (6.7×10^{-4})	6.7×10^{-3} to 3.3×10^{-3}* (6.7×10^{-4})
Resolution:** TV lines, limiting Line Pair/mm	4000* (8000) 4000* (8000) 79* (158)	7000* (10,000) 7000* (10,000) 69* (98)
Image Format (mm)	25.4 x 25.4	50.8 x 50.8
Dynamic Range (without adjustment)	100:1	100:1
Storage	80% at 10 sec.	80% at 10 sec.
Ruggedized	Partial* (Yes)	No* (Yes)
Length (cm) Mass including Yoke (kg)	approx. 20.3* (22.9) 4.5	45.7 approx. 13.5* (9.1)
Deflection and Focus	All Mag.	All Mag.

NOTES

* Potential capabilities shown in parentheses.

** Resolution based on open shutter operation; degradation results for operation in a shuttered mode.

6.1.4 SEC Vidicon Tubes

The SEC (Secondary Emission Conduction) vidicon is a high sensitivity tube which utilizes an SEC target developed by the Westinghouse Electric Corporation (Ref. 6-9 and 6-10). The two principal advantages of the SEC camera tube are a relatively high signal-to-noise ratio and a high signal amplification prior to target readout. The SEC vidicon achieves high gain with direct beam readout, eliminating the need for image intensifier or return beam electron multiplier techniques. The signal amplification principle also lends itself to unique target-gain control methods which can provide camera operation for an unusually wide range of illumination inputs.

The operation of the SEC vidicon tube is based on conduction by secondary electrons liberated by primary electron bombardment. The tube consists basically of a photoemissive cathode, the SEC target and a direct beam readout gun. Photoelectrons are accelerated and focused onto the target; secondary electrons produced in the dielectric layer of the target result in a multiplication of the photoelectron image current. An electron beam reads and erases the charge pattern at the target and generates the output video signal.

The performance and physical characteristics of SEC vidicon tubes are presented in Table 6-6 (Ref. 6-3 and 6-6). The illumination and modulation transfer functions are presented in Figures 6-2 and 6-3 respectively, for a typical SEC tube. At the present time, SEC tube resolution is poorer than of conventional vidicon camera tubes. Since SEC resolution is limited by target thickness and target mesh requirements, a significant advance would be required to achieve competitive resolution capability.

6.1.5 Plumbicon Tubes

The Plumbicon, developed and produced by the Philips Company of The Netherlands is characterized by small size, simplicity of construction and operation, low dark current and relatively good sensitivity, speed and resolution. The tube offers superior picture quality and speed at low illumination levels in comparison to typical vidicon performance. The Plumbicon is widely used in commercial television, especially color television applications. The tube requires automatic exposure control to maintain the incident light at a non-destruct level.

TABLE 6-6 SEC VIDICON PERFORMANCE AND PHYSICAL CHARACTERISTICS

SENSOR	2" SEC (Ref. 6-3)	3.2" SEC (Ref. 6-6)
Sensitivity, at 10:1 S/N: (meter-candle-seconds)	4.7×10^{-4}* (6.7×10^{-5})	6.7×10^{-4}
Resolution:** TV lines, limiting Line Pair/mm	300* (600) 11* (22)	1,000 24
Image Format (mm)	14 x 14	28 x 21
Dynamic Range (without adjustment)	60:1* (100 to 150:1)	100:1
Ruggedized	Partially* (Yes)	Yes
Length (cm)	22.9	44.5
Mass including Yoke (kg)	0.23	-
Deflection and Focus	Electrostatic	Electrostatic

NOTES

* Potential capabilities shown in parentheses.

** Resolution based on open shutter operation; degradation results for operation in a shuttered mode.

The Plumbicon uses a multilayer photoconductor, but is otherwise functionally similar to the vidicon tube. The use of the photoconductor, composed of layers of PbO and SnO_2, results in low dark current and good sensitivity characteristics (Ref. 6-11 and 6-12). The spectral sensitivity more closely matches that of the human eye than do the sensitivities of the vidicon or image orthicon.

The performance and physical characteristics of a Plumbicon tube are shown in Table 6-7 (Ref. 6-7). The illumination and modulation transfer function characteristics are shown in Figures 6-2 and 6-3, respectively. The tubes are now manufactured in The Netherlands, but will be produced by the Amperex Corporation in the United States by early 1968. The Plumbicon is not currently available in a space ruggedized form, since it is primarily intended for commercial applications (Ref. 6-13).

6.1.6 Comparison of Electro-Optical Sensors

Comparisons have been made of the capabilities of various electro-optical sensors considered for the Voyager photographic imaging system. The major characteristics of these tubes are summarized in Table 6-8. The vidicon and return beam vidicon sensors are considered to be most suitable for use during the mid 1970's. This determination is based upon the overall performance of these tubes, and particularly upon the excellent potential resolution capability claimed for the future.

TABLE 6-7 PLUMBICON PERFORMANCE AND PHYSICAL CHARACTERISTICS

SENSOR	1.3" PLUMBICON
Sensitivity, at 10:1 S/N: (meter-candle-seconds)	$\sim 2 \times 10^{-2}$
Resolution:** TV lines, limiting Line Pair/mm	600* (800) 19* (25)
Image Format (mm)	12 x 16
Dynamic Range (without adjustment)	200:1
Target	Photoconductor PbO
Ruggedized	No* (Yes)
Length (cm)	21
Mass including Yoke (kg)	1.1
Deflection and Focus	All Mag.

NOTES

* Potential capability in parentheses.

** Resolution based on open shutter operation; degradation results for operation in a shuttered mode.

TABLE 6-8 ELECTRO-OPTICAL SENSOR SUMMARY CHART

Type	Size (inches)	Format Width (mm)	Resolution (lp/mm) Present	Resolution (lp/mm) Potential (5 years)	Sensitivity (meter-candle-seconds)	Dynamic Range	Tube Mass (kg)
Vidicons*	0.5	6	31	39	6.7×10^{-2}	100:1	0.45
	1	11	44	62	3.3×10^{-2}	100:1	1.35
	2	25	70	100	1×10^{-2}	100:1	4.5
Return Beam Vidicons*	2	25	79	158	$\sim 1 \times 10^{-3}$	100:1	4.5
	4.5	50	69	98	$\sim 5 \times 10^{-3}$	100:1	13.5
Image Orthicon	2	25	15	20	2.3×10^{-5}	100:1	2.3
SEC Vidicon	2	14	11	22	5×10^{-4}	60:1	0.23
Plumbicon	1	12	19	25	$\sim 2 \times 10^{-2}$	200:1	1.1

* Most suitable electro-optical sensor.

6.2 SILVER HALIDES

Photographic cameras using silver halide sensors are the primary means for acquiring mapping and reconnaissance imagery. Silver halide materials offer enormous latitude in speed, resolution, contrast and spectral response and do not require an independent storage medium.

The recently completed Lunar Orbiter missions demonstrated the value of film camera systems for obtaining imagery from orbital vehicles. The Lunar Orbiter camera systems used a silver halide film imaging system to provide high quality imagery of virtually the entire moon. Medium and high resolution photographic data of large near and farside areas of the lunar surface were obtained with resolution sufficient for detailed examination and final selection of potential Apollo landing sites.

The Voyager missions to Mars are of relatively long duration; i.e., up to 8 months enroute and 6 months in orbit. Of particular interest for such a long term mission are the film processing requirements and the sensitivity to radiation of silver halide films. The use of silver halides in a Voyager mission requires a chemical processing material capable of long term storage before use. In addition, since silver halide emulsions are generally sensitive to the types of radiation to be encountered during the mission (see Section 2.8), an analysis of film suitability and shielding requirements is essential.

The capabilities of specific silver halide film types and processing materials, as well as radiation effects and shielding requirements are presented in this section.

6.2.1 Silver Halide Characteristics

Photographic emulsions are suspensions of silver halide crystals, usually in a gelatin medium. Upon exposure to incident light, electron-hole charge pairs are produced in the silver halide and a permanent latent image is formed. When treated with a chemical developer, the exposed silver halide becomes visible and the unexposed and undeveloped silver halides are removed. The speed, density range and contrast properties of silver halide emulsions are functions of the inherent sensitivity of the material to light and the developing process.

The characteristics of silver halide emulsions are generally expressed in terms of speed ratings, density-log exposure curves, time-gamma curves, reciprocity data and the spectral sensitivity in response to a recommended development procedure. Resolution is generally expressed in terms of modulation transfer function characteristics, although the spread function is sometimes used.

Candidate films for the Voyager photographic mission are listed in Table 6-9. Modulation transfer functions and spectral response data for some of these Eastman Kodak films are presented in Figure 6-4, (Ref. 6-14). Of these films, SO-243, 3404 or SO-230 appear to be the most suitable, primarily because of high resolution capability, good photographic speed, and relative insensitivity to stray radiation (as compared to other silver halide films). Kodak's SO-243 film has been used for many years in high altitude reconnaissance photography. It is a very fine grain film, possesses very high resolution capability at both high and low contrast, and has good photographic speed. In addition, SO-243 is easily and quite satisfactorily processed with a monobath saturated web technique or hydrophilic layer processing technique as would be required for space processing. The SO-243 film has been used for the lunar mapping missions.

SO-230 is a film recently developed by Eastman Kodak, (Ref. 6-15). At this time, complete sensitometric data of this film is not available (the film itself will not be available until early 1968). However, preliminary information on SO-230 indicates that its performance will be similar to that of 3404 film, but approximately 4 times as fast.

Thin base films, e.g., 3404 and SO-230, are considerably lighter than the estar or triacetate base films. However, a dye backing is usually placed on the thin base films to prevent image degradation by light reflected back from the base. If not removed during processing, the dye adds a density of about 0.2 to the negative. The dye is removable by conventional processing, but would not be removed by space processing techniques (see Section 6.2.2). The monobath processing chemicals used for inflight processing only contact the emulsion side of the film and, therefore, would not remove the dye material. The triacetate base SO-243 film does not have a dye backing and is, therefore, more suitable for spaceborne processing.

6.2.2 Space Processing of Silver Halide

The ultimate quality and performance parameters obtained from

TABLE 6-9 SILVER HALIDE CHARACTERISTICS CHART

Kodak Film Types	Sensitivity (meter-candle-seconds)	AEI	Resolution (lp/mm)			Mass kg/m^2	Description and Remarks
			Contrast 1000:1	Contrast 2:1	Contrast 1.6:1		
High Definition, SO-243	3.1×10^{-1}	1.6	640	296	230	0.181	High altitude film; ultra-fine grain; high acutance; triacetate base.
High Definition, 3404	3.1×10^{-1}	1.6	670	295	225	0.107	High altitude, stable-platform film, estar thin base, dye backing.
High Definition, SO-230	8.3×10^{-2}	6	670	295	225	0.107	Similar to 3404, but higher speed.
Fine Grain, SO-206	8.3×10^{-2}	6	435	168	124	0.107	High altitude film; estar thin base, dye backing.
Fine Grain, SO-226	8.3×10^{-2}	6	435	168	124	0.156	High altitude film; estar base.
Panatomic X, 3400	2.5×10^{-2}	20	188	86	68	0.107	General usage; estar thin base.
Panatomic X, SO-136	2.5×10^{-2}	20	210	90	68	0.161	Fine grain mapping; estar base.

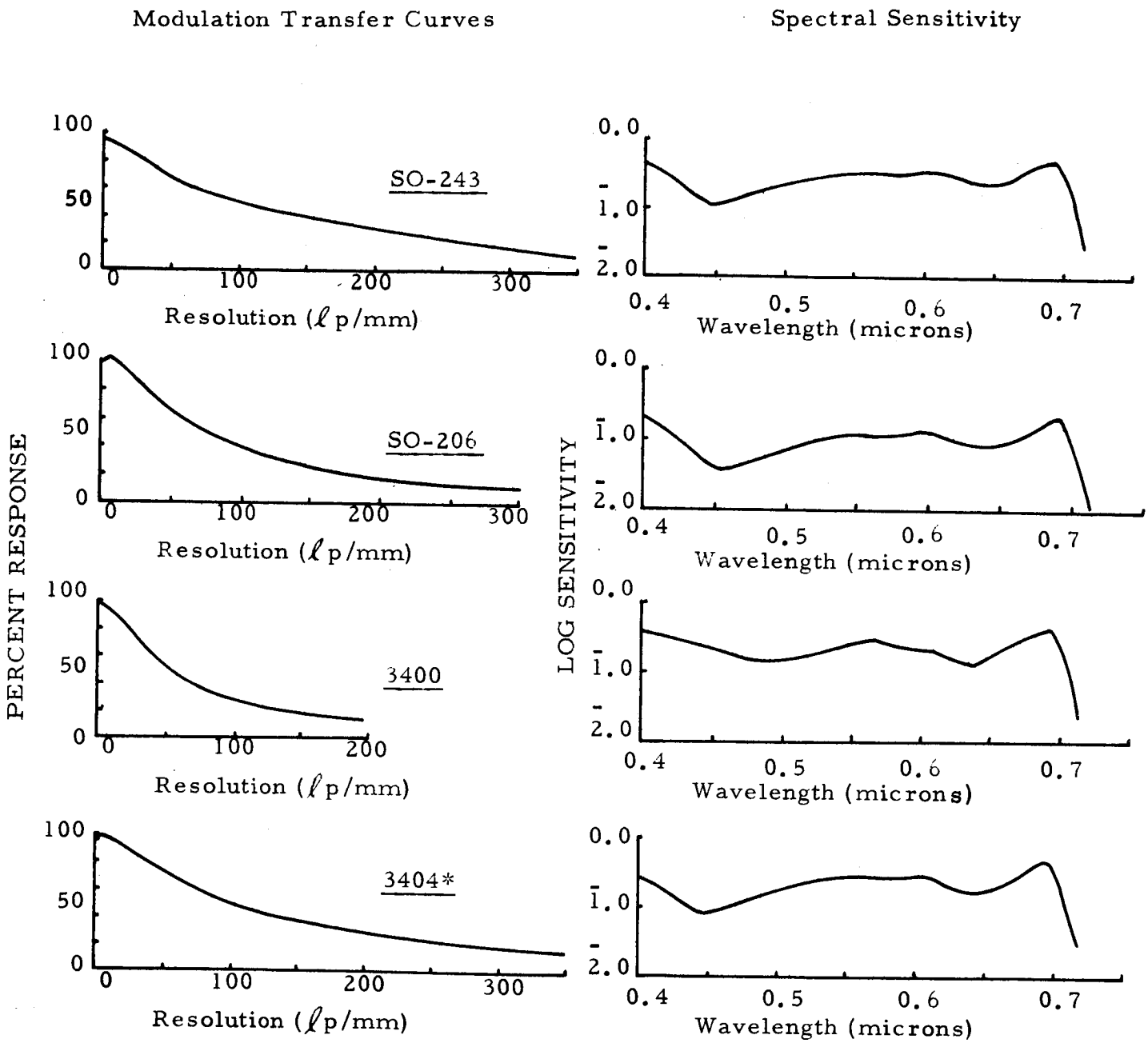

*Similar to SO-230 Characteristics

FIGURE 6-4 MODULATION TRANSFER FUNCTIONS AND SPECTRAL CHARACTERISTICS OF KODAK FILMS

gelatin silver halide materials are dependent on the chemical processing and general environmental handling of the film before, during, and after exposure and processing. Therefore, the unusual conditions inherent in space flight place severe restrictions on the means by which an aqueous solution may be applied to an exposed film to reduce the exposed silver halide to silver and remove the unexposed silver halide material.

The two promising techniques available for inflight processing applications are the Kodak Bimat and Fairchild Fairweb chemical monobath processes. The suitability of these inflight processing materials for space missions is, however, a function of many factors.

A satisfactory processing material must provide sufficient processing fluid in a reasonably sized format for simple and uniform application. It should be capable of withstanding temperature, pressure, vibration, tension and acceleration variations. The material cannot break down upon separation from the processed photographic film, nor should it remove portions of the gelatin from the film.

An additional major processor characteristic relates to the storage capability of the processing materials. A long term storage capability; i.e., at least one year, must be provided without dry-out or loss of chemical potency.

6.2.2.1 Kodak Bimat Process - The Kodak Bimat process uses a chemical monobath processing solution in a gelatin layer coated on a film base (Ref. 6-16). It has been used successfully in the Lunar Orbiter system.

The sensitometric quality of Bimat processed imagery is generally similar to that of laboratory processed film. However, the hydrophilic gelatin layer containing the processing chemicals sometimes separates from the film base causing small spotting on the processed film. Long stationary contact of the Bimat material with the film must be avoided to prevent adhesion and additional film marking. Misalignment of the film and Bimat is difficult to correct since the Bimat adheres to the film. The liquid content of Bimat is approximately 65 gm/m^2, but not all of the chemicals are released for processing.

The major current limitation of Bimat processing is its short term

storage life. The Bimat storage temperature is critical; the material cannot be frozen or subjected to temperatures higher than about 310°K. However, the storage life can be significantly increased when the material is stored at temperatures just above freezing (Ref. 6-17). Kodak is presently attempting to develop an extended life Bimat processing material for use in long term planetary space missions.

6.2.2.2 Fairchild Fairweb Process - The Fairweb processing technique, formerly known as PoroMat, employs an inert microporous, polyvinyl chloride web impregnated with the processing solution. This technique has been used in operational aerial reconnaissance systems. Many aspects of the Fairweb technique for space and planetary applications have been demonstrated in a laboratory film processor built for NASA under contract to Jet Propulsion Laboratory (Ref. 6-18). The quality of Fairweb processed imagery is similar to that of laboratory processed film. Figure 6-5 is a sensitometric curve comparing Fairweb with Kodak D-76 processed SO-243 high definition film (Ref. 6-18). The processes can be fairly well matched, or the chemicals in Fairweb can be modified to satisfy just about any desired sensitometric effect.

The impregnated web is brought into contact with the silver halide emulsion for processing. The processing liquid adheres to the silver halide emulsion by capillary action. The solution content of the web is approximately 165 gm/m^2 and virtually all the liquid in the web is available for processing. The web may be stripped from the film immediately upon completion of processing for drying, scanning, or projection. Alternately, the web may be retained in contact until it can be conveniently removed. In case of misalignment between the film to be processed and the saturated web, the web corrects itself by sliding or folding.

Fairweb storage capability of 24 months has been demonstrated and tests have indicated no substantial degradation of performance. This has been accomplished by encapsulating the web material in a flexible, heat sealable, plastic sandwich to prevent oxidation and evaporation of the chemicals. The web remains sealed until needed for processing, at which time the envelope is opened and the web is brought into contact with the exposed film. The Fairweb material can be frozen indefinitely for long term storage and can withstand temperatures up to about 360°K. Table 6-10 presents a comparison of Fairweb and Bimat silver halide processing techniques. On the basis of storage

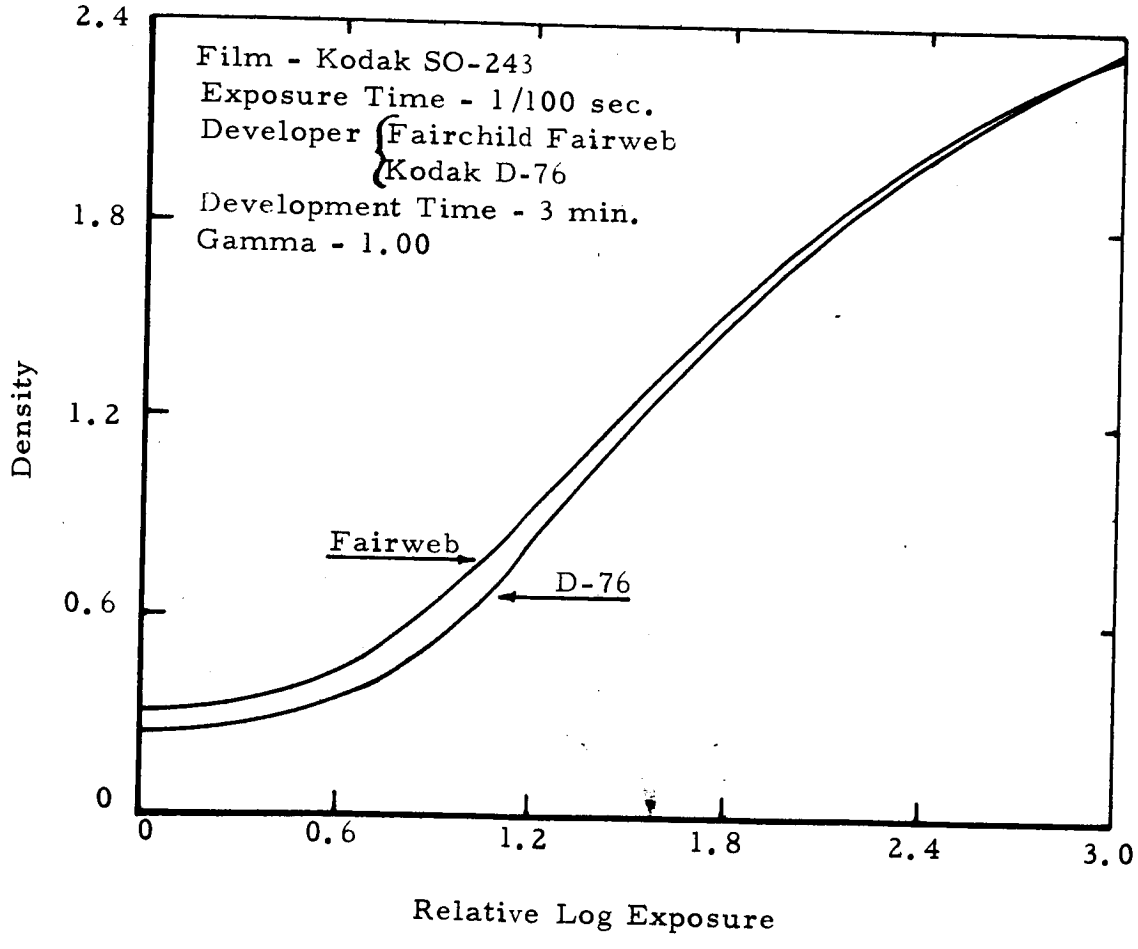

FIGURE 6-5 COMPARISON OF FAIRCHILD FAIRWEB WITH KODAK D-76 PROCESSED SO-243 HIGH DEFINITION FILM

TABLE 6-10 SILVER HALIDE PROCESSING TECHNIQUES FOR SPACE APPLICATIONS

ITEM	FAIRWEB* (SATURATED WEB)	BIMAT
Material	Chemical monobath processing solution in an inert microporous web.	Chemical monobath processing solution in a gelatin layer, coated on a film base.
Processing Ability	Quality of processed imagery similar to lab processed film.	Quality of processed imagery similar to lab processed film.
Characteristics	Chemicals do not react with web material; processing liquid available by capillary action with film; solution content about 165 gm/m^2 and virtually all the liquid is available for processing.	Gelatin hydrophilic layer can separate from base film; soft, expanded gelatin layer has limited stability; processing is accomplished by physical equilibrium state of hydrophilic layers; solution content about 65 gm/m^2, but not all liquid is available for processing.
Storage Qualities	Storage capability of 24 months has been demonstrated; material can be frozen for storage.	Extended storage capability has not been demonstrated; storage temperature is critical; cannot be frozen.
Material Handling	In case of misalignment between the film and the saturated web, the web corrects itself.	In case of misalignment between the film and Bimat material, Bimat cannot correct itself.

*Currently most suitable processing material.

life alone, Fairweb is currently the more suitable silver halide processing material for planetary reconnaissance missions.

6.2.3 Film Radiation Shielding Requirements

Adequate radiation shielding requirements for specific photographic films in long term Martian orbital mission applications must be determined. More precisely, the choice of film type and the corresponding shield thickness requirement must be optimized within an acceptable limit of shielding weight, so that radiation fogging does not become excessive. A maximum allowable net density due to radiation fogging of less than 0.3 with a 90 percent probability has been established, for purposes of the analysis which follows. This analysis is based upon a 340 day (about eleven month) mission, equivalent to the maximum assumed transit time of 240 days plus 100 days in orbit.

The radiation shield would be placed around the film cassette. Additional shielding would be provided by the camera housing, the spacecraft, and the film itself, but this additional shielding is not considered in the analysis. A substantial increase over the dosage discussed here would be required to fog all the film contained in the cassette. Damage to the film when out of the cassette is minimized by processing within a few hours after exposure. Since some warning of an expected solar flare can be given, a particular exposure cycle could be delayed on ground command if it were to occur during a solar event.

The sources of radiation are the Van Allen belts, solar-flare effects and galactic radiation (see Section 2.8). A relatively short time will be spent traversing the two Van Allen belts, and since the amount of protons encountered and their energy levels are lower than that of the solar flares, these radiation belts will not enter the shielding considerations in a primary way. Electrons are not important outside the Van Allen belts. Similarly, gamma rays and neutrons are not a major factor (Ref. 6-20, 6-21).

The galactic cosmic radiation components are largely of such high energy as to be, for practical purposes, unshieldable. As stated in Section 2.8, about 2 rads per month of such radiation can be expected, which immediately precludes the use of all but the very slow films. The main problem, however, is to shield against solar flare radiations,

consisting largely of protons with a smaller and perhaps marginally significant number of α-particles in addition.

The dosage in rads to be expected during various Mars missions for different aluminum and polyethelene shield thicknesses has been determined by Hill, Ritchie and Simpson (Ref. 6-22). While this was done to estimate biological radiation hazards, the results also can be applied to analyze film radiation effects. The effects of protons on various films have been measured against their doses in rads for several proton energies. In general, higher energy protons have a larger effect on film for the same rad dosage than do lower energy protons. However, within a considerable range of proton energies, slower films tend to respond more to the number of rads involved than to the number of particles or to the energy of the particles comprising that rad dosage.

Considering that protons having energies above about 200 MEV do not statistically occur in very large numbers in solar flares (Ref. 6-20, 6-22) and moreover have less effect on film per particle than lower energy protons, it is seen that very few rads will be delivered by such protons. Protons above about 200 MEV move too fast to interact electrically with bound electrons within the film gelatin long enough to produce much ionization, so that a low contribution in rad dosage results. It is for this same reason that such high energy protons are difficult to shield, i.e., they do not give up their energy to the electrons in the shielding medium.

From the foregoing, the rads delivered may be safely assumed to be coming entirely from proton energies of the order of 100 MEV, since this is higher than the actual average proton energy (Ref. 6-20, 6-22) and thus represents a greater film effect for a given rad exposure than would actually occur. (Proton energies much above 100 MEV can occur, but these are related to very low probability flare events, not included in the stipulated 90% probability of obtaining net fog densities less than 0.3.)

The effects of proton exposure on aerial films has been investigated experimentally by Kodak and Langley Research Center personnel. Proton exposure data supplied by Kodak is presented in Figures 6-6a, 6-6b and 6-6c for Type SO-243 and SO-206 films. The shielding requirements for Voyager missions have been established for these film types.

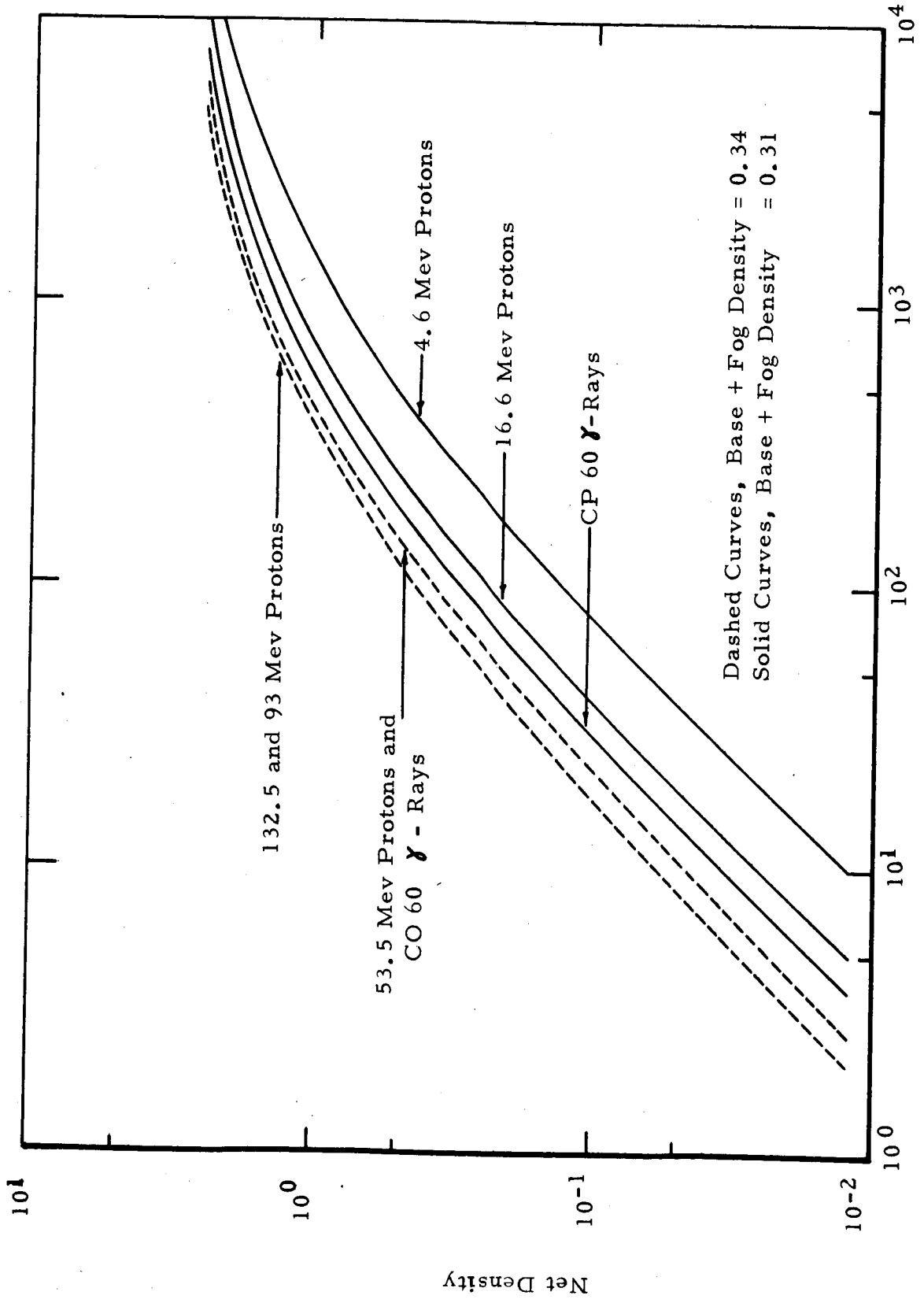

FIGURE 6-6a RADIATION EXPOSURE FOR KODAK SO-243 HIGH DEFINITION AERIAL FILM (GRAY BASE) - BIMAT PROCESSED

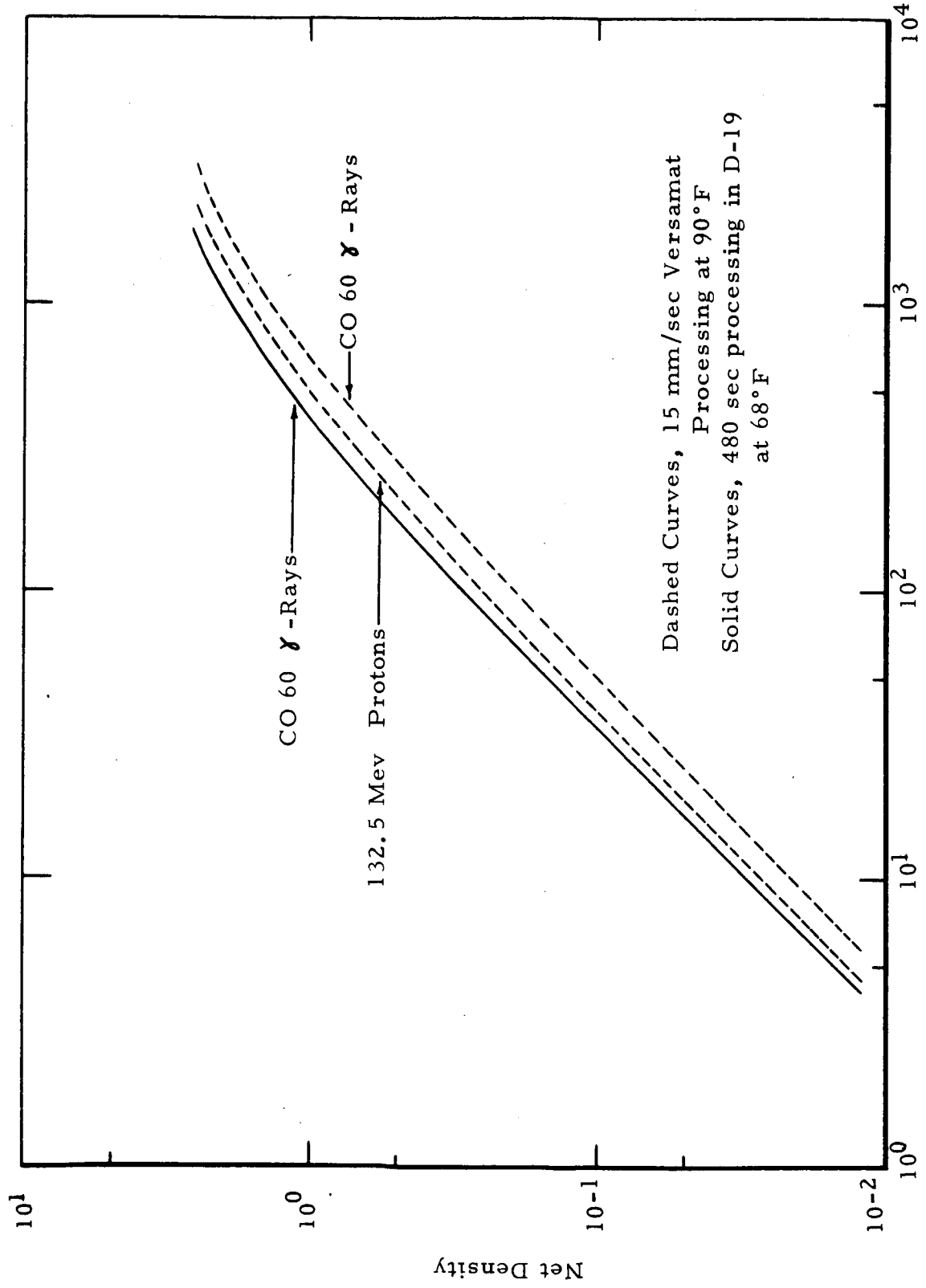

FIGURE 6-6b RADIATION EXPOSURE FOR KODAK SO-243 HIGH DEFINITION AERIAL FILM (GRAY BASE)

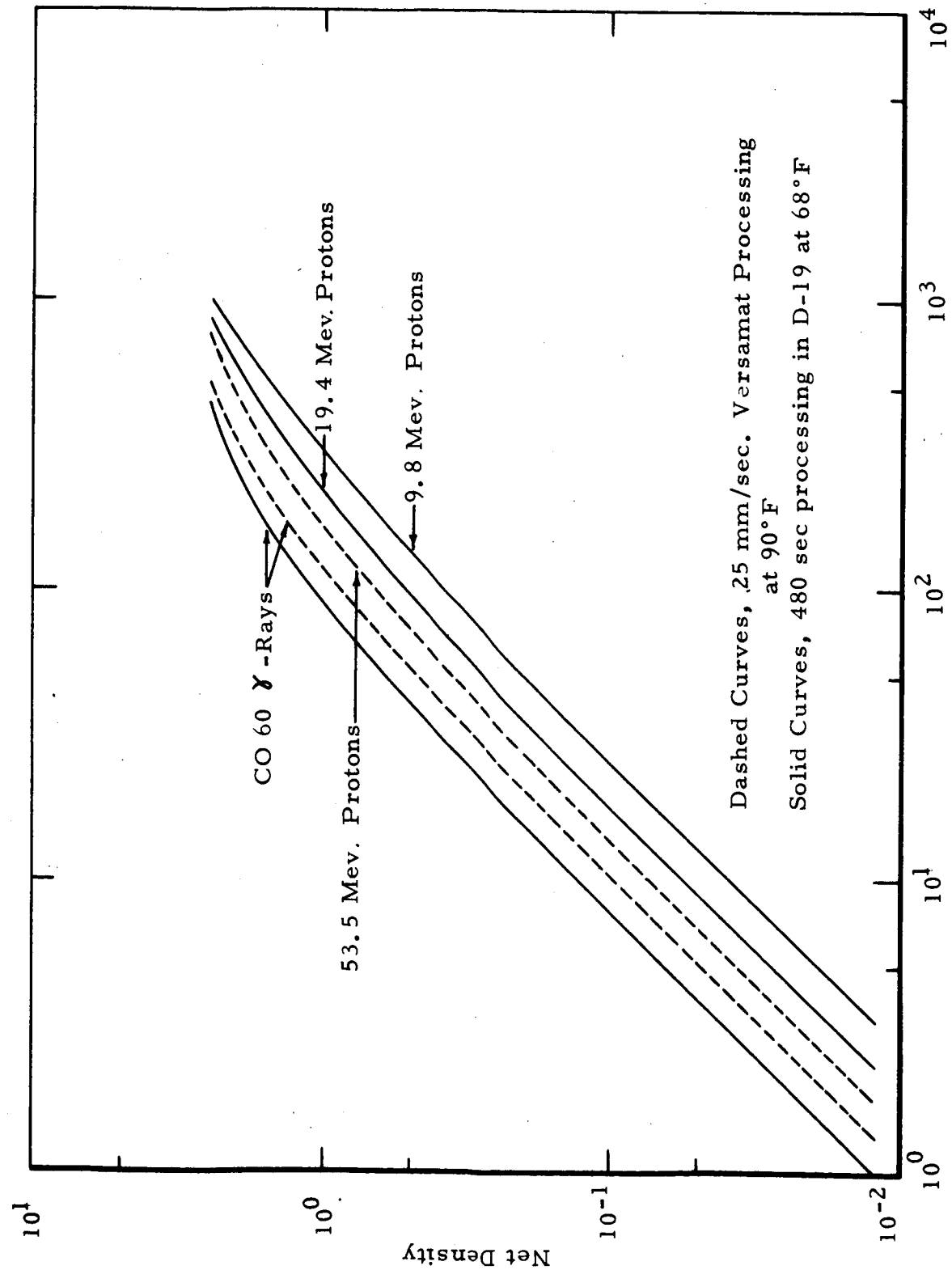

FIGURE 6-6c RADIATION EXPOSURE FOR KODAK SO-206 SPECIAL AERIAL NEGATIVE FILM (ESTAR THIN BASE)

6.2.3.1 Type SO-243 Film Shielding Requirements - Figure 6-6a presents radiation exposure data for Bimat processed Type SO-243. The solid line (film/processing schedule #2) Cobalt 60 γ-ray curve of this figure corresponds fairly well to the curve in Figure 6-6b for the standard 8 minute D-19 developer and, therefore, can be considered to be a good "standard" with which to evaluate radiation effects.

The dashed curve in Figure 6-6b is for 132.5 MEV protons (which is in the order of the 100 MEV level of interest) using the film/processing schedule #1 development process. By comparing the dashed and solid Cobalt 60 γ-ray curves in Figure 6-6b and extrapolating to a "standard" Bimat process for 132.5 MEV protons, a 0.3 density would result from an exposure of about 85 rads, which may be considered to be the total mission radiation exposure limit. Deducting the unshieldable galactic radiation of 2 rads per month for the eleven month mission leaves 63 rads as the maximum dosage to be permitted to pass through the shielding.

Rad dosages due to solar flare protons and alpha rays have been computed as a function of aluminum and polyethylene shielding thickness for a 14.5 month 1977-8 Mars mission (Ref. 6-22). The dosage data, scaled down for an eleven month mission, is presented in Figures 6-7a, and 6-7b. The solar flare damage information for the mathematical model was obtained from the solar cycle 19 profile (1954-1964). As indicated in Section 2.8, a mission in 1977 can be expected to encounter more radiation than a mission in 1973 or 1975. Also, the dosage was computed on the basis of an Earth-return trajectory passing inside the orbit of Venus, which, being nearer the sun, receives stronger flare radiation than Mars. Applying these considerations thus serves to introduce an additional design safety factor.

Figure 6-7a indicates that an aluminum shield thickness of about 10 gm/cm^2 provides a 90% probability that no more than 63 solar flare proton rads will be received during the eleven month mission. (The effects of solar flare α-rays are also shown, but do not significantly add to the shielding requirements.)

Similarly, for the case of polyethylene shielding (Figure 6-7b) about 8 gm/cm^2 would be required to provide a 90% probability that no more than 63 solar flare proton rads will be received during the mission. The shielding mass required for 70 mm SO-243 film is shown in Figure 6-8 as a function of film length for specific shielding thicknesses.

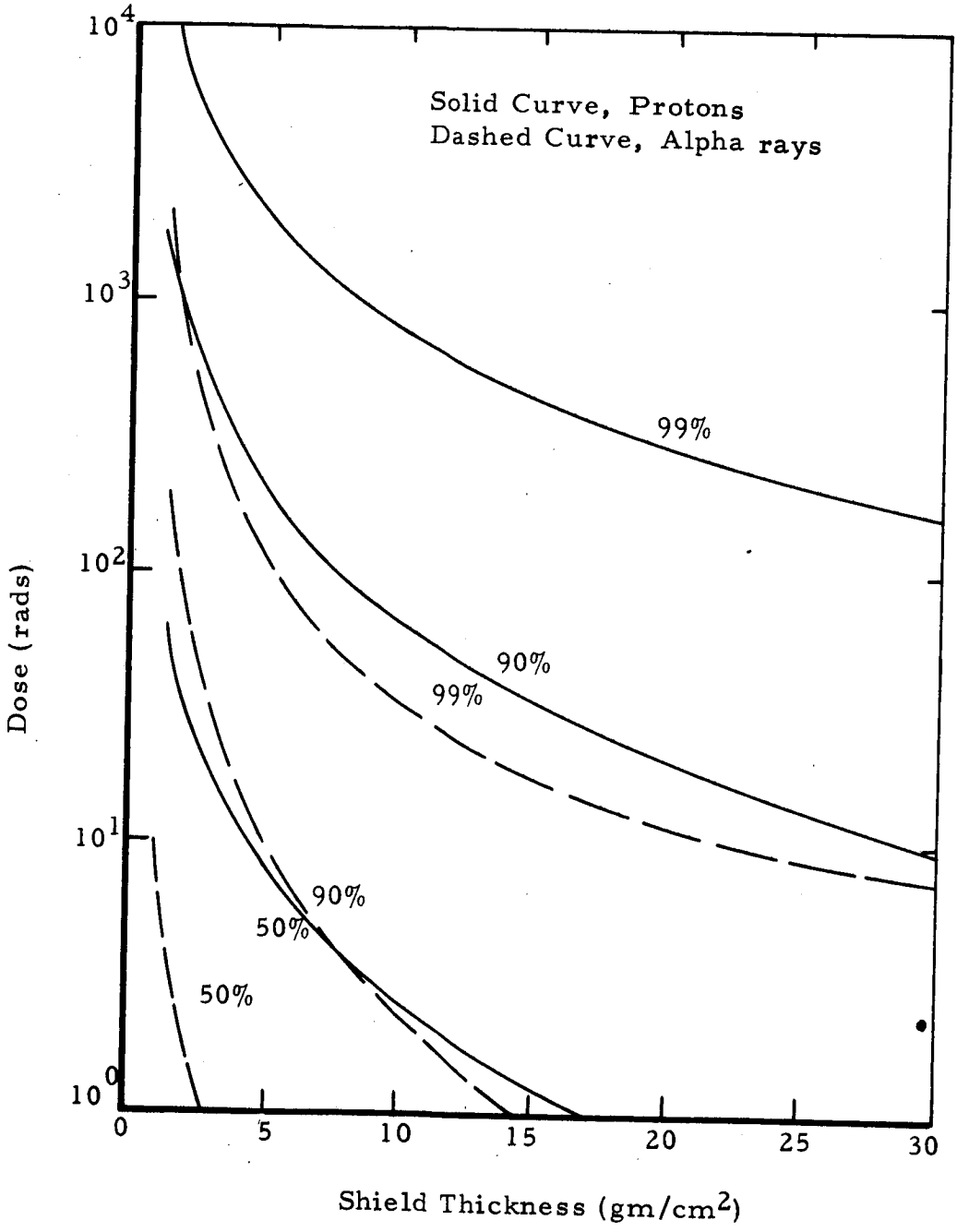

FIGURE 6-7a EXPOSURE DOSE VERSUS ALUMINUM SHIELD THICKNESS FOR A MARS MISSION

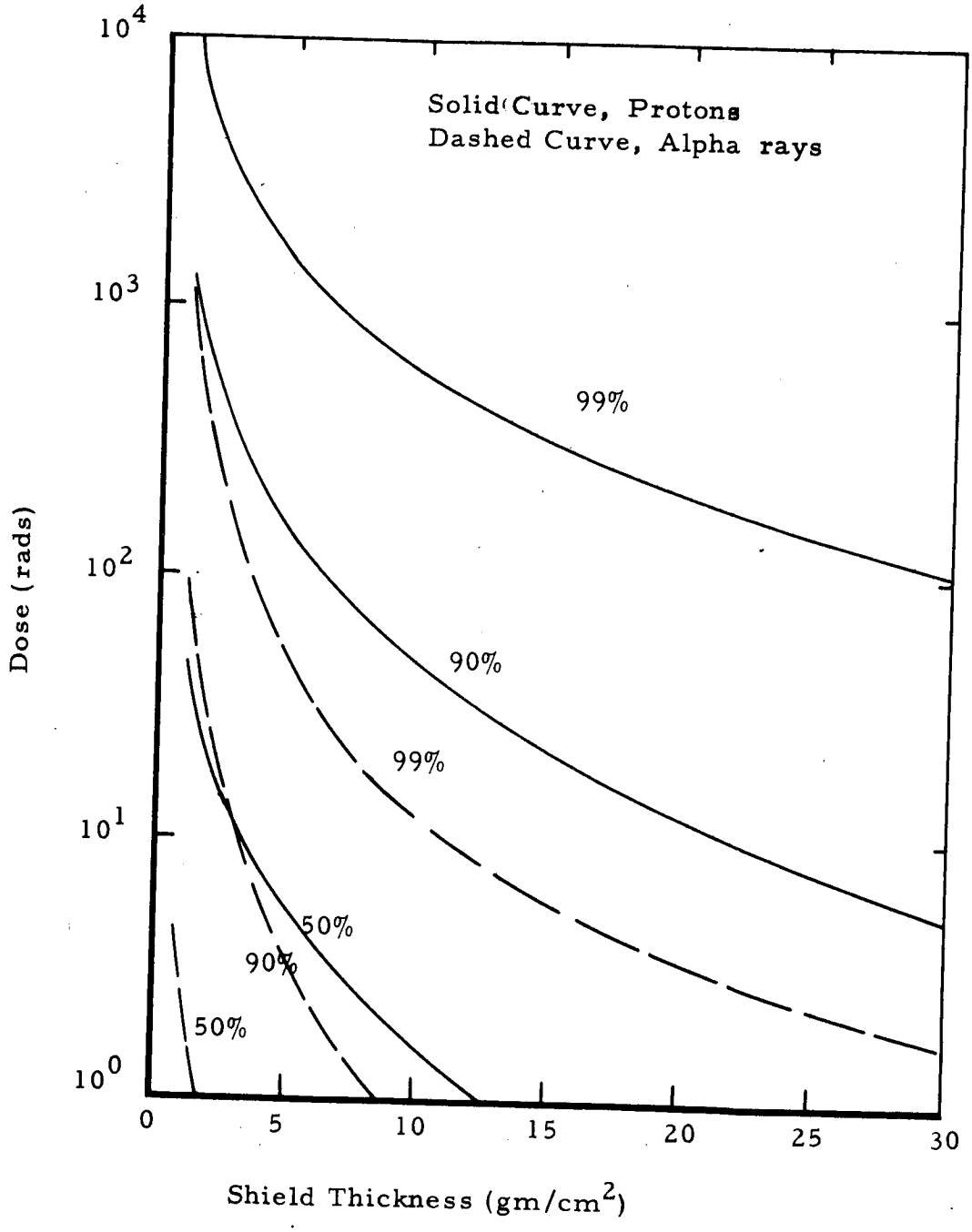

FIGURE 6-7b EXPOSURE DOSE VERSUS POLYETHYLENE SHIELD THICKNESS FOR A MARS MISSION

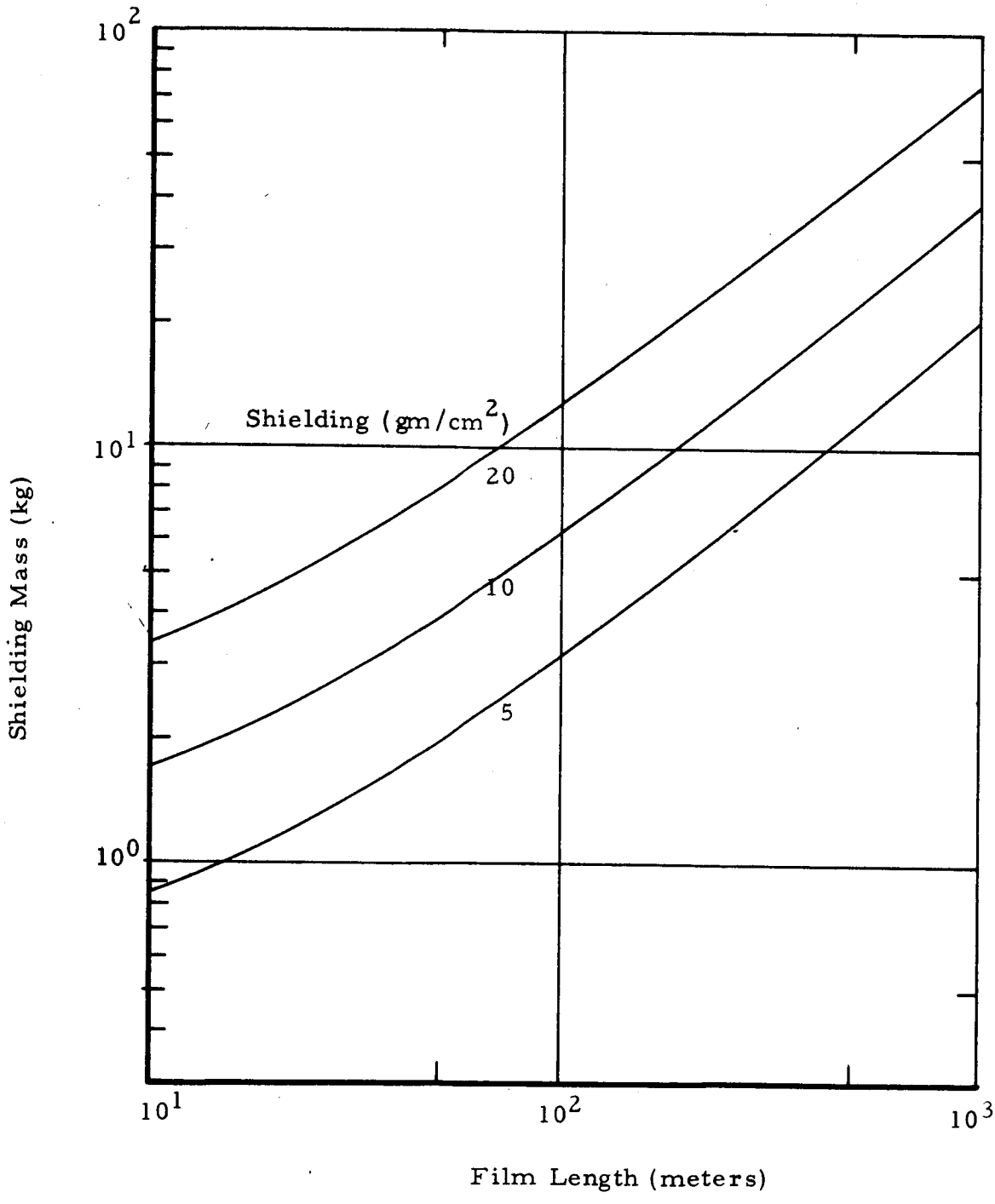

FIGURE 6-8 SHIELDING MASS VERSUS FILM LENGTH FOR 70 mm SO-243 FILM

6.2.3.2 Type SO-230 Shielding Requirements - There is no available data on the response of the new SO-230 film to proton exposures. It is, therefore, necessary to estimate required shielding thickness by relating it to a film having similar sensitivity, such as SO-206 (both films have an aerial exposure index of 6). It appears that SO-206 can be regarded as a safe equivalent of SO-230 for shielding computation purposes, for if a departure from equal sensitivities did occur for the case of proton radiation, the finer grained SO-230 film would, if anything, become the slower film.

While no Bimat process information is available on SO-206, Versamat data is available. Extrapolating from the data in Figure 6-6c, a net density of 0.3 results from about a 35 rad dose of proton radiation of the order of 100 MEV. Using the same Versamat process for SO-243 film (Figure 6-6b), a 120 rad dose of similar radiation results in a net density of 0.3. Thus, the ratio of speeds between SO-206 and SO-243 for this type of proton energy and Versamat processing schedule is about 3.5. A different gauge of their speed ratio can be obtained by comparing their response to visible light for some specific developer. Using their respective H&D curves corresponding to visible light exposure and the use of D-76 developer for 8 minutes (the choice of developer and development time is quite arbitrary provided these are the same for both films), the ratio of these exposures is also about 3.5. This suggests that the ratio of sensitivities of two different types of film for the same type of radiation and development process does not vary strongly, if they are subsequently compared for some other type of radiation and some other development process.

Using this concept of constancy of ratio of sensitivities between two films, an "inherent sensitivity ratio" of about 3.5 can be assigned between SO-206 and SO-243 films. Thus, since Bimat processed SO-243 obtains a net density of 0.3 for about 85 rads of 100 MEV proton radiation, it can be concluded that Bimat processed SO-206 obtains this same density from 24 rads of 100 MEV proton radiation. Therefore, since 22 rads are expected from galactic radiation alone, it follows that SO-206 film cannot be used. Hence, SO-230 film, which was equated to SO-206 in terms of exposure sensitivity, cannot be seriously considered for the assumed mission.

This conclusion is tentative since experimental data on SO-230 film for proton exposure is not available. It is conceivable that SO-230 film, being of much finer grain structure than other films of Aerial Exposure Index 6, may "revert to type" for proton exposures and

become slower as do other very fine grain films. (This would render SO-230 film an exception to the general rule of "constancy of ratio of sensitivities," but this is conceivable, since it is already quite atypical in that its speed, for visible light at least, is several times larger than would be expected in view of its very high resolution.) If this proves to be the case, namely, that the effective AEI value for SO-230 film is found to be considerably less than 6 under proton exposure, then the question of its applicability would have to be re-examined.

6.2.3.3 Radiation Sensitivity of Processing Materials - The effect of radiation on processing materials as well as film must be considered since the processing material is equally likely to be subjected to radiation. However, processing chemicals have been subjected to incident dosages of 1,000 rads without noticeable damage.

The polyvinyl chloride structure of Fairweb has been subjected to radiation sterilization in another application without deleterious effect. Bimat processing material has been irradiated with 1,000 rads of proton exposure without any significant changes in processing characteristics.

6.3 TAPE SENSOR SYSTEMS

Various promising tape sensor systems have been evaluated for Voyager mission applications. The basic tape materials considered include: dielectric tape, electrostatic tape and photoplastic tape. Each of these materials provides both a sensing and a storage capability, and each offers the advantage of reuseability. The dielectric tape and electrostatic tape systems utilize video techniques in conjunction with the tape material to record and readout data. The photoplastic tape system employs thermal and optical techniques for recording and reading data. The operation and performance characterisitics of these tape sensors are described in the following subsections.

6.3.1 Dielectric Tape

Dielectric tape camera systems, under development by RCA for a number of years, are capable of both sensing and storing an optically imaged scene. The tape (sensor) material can be read-out or stored for future readout. The major advantages include good speed, all electronic (non-chemical) processing, reuseability and a relative insensitivity to radiation.

The basic four layer dielectric tape material consists of a transparent polyester base, a transparent metallic conducting layer, a photoconductive layer and a transparent insulating layer of polysterene. The image is stored on the insulating layer.

Three electron guns are required in a dielectric tape system. One gun is used for charging the tape material, a second for the recording operation and the third for readout (Ref. 6-23, 6-24). The tape material is prepared by scanning the insulating layer with the electron gun, while simultaneously illuminating the tape with light considerably brighter than the expected scene illumination. A uniform tape potential is established and all previously stored data is removed as a result of the process.

In the recording operation, the scene is optically focused upon the photoconductor as it is simultaneously flooded with an electron beam. The insulator surface becomes positively charged with respect to the metallic layer, with the charge a function of the illumination variations in the scene. A charge pattern corresponding to the optical scene remains on the dielectric tape for read out or storage for future readout. The spectral response of the tape is a function of the photoconductive material selected. The response peaks in the visible but is not as wide as the silver halide response.

The readout process converts the charge pattern on the insulator into an electrical output signal. Readout can be accomplished either by using standard vidicon techniques or by using return beam modulation and electron multiplication as an image orthicon.

Currently, dielectric tape sensor systems are limited by low resolution compared to vidicon tubes and silver halide films. A 35 mm dielectric tape camera designed by RCA (Ref. 6-23, 6-25) for meteorological applications (Nimbus) provides a resolution capability of about 12 line pair/mm. (Other characteristics of this system are given in Table 6-11.) An experimental system with an approximate 40 to 50 line pair/mm capability was designed for the Air Force. The electron beam readout currently limits system resolution. Higher resolution of about 80 to 90 line pair/mm has been predicted for the 1970's, if adequate support is provided for the required development work.

6.3.2 Electrostatic Tape

Westinghouse Electric Corporation has been conducting a research program to develop an electrostatic tape camera system suitable for reconnaissance under adverse illumination conditions. The system is to provide good resolution and a large information storage capacity on a reuseable sensor/storage medium, which is not damaged by radiation.

An electrostatic tape camera, incorporating an endless metal tape loop as the storage surface, has been built for the Air Force (Ref. 6-26). The tape is a grooved metallic material with a dielectric deposited on the long surfaces of the grooves (Ref. 6-27). Grooves on the grating storage tape are generally spaced 6000 grooves/inch. Electron beam guns are used to prime, write, read and erase the tape. The optical image, converted to a photoelectron charge pattern, is focused onto the primed dielectric surfaces of the tape and stored as an electrostatic charge pattern.

Reading of stored pictures is accomplished by a high resolution electron beam in much the same manner as in an image orthicon camera. After reading, the pictures may be erased electronically so that the electrostatic storage tape is reuseable. Tapes can be read-out immediately or stored; data has been stored on the tape for up to 60 hours without apparent degradation.

TABLE 6-11 METEOROLOGICAL DIELECTRIC TAPE CAMERA SYSTEM CHARACTERISTICS

Designated Space System	Nimbus
Tape Length (m) Image Format (mm)	30.5 18.4
Resolution: TV lines Line Pair/mm	 436 12
Sensitivity (meter candle seconds) Dynamic Range	3×10^{-2} 33:1
Optics: F/No. Focal Length (mm)	 f/2.5 127
Camera Physical Char.: Mass (kg) Max. Power (watts)	 38 30

An Electrostatic Latent Image Development process may be incorporated to considerably raise the effective photographic speed index for the electrostatic camera system. This is accomplished by driving the exposed tape past a line flood beam of electrons. The process can be used to enhance contrast for low level signals, but introduces additional noise and is not recommended if longer exposure times are possible.

The developmental electrostatic tape camera built by Westinghouse for the Air Force has a 450 mm endless tape loop, enough for 18 frames with with a 25 mm square format. The system provides a limiting resolution of 50 line pair/mm with a signal-to-noise ratio in excess of 100.

Westinghouse has proposed orbital electrostatic tape systems for space mapping missions. Table 6-12 presents the characteristics of such a system. Although the electrostatic tape process is highly developmental, Westinghouse indicates that an operational system could be available in the 1970's.

6.3.3 Photoplastic Tape

The photoplastic tape process, developed by the General Electric Company, is based upon the deformation by heating of a light sensitive thermoplastic photoconductive medium (Ref. 6-29, 6-30). The photoplastic sensor/storage material is inherently capable of extremely high resolution and is reuseable. However, the material generally exhibits slow photographic speed and requires high power output for processing and erasure.

The photoplastic tape material process is based to some extent on the development of thermoplastic film, also by General Electric. Thermoplastic film, however, is not a sensor medium; it is used as a recording device in conjunction with radar or infrared sensors (Ref. 6-34, 6-35). An Air Force thermoplastic recording system is currently under development (Ref. 6-36, 6-37). This system provides 8000 by 5000 picture elements on a 75 by 50 mm tape area. The tape has a 10 megacycle recording bandwidth and a dynamic range capability of better than 100 to 1.

The photoplastic film is a photoconductive thermoplastic material. The material is sensitized before use by depositing a uniform electrical charge on its surface with a corona discharge device. This surface charge is dissipated due to the photoconductivity induced in the

TABLE 6-12 ELECTROSTATIC TAPE CAMERA SYSTEM CHARACTERISTICS

SYSTEM CHARACTERISTICS	Medium Ground Resolution System	High Ground Resolution System
Tape Length (mm)	450	450
Tape Width (mm)	35	35
Image Format (mm)	25x25	25x25
Resolution (lp/mm)	50	50
Number of Pictures/Tape	18	18
Sensitivity (meter candle second)	10^{-2}	10^{-2}
Dynamic Range	100:1	100:1
Optics:		
F/No.	f/16	f/16
Focal Length (mm)	560	5600
Field of View (deg)	3.7	0.37
Mass (kg)	1.4	23
Camera Physical Char.:		
Mass (kg)	20	42
Power (watts)	-	-

material upon exposure to an image. A real image is formed by heating the film to the flow point of the thermoplastic. When cooled, the deformations corresponding to the recorded image can be viewed with a Schlieren projection system. The light intensity of the projected image is dependent upon the depth of film deformations.

The material can be erased for reuse with the application of approximately twice the heat required for development. The reuseability of photoplastic is limited by the decomposition due to heating and the degree of cleanliness of the environment.

Photoplastic materials generally have not offered spectral sensitivities as broad as those of silver halides. However, a new type has been developed which offers improved red sensitivity and is responsive from the ultraviolet to the near infrared (Ref. 6-31).

Theoretical predictions of resolution are for better than 1000 line pair/mm; 360 line pair/mm have already been achieved in the laboratory (Ref. 6-32). Photographic speeds of ASA 30 have been reported; however, high resolution has been obtained only at low ASA speeds. Typical performance of the photoplastic film is 150 to 200 line pair/mm but at a questionable ASA speed range of 1 to 3.

6.3.4 Comparison of Tape Sensors

All three of the candidate tape sensor systems must be currently considered to still be in a developmental state. Dielectric tape systems are probably in the most advanced state of development for space applications, but substantial capability improvements are required for Voyager type applications.

Electrostatic tape systems appear promising for planetary type missions, but would need extensive development. Photoplastic tape devices currently do not appear suitable for orbital planetary photographic sensors. The characteristics of the three tape materials are compared in Table 6-13.

TABLE 6-13 COMPARISON OF DIELECTRIC, ELECTROSTATIC AND PHOTOPLASTIC TAPE MATERIALS

SENSOR	MFG.	RESOLUTION (lp/mm)	SENSITIVITY (meter-candle-seconds)**	COMMENTS
Dielectric Tape*	RCA	12 to 50	10^{-2}	Meteorological system: 12 lp/mm with growth to 40-50 lp/mm; Air Force developmental system: 45 lp/mm, program terminated.
Electrostatic Tape*	West.	50	10^{-2}	System proposed by Westinghouse for orbital mapping; moderate resolution, data storage on tape loop in a vacuum compartment, needs developmental work.
Photoplastic Tape	G. E.	200	10^{-1}	Current application as a copy and recording media, potential speed improvement, high density recording media, high resolution potential, Schlieren optics required for viewing.

*Most suitable of these sensors.

**Approximate values.

6.4 OTHER SENSOR MATERIALS

Several other sensor materials have been considered for Voyager mission applications. Included are electrophotography, dry silver, frost xerography, RS and diazo. Each of these sensors is capable of achieving high resolution, but at relatively slow speeds. Based on current data, these sensors are considered more suitable for copying applications. The primary characteristics of each of the sensor materials are described in the subsections which follow.

6.4.1 Electrophotography

Electrophotography is currently used in commercial copying equipment (e.g., Zerox and Electro Fax). In the dry, non-chemical xerographic process, an electrostatic latent image, formed on a photoconductive layer by the exposure, is made visible by the deposition of a fine powder material on the charged areas (Ref. 6-38).

The xerographic process currently provides a resolution in the order of 15 line pair/mm. Specialized liquid and colloidal suspension techniques can produce resolution capability of 200 to 600 line pair/mm (Ref. 2-39). The speed of electrophotographic materials is limited to about ASA 15 and both spectral sensitivity and tonal quality are poor. Considerable effort is being expended to improve the process, but almost exclusively for duplication applications.

6.4.2 Dry Silver

The dry silver photographic process, developed by the 3M Company, uses a silver halide material combined with image forming materials. Upon exposure to light, the silver from the silver halide catalyzes the constituents of the image forming materials and a silver image is formed after the application of heat.

Resolution in the order of 1500 line pair/mm has been achieved but at a low ASA equivalent speed of 10^{-3} (Ref. 6-40). Faster speeds up to about an ASA of 10^{-1} are possible for such applications as electron beam recording.

6.4.3 Frost Xerography

The Xerox Corporation has developed a process to permit an electrostatic image to be transferred to a thermoplastic film which is then heated to create the image deformation pattern. The process is somewhat

similar to the photoplastic method, except that a conducting liquid is incorporated to transfer the charge. The material is reuseable and the images are transparent and suitable for projection viewing.

Resolutions on the order of 100 line pair/mm can be obtained, but only at low speeds. A resolution of 21 line pair/mm has been obtained at an equivalent ASA of 100 (Ref. 6-41, 6-42). Image uniformity and spectral response are poor by comparison to silver halide performance. In addition, the process is mechanically complex and therefore not currently suitable for space application.

6.4.4 RS Process

RS is a relatively new photographic process developed by the Itek Corporation (Ref. 6-43). In the conventional silver halide process, the photoconductor is the source of image material. In the RS process, the image material is added during processing. The RS material has excellent shelf stability, including stability to heat, gamma and x-ray radiation; can be manufactured in actinic light; and can be processed rapidly. However, the material is slow with an approximate speed of ASA 2×10^{-2}. As a copy material, at high contrast, it is capable of resolving up to 600 line pair/mm. In addition, the material is grainless and has good tonal and spectral qualities.

6.4.5 Diazo

The diazo process involves the use of dyes sensitive in the ultraviolet and violet portion of the spectrum. When exposed to radiation, the diazonium molecule is decomposed and nitrogen is released from the molecule. The product is relatively colorless and is inactive during further exposure. A coupler reacts with the unexposed diazonium after the application of a mild neutralizing alkali to produce a visible image in the unexposed areas.

Diazo materials are used primarily as a recording media. They possess high resolution capability of approximately 2000 line pair/mm, but have slow speeds in the order of ASA 10^{-4}. The slow speed and limited spectral sensitivity are prohibitive for reconnaissance purposes.

6.5 SENSOR SUMMARY

A summary of the relative advantages and disadvantages of the promising sensor candidates for the Voyager mission is presented in Table 6-14. These are vidicons, return beam vidicons, silver halide film (SO-243), dielectric tape and electrostatic tape. The potential resolution capabilities for the 1970's are indicated in terms of suitability for use in high and/or medium resolution cameras.

The three particular sensors selected for the purpose of systems analysis (see Section 8) are the one inch vidicon, two inch return beam vidicon, and 70 mm SO-243 film. The one inch vidicon system was selected because of its prior space experience. The two inch rather than the four inch return beam vidicon was selected because of mass considerations. The 70 mm SO-243 film was chosen because of its use on the Lunar Orbiter and the radiation considerations discussed in Section 6.2. Neither of the tape systems were included primarily because of their developmental status.

TABLE 6-14 COMPARISON OF SENSORS FOR VOYAGER MARTIAN MISSION APPLICATIONS

Sensor	Advantages	Disadvantages	Camera Resolution Capability	
			Early 70's	Late 70's
Vidicon	a) reusable with magnetic tape b) good speed c) insensitive to radiation d) space proven	a) needs separate storage b) limited format c) resolution less than film	medium	medium
Return Beam Vidicon	a) good speed b) reusable with magnetic tape c) insensitive to radiation d) excellent resolution potential	a) needs separate storage b) limited format c) more complex than vidicon d) still developmental	medium	high and medium
Silver Halide (SO-243)	a) excellent resolution b) self-contained data storage c) flexible readout rates d) large storage capacity e) delayed readout capability f) space proven g) wide-flat spectral response h) excellent geometric fidelity	a) requires chemical processing b) radiation sensitive c) not reusable	high and medium	high and medium
Dielectric Tape	a) reusable material b) speed equal to vidicon c) insensitive to radiation d) self-contained data storage	a) currently low resolution b) complex c) limited format d) still developmental	medium	medium
Electrostatic Tape	a) reusable material b) good speed c) insensitive to radiation d) self-contained data storage	a) currently low resolution b) complex c) limited format d) still developmental	-	medium

6.6 REFERENCES

6-1 "Space Television Cameras," RCA Astro-Electronics Division, August 1967

6-2 HELSER, L., HOAGLAND, K. and LUVALLE, J., "Survey of Electrical-Chemical-Optical Transducers for the Visible Spectrum," Fairchild Space and Defense Systems, Report SME-AY-23, September 1963

6-3 "Television Sensor Performance and Characteristics," RCA Astro-Electronics Division, August 1967

6-4 "Vidicon Type 8051 and Image Orthicon Type 7967 Tube Data Sheets," RCA Electronic Components & Devices, March 1966

6-5 "Developmental Type C23061A Two-Inch Return Beam Vidicon," RCA Industrial Tube Division, October 1967

6-6 "SEC Vidicon Type WX - 5419B Technical Data Sheet," Westinghouse Electric Corporation - Electronic Tube Division, January 1967

6-7 "Plumbicon Type 55875 Data Sheet," Amperex Electronic Corporation, June 1965

6-8 HOUSE, R.A., Personal Communication, RCA Astro-Electronics Division, September 1967

6-9 GOETZ, G. W., et al, "Westinghouse SEC Camera Tubes," Advances in Electronics and Electron Physics, Volume 22, September 1965

6-10 Personal Communication at Westinghouse Seminar, September 1967

6-11 VAN DOORN, A. G., "The Plumbicon Compared with Other Television Camera Tubes," Philips Technical Review, Volume 27, No. 1, 1966

6.6 REFERENCES (continued)

6-12 DE HAAN, E. F., VAN DER DRIFT, A., SCHAMPERS, P. P. M., "The Plumbicon, A New Television Camera Tube," Philips Technical Review, Volume 25, No. 6-7, 1963-1964

6-13 BIRNSTEIN, P., Personal Communication, Amperex Electronics Corporation, September 1967

6-14 Eastman Kodak Film Data Sheets

6-15 SHEA, W. E., Personal Communication, Eastman Kodak, September and October 1967

6-16 "An Introduction to Kodak Bimat Transfer Processing System," Eastman Kodak, Pamphlet P-65, 1966

6-17 TURK, E., Personal Communication, Eastman Kodak, October 1967

6-18 "Camera and Film Processor for JPL," Fairchild Space and Defense Systems, Engineering Report SME-AF-22, August 1965

6-19 Supplement to above report (Ref. 6-18), November 1966

6-20 SCOTT, W. W., "Estimates of Primary and Secondary Particle Doses Behind Aluminum and Polyethylene Slabs Due to Incident Solar-Flare and Van Allen Belt Protons," Radiation Shielding Information Center, Oak Ridge National Laboratory, July 1967

6-21 LEACH, E. R., FAIRAND, B. P., and BETTENHAUSEN, L. H., "The Space Radiation Environment and Its Interactions with Matter," Radiation Effects Information Center, Battelle Memorial Institute, January 1965

6-22 HILL, C. W., RITCHIE, W. B. and SIMPSON, K. M. JR., "Data Computation and Evaluation of Space Shielding Problems: Volume III, Radiation Hazards in Space," Lockheed Aircraft Corporation, April 1966

6.6 REFERENCES (continued)

6-23 FREEDMAN, L. A., "A Dielectric-Tape Camera for Meteorological Applications," Supplement to IEEE Transactions on Aerospace and Electronic Systems, Volume AES-2, No. 4, July 1966

6-24 BELLER, W. S., "Dielectric Camera Ready for Space Use," Missiles and Rockets, 18 April 1966

6-25 HOUSE, R. A., FREEDMAN, L. A., BINLEY, J., Personal Communication, RCA Astro-Electronics Division, September-October 1967

6-26 "Electrostatic Tape Recording for Orbital Mapping," Westinghouse Electric Corporation, Westinghouse Aerospace Division Report, July 1967

6-27 JENSEN, A. S., REININGER, W. G., LIMANSKY, I., "The Grating Storage Target," Advances in Electronics and Electron Physics, Volume 22, Photo-Electronic Image Devices Third Symposium, Published by Academic Press, 1965

6-28 JENSEN, A. S., Personal Communication, Westinghouse Aerospace Division, October 1967

6-29 GAYNOR, J., AFTERGUT, S., "Photoplastic Recording," Photographic Science and Engineering, Volume 7, No. 4, July-August 1963

6-30 AFTERGUT, S., GAYNOR, J., WAGNER, B. C., "Sensitometric Study of Photoplastic Films," Photographic Science and Engineering, Volume 9, No. 1, January-February 1965

6-31 BARTFAI, J. J., OZAROW, V., GAYNOR, J., "Red-Sensitive Photoplastic Recording Film," Photographic Science and Engineering, Volume 10, No. 1, January-February 1966

6.6 REFERENCES (continued)

6-32 AFTERGUT, S., BARTFAI, J.J., GAYNOR, J., "Photoplastic Recording for Electro-Optical Photography," Photographic Science and Engineering, Volume 9, No. 2, March-April 1965

6-33 AFTERGUT, S., and PASHLER, P., Personal Communication, General Electric Research and Development Center, September 1967

6-34 GLENN, W.E., "Thermoplastic Recording: A Progress Report," Journal of the SMPTE, Volume 74, August 1965

6-35 KIRK, N., "Thermoplastic Recording Tape Systems," Journal of the SMPTE, Volume 74, August 1965

6-36 "Air Force Gets Recorder - Display," Electronic News, 21 August 1967

6-37 "A Real Time Airborne Recorder - Display System," Signal, August 1967

6-38 NEBLETTE, C.B., "Electrophotography," Photography - Its Materials and Processes, New York, D. Van Nostrand Company, 1962

6-39 NEWMAN, A.A., British Journal of Photography, September-October 1964

6-40 HARRIMAN, B.R., "Progress in Dry Photography,"SPSE Symposium on Unconventional Photographic Systems, October 1967

6-41 BICKMORE, J.J., CLAUS, C.J., "Charge Transfer Frost Xerography," Photographic Science and Engineering, Volume 9, No. 5, September-October 1965

6-42 URBACH, J.C., "The Role of Screening in Thermoplastic Xerography," Photographic Science and Engineering, Volume 10, No. 5, September-October 1966

6-43 BERMAN, E., "The Itek RS Process," SPSE Symposium on Unconventional Photographic Systems, October 1967

SECTION 7

CONVERSION SUBSYSTEM ASSESSMENT

Information discerned by the optical and photosensor subsystems must be stored and converted into a form suitable for transmission from the orbital vehicle to the Earth. A data storage capability is required to reconcile the need for the rapid acquisition of imaging data with the much slower readout needed to restrict the data rate to the available capacity of the bandwidth limited communications system. Direct or real time readout is further precluded by interruption of the communications line-of-sight path during the portions of the orbit involving an Earth occultation by the Martian planet, as viewed from the spacecraft; since electrical power is obtained by conversion of solar energy, the communications also may be interrupted when the spacecraft is shadowed from the Sun by Mars (see Section 4).

Conversion subsystem factors which have been considered include:

- anticipated communications system capability
- mission data acquisition requirements
- mission data storage requirements
- capabilities of selected data storage media (i.e., magnetic tape recorder and photographic film)
- data readout techniques and capabilities
- optimum bandwidth utilization.

7.1 MISSION DATA HANDLING CAPABILITY AND REQUIREMENTS

The potential bandwidth capacity for the Voyager spacecraft-to-Earth communications link and the total amount of information which can be transferred to Earth during the postulated Voyager mission lifetime without violating the channel capacity restrictions have been evaluated. Consideration has been given to both microwave and optical (laser) transmission systems.

7.1.1 Spacecraft Data Transmission Capability

Spacecraft data handling capacity is increasing significantly; the Mariner IV system operated at 8-1/3 bits per second, whereas the 1969 Mariner mission to Mars is expected to utilize a 16,200 bit per second data transmission rate (Ref. 7-1). This improvement has been achieved by extension of present day techniques and primarily by the shift from a 25.9 meter to a 64 meter antenna dish at the ground station(s). Wideband RF links using high power output klystron tubes have been proposed with data rate capabilities in the megabits per second range (Ref. 7-2 and 7-3). However, the data rate capability for the deep space network (DSN), up to the year 1976, using three 64 meter antenna stations and a third generation computer system is expected to be 16,200 bits per second (Ref. 7-4).

The application of laser transmission system techniques to provide a broadband optical communications link has created considerable interest (Ref. 7-5). The general consensus, however, reflects the superiority of the microwave approach for the missions and time period under consideration (Ref. 7-6, 7-7 and 7-8).

A recent, comprehensive, study program, conducted by the Aerospace Group of Hughes Aircraft Company, provides a comparative assessment of 2.3 GHz microwave and 10.6 micron laser systems as applied to the communication and tracking requirement for interplanetary space missions (Ref. 7-9). Figure 7-1 shows the decided weight advantage of the microwave system for the Mars mission and data rates of interest. A study performed by NASA-Ames Research Center personnel similarly concludes that for mid-1970's Mars missions, the optimum telemetry link should be in the microwave band around 10 Gigahertz (Ref. 7-10).

7.1.2 Mission Data Rate Requirements

Figure 7-2 illustrates the total number of bits required to provide various percentages of ground coverage of the Martian planet for different ground resolutions. Six bit intensity encoding (64 intensity levels) is assumed, with a line pair required to describe each minimum discernible ground resolution element (i.e., for a 1 meter ground resolution, a 1 square meter area would be described by 4 resolution elements, with each element description containing 6 bit information).

Since the communications link represents one of the most significant constraints on the information gathering potential of a mission, the total

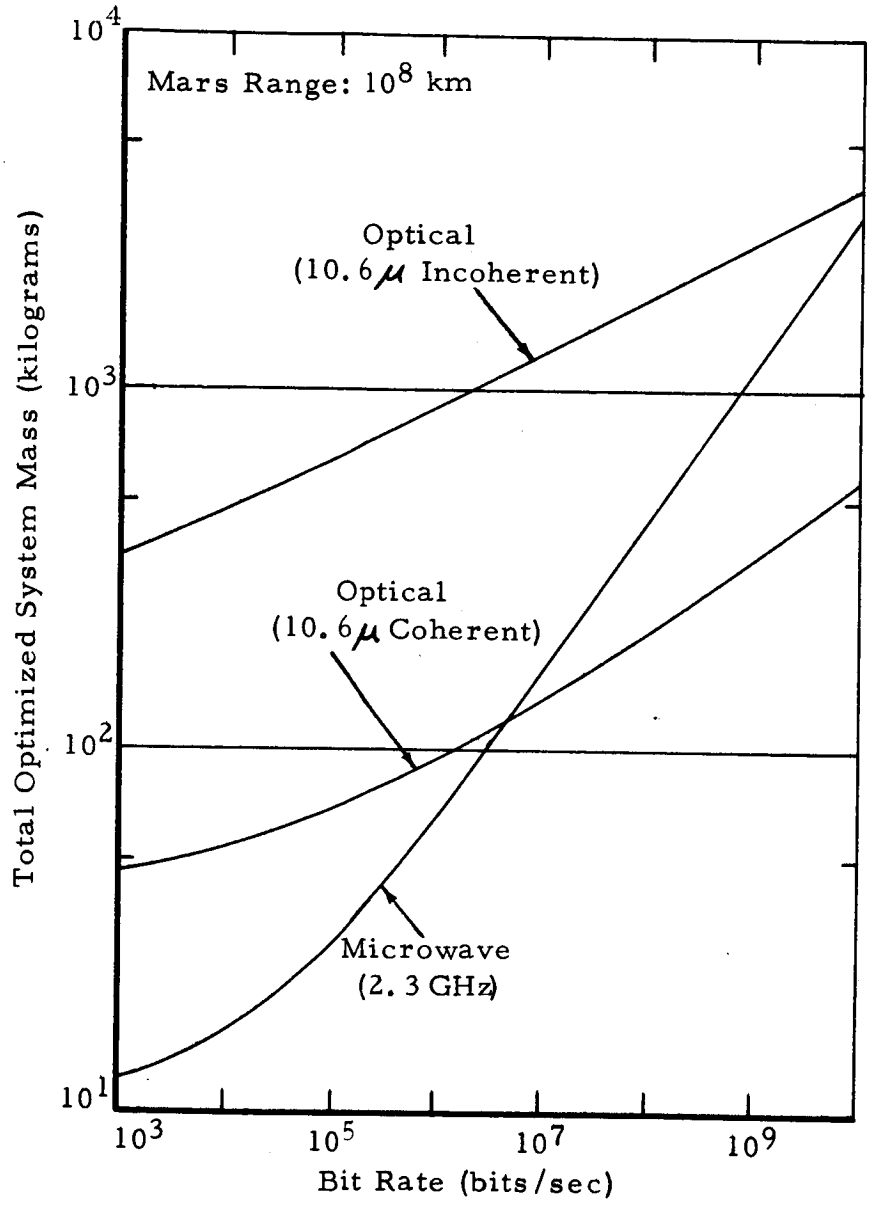

FIGURE 7-1 COMPARISON OF MICROWAVE AND OPTICAL TOTAL COMMUNICATION SYSTEM MASS VS. BIT RATE

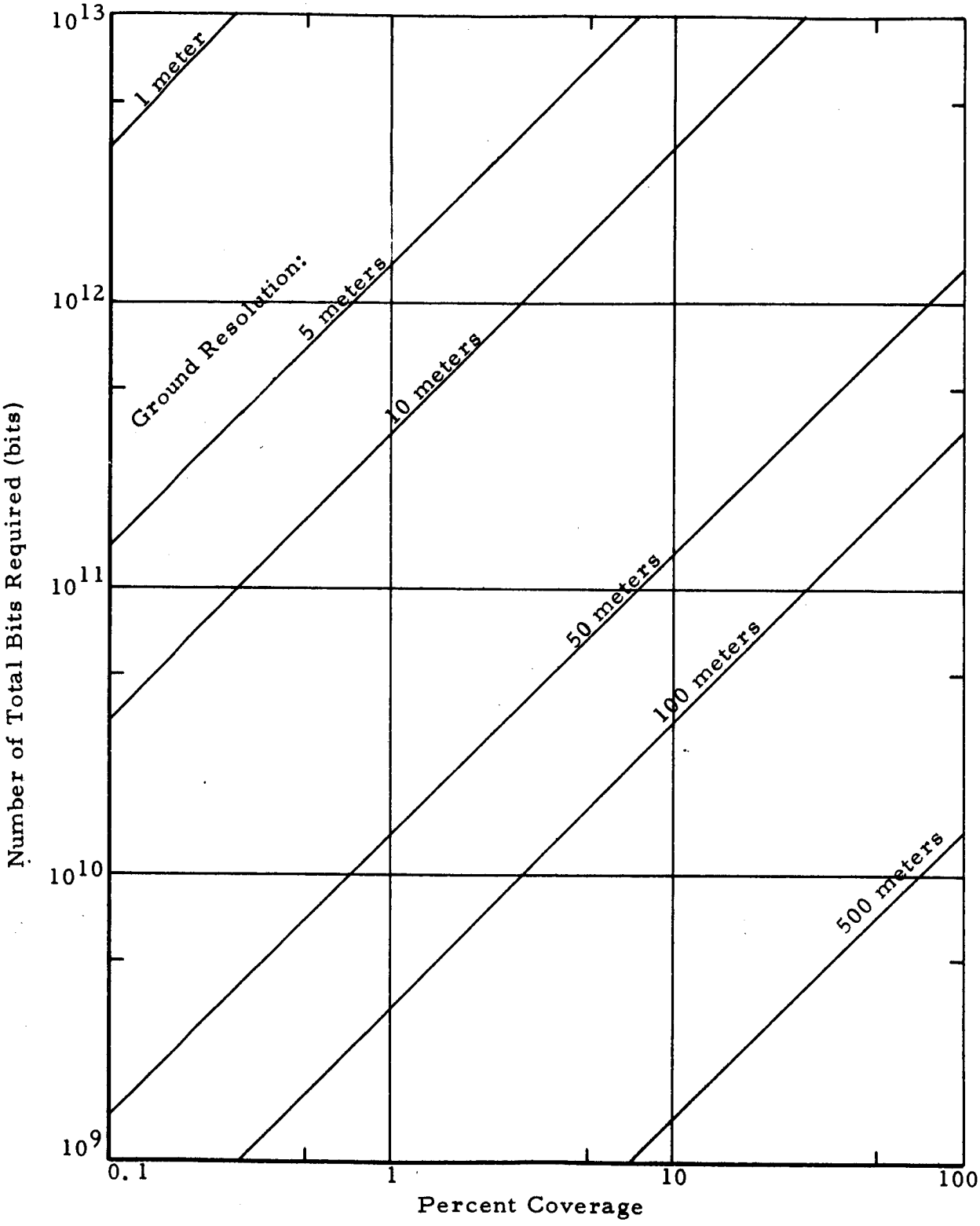

FIGURE 7-2 DATA TRANSMISSION REQUIREMENTS VS. PERCENT COVERAGE (6 bit encoding, 2 scan lines/resolution element)

number of bits transmitted is plotted parametrically as a function of mission life in Figure 7-3 for a range of discrete bit rates. Computer runs for several types of elliptical orbits with different periapsis values were examined to determine the time available for data acquisition with good ground resolution. Limiting the maximum altitude for image data acquisition, to about three times periapsis, a typical imaging time of less than 10 percent of the orbital period is obtained (see Section 4). Considering the possible loss of Earth line-of-sight and a non-simultaneous maximum Sun occult, a reasonable data transmission time of approximately 67% of total time in orbit has been assumed. (See Appendix C for minimum line-of-sight times for a wide range of possible orbits.)

The results of the above mission considerations in terms of their impact on the data handling requirements are summarized in Table 7-1 for a mission of 100 days in orbit, and in Table 7-2 for a mission of 200 days in orbit. Orbital mission constraints are neglected for these calculations (see Section 4). It must also be noted that the data acquisition rates are average rates and are not necessarily consistent with the data record rates associated with each type of sensor. The data link channel capability for the 1969 Mariner mission of 10^4 bits per second is certain, while a channel capacity for the mid-1970's of 10^5 bits per second can be projected. According to Ref. 7-11, a maximum communication rate of 15,000 bits/sec. should be considered at the initiation of imagery data transmission by the Voyager, with the maximum rate decreasing to approximately 5,000 bits/sec. by six months, due to the increase in Mars-Earth distance (see Appendix C). A 10^6 bits per second rate is presented as an upper bound for the time period under consideration.

Conclusions concerning data link limitations which can be drawn from the information in Tables 7-1 and 7-2, for the cases assumed are:

- Complete coverage of the Martian planet with 100 meter medium resolution system cannot be transmitted in 200 days with a 10^4 bits/second data rate, even if only this single sensor uses the data link.

- Complete coverage of the planet cannot be transmitted in 100 days with resolutions of 50 meters or better, even with the projected 10^5 bits/second transmission system capability.

- Virtually complete coverage (88%) can be transmitted in 200 days with a fixed resolution of 50 meters and a data rate of 10^5 bits/second.

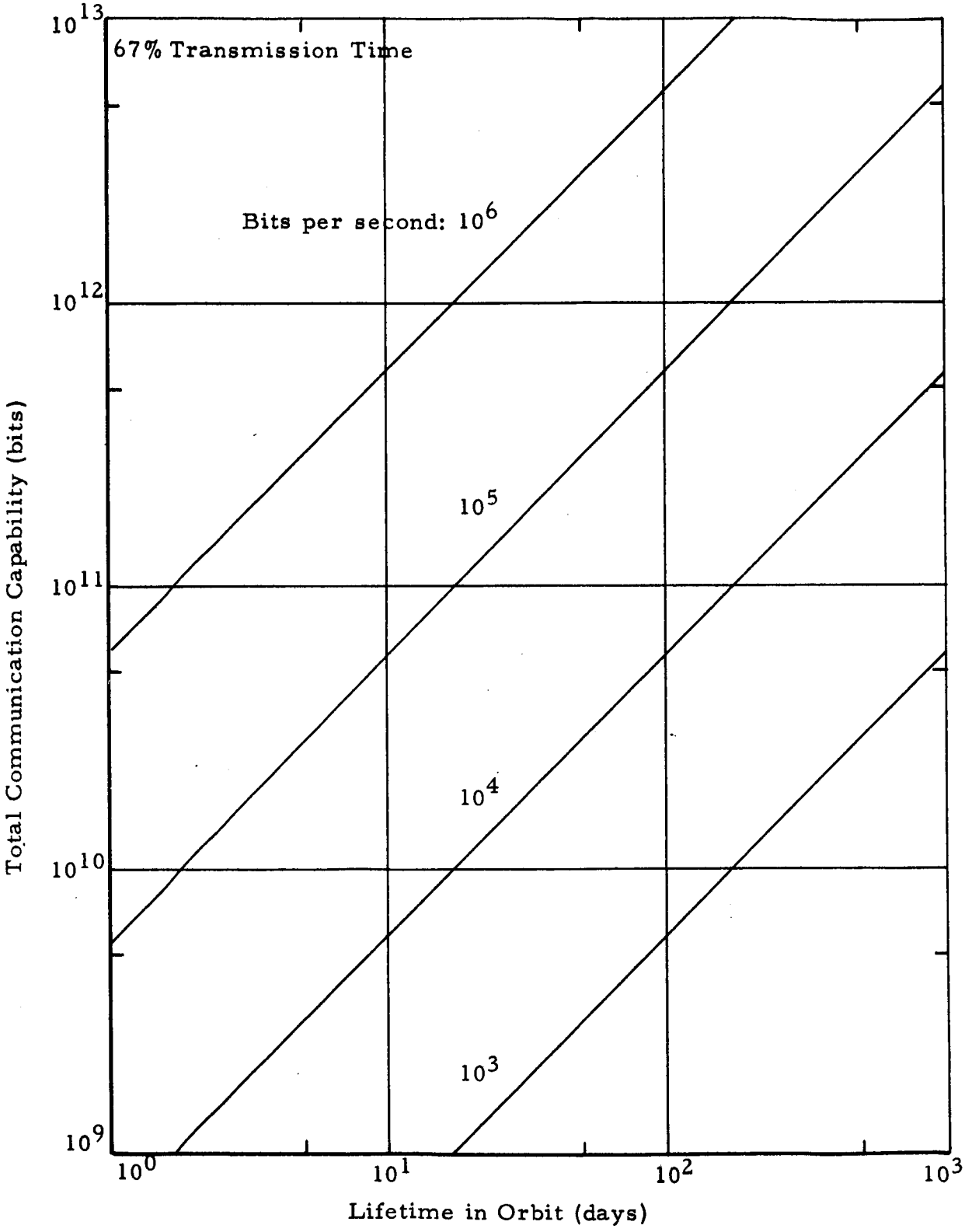

FIGURE 7-3 PLANETARY SPACECRAFT COMMUNICATIONS AS A FUNCTION OF MISSION LIFE

- With a dual sensor system, the minimum acceptable medium resolution (40 to 70 meter) coverage, specified in Table 3-4 (30°N to 30°S latitude), plus the high resolution (5 meter) spot coverage, equal to one percent of total medium resolution coverage, can be transmitted in 200 days with a data rate of 10^5 bits/second.

TABLE 7-1

DATA TRANSMISSION PARAMETERS*, 100 DAYS IN ORBIT

Parameter			
Transmission System Capability (bits/second)	10^4	10^5	10^6
Total Data, 100 days in orbit (bits)	6×10^{10}	6×10^{11}	6×10^{12}
Percent Planetary Coverage, Single Sensor:			
a) 100 meter resolution sensor	17%	>100%	>100%
b) 50 meter resolution sensor	4.4%	44%	>100%
c) 5 meter resolution sensor	0.04%	0.44%	4.4%
Percent Planetary Coverage, Dual Sensors:**			
a) 50 meter resolution sensor (medium)	2.2%	22%	>100%
b) 5 meter resolution sensor (high)	0.02%	0.22%	2.2%

* Assuming 67% transmission time and 6 bit encoding.

** Each sensor uses half of total data transmission capability.

TABLE 7-2

DATA TRANSMISSION PARAMETERS*, 200 DAYS IN ORBIT

Parameter Transmission System Capability (bits/second)	10^4	10^5	10^6
Total Data, 200 days in orbit (bits)	1.2×10^{11}	1.2×10^{12}	1.2×10^{13}
Percent Planetary Coverage, Single Sensor:			
a) 100 meter resolution sensor	34%	>100%	>100%
b) 50 meter resolution sensor	8.8%	88%	>100%
c) 5 meter resolution sensor	0.09%	0.88%	8.8%
Percent Planetary Coverage, Dual Sensors:**			
a) 50 meter resolution sensor (medium)	4.4%	44%	>100%
b) 5 meter resolution sensor (high)	0.04%	0.44%	4.4%

* Assuming 67% transmission time and 6 bit encoding.

** Each sensor uses half of total data transmission capability.

7.2 DATA STORAGE CAPABILITY

The Voyager orbiting vehicle is likely to acquire large quantities of imagery data at the relatively low altitudes near periapsis. The major portion of the time during the remainder of the orbit would be used for a relatively slow data readout and transmission back to Earth. This basic incompatibility between the need for rapid acquisition of data and inability of the spacecraft to transmit this information at a very high rate requires that some form of data storage be provided in the spacecraft to serve as a buffer. In the case of photographic film, the detection and storage functions are combined in one medium. For vidicon systems, in applications such as the Voyager Martian missions, a buffer storage device such as a magnetic tape recorder is required to permit rapid sequential picture data acquisition and relatively slow playback at the spacecraft communication rate.

The discussions in the following section are confined to those storage techniques which have high energy density capability, rapid data loading rates and large total capacity. In addition, the devices must be compatible with space environmental, reliability, vehicular configuration, weight and power constraints. The two materials for image data storage which meet these qualifications and have been successfully utilized in space programs are magnetic tape and silver halide film emulsions. Since the use of dielectric, thermoplastic and photochromic tape materials as storage media are still in a development stage (see Section 6) and the various laser schemes are even further off in the future, they are not considered in the detailed discussions which follow.

7.2.1 Magnetic Tape Recorders

The two standard magnetic tape recording techniques are longitudinal and transverse recording (Ref. 7-12). In the longitudinal system, the tape is transported past a stationary head to create a linear track along the length of the tape. In a transverse recording system the rotating multiple recording head is used to lay down a skewed data track across the width of the tape, with the tape being simultaneously transported in the longitudinal direction as before.

Transverse recording increases the relative tape-to-record head speed and permits the recording of wider bandwidth data for a given tape speed. To increase the total information storage capacity per unit length, in longitudinal recording, use of linear multiple tracks and wider tapes are employed. The data input handling rates may be

increased by faster tape speeds, increased bit packing density and parallel rather than serial recording of data. The use of parallel recording introduces the need for multi-track recording heads and buffer storage units to transform the serialized data stream into parallel word blocks and to reconstruct the data on playback. Aside from the additional circuit complexity, alignment problems of track-to-track data registration are introduced and the maximum achievable single channel bit packing density can no longer be utilized.

Digital recording can be performed by pulse saturation recording or carrier modulation recording. Pulse saturation recording bit density is ultimately limited by the oxide thickness, but recording densities up to 4 kilobits per cm have been reported (Ref. 7-13). However, the data packing density constraints imposed by the oxide thickness can be circumvented by applying the digital data to the tape by means of a modulated carrier. High density digital recording systems developed by Leach Corporation (Ref. 7-14) record about 4 kilobits per track cm with demonstrated error rates of less than 1 in 10^8. Improvements to about 12 kilobits per cm with an error rate of 1 in 10^9 are projected and techniques are in development which can provide packing densities as high as 35.4 kilobits per cm.

The characteristics of the Mariner IV tape recorder and an advanced Mariner series recorder are presented in Table 7-3. These recorders, developed by Raymond Engineering Laboratory, Inc. (Ref. 7-15), feature extremely low playback tape speeds with high record-to-playback ratios.

Consideration has been given to the representative performance of magnetic tape recorders for the Voyager applications of the mid 70's. When coupled with a bit packing capability of 4 kilobits per cm, a data acceptance rate of 1×10^6 bits per second per track results. The upper limit of tape speed is about 500 cm per second, but for an orbital mission duration of 100 days, a more moderate tape speed of 250 cm per second is recommended (Ref. 7-14). A typical flight tape recorder using 550 meters (1800 feet) of 0.637 cm (0.25 inch) wide mylar 6 track tape could store up to 12×10^8 bits. Such a system would have a mass of approximately 5.5 kilograms, a specific storage mass of 2.2×10^8 bits per kilogram and a data storage density of 6.6×10^7 bits per cubic centimeter. Record-to-playback speed ratios as high as 2000 to 1 can be built with a power requirement of from 5 to 25 watts as a function of tape speed (Ref. 7-16).

TABLE 7-3 MARINER TAPE RECORDER CHARACTERISTICS

Characteristics	Mariner IV Recorder	Advanced Mariner Recorder
Tape Length (meters)	100	550
Tape Width (mm)	6.35	25.4
Total Storage Capacity (bits)	5.2×10^6	1.5×10^8
Recording Speed (cm/sec)	32	61
Recording Rate (bits/sec)	10.7×10^3	84×10^3
Playback Rate (bits/sec)	8-1/3	84 to 672
Minimum Playback Speed (cm/sec)	25×10^{-3}	61×10^{-3}
Maximum Record/Playback Ratio	1284:1	1000:1
Power Consumption (watts)	3 to 4	3 to 16
Transport Mass (kg)	4.2	10.9

Rotary head magnetic tape recorders may provide an excellent capability for Voyager mission applications, but have not yet been fully developed for space use. Proposed systems can handle total data storage in the order of 10^{10} bits. A 220 kilogram rotary head recorder to handle 50 minutes of 10×10^6 bits per second serial stream data can store approximately 3×10^{10} bits (Ref. 7-17). This corresponds to a specific storage mass of 6.6×10^8 bits per kilogram.

A rotary head wide-band tape recorder design under consideration for Apollo program use is theoretically capable of handling the digital equivalent of 8×10^6 bits per second and can store up to 1.44×10^{10} bits (Ref. 7-18). This system would provide a specific storage mass of about 1×10^9 bits per kilogram and a data storage density of 8.8×10^5 bits per cubic centimeter.

A recent tape transport design development by C. W. Newell promises to provide a radical new approach to low cost, high performance tape recorder design (Ref. 7-19). Only three moving parts are required for the transport. A single large drive capstan is located between and in contact with both rolls of tape. Tape speed upper limits of from about 25 to 100 meters per second and bandwidths from 10 to 50 MHz are claimed, but it is too early to ascertain the impact of this concept on spaceborne recorders.

7.2.2 Photographic Film Storage

Film is a strong candidate as a combined sensor storage medium for the Voyager imaging system. As a storage material, very fine-grained, low-sensitivity film can provide an information storage density of 1.6×10^8 bits per square cm. (Ref. 7-20). A maximum bit capacity of 10^6 bits/cm^2 is theoretically available at high contrast for the Kodak Type SO-243 film selected in Section 6.2, (Ref. 7-21).

The length of film required as a function of resolution and percent coverage of the Martian surface is presented in graphical form in Figures 7-4a, b and c. A 70 mm format was considered with a nominal overlap in coverage of 10% on each frame, and a standard 70 mm spacing of 4.6 millimeters between frames. Ground resolutions of 1, 10 and 100 meters were plotted for system resolutions of 50, 100 and 200 lp/mm. Similarly, Figures 7-5a, b and c illustrate the film and Fairweb saturated web processing mass requirements as a function of percent coverage of the Martian surface. Core weights for the film and processing material spools are included. The total data bit capacity of the film, based on 6 bit encoding is also shown in Figures 7-4 and 7-5.

These curves give some insight into the trade-offs that can be made in attempting to satisfy mission goals in terms of coverage of the Martian surface and desired ground resolution. If the mass available for the film and processing is fixed, the maximum amount of coverage can be determined for a selected ground resolution and system resolution. Conversely, if the amount of desired coverage is known, length and mass of film and processing material can be determined as a function of ground and system resolution.

Complete coverage of the planet surface with a 100 line pair/mm system resolution and a 100 meter ground resolution can be obtained with only about 30 meters (mass of about 1 kilogram) of 70 mm film and processing material (see Figures 7-4b and 7-5b). An additional 30 meters of film (and a 1 kilogram mass) could provide 1 percent of Martian surface coverage at 10 meter ground resolution. The total data bit capacity for such a nominal dual imaging system is approximately 10^{12} bits, an amount which could reasonably be transmitted in 200 days using the projected 10^5 bits/second data rate discussed in Section 7.1. However, Figure 7-3 indicates that the communication system would be bit limited and unable to handle the required amount of data in less than approximately 180 days.

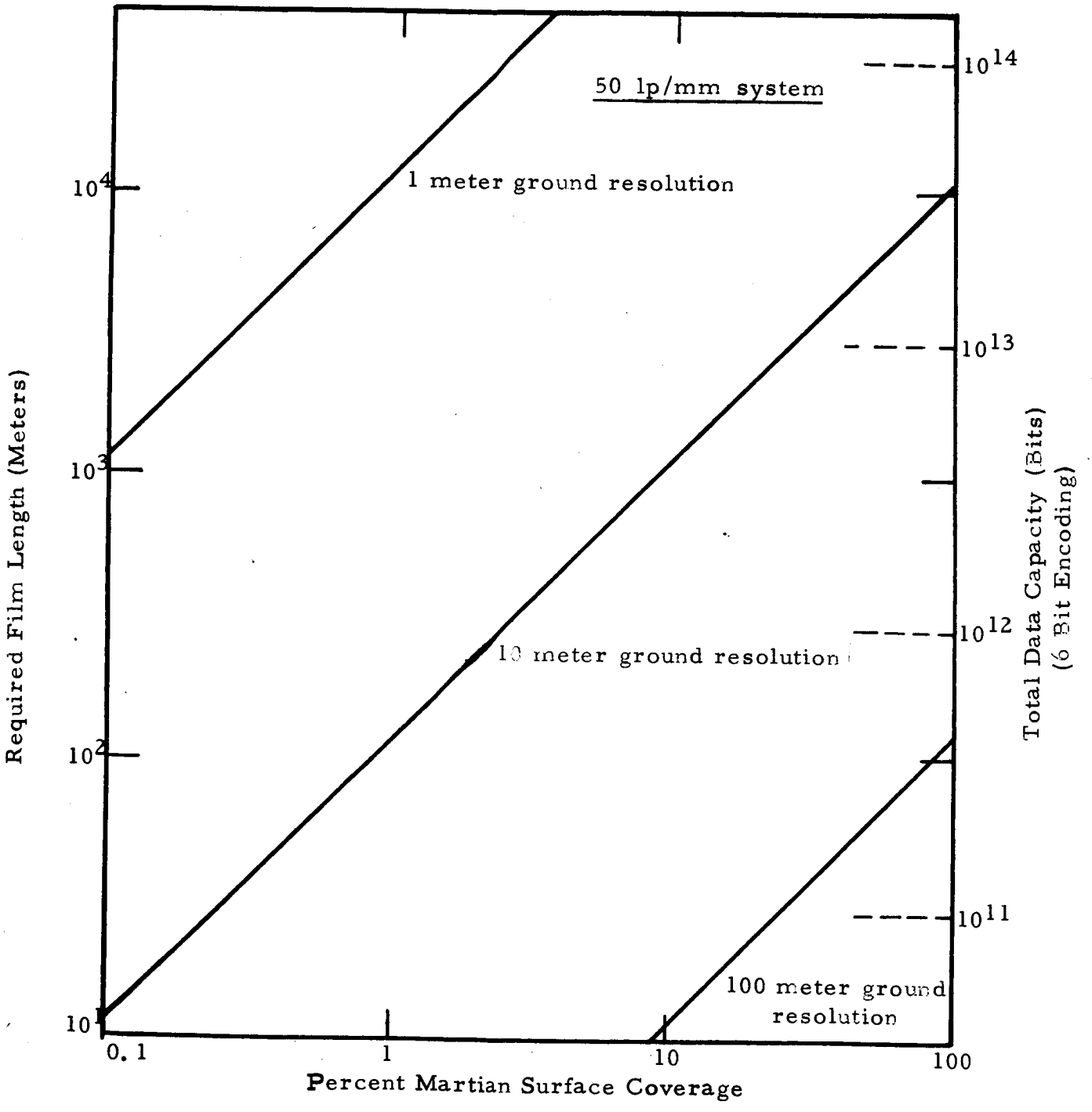

FIGURE 7-4a PERCENT COVERAGE OF MARS VS REQUIRED 70 mm FILM LENGTH (Assuming 10% Overlap, 4.6 mm Frame Spacing)

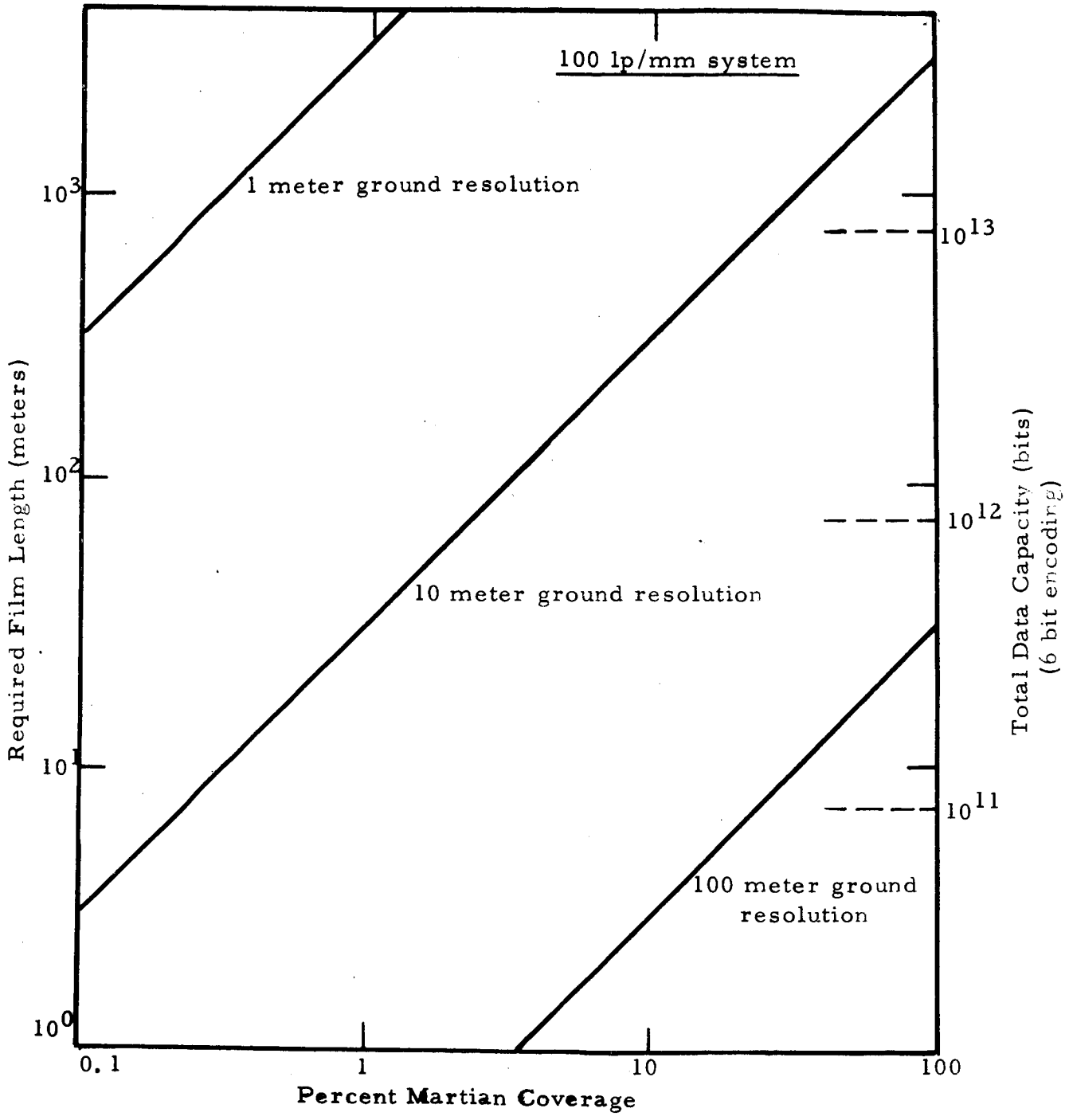

FIGURE 7-4b PERCENT COVERAGE OF MARS VS REQUIRED 70 MM FILM LENGTH FOR A 100 LP/MM SYSTEM (assuming 10% Overlap; 4.6 mm Frame Spacing)

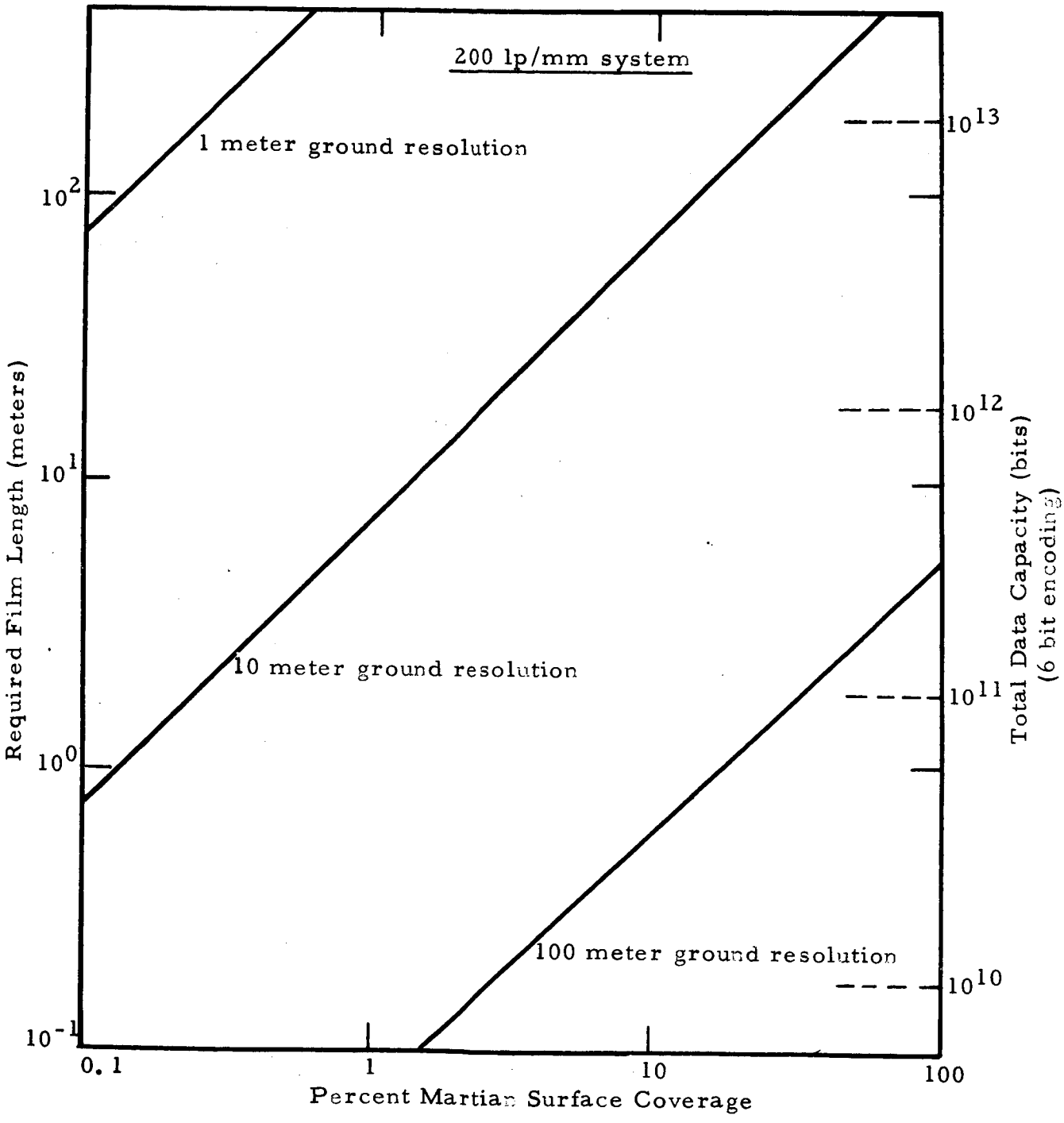

FIGURE 7-4c PERCENT COVERAGE OF MARS VS REQUIRED 70 MM FILM LENGTH FOR A 200 LP/MM SYSTEM (assuming 10% Overlap, 4.6 mm Frame Spacing)

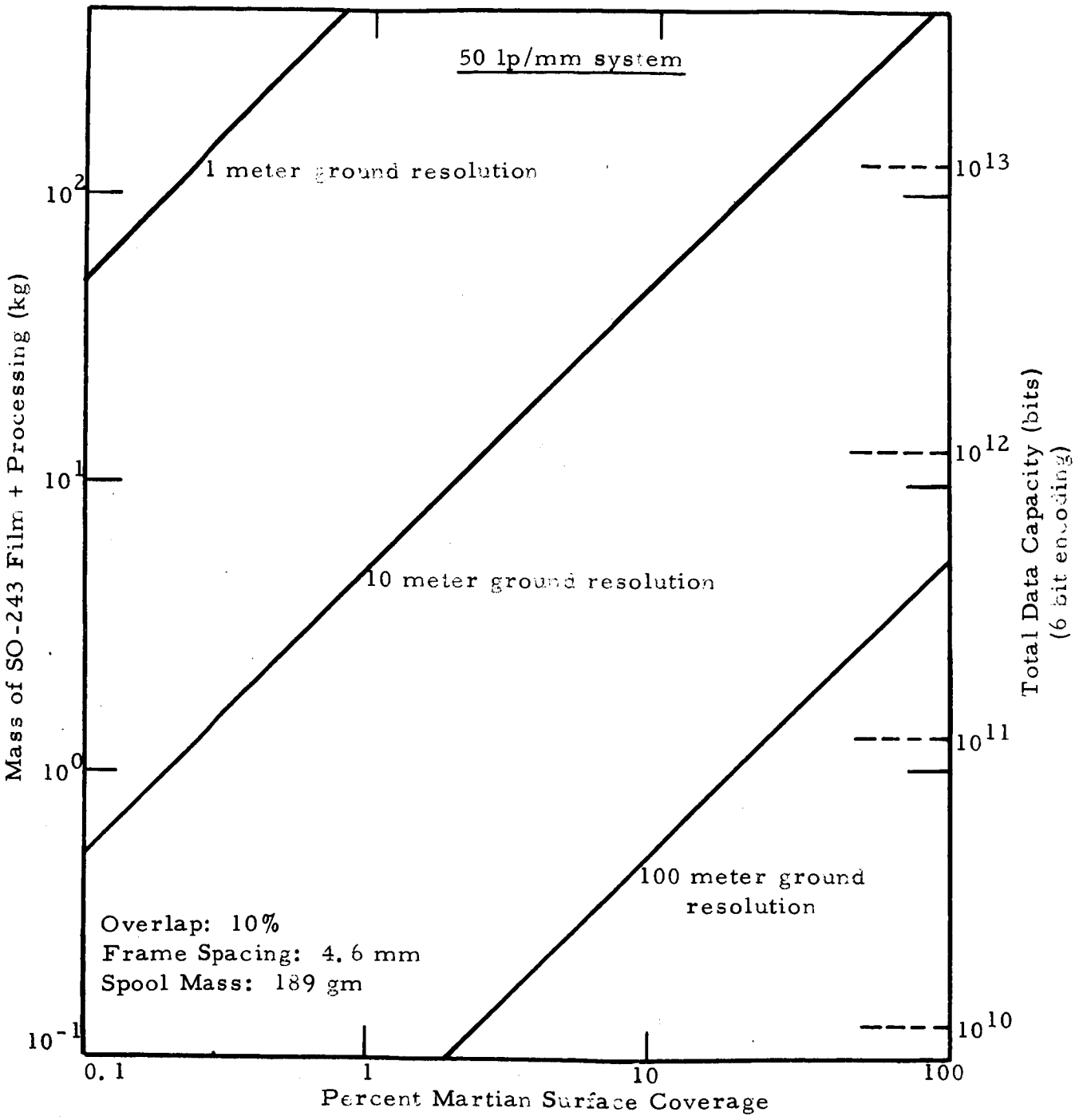

FIGURE 7-5a PERCENT COVERAGE OF MARS VS MASS OF REQUIRED 70 MM FILM AND PROCESSING MATERIAL FOR A 50 LP/MM SYSTEM

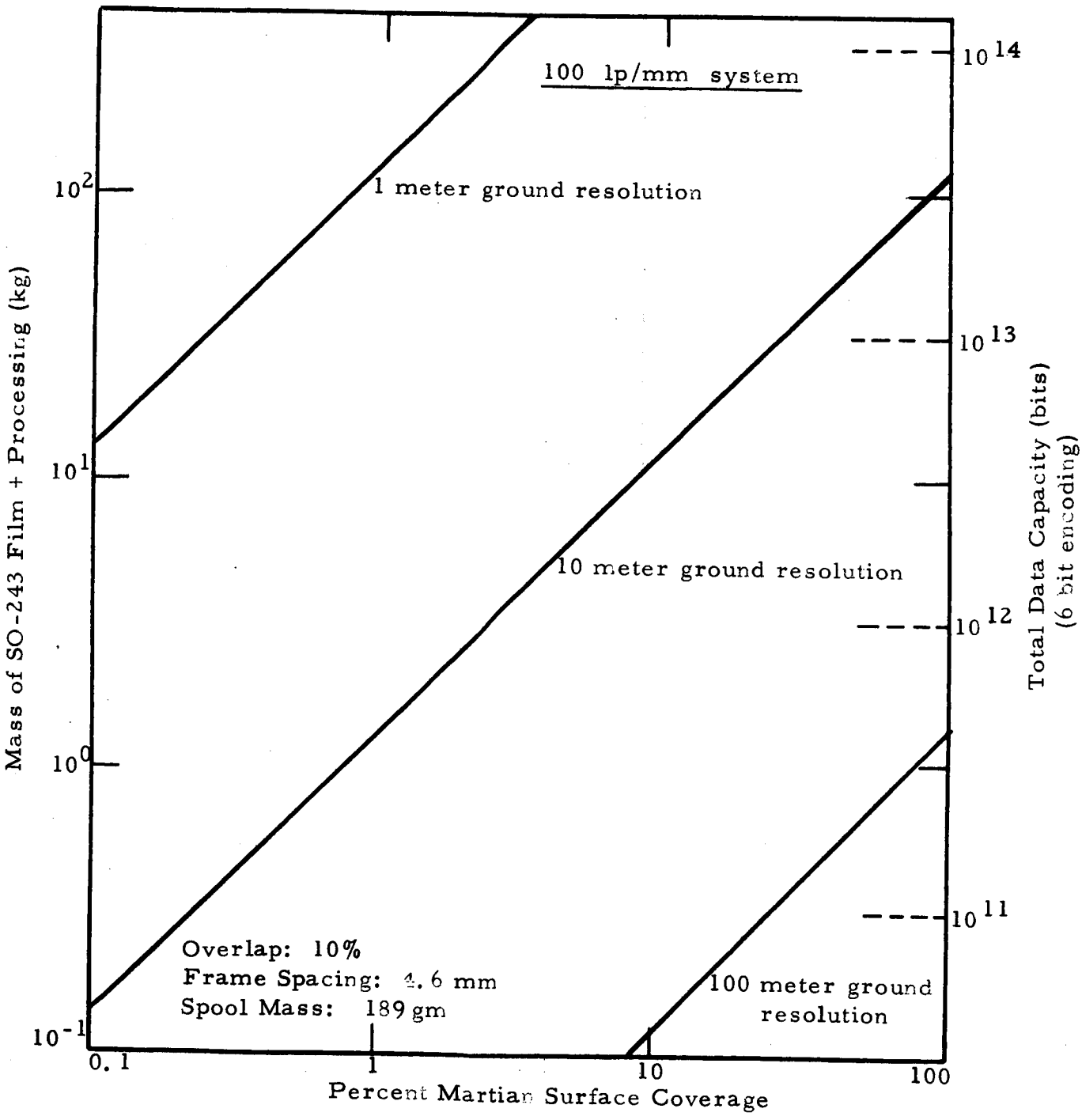

FIGURE 7-5b PERCENT COVERAGE OF MARS VS MASS OF REQUIRED 70 MM FILM AND PROCESSING MATERIAL FOR A 100 LP/MM SYSTEM

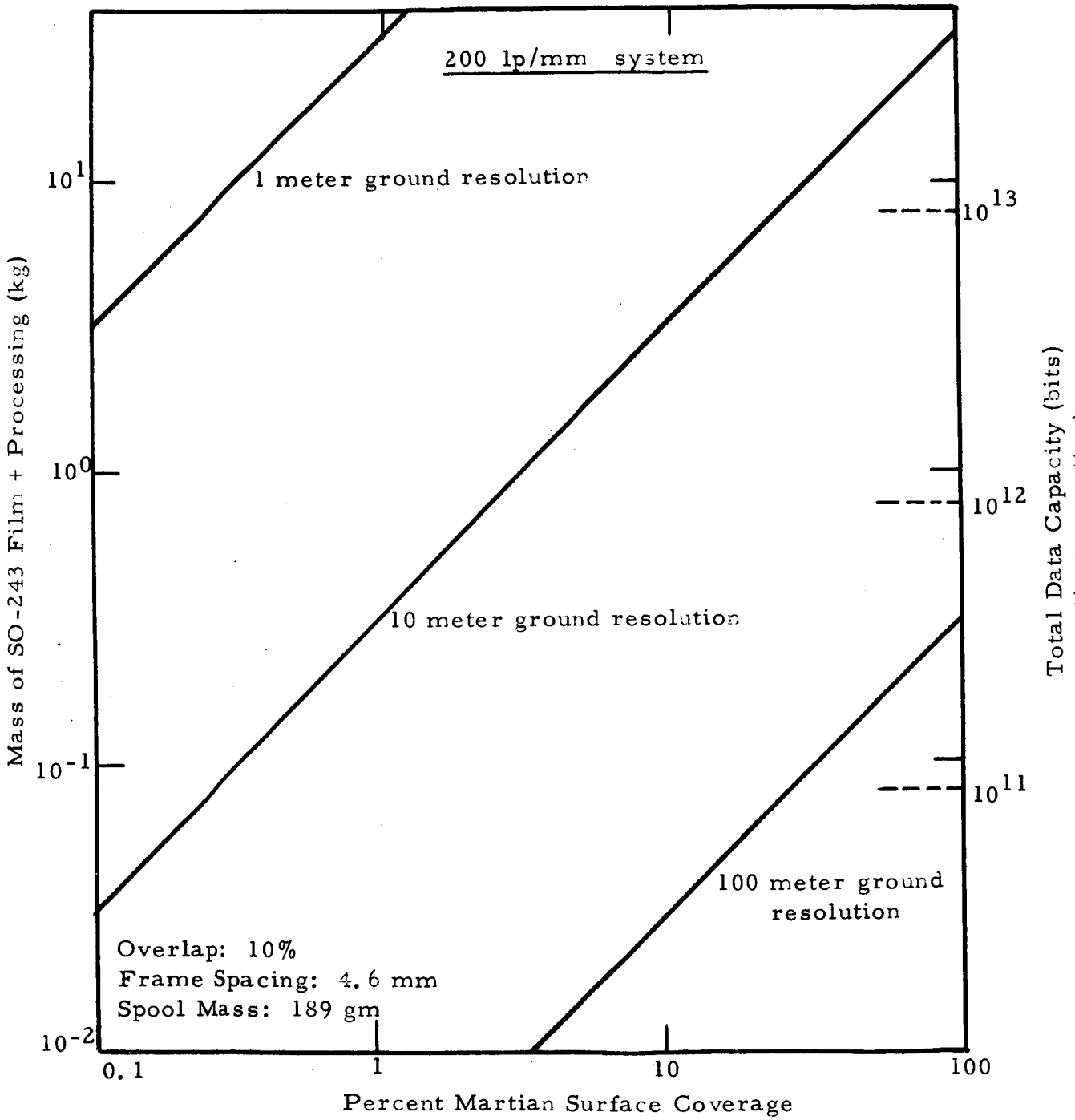

FIGURE 7-5c PERCENT COVERAGE OF MARS VS MASS OF REQUIRED 70 MM FILM AND PROCESSING MATERIAL FOR A 200 LP/MM SYSTEM

7.3 DATA READOUT TECHNIQUES

The two most promising image data gathering sensors, viz. photographic film and the vidicon sensors (see Section 6.5) both involve the use of a storage medium to reconcile the incompatibility of the rapid data acquisition process to the slow data transfer rate imposed by the communications link limitations. Electro-optical sensor data is stored on magnetic tape in a serialized form readily adapted on playback to be fed into the communications system, with a minimum of additional signal processing. Film which admirably combines the function of a high resolution sensor and a high density permanent information storage medium requires an auxiliary scanning device to convert the imagery to a usable electronic signal of serialized data.

The film system incorporates several major advantages which are not as readily achieved by electro-optical systems. A multiple scan resolution capability is readily implemented for a film system. High resolution imagery can be coarse scanned and transmitted to the ground to determine which frames should be scanned out and transmitted at high resolution. Since the film record is permanent, individual frames can be recalled, scanned and retransmitted.

The two major types of film scanners, i.e., flying spot scanners and electro-mechanical scanners are described in the following subsections.

7.3.1 Flying Spot Scanners

The most prevalent film scanning method to convert the photographic image to an electronic signal employs the flying spot scanner. Although the film frame may be held stationary while it is sequentially illuminated by an electronic raster scan generated on the face of a CRT, these conventional television approaches have neither the resolution capability (in picture elements per frame) nor the dynamic range to satisfy the mission resolution performance requirements. In general, for the subject application, raster scanner approaches offer no advantages over line scanners. Since relative motion between film and scanner is still required between frames for raster scanning, continuous film drive for line scanning simplifies scanner design with little additional complexity for the film handling mechanism.

In the basic electronic line scanner, film is continuously transported at right angles to the direction of scan such that the film is displaced by one picture element after each complete line scan. Two typical electronic line scan approaches are:

- Cathode ray tube flying spot scanner with photomultiplier tube sensor.

- Vidicon or image orthicon scanning of an illuminated line.

The two approaches are constrained by the approximately five thousand elements/scan line upper limit for such electro-optical devices. Segmentation techniques impose severe dimensional accuracies and repeatability requirements on the use of electronic beam scanners.

The line scan tube readout technique, successfully used for the Lunar Orbiter missions, demonstrates the high quality performance potential inherent in the film and scanner readout system approach. Since a detailed, comprehensive description of the Lunar Orbiter-Readout hardware and its performance characteristics is readily available in the literature (Ref. 7-22) only a few key points will be mentioned here. A special rotating anode line scan tube, developed by CBS Laboratories, generates an extremely intense, fine spot of light, which is optically minified to a spot diameter on the film of 6 microns. While the flying spot scanner tube electronically generates a line scan by deflecting the electron beam, the light is focused on the film through a mechanically driven scanning lens. When the rectangular framelet is completely scanned the film is advanced 2.54 mm for the next framelet to be read out. The light passing through the film is collected and converted to an electrical signal by a high gain photomultiplier tube. The readout equipment is capable of providing resolution in excess of 100 lines/mm for 3:1 contrast targets. Some of the problems inherent with this type of system include:

- limited guaranteed lifetime of rotating anode line scan tube

- high voltage requirements for CRT and photomultiplier tube

- maintenance of uniform spot size, intensity and sweep linearity

- long term gain stability for PM tube.

7.3.2 Electro-Mechanical Scanners

Another technique for high resolution film readout is being developed at present under a NASA contract at Fairchild Space and Defense Systems. The scanner combines the linearity, simplicity and repeatability of mechanically-traversing precision lead-screw scanning with the low power, weight and volume, high reliability, long-life characteristics of solid state light sources and detectors. The use of a gallium arsenide photo-emitter single point light source and a phototransistor detector eliminates the requirement for high voltages. This scanner is expected to be compatible with a range of data rates from the lowest bit rates previously used up to the 10 to 20 kilobit range.

Developments in solid state technology in the form of linear arrays of photo-emitters and detectors can extend the range of readout rates to the megabit per second region by combining the mechanical X-Y traversing scan motion with a simultaneous rapid electrical scan readout of the array. Fairchild Space and Defense Systems recently has completed a design study for an advanced high rate, high resolution electro-mechanical traversing line scanner (Ref. 7-23). This unique system utilizes the solid state linear integrating phototransistor array and associated scan generator developed by the Fairchild Semiconductor Division. Existing photodiode and phototransistor arrays with packing densities of up to 240 elements per cm have been used and evaluated.

The scanning system can provide high photogrammetric accuracy and promises reliability, ease of operation, compaction, low weight and low power consumption. Resolutions of 150 line pair/mm and a transmission bandwidth of 25 Megahertz are predicted with this approach. Such scanner capabilities are far in excess of available or anticipated transmission equipment data rates for near future planetary orbital reconnaissance programs.

7.4 BANDWIDTH UTILIZATION

Two approaches can be taken to effect an increase in the acquisition of useful information with a limited data link capability. The first involves the application of judicious mission planning techniques, to carefully allocate initial data acquisition to those areas which have the highest probability of containing items of interest to the scientific community. However, once acquired, effective data handling and management techniques must be applied. The permanent storage and readily implemented coarse scan quick-look features of a film system can be a valuable asset in achieving maximum control for missions that permit ground command decisions to influence data acquisition during the remainder of the mission.

More efficient data encoding techniques and methods for removal of the vast amount of redundant information frequently encountered in visual data can be used to reduce the information bandwidth requirements. A communication system includes the source coder at the transmitter, which converts the input data into a sequence of code bits of minimum possible length,and the receiver source decoder, which performs the inverse operation of reproducing the source data from the code bits. The operation of source coding and decoding is denoted as data conditioning and reconstruction.

Data conditioning offers the possibility of an increase in the information rate of a communication system after optimum coding and modulation techniques have been applied to the system. The information rate increase is realized by transforming the source data, by an elimination of redundancy, into a form in which fewer symbols are required to describe the data. Table 7-4 presents estimates of digital source bit rate reduction possible for various data compression schemes (Ref. 7-24). A great deal of work has gone into reducing the bandwidth requirements for digital facsimile and TV transmission, and data compression ratios ranging from 2:1 to 6:1 have been reported (Refs. 7-25, 7-26, 7-27, 7-28).

It must be noted that the realization of advantages derived from use of data compression techniques comes only at the expense of system complexity, power, mass, volume and reliability. Therefore, a careful assessment of potential system performance enhancement versus the system penalties incurred must be made before a decision is made to incorporate any type of data compaction schemes.

TABLE 7-4 DIGITAL SOURCE BIT RATE REDUCTION BY DATA CODING

Type of Data and Bandwidth	PCM Equivalent	Delta Coding	Multiple Interlace Encoding	Predictive Coding
Scientific, 0 to 1 KHz	Up to 18 kilobits/ second	-	-	Up to 6 kilobits/ second
Engineering, 0 to 1 KHz	Up to 18 kilobits/ second	-	-	Up to 6 kilobits/ second
Pictorial information (real-time TV), 4 MHz	48 megabits/ second	24 megabits/ second	12 megabits/ second	-
Pictorial information (one frame per 12.5 seconds), 10 MHz	120 kilobits/ second	60 kilobits/ second	30 megabits/ second	-

Unfortunately, since relatively little is known about the Martian planet, the preservation of the data quality must remain a primary objective. Thus, until a more detailed body of scientific knowledge is built up, many of the data compression schemes cannot be considered for the initial reconnaissance missions.

7.5 REFERENCES

7-1 EASTERLING, M., Jet Propulsion Laboratory Letter: 330-MFE: ljb, 28 July 1967

7-2 WOOD, L.H., VACHON, R.I., PRASTHOFER, W.P., "Photographic Exploration of Mars with Solar-Electric Propulsion"

7-3 WOOD, L.H., STONE, N.H., and FLECK, H.A., "An Application of Solar-Electric Power to a Sophisticated Planetary Surface Observation System," AAS67-432 (PS-22)-1

7-4 HEFTMAN, K., and RENZETTI, N.A., "Data Return Capabilities of the Deep Space Network in the 1970's," Jet Propulsion Laboratory, AIAA Paper, No. 67-648, August 28-30, 1967

7-5 BROOKNER, E., KOLKER, M., WILMOTTE, R.M., "Deep-Space Optical Communications," IEEE Spectrum, January, 1967

7-6 GUBIN, S., MARSTEN, R.B. and SILVERMAN, D., "Laser Versus Microwaves In Space Communications," AIAA Journal of Spacecraft and Rockets, June 1966

7-7 REINBOLT, E.J., and RANDALL, J.L., "How Good Are Lasers for Deep-Space Communications?" Astronautics and Aeronautics, April 1967

7-8 RECHTIN, E., "How Good Are Lasers," Letters Dept., Astronautics and Aeronautics, October 1967

7-9 "Fifth Quarterly Report for Parametric Analysis of Microwave and Laser Systems for Communication and Tracking," Hughes Aircraft Company, Report No. P67-09, December 1966

7-10 DIMEFF, J., GUNTER, W., JR. and HRUBY, R., "Spectral Dependence of Deep-Space Communications Capability," NASA-Ames Research Center, IEE Spectrum, September 1967

7.5 REFERENCES (continued)

7-11 CAMPEN, C., Personal Communications, Voyager Interim Project Office, Pasadena, California, August 1967

7-12 ATHEY, S.W., "Magnetic Tape Recording," NASA SP-5038, January 1966

7-13 NORRIS, K.A., "A Technique for High Density Digital Magnetic Recording," Leach Bits, August 1967

7-14 MUENCH, J., Personal Communications, Leach Corporation, October-November 1967

7-15 "High Reliability Tape Recorders/Reproducers for Rugged Environments," Raymond Engineering Laboratory, Inc., 1967

7-16 "Leach Satellite Tape Recorders - Series 2000," Leach Corporation, Bulleting SR2000-866, 1966

7-17 YOUNG, R.E., Personal Communication, Market Development Manager, Ampex Corporation, November 1967

7-18 "RCA Aiming at Aircraft Market for Recorders," Aerospace Technology, October 9, 1967

7-19 "Tape Transports Are Here to 'Play'," Brogan Report, Volume 1, No. 2, Fall 1967

7-20 CLARK, G.L., "High-Speed Data Recording," Electro-Optical Systems Inc., Photographic Science and Engineering, Volume 8, No. 1, January-February 1964

7-21 ALTMAN, J.H. and ZWEIGH, H.J., "Effect of Speed Function on the Storage of Information on Photographic Emulsions," Eastman Kodak Co., Photographic Science and Engineering, Volume 7, No. 3, May-June 1963

7-22 JENSEN, A. et al, "Lunar Orbiter Readout" Journal of the SMPTE, Volume 76, August 1967

7-23 BASHE, R., "High Rate, High Resolution Film Scanning," Fairchild Space and Defense Systems, Tech. Memo. SME-AT-2, August 1966

7.5 REFERENCES (continued)

7-24 STOKES, L.S. and BRINKMAN, K.L., "Fourth Quarterly Report for Parametric Analysis of Microwave and Laser Systems for Communication and Tracking," Hughes Aircraft Company, Report No. P66-213, September 1966

7-25 GOLDSMITH, C.T., "Bandwidth Reduction for Facsimile," Fairchild Space and Defense Systems, Report S.I. 920,134, August 1967

7-26 GRUEN, H. and OLEVSKY, B., "Increasing Information Transfer," Philco Corporation, Space/Aeronautics, February 1965

7-27 WHELAN, J., "Digital TV Bandwidth Reduction Techniques as Applied to Spacecraft Television," RCA Astro-Electronics Division, J. Spacecraft, Volume 3, No. 4, May 1966

7-28 STUMPFE, J.W., "Redundancy Reduction Techniques and Applications," Radiation Inc., Telecommunications, October 1967

SECTION 8

PHOTOSYSTEM TRADE-OFF ANALYSES

The overall photosystem, consisting of the optical, photosensor and conversion subsystem elements, is considered in this section. The photosystem trade-off analyses have been necessarily limited in scope, in keeping with the funding and schedule restrictions of the study program. Preliminary imaging system designs should be prepared and more comprehensive system analysis trade-offs should be performed.

For purposes of comparison, the trade-off analyses are based on three systems, each using a different photosensor. These systems are a film system using 70 mm, SO-243 film and two electro-optical systems, one using a one inch vidicon tube and the other a two inch return beam vidicon tube. Of the photosensors considered for the Martian orbital mission, these three are the prime candidates (see Section 6.5). Both vidicon and film systems have been flown successfully in space missions. The selection of SO-243 film is based on radiation shielding considerations (see Section 6.2.3). The return beam vidicon is included because of its promise as a high resolution electro-optical sensor in the 70's.

The three systems are first compared in terms of the total system mass required as a function of ground resolution obtainable. Then the three sensor systems are compared on the basis of the coverage they provide. Finally, other important system considerations are discussed, and an overall comparison is made for these candidate sensor systems.

8.1 SYSTEMS COMPARISON: GROUND RESOLUTION

A series of general system parameter values have been assumed in order to establish a basis for comparing the ground resolution provided by individual sensor systems.

A mission lifetime of 100 days in orbit was selected because it is approximately midway between the minimum mission life of 30 days and the desired life of 6 months that were specified for this study. Analyses are also made for a mission lifetime of 200 days in orbit in order to illustrate the effect of extended mission life on the system comparisons.

An altitude of 1,000 km was selected for analysis as a nominal value that lies between an anticipated periapsis of, perhaps, 500 km, and a maximum imaging altitude of approximately three times that value, or 1,500 km. A velocity/altitude (V/H) ratio of 3×10^{-3} radians/second was used since this is a typical value for the assumed imaging altitude (see Section 5.1.2). An image motion compensation error of 0.2% for forward motion (FMC) is assumed since this is approximately the anticipated state-of-the-art capability for the early Martian missions. It is assumed, based on information received from vehicle manufacturers, that the vehicle or a stabilized platform will provide an RMS stability error rate of 10^{-5} radians/second.

A scene brightness of 700 candela/meter^2 was assumed based on available photometric data. Contrast for the scene being imaged was selected to be 1,000:1 for the purpose of the analysis; this choice was made primarily due to the lack of low contrast information for the return beam vidicon. A range of communication data rates of 10^4 to 10^6 bits/second was selected in order to include consideration of the data rates that are anticipated for the early Voyager missions (about 10^4 to 5×10^4 bits/seconds) as well as a megabit/second rate that eventually may be achieved by future r.f. or laser communication systems (see Section 7).

A summary of the assumed parameters for the example systems is presented in Table 8-1. The values indicated are not necessarily optimum for the mission, but have been established solely as a basis for parametric comparison.

TABLE 8-1 COMMON SYSTEM PARAMETERS ASSUMED FOR EXAMPLE SYSTEMS COMPARISONS

PARAMETER	VALUE
Altitude	1,000 km
Velocity/Altitude (V/H)	3×10^{-3} radians/second
FMC Error	0.2%
Vehicle Stability	10^{-5} radians/second
Scene Brightness	700 candela/meter^2
Contrast	1,000:1
Intensity Encoding	6 bits
Relative Transmission Time	67%
Communication Data Rate	10^4 to 10^6 bits/second
Mission Lifetime (In Orbit)	100 and 200 days

In addition to the parameters that are identical for the individual sensor systems being compared, there are many characteristics that are necessarily different for the three systems. These characteristics are presented in Table 8-2. The estimated ranges of system static resolution are based on the present and future subsystem performance data previously discussed in this report. The lens f/numbers, type T/ numbers and the exposure time are based on sensor sensitivity and resolution data given in Section 6, as well as optical subsystem considerations discussed in Section 5.1, but the values chosen are not necessarily optimum for this application. Additional detailed system analysis will be required after the mission objectives, orbital characteristics, communication capability and mission duration have been firmly established.

Camera mass (not including optics) is based on the design shown in Figure 8-1 for the film system on data presented in Table 6-2 for the two inch return beam vidicon system and on the Mariner '69 camera for the one inch vidicon system. Recorder mass is based on use of a rotary head recorder with the return beam vidicon and a linear recorder with the vidicon (see Section 7). Radiation shielding mass for the film system is based on Figure 6-8 and the shielding requirement for SO-243 film of 8 gm/cm^2 of polyethylene, both given in Section 6.2.3. Optical subsystem mass estimates are based on Figure 5-2 in Section 5.1.1.

The resolution performances as a function of total mass for the three individual sensor systems being compared are shown in Figures 8-2, 8-3 and 8-4 for a mission life of 100 days and a data link rate of 10^4 bits/second. (Total system mass includes consideration of camera, film or recording tape and shielding.) The ground resolution indicated represents the resolution at the nadir in meters per line pair.

The performance of each sensor system is shown as a band because a range of system static resolution is assumed for each. In order to compare the three sensor systems, the average values for these static resolution ranges were used, as shown in Figure 8-5a. Figure 8-5b is similar, but for a communication data rate of 10^5 bits/second. Finally, a similar comparison is made for a mission life of 200 days, again for data transmission rates of 10^4 and 10^5 bits/second (Figures 8-6a and 8-6b).

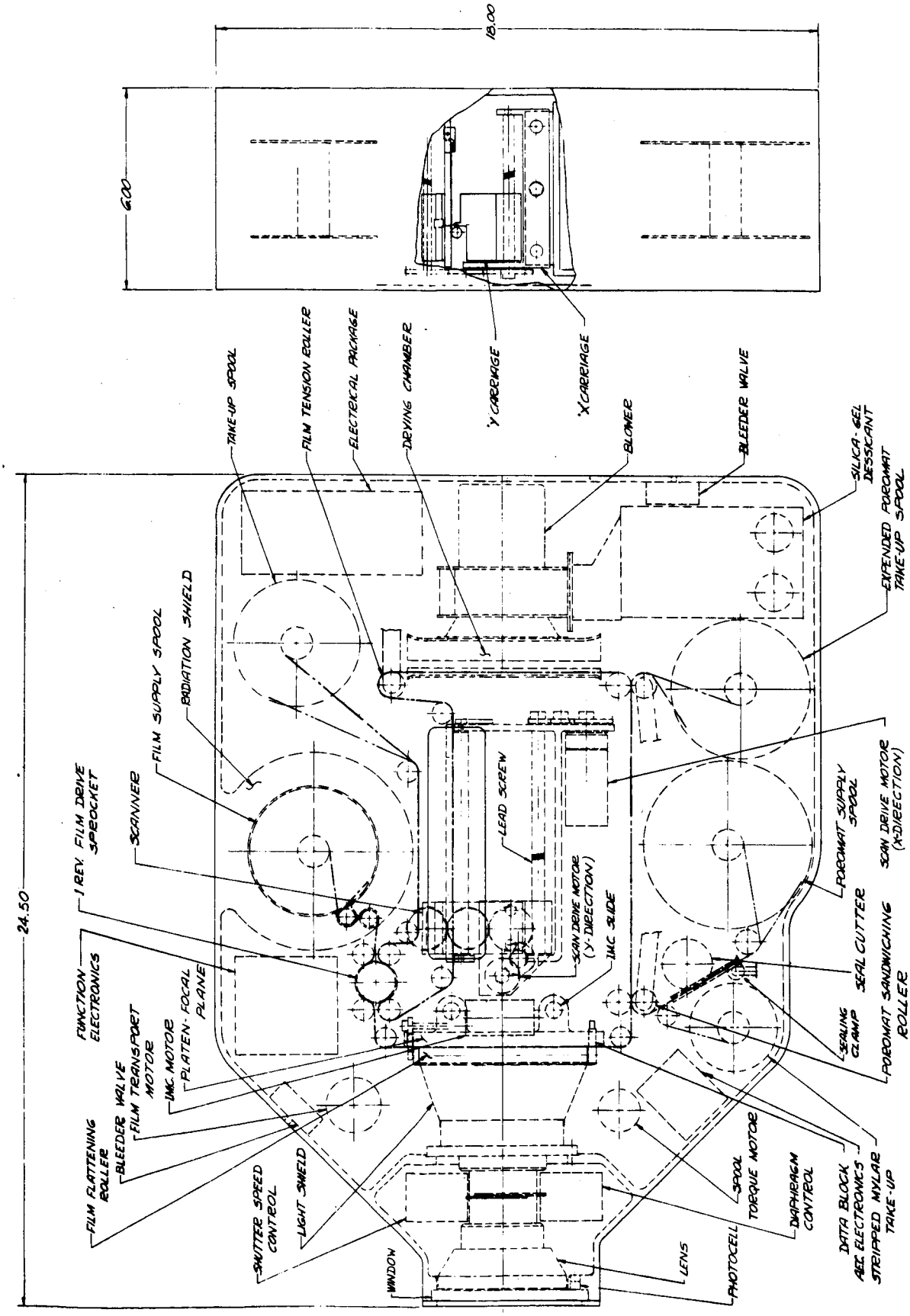

FIGURE 8-1 TYPICAL MARTIAN ORBITER FILM CAMERA

TABLE 8-2 INDIVIDUAL SENSOR SYSTEM CHARACTERISTICS ASSUMED FOR SYSTEMS COMPARISON

Parameter	70 mm SO-243 Film Scanner	2-inch Return Beam Vidicon Camera	1-inch Vidicon Camera
Range of Static System Resolution (lp/mm)	80 to 120	50 to 100	35 to 50
Lens f/number	5	8	7
Lens Type	Catadioptric	Refractive	Refractive
Lens T/number	7	10	8.8
Exposure Time (milliseconds)	25	0.18	6
Format Width (mm)	57	25	11
Camera Mass (kg)	21	14	9
Recorder Mass (kg)	N/A	12	6
Radiation Shielding (gm/cm^2)	Polyethylene: 8	N/A	N/A

Total system mass is not included because the mass of the optics and shielding are variables. Examples of total system mass for both high and medium resolution sensing are presented on page 8-14 for the three individual sensors.

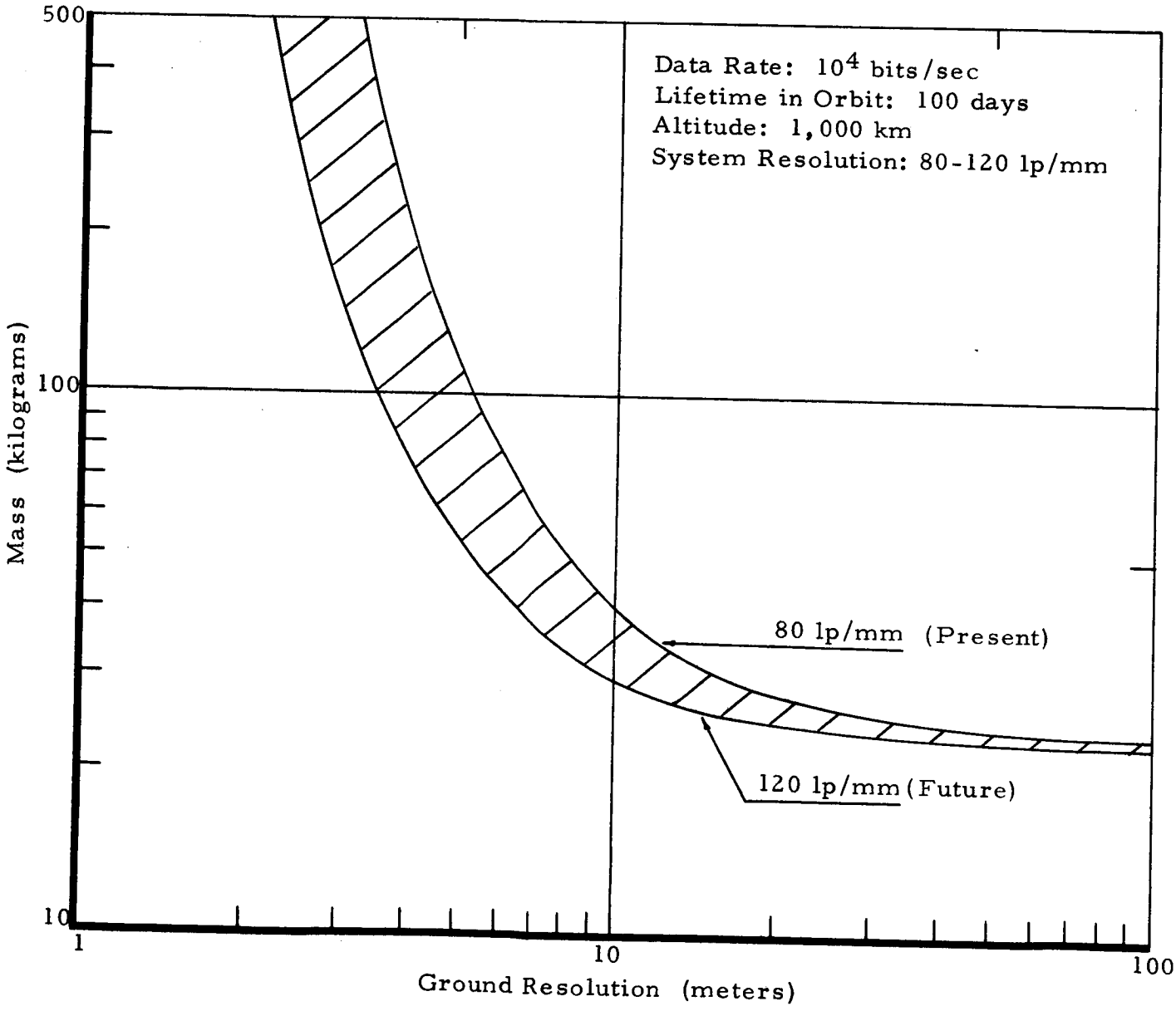

FIGURE 8-2 FILM SYSTEM MASS AS A FUNCTION OF GROUND RESOLUTION (10^4 bits/sec Data Rate)

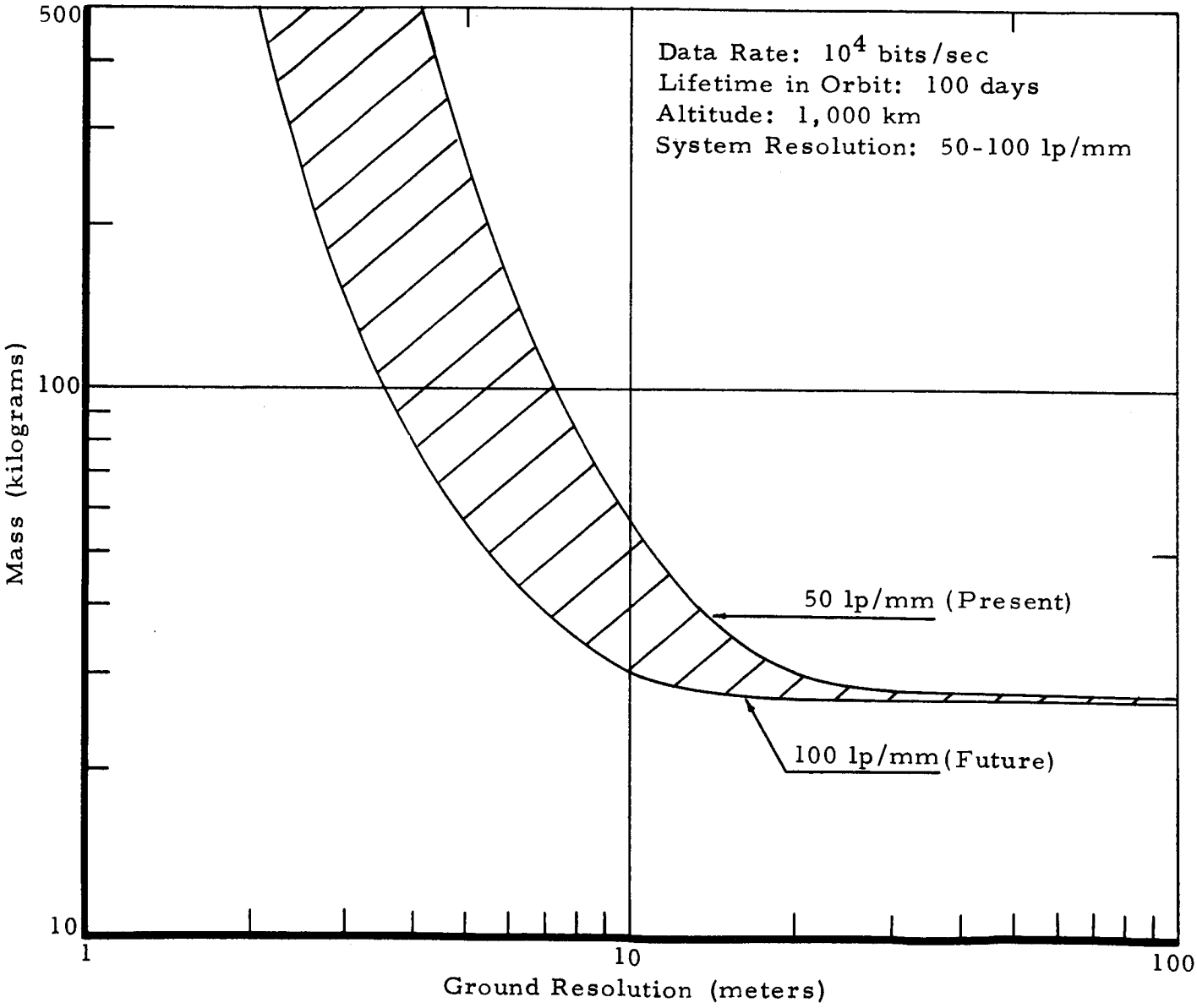

FIGURE 8-3 RETURN BEAM VIDICON SYSTEM MASS AS A FUNCTION OF GROUND RESOLUTION (10^4 bits/sec Data Rate)

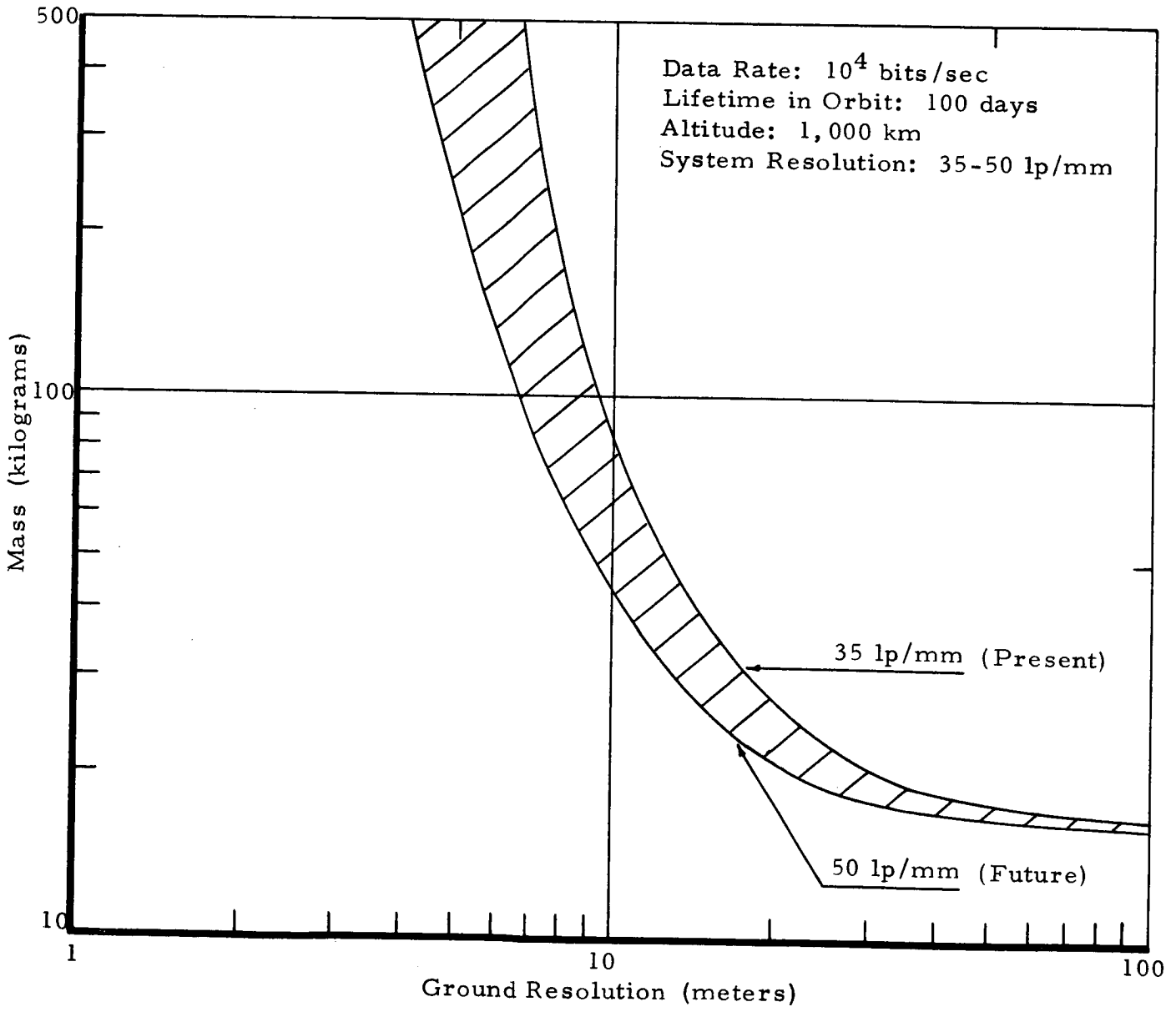

FIGURE 8-4 VIDICON SYSTEM MASS AS A FUNCTION OF GROUND RESOLUTION (10^4 bits/sec Data Rate)

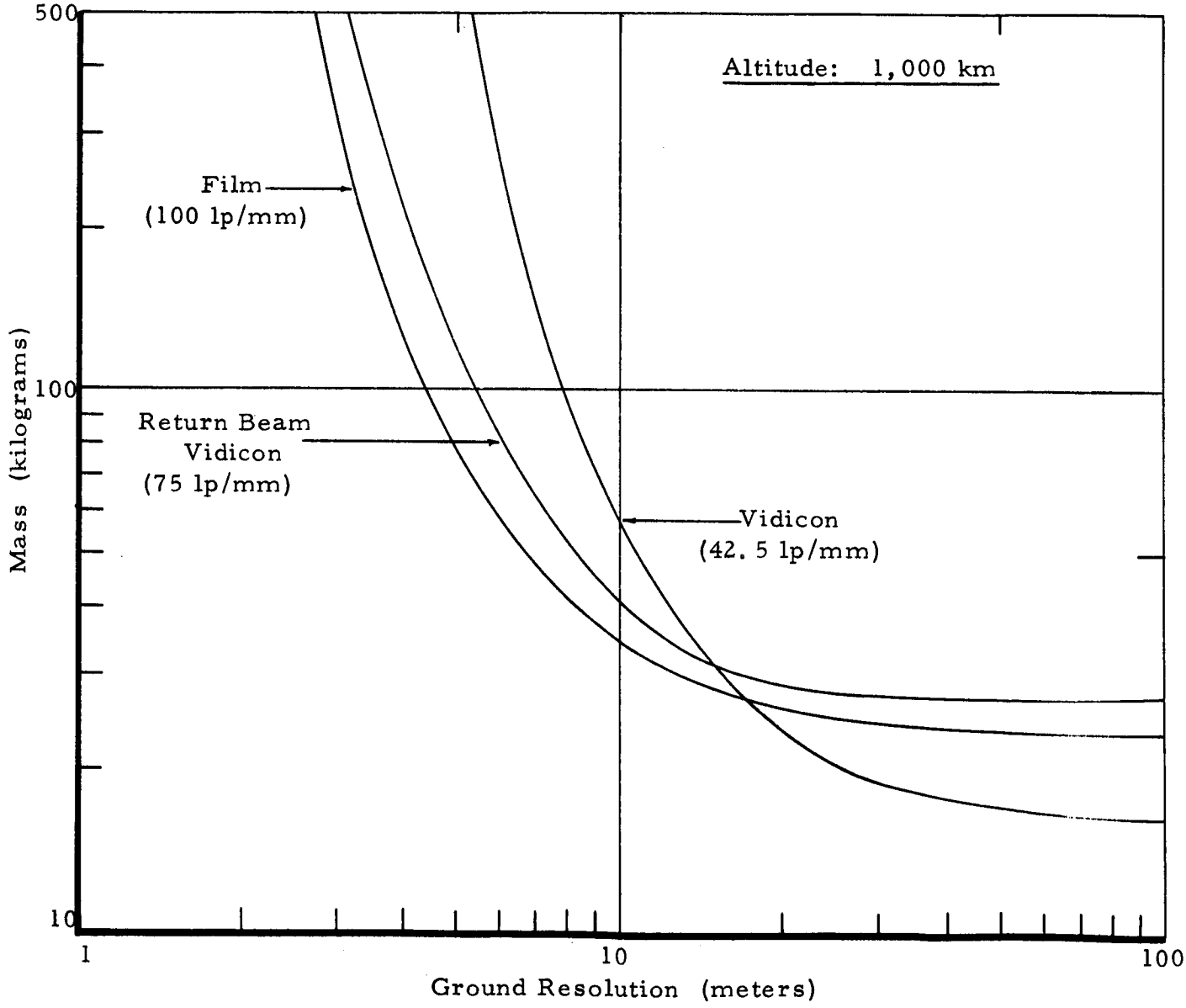

FIGURE 8-5a COMPARISON OF SYSTEMS MASS VS RESOLUTION; 100 DAYS IN ORBIT (10^4 bits/sec Data Rate)

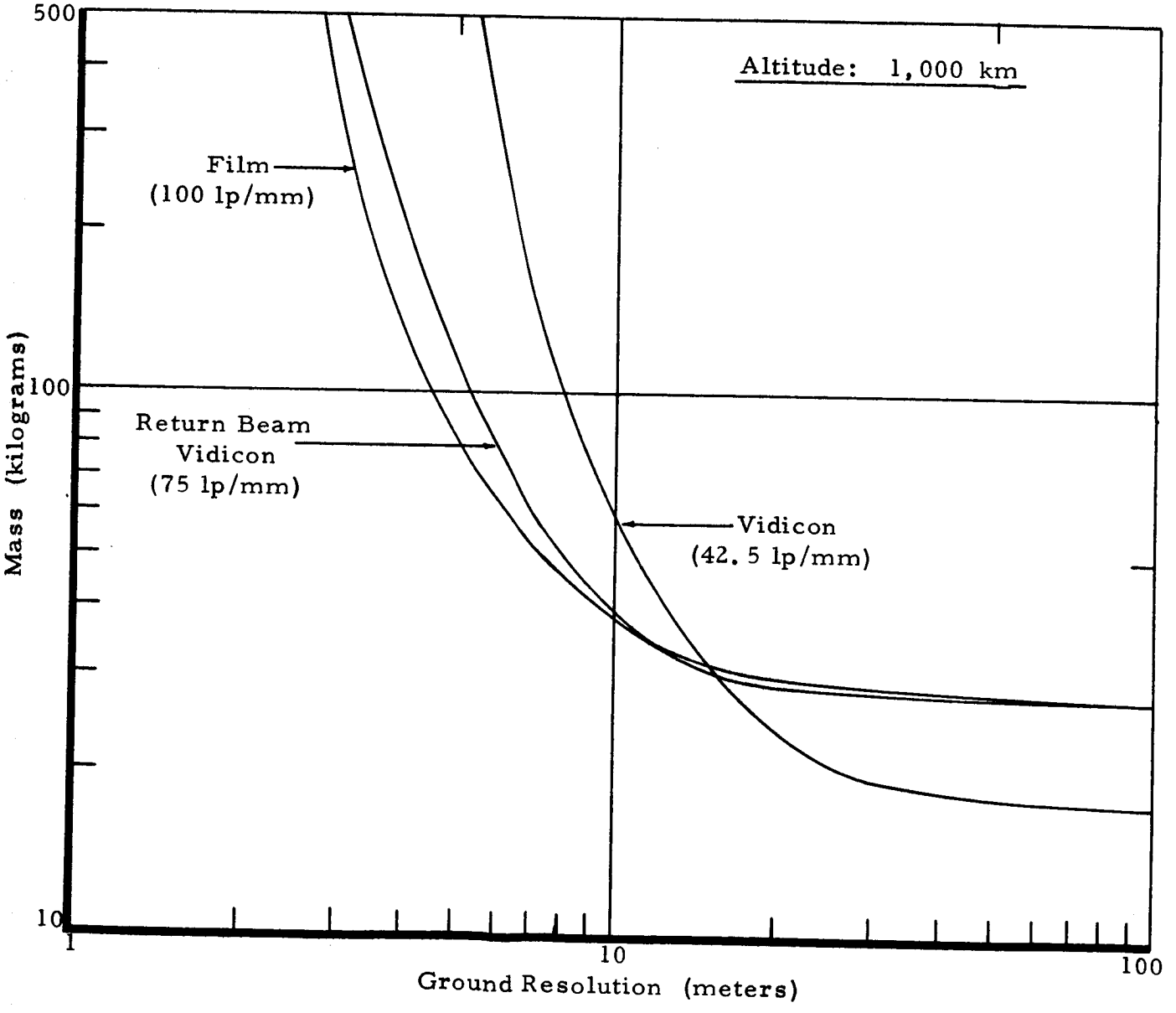

FIGURE 8-5b COMPARISON OF SYSTEMS MASS VS RESOLUTION; 100 DAYS IN ORBIT (10^5 bits/sec Data Rate)

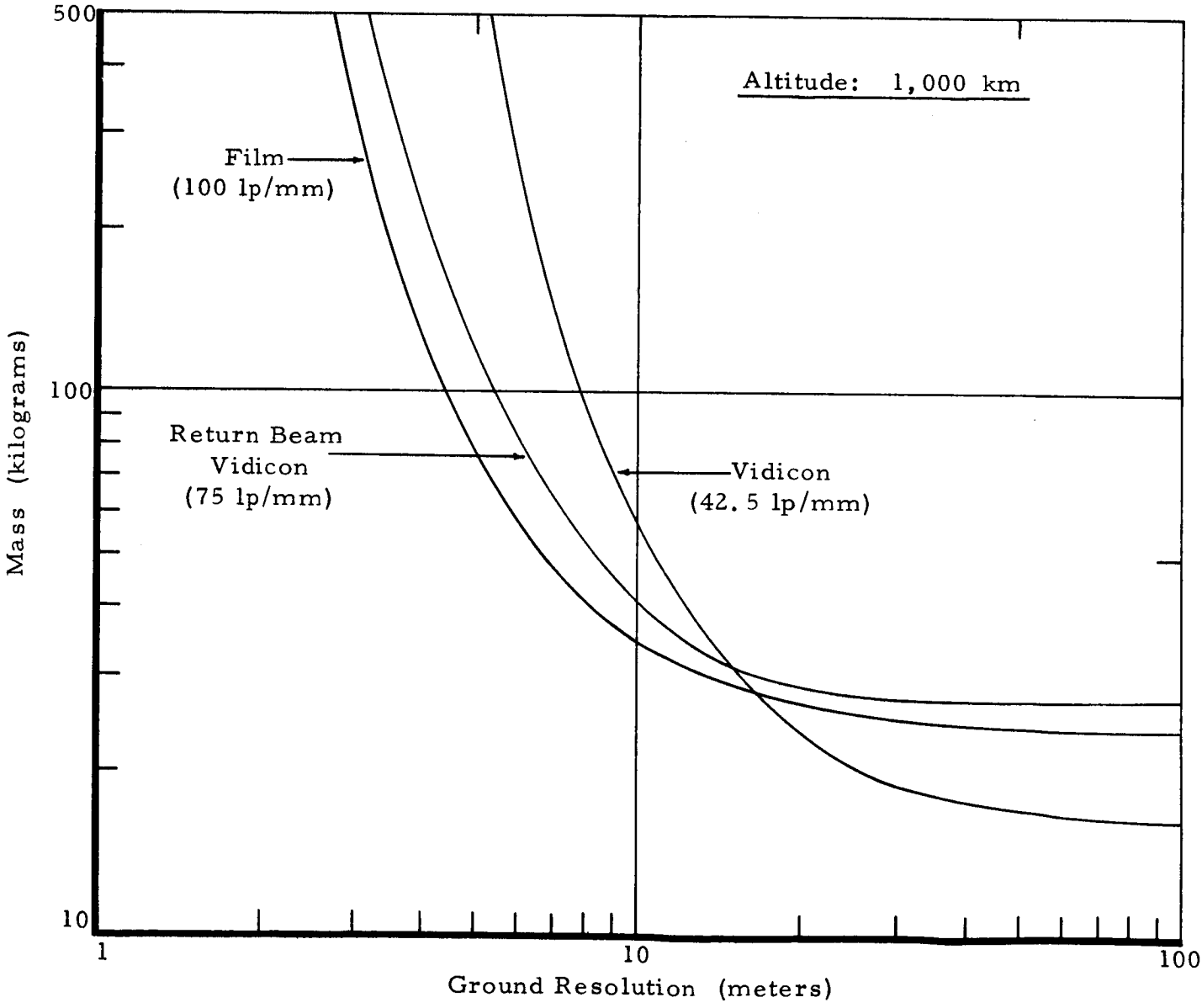

FIGURE 8-6a COMPARISON OF SYSTEMS MASS VS RESOLUTION; 200 DAYS IN ORBIT (10^4 bits/sec Data Rate)

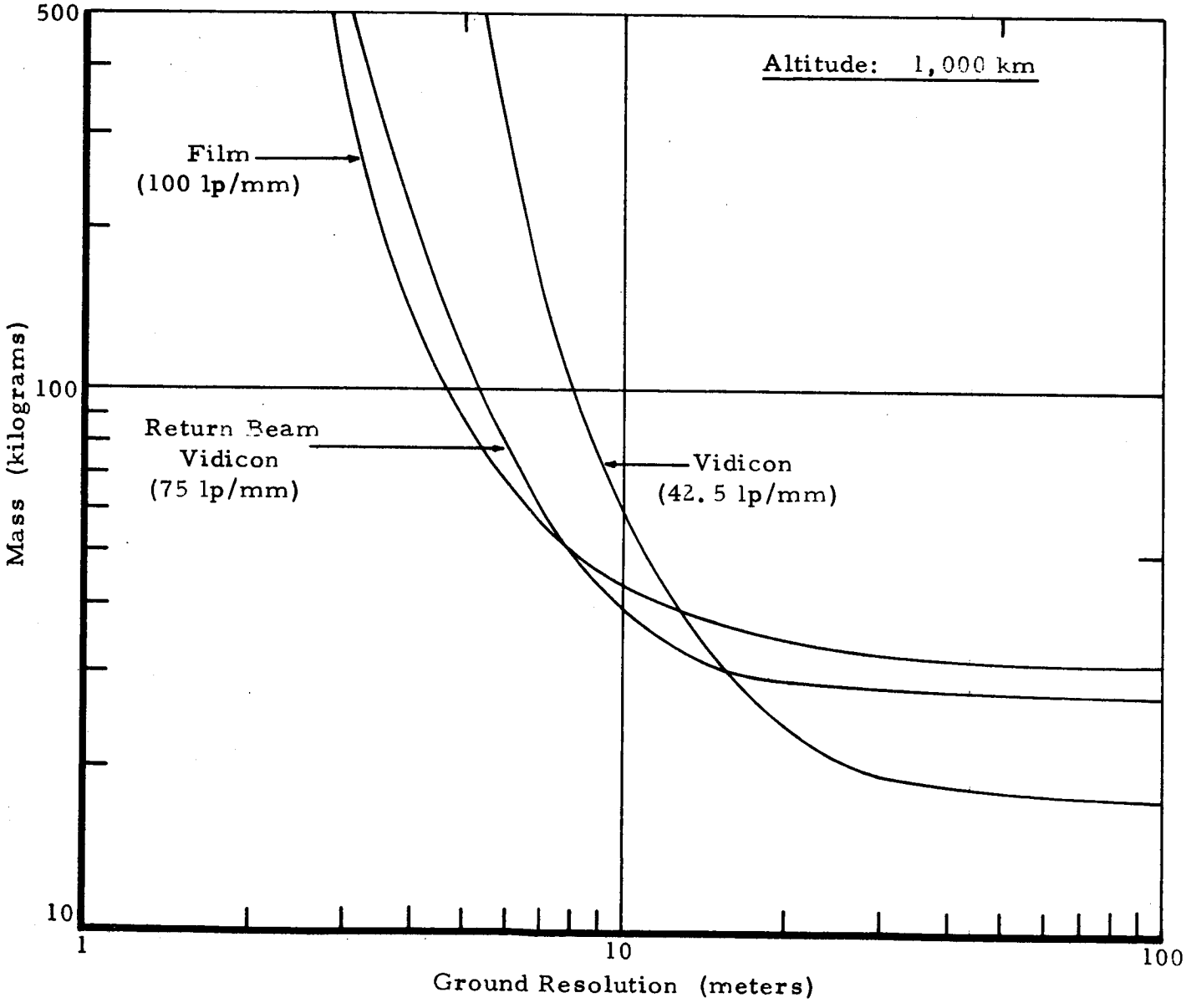

FIGURE 8-6b COMPARISON OF SYSTEMS MASS VS RESOLUTION; 200 DAYS IN ORBIT (10^5 bits/sec Data Rate)

Some of the conclusions that can be drawn from inspection of these curves, for the conditions assumed and for the three individual sensors compared are:

- The film system has the least mass for high resolution sensing. This holds true for the 200 day as well as the 100 day missions. For example, for a 100 day mission a data rate of 10^4 bits/second and a 5 meter ground resolution, a system mass of about 80 kilograms for the example film system, 120 kilograms for the return beam vidicon system and over 500 kilograms for the vidicon system.

- Resolution significantly better than 5 meters can be achieved only by exceeding the guideline mass of 80 kilograms, even if only a single film sensor is used.

- The one inch vidicon system has the least mass for medium resolution photography by an individual sensor. For example, for a 100 day mission, a data rate of 10^4 bits/second and 50 meter ground resolution, a system mass of about 17 kilograms is required for the example vidicon system, 24 kilograms for the film system, and 27 kilograms for the return beam vidicon system.

- There is not a significant amount of mass savings realized by degrading the resolution from roughly 30 meters to 100 meters. However, the resolution degradation does allow for improvements in coverage. This is discussed more fully in the next subsection.

- For an increase in data rate from 10^4 to 10^5 bits/second, there is no significant change in the relative rating of film and the vidicons. However, for a rate of 10^6 bits/second or higher the ranking of the vidicons relative to film improves.

8.2 SYSTEMS COMPARISON:GROUND COVERAGE

An important reason for minimizing the number of photographs required to achieve a given coverage is the resulting simplification in handling the imagery after it is returned to Earth. The large amount of imagery that will be obtained because of the orbital nature of the mission, in contrast to the amount of imagery obtained on a fly-by mission such as Mariner '64 or Mariner '69, makes this a particularly significant factor. The anticipated highly elliptical orbits will result in photography that is made more difficult to handle effectively, because of the resulting photo-to-photo variations in resolution, scale and coverage as a function of altitude. The resolution and coverage variations are illustrated in Figure 8-7.

The number of photos required to provide a stated percentage coverage of the planet is a function of the sensor format and the ground resolution capability required. Assuming no overlap and a square format, the number of photos required with 100 meter ground resoultion is shown in Figure 8-8a for the one inch vidicon, two inch return beam vidicon, and 70 mm film systems discussed in the previous section, as well as for 35 mm film. Figures 8-8b and c are similar curves for a ground resolution of 10 meters and 1 meter, respectively.

As can be seen from the figures, 70 mm film requires the least number of pictures and the one inch vidicon requires the most. If film is used in an extended length format (e.g., 57 x 220 mm), then the number of photographs it requires is reduced even further.

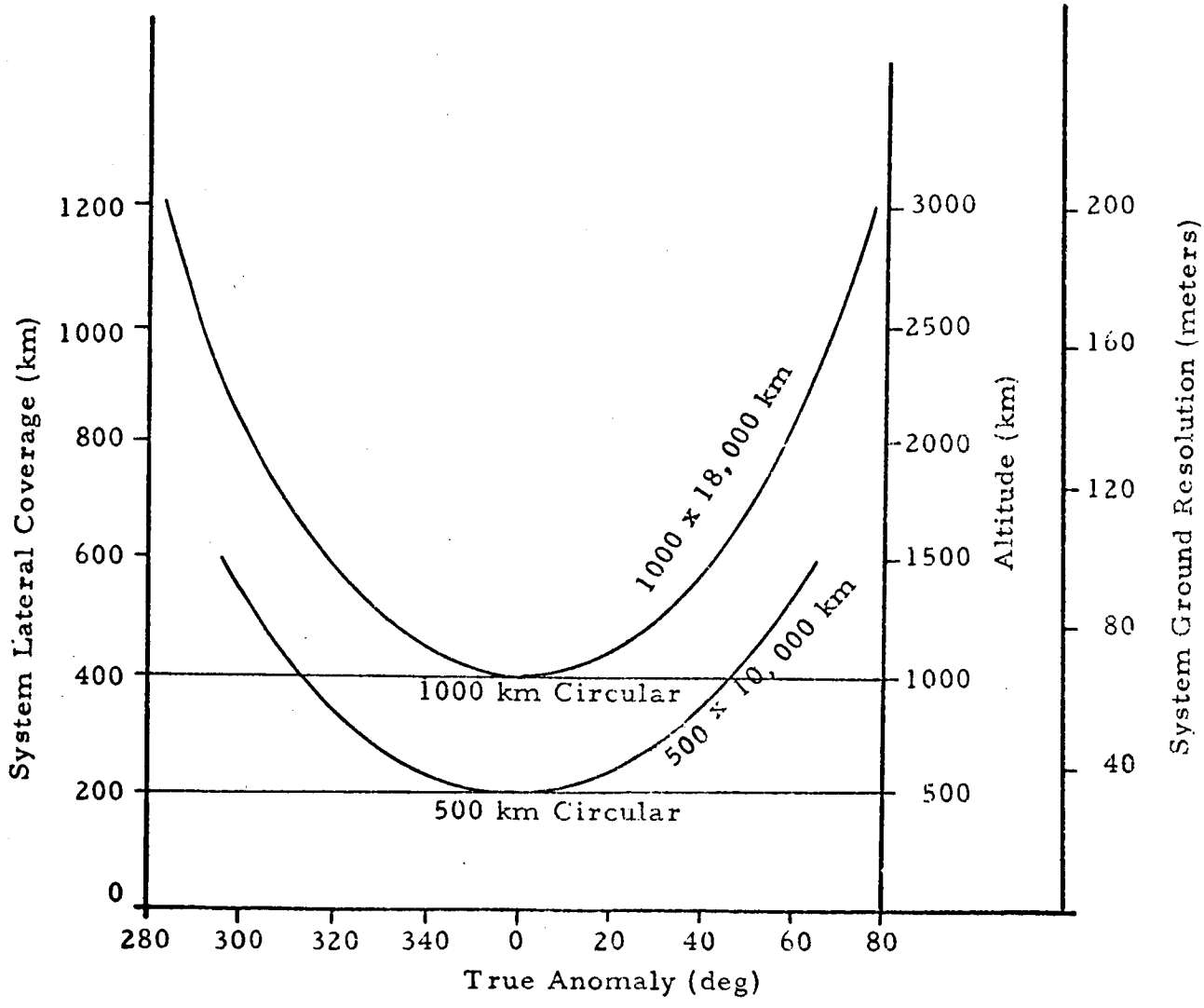

COMPARISON OF PHOTO-SYSTEM PARAMETERS FOR SELECTED ORBITS
(150 mm focal length, 100 lp/mm system resolution, 70 mm format)

FIGURE 8-7

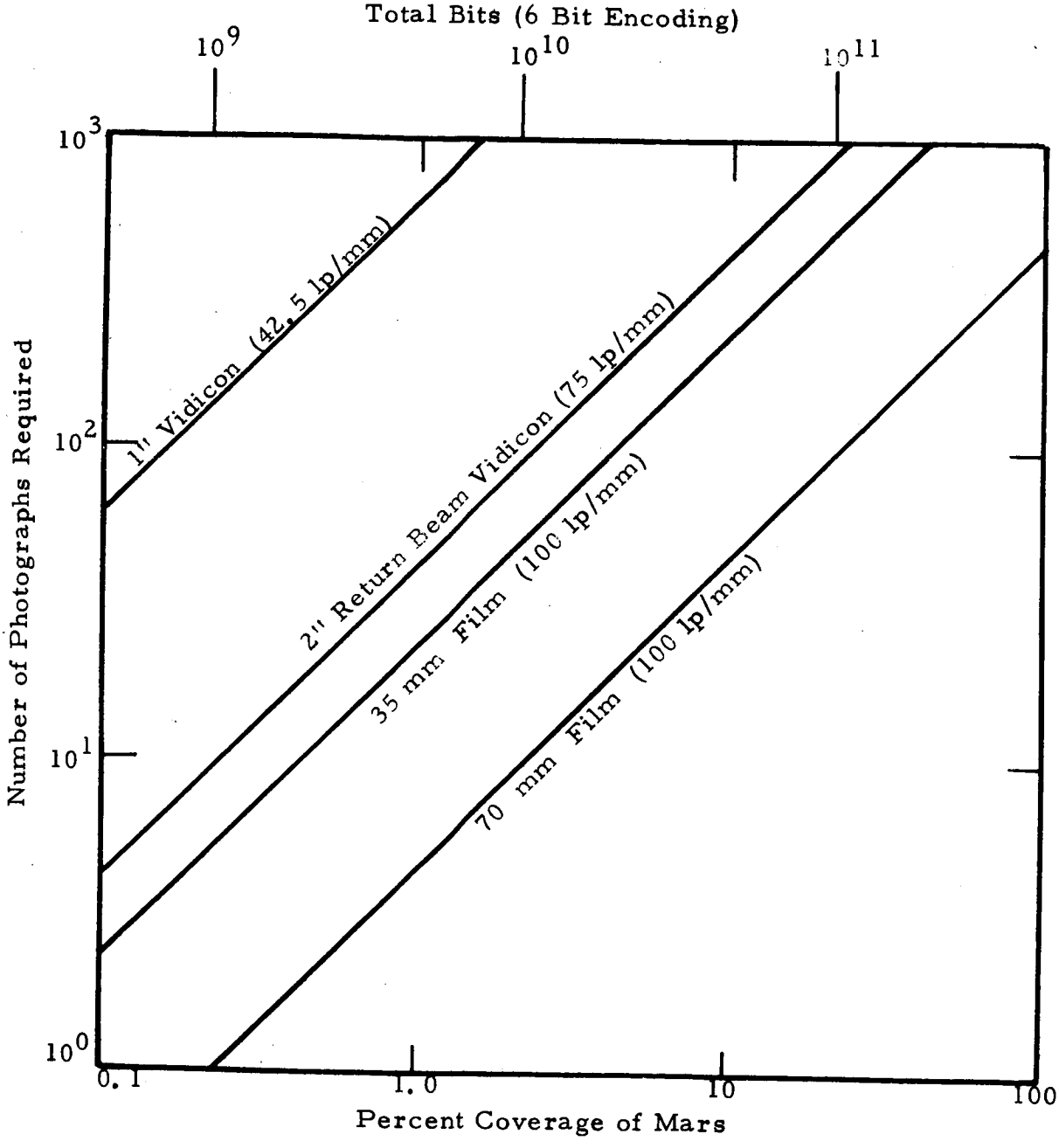

FIGURE 8-8a PERCENT PLANET COVERAGE VS NUMBER OF PHOTOGRAPHS REQUIRED (100 Meter Ground Resolution)

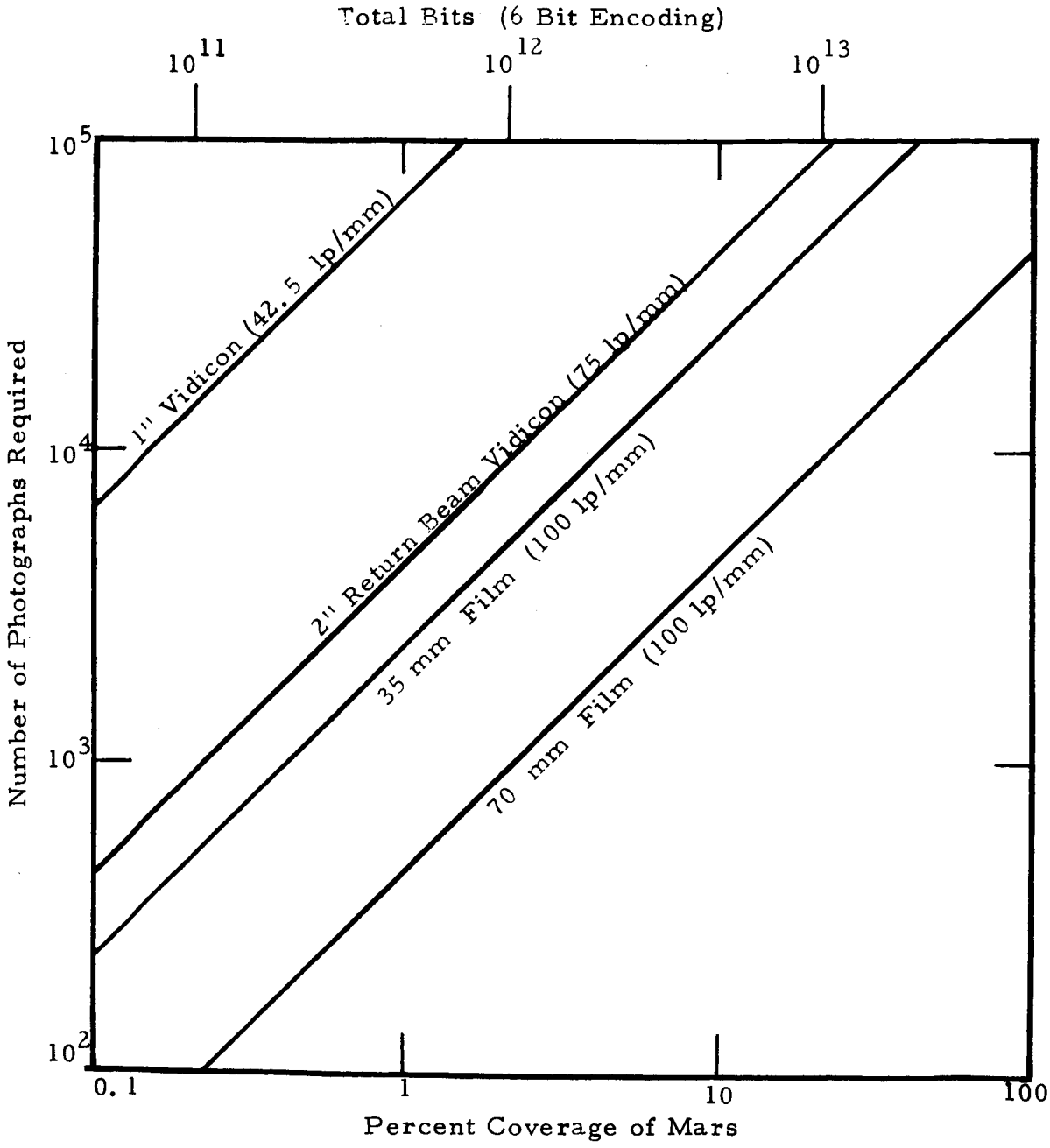

FIGURE 8-8b PERCENT PLANET COVERAGE VS NUMBER OF PHOTOGRAPHS REQUIRED (10 Meter Ground Resolution)

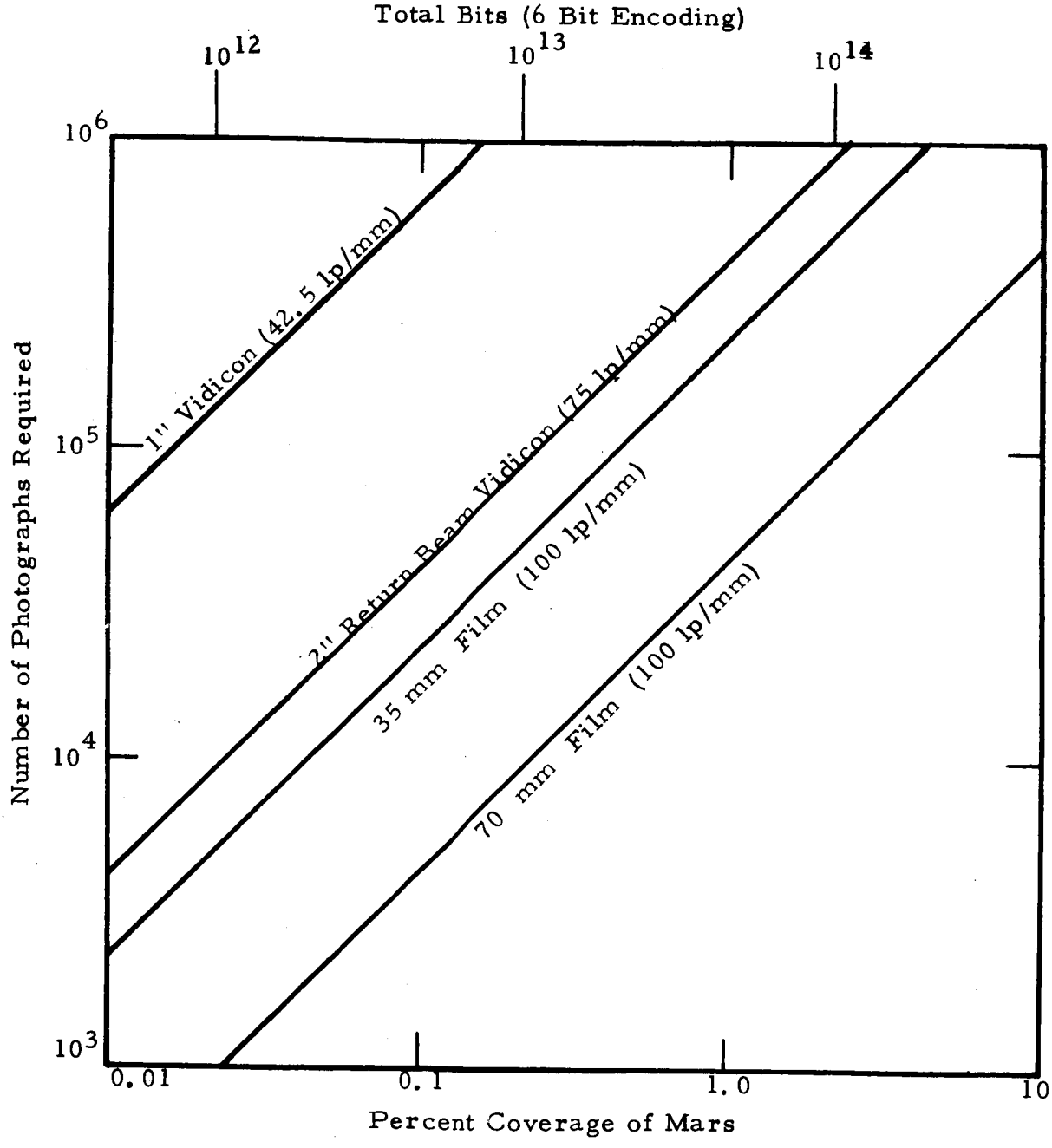

FIGURE 8-8c PERCENT PLANET COVERAGE VS NUMBER OF PHOTOGRAPHS REQUIRED (1 Meter Ground Resolution)

8.3 SYSTEM COMPARISON: OVERALL CONSIDERATIONS

In the preceding sections, individual sensor systems were compared on the basis of resolution as a function of system mass and the number of pictures required to provide a given coverage. In this section, other systems considerations including dual resolution capability (both high and medium resolution from one photo system), multi-spectral, stereo, and mapping capability, and additional important system criteria are discussed, and the candidate sensor systems are compared.

8.3.1 Dual Resolution Capability

To convert the individual sensor systems previously discussed into systems with a dual resolution capability requires, first of all, the use of two separate lenses, unless a zoom lens with sufficient range to cover the two different resolution levels is used. Because of the moving parts required by zoom lenses, the difficulty of achieving high resolution performance with these lenses, and the impossibility of simultaneously obtaining high and medium resolution imagery unless two separate lenses are used, the zoom lens does not appear to be a suitable method for providing a dual resolution capability. (An application for which the zoom lens is better suited is that of providing a fixed ground coverage area for a given sensor by compensating for the altitude variations that occur in the highly elliptical orbits that are anticipated.) In addition to the requirement for two lenses, two separate sensor surfaces must be available. This can be supplied in a film system by imaging, simultaneously if desired, onto two separate parts of the film transport strip. Since this approach cannot be used for the vidicons, an additional camera head would be required.

8.3.2 Multi-Spectral Capability

Multi-spectral imagery can be provided by any of the sensor systems through the use of a filter wheel, as discussed in Section 5.3. To obtain color photos the preferred approach with a film system would again be to image simultaneously at multiple places on the film strip, while the vidicons would again use multiple camera heads.

8.3.3 Stereo Capability

Stereo capability can be provided by imaging with a fixed camera and using frame overlap, or by the use of convergent camera (see Section 5.2). For the fixed camera approach, the larger format sizes as well as the higher resolution provided by film results in better stereo performance than that of the vidicon sensors. If stereo is to be provided by vidicons, the convergent camera approach using two camera heads would probably be the method employed.

8.3.4 Mensuration Capability

The mensuration capability of film is certainly better than that of vidicons because of the greater geometric fidelity of film. This advantage can, however, be dissipated if the other elements in the system, particularly the scanner, are not relatively free from geometric distortion. Mechanical scanning devices have an advantage over electron beam scanners in this regard.

8.3.5 Data Readout Flexibility

The degree of data readout flexibility for a photosystem is a function of the range of rates at which sensor data can be transferred to the storage medium (if the two are separate), the range of rates at which the imagery data can be transferred from the storage medium to the communication subsystem, and various readout options such as coarse scan, repeated readout, and delayed readout (see Section 7). The transfer of data from the sensor to the storage medium is not applicable to film, but does apply to the vidicons. The two inch return beam vidicon requires a considerably higher data input rate to the storage device than does the one inch vidicon because of the better resolution and larger format of the return beam device (the ratio is roughly 4:1 for continuous coverage for the sensors used in the systems comparison).

Transferring the information from the storage medium to the data link is required for all of the sensors. The requirement to match the film scanning rate to the communication bandwidth can be fulfilled by electronic (CRT) or electro-mechanical scanners for the range of bandwidths anticipated for the Voyager mission (see Section 7). For the vidicons, the ratio between the input rate to the storage medium and its output rate to the data link, e.g. the tape recorder playback ratio, can be a problem. There is a question about the feasibility of achieving these ratios with a rotary head tape recorder, the type usually considered for use in conjunction with return beam vidicons.

An important additional consideration is the need to continuously feed data to the tape recorder for the portion of the orbit during which the pictures are being taken. Otherwise the tape recorder would have to be started and stopped for each picture so that no gaps would occur later during transmission. This would further reduce the life expectancy of the recorder, the component that would probably limit the system lifetime even if it is cycled only once per orbit, first recording and then reading out.

8.3.6 Dual Resolution Readout

A readout option that is definitely of interest for the Voyager mission is the preliminary coarse scanning of stored imagery for the purpose of either establishing the order of detailed picture readout or selecting the pictures to send and to omit. The latter application is particularly appealing because the mission is limited by the data link bandwidth, at least until megabit and higher data rates become available. Preliminary coarse scanning can certainly be implemented with film systems; its accomplishment with systems using tape recorder storage is doubtful.

8.3.7 Repeated Readout

Repeated readout of picture data can be employed to reduce the number of errors (i.e., improving the signal to noise ratio), increasing the confidence in a photo that is of special interest. It is fairly simple to include the capability for repeated readout in a film system or in a system using tape recorder stoarge. However, an orbiting system using

a tape recorder is usually designed so that all of the information acquired during a given orbit is read out during that orbit, although this does not have to be the case. Additional tape can be included to allow for data storage for two or more orbits.

8.3.8 Delayed Readout

The capability to delay the readout of data can be useful for several reasons. The transmitting time on a particular orbit or sequence of orbits may be limited because Mars occults the Voyager vehicle and the Sun or the Earth for part of most orbits. There may be an above average number of photos of interest on a particular orbit or sequence of orbits. The receiving ground station may be unavailable for a period of time. The latter is a particularly important consideration because of the anticipated duration of the orbital mission. It seems possible that the requirements of other missions (e.g., Voyager twin or Mariner mission) may precipitate conflicts for ground station facilities at some time during a Voyager mission of many months duration. Implementation considerations are similar to those discussed above for repeated readout. The capability can be included not only in film systems, but also in systems using tape recorder storage if enough tape is added to provide storage for the required number of orbits.

8.3.9 Lifetime Limitations

For film systems, a limitation on the mission life is of course imposed by the amount of film and processing material that is carried, although this limitation is not a serious one for the communication rates and orbiting mission times anticipated for Voyager. For example, a data bit rate of 5×10^4 bits/second for a period of 100 days would result in the transmission of about 3×10^{11} bits (see Figure 7-3), which would require only about a 15 meter roll of 70 mm film for a 100 lp/mm system resolution (see Figure 7-4b). For the same data rate, and 200 days in orbit, a 30 meter roll of film would be required. For the vidicon systems, tape recorder wear is the most probable limitation on mission lifetime.

8.3.10 Development Risks

The film and one inch vidicon systems are considered to entail little development risk because similar systems have been proven in space. The return beam vidicon system is estimated to have a higher development risk primarily because of the current status of the tube and its associated recorder.

8.4 SYSTEMS COMPARISON: SUMMARY

Table 8-3 summarizes some points of comparison between the film, return beam vidicon, and vidicon photo systems. An examination of the table shows that, for the assumed mission characteristics, the film system provides the best high resolution capability. For a medium resolution capability, the choice is not as clear; the vidicon system has the minimum mass, but the film system offers the advantage of requiring significantly fewer pictures. For a dual resolution capability, a film system is the superior choice for the Voyager mission configuration.

Although not indicated in the table, various combinations of these sensors are certainly possible to provide dual resolution capability. One possible combination system is a film sensor for high resolution imagery and a one inch vidicon sensor for the medium resolution capability.

TABLE 8-3 PHOTO SYSTEM COMPARISON SUMMARY*

Parameter	70 mm Film	2 inch Return Beam Vidicon	1 inch Vidicon
High Resolution Performance	1	2	3
Medium Resolution Performance	2	2	1
Dual Resolution Capability	1	2	2
Number of Pictures Required	1	2	3
Mensuration Capability	1	2	2
Storage Requirements	1	3	2
Processing Requirements	2	1	1
Susceptibility to Radiation	2	1	1
Data Readout Flexibility	1	2	2
Development Risk	1	2	1

* Numbers indicate relative ranking: 1:best; 3: poorest.

APPENDIX A

CHARACTERISTICS OF MARTIAN ORBITS

Martian orbit characteristics which are useful in reconnaissance system analyses are presented parametically in this appendix. Data on both circular and elliptical orbits are included as well as orbit perturbation effects due to planetary oblateness and atmopsheric drag. Orbital geometry and nomenclature are defined in Figures A-1 and A-2.

A. 1 Circular Orbits

The well known relationships between orbit altitude, velocity, and the period of an orbital revolution are briefly stated here for convenience; they are referenced in explaining other derivations throughout this report.

Let:

R = mean radius of Mars

h = height of satellite above Martian surface

r = distance from center of Mars to satellite = R + h

v = velocity of satellite in orbit

G = universal gravitational constant

M = mass of planet

The velocity of a satellite in circular orbit is:

$$v = \sqrt{\frac{GM}{r}} = \sqrt{\frac{GM}{R+h}} \qquad (1)$$

Both G and M are constants, so let GM = K. For orbit altitude expressed in kilometers,

$$K = 4.2906 \times 10^4 \text{ kilometers}^3/\text{seconds}^2$$

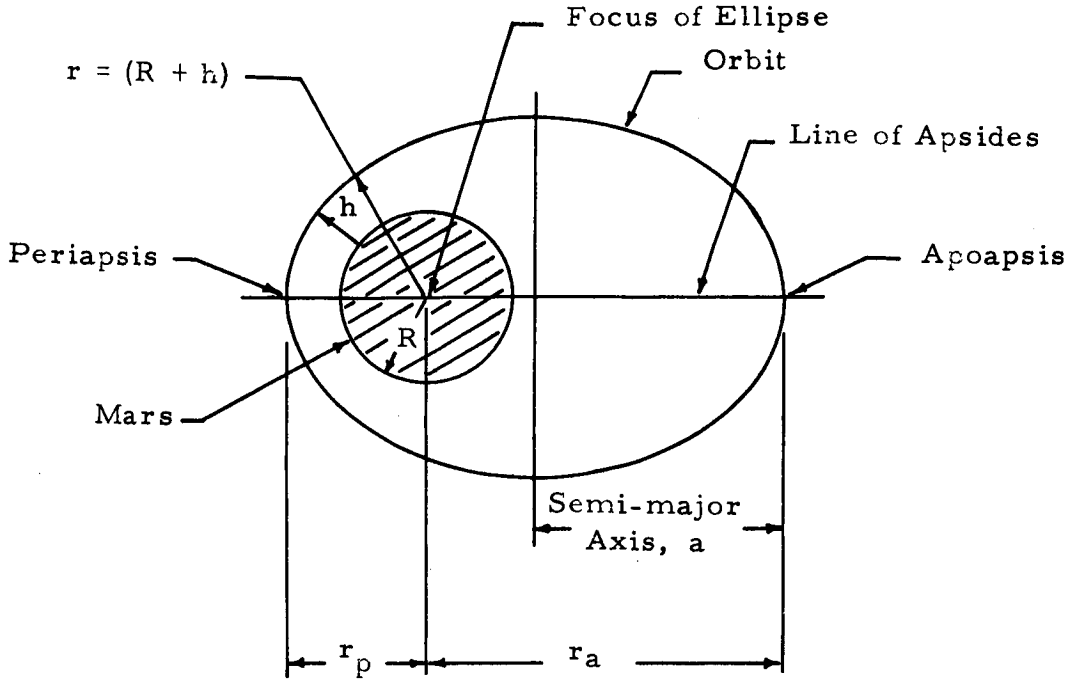

GEOMETRY AND DEFINITIONS FOR ELLIPTICAL ORBITS

FIGURE A-1

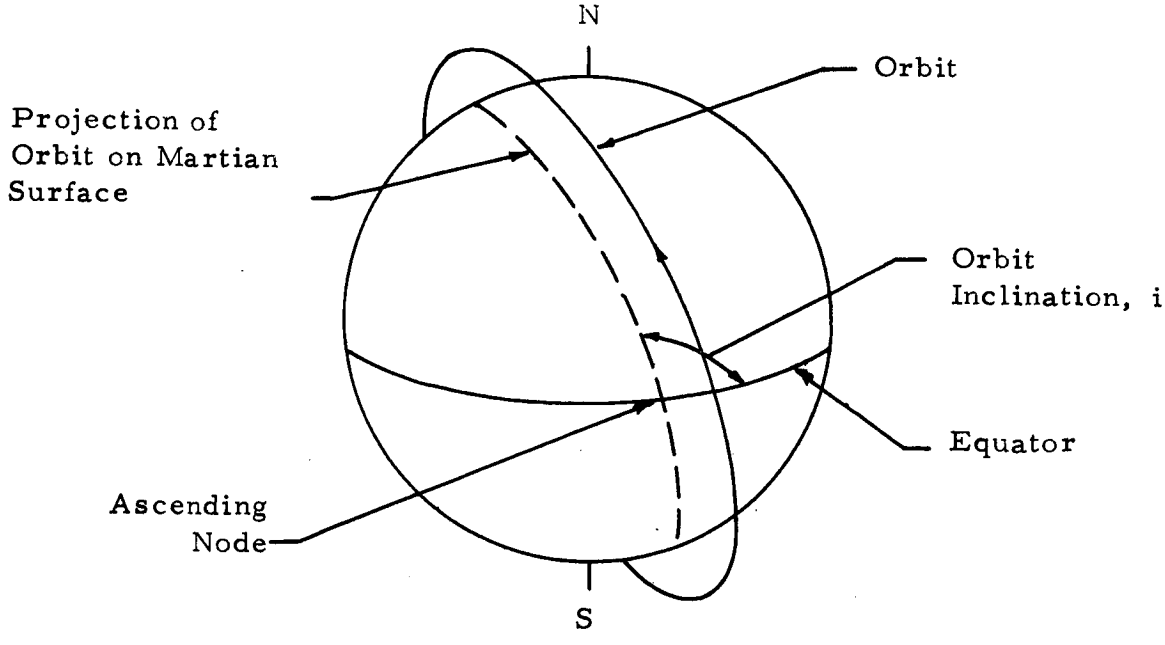

ORBITAL DEFINITIONS

FIGURE A-2

Accordingly

$$V = \frac{207}{\sqrt{r}} \quad \text{km/sec.}$$

Circular orbital velocity is plotted as a function of the ratio of orbit radius to Martian radius in Figure A-3 and versus orbit altitude in Figure A-4.

For photographic experiments, the more crucial velocity is that over the planet's surface. Neglecting, for the present, the effects of planet rotation and letting v_g' be velocity over the surface of a non-rotating Mars

$$v_g' = \left(\frac{R}{R+h}\right) v = \left(\frac{R}{R+h}\right) \sqrt{\frac{K}{R+h}} \quad \text{km/sec} \qquad (2)$$

Ground velocity is presented in Figure A-4 versus orbit altitude for the nonrotating planet case.

The orbital period for a circular orbit about Mars can be determined by noting that

$$P = \frac{2\pi(R+h)}{v} = 2\pi \frac{(R+h)^{3/2}}{\sqrt{K}} \quad \text{sec.} \qquad (3)$$

when h is expressed in kilometers. The time to complete a circular orbit about the planet Mars is presented in Figure A-3 as a function of the ratio of orbit radius to planet radius, and as a function of orbital altitude in Figure A-4.

A.2 Elliptical Orbits

Voyager orbits about Mars can be expected to be quite elliptic due to consideration of over-all mission objectives and system constraints. For convenience in visualizing elliptical orbits, apoapsis altitude is plotted versus periapsis altitude in Figure A-5 (Ref. A-2) for several

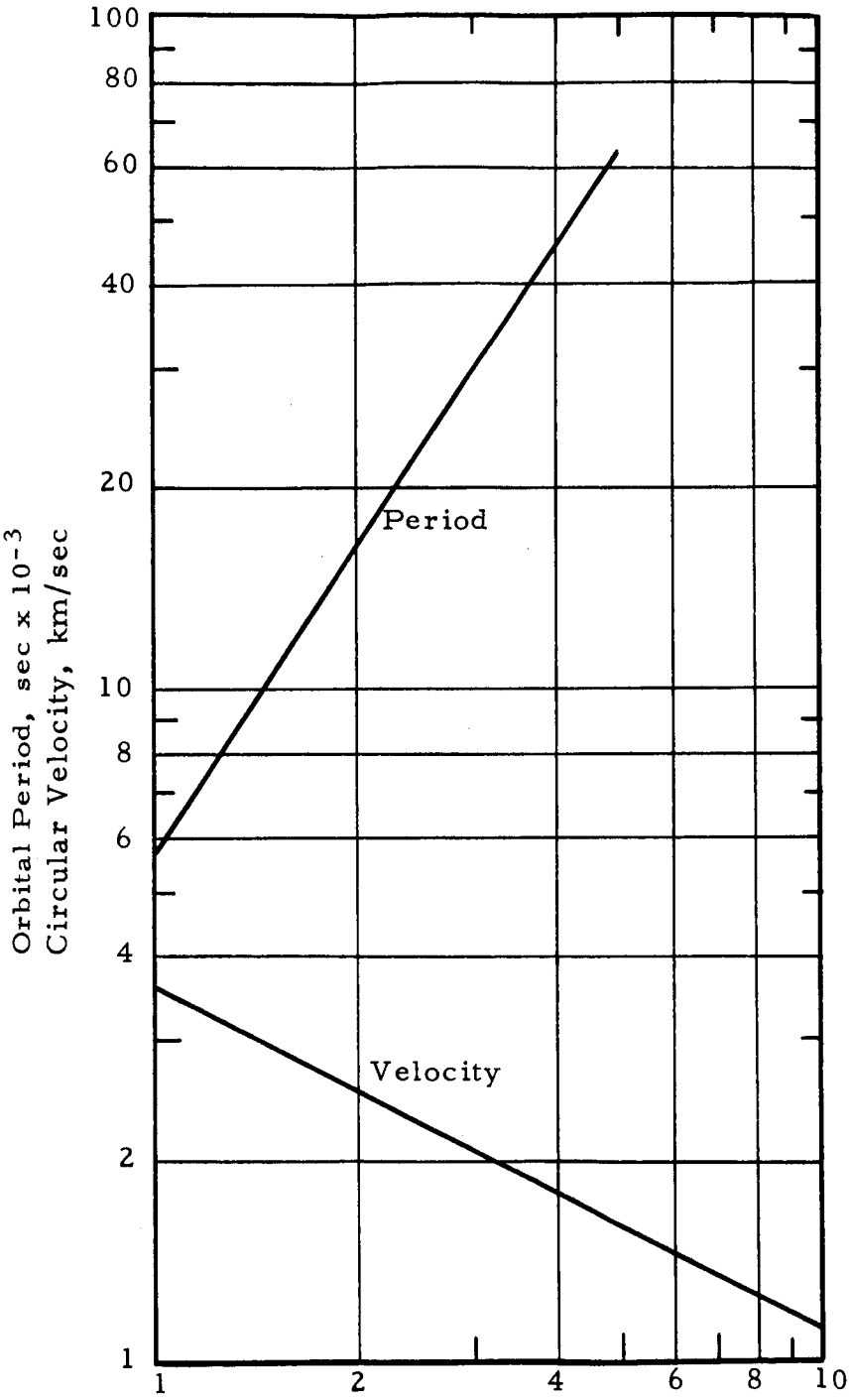

CIRCULAR ORBITAL VELOCITY AND PERIOD ABOUT MARS

FIGURE A-3

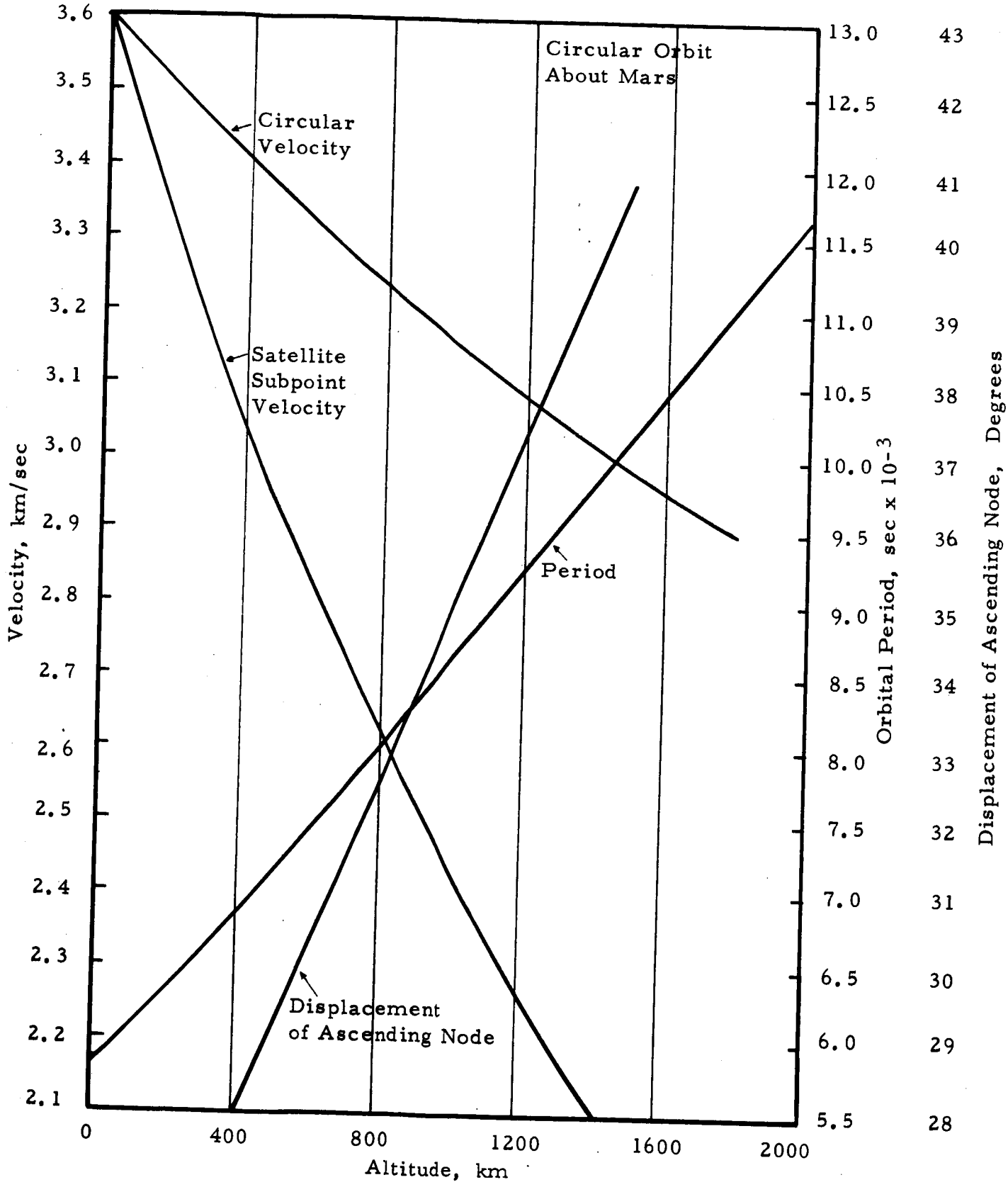

ORBITAL VELOCITY, SUBPOINT VELOCITY, ASCENDING NODE AND ORBITAL PERIOD VS. ORBIT ALTITUDE
FIGURE A-4

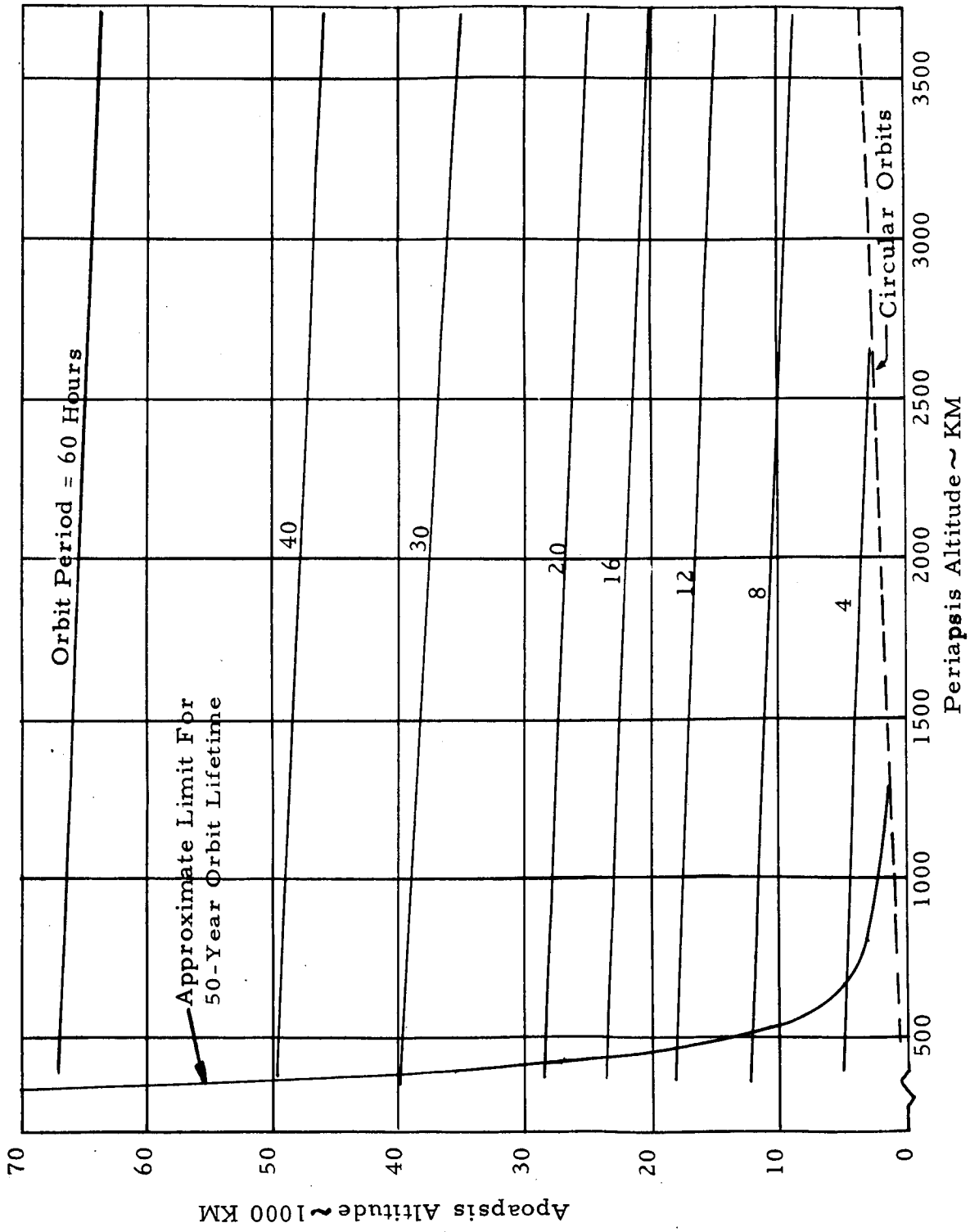

APOAPSIS VERSUS PERIAPSIS ALTITUDES OF ORBITS ABOUT MARS

FIGURE A-5

orbit periods. Minimum periapsis altitude for a 50 year orbit lifetime is also indicated. This is necessary to meet planetary quarantine constraints. The curve, from Reference A-2, is based on current conservative estimates of the atmosphere of Mars, and on a spacecraft m/C_DA of 0.25 slug/ft^2; this is a typical value for a solar powered-spacecraft. A more detailed discussion of orbit decay is given in paragraph A.5.

Recent discussions with NASA personnel of the Marshall Space Flight Center and from the Voyager Interim Project office indicate current thinking is that the spacecraft should not impact the planet with unsterilized elements for a period of 20 years after initial orbit of Mars. Depending upon the atmospheric model used in the orbit decay analysis, orbits having periapsis altitudes as low as 200 km can satisfy a 20 year requirement.

The ratio between ground velocity and altitude, commonly known as V/H, is of importance in defining the resolution of imaging systems, and in evaluating the need for image-motion compensation. The maximum V/H for a given orbit occurs at periapsis, when velocity is highest and altitude is lowest. As shown in Figure A-6, the ratio is primarily dependent upon altitude, reflecting the fact that large differences in orbit period cause relatively small differences in periapsis velocity.

Characteristics of three specific example trajectories having periods of 7, 9.5 and 40 hours are illustrated in the following figures. The altitude above the planet surface at periapsis versus orbit eccentricity is shown in Figure A-7. The variation of orbital period with the semi-major axis of the elliptic orbit is presented in Figure A-8.

An important input to photographic system design is the change in altitude as the spacecraft moves from periapsis. This parameter is presented in Figure A-9 as a function of angle away from periapsis, for orbits having periods of 7, 9.5 and 40 hours. It can be seen that a significant increase in altitude will occur at approximately 45° from periapsis for each of the orbits. Hence, extremely long picture taking cycles would not be very profitable from elliptical orbits having eccentricities in the range indicated, since ground resolution decreases with increasing altitude.

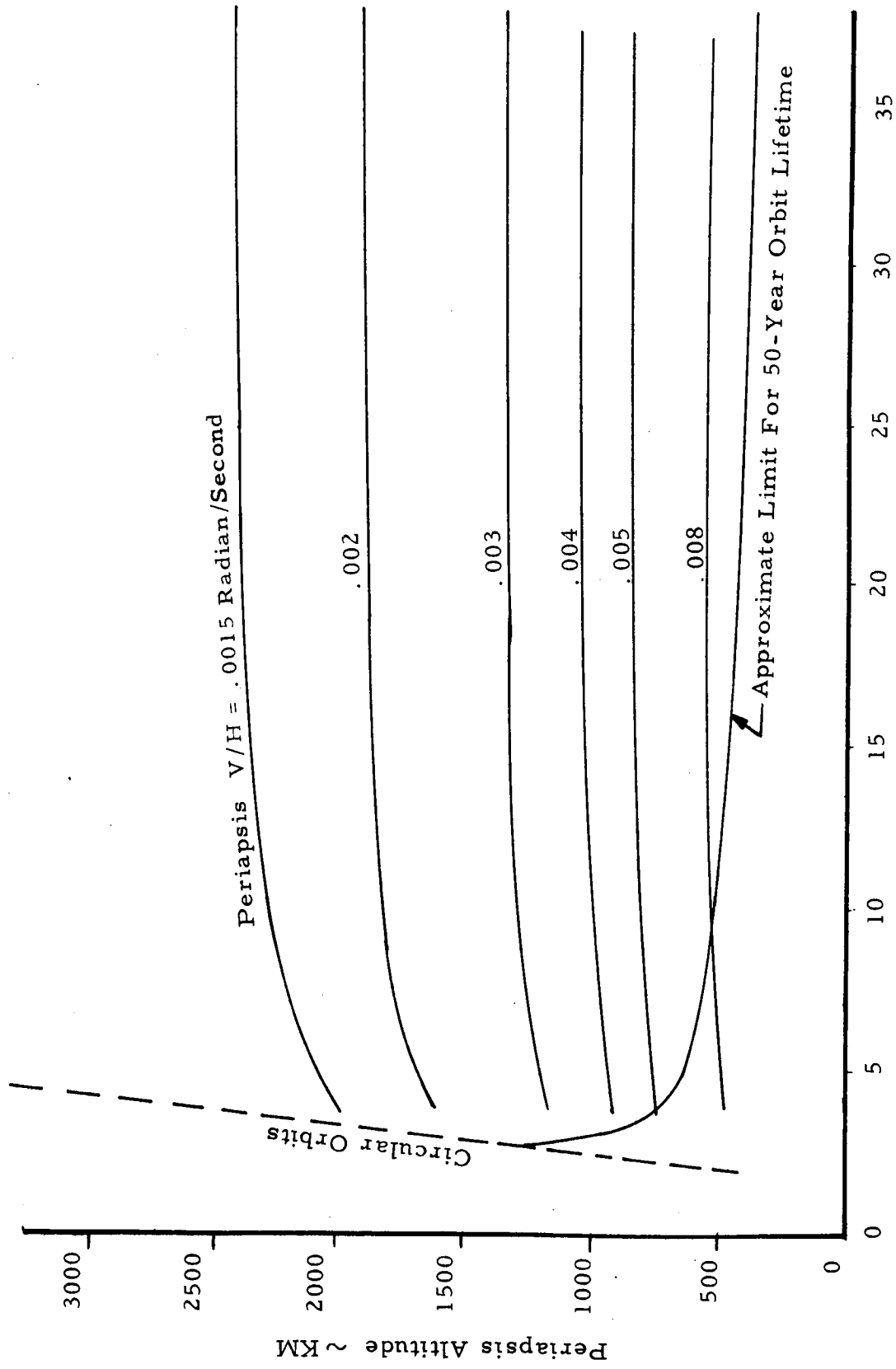

PERIAPSIS V/H FOR ORBITS ABOUT MARS

FIGURE A-6

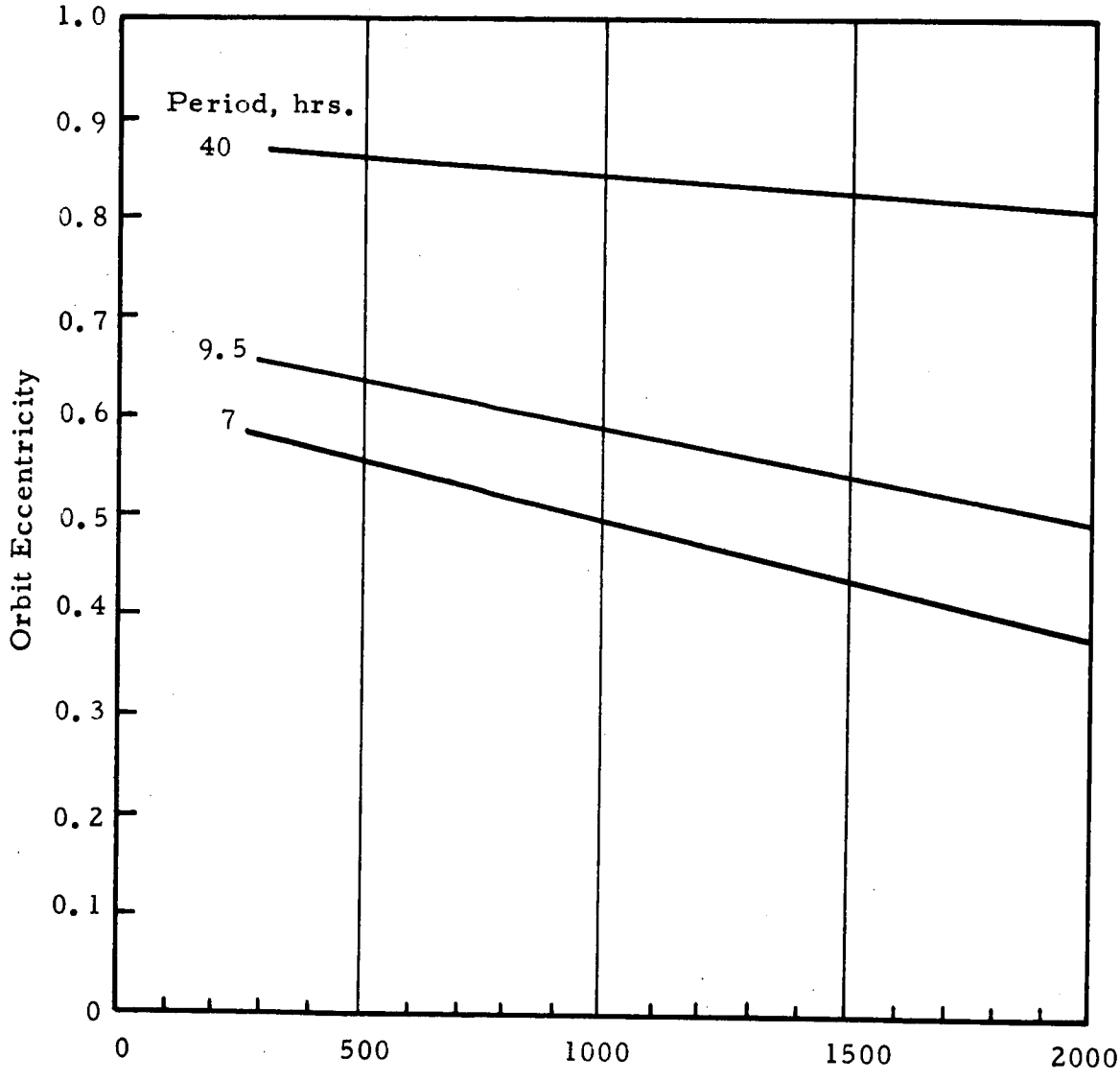

ORBIT ECCENTRICITY VS. PERIAPSIS ALTITUDE

FIGURE A-7

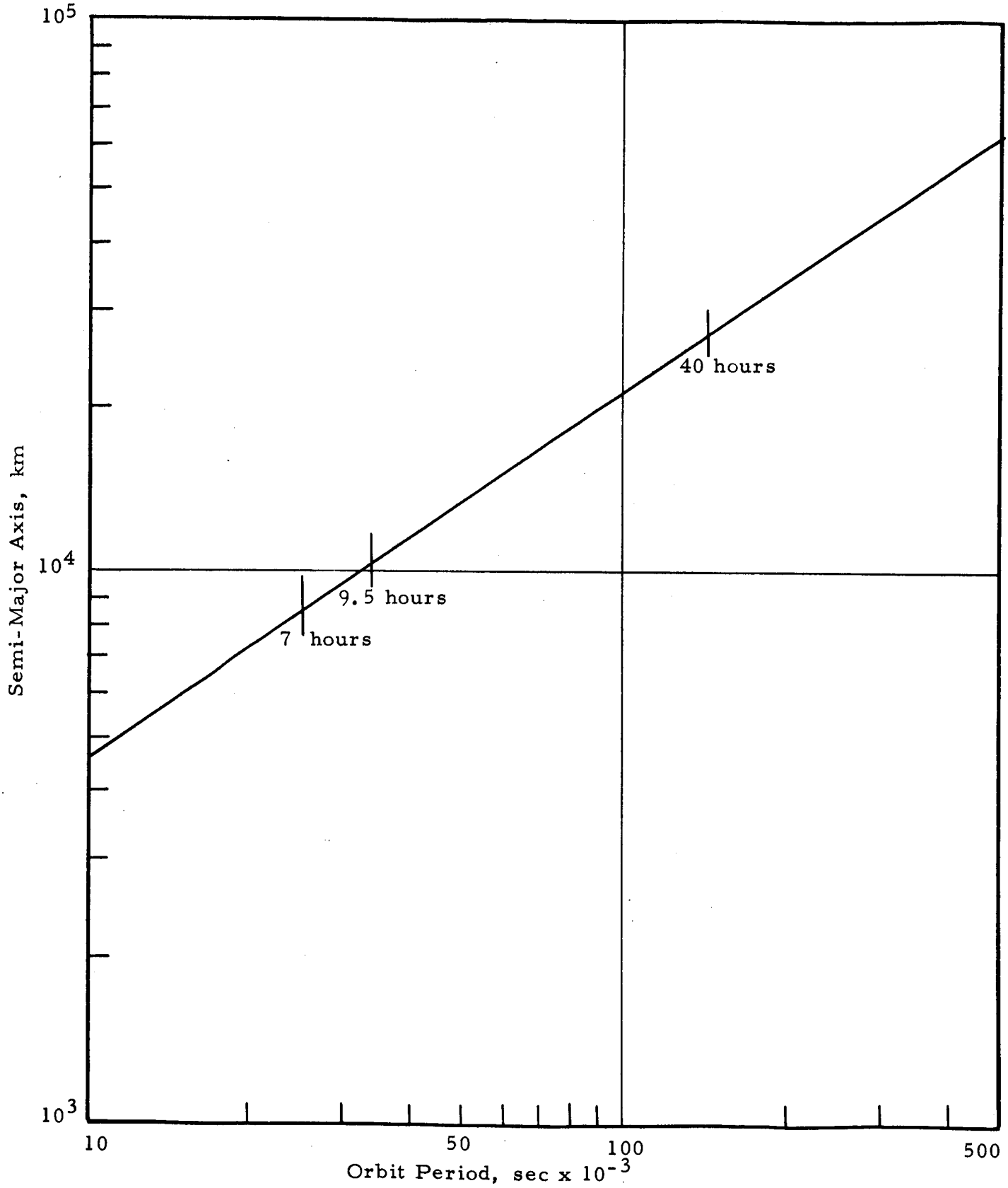

ORBIT PERIOD VS. SEMI-MAJOR AXIS
FIGURE A-8

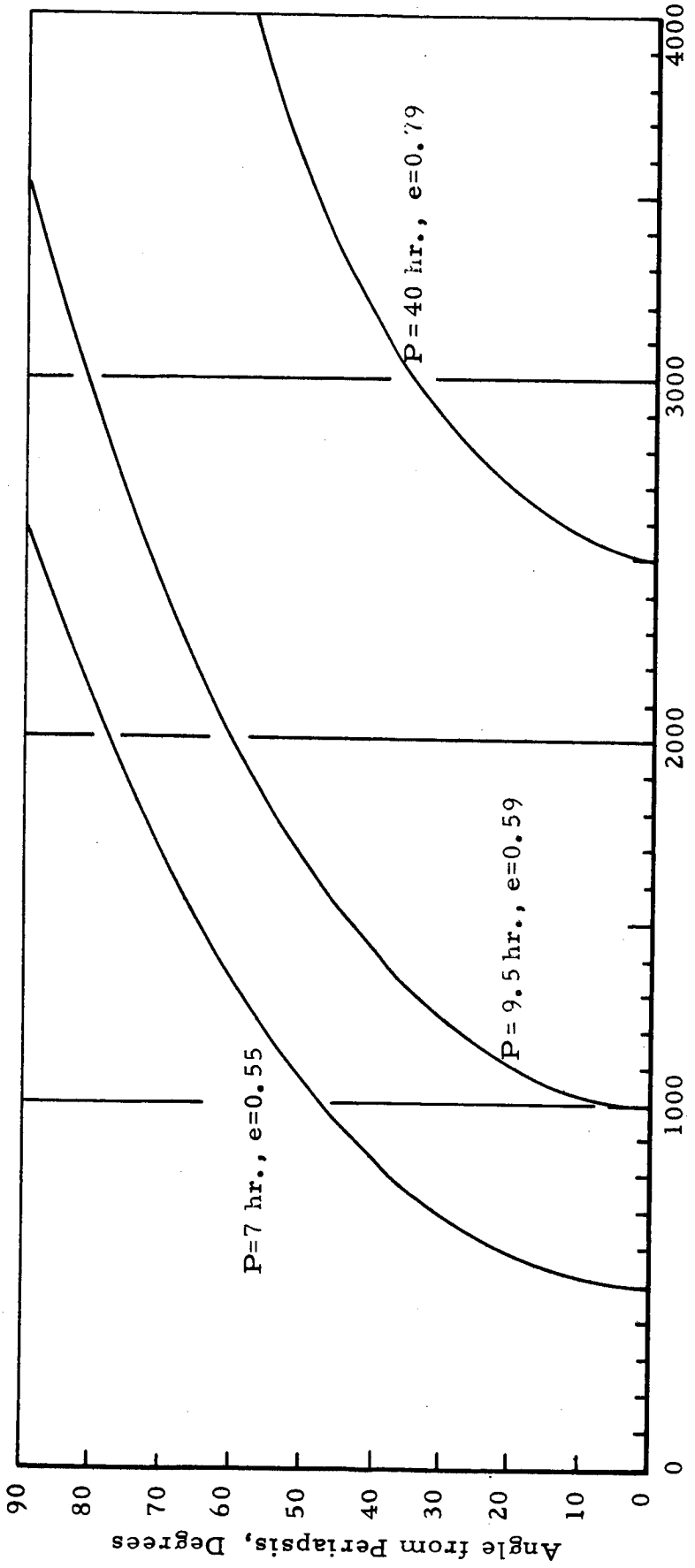

SPACECRAFT ALTITUDE VS. ANGLE FROM PERIAPSIS
FIGURE A-9

As noted previously, an important parameter necessary for the evaluation of image smear and determining shutter speed is the ground velocity of the spacecraft. This is shown for three eccentricities in Figure A-10 (nonrotating planet). The maximum velocity occurs at periapsis and, for example, will be 3.4 km/sec for the 7 hour, 500 km periapsis altitude orbit.

A.3 Orbit Inclincation and Ascending Node

So far, only the shape of an orbit has been considered. Its orientation in space will now be discussed. The orientation of the orbit plane is specified in terms of the inclination and of the ascending node.

The orbit inclination, i, is the angle between the planet's equatorial plane and the plane of the orbit. The orbit inclination determines the maximum latitude over which the orbit passes. The orbit will cross or reach all latitudes $\leq$ i. Thus, the inclination places one limitation on the extent of planet coverage a satellite can provide and will be a major parameter to be considered in selecting the optimum orbit.

Consideration of Martian surface area coverage requires the performance of trade-off studies of satellite period, planet rotation and orbit orientation with respect to the sun. It is possible to vary the orbit inclination by propulsive means; however, as can be seen by the plot in Figure A-11, rather small changes in orbit inclination requires that significant ΔV capability be provided, which in turn dictates propulsion system weight. According to Reference A-3, the Voyager orbiter will have a ΔV capability for in-orbit maneuvers of 6500 ft/sec.

The other aspect of orbit orientation is given by specifying the ascending node, the point of northbound equator crossing of the satellite. Since the planet is rotating continually, the primary coordinate system for specifying ascending node is right ascension (the astronomical equivalent of longitude).

A.4 Effects of Mars Rotation

Because of the rotation of Mars, the subpoint track (the projection of the satellite positions on the Martian surface) does not retrace from one orbit to the next (with the exception of the special case of equatorial

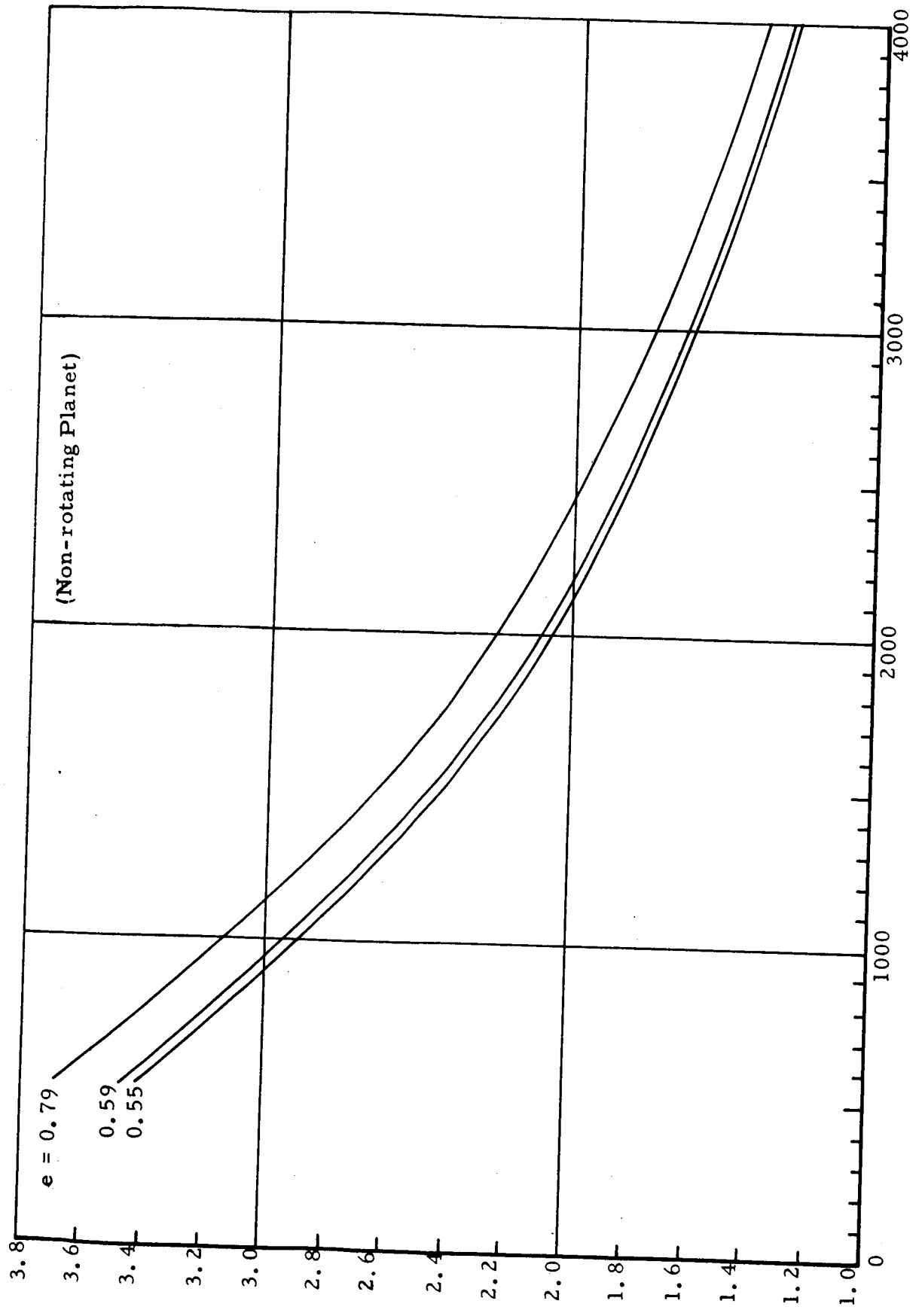

SATELLITE SUBPOINT VELOCITY AT PERIAPSIS

Figure A-10

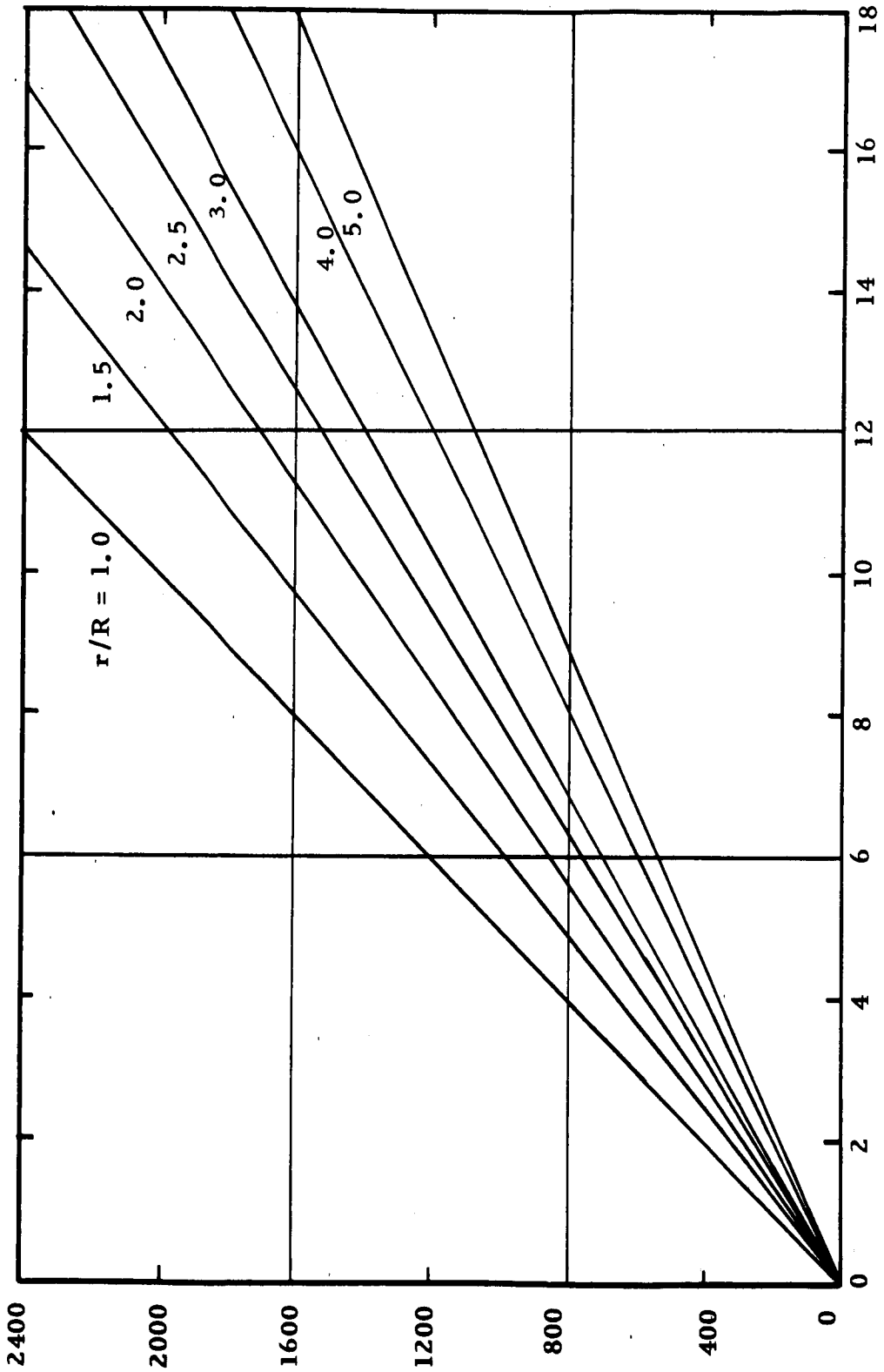

VELOCITY INCREMENT REQUIRED TO ROTATE CIRCULAR ORBIT PLANE

Figure A-11

orbits, i = 0° or 180°). Rather, the ascending node and the subpoint of every point on the orbit are displaced westward by an amount in longitude equal to the angular rotation of Mars during an orbital period.

Since Mars rotates 360° in 24 hours and 37.38 minutes (i.e., angular rate = 4.07×10^{-3} deg/sec), this longitudinal displacement from one orbit to the next, $\Delta\lambda$, is given by

$$\Delta\lambda = (4.07 \times 10^{-3})\, P, \text{ degrees}$$

where P is the orbital period in seconds. $\Delta\lambda$ is plotted versus altitude in Figure A-4.

Because of the Martian rotation, the subpoint track and the instantaneous intersection of the orbital plane and the Martian surface are not the same. The heading line is the instantaneous projection on the surface of the orbital plane. Looking along the orbit in the direction of the satellite motion, the heading line is directed slightly to the east of the subpoint track (except at the northernmost and southernmost limits of the orbit, where the heading line is tangent to the subpoint track).

These differences between the subpoint track and the heading line may be significant if the photographic experiment design is to be precise. For a satellite with three axis stabilization (such as Nimbus), a sensor rotating about an axis parallel to the satellite roll axis (the satellite velocity vector for perfect stabilization) will produce a scan perpendicular to the heading line, rather than to the subpoint track. The Nimbus radiometers have such a scanning pattern, and neglect of this matter can lead to errors of up to 1.5° of great circle arc in the geographical location of observed points.

The satellite velocity over the surface of a nonrotating planet, v_g', was related earlier to the orbit velocity, v, by Equation 2. v_g' can be resolved into its latitudinal and longitudinal components to determine the actual satellite velocity over the planet's surface (that along the subpoint track). Obviously, the rotational velocity of the planet only adds to the longitudinal component of the satellite velocity. The contribution to ground velocity of the subpoint track due to planet rotation

is negligible during that portion of the orbit when imaging is to be obtained and can be ignored in photographic IMC considerations.

A.5 Orbit Perturbations and Satellite Lifetime

For observational reasons, a low periapsis altitude is highly desirable. In order to avoid contaminating the surface of Mars with an unsterilized space probe, NASA had established the ground rule that those probes which orbit the planet must have a lifetime of at least fifty years*. Since the properties assumed or estimated for the Martian atmosphere strongly affect the lifetime, the range of uncertainties in the proposed models of this atmosphere cause wide variations in the minimum altitude allowed for the orbiter. In addition, Martian oblateness and the solar gravitational field cause perturbations in the height of periapsis above the planet's surface and the location of the periapsis subpoint and these perturbations are directly tied to the specific mission chosen. Consequently, an evaluation of the effect of these variations on the operating altitudes is necessary to assess their importance in the design of the probe itself and in the selection of the mission constraints that determine the choice of the orbit about Mars.

A.5.1 Orbit Decay Due to Atmospheric Drag - The most significant area in estimating the lifetime of a near-Mars satellite is the choice of the atmosphere model. Since the properties assumed or estimated for the Martian atmosphere so strongly affect the lifetime predictions, the range of uncertainties in the models that have been proposed by both NASA and industry cause extremely wide variations in any mission analysis conclusions (Ref. A-4).

Figure A-12 shows the estimated lifetime of Martian satellites based on two atmosphere models, the maximum and the mean of NASA TN D-2525 (Ref. A-5), as a function of initial periapsis altitude and eccentricity. Note the factor of about 500 between the lifetimes predicted for these two models. Clearly, any gain in the knowledge of the atmospheric structure results in a large reduction in lifetime uncertainty.

---

*Recent discussions with NASA personnel of the Marshall Space Flight Center and the Voyager Interim Project Office indicate that this restriction will probably be 20 years, or less.

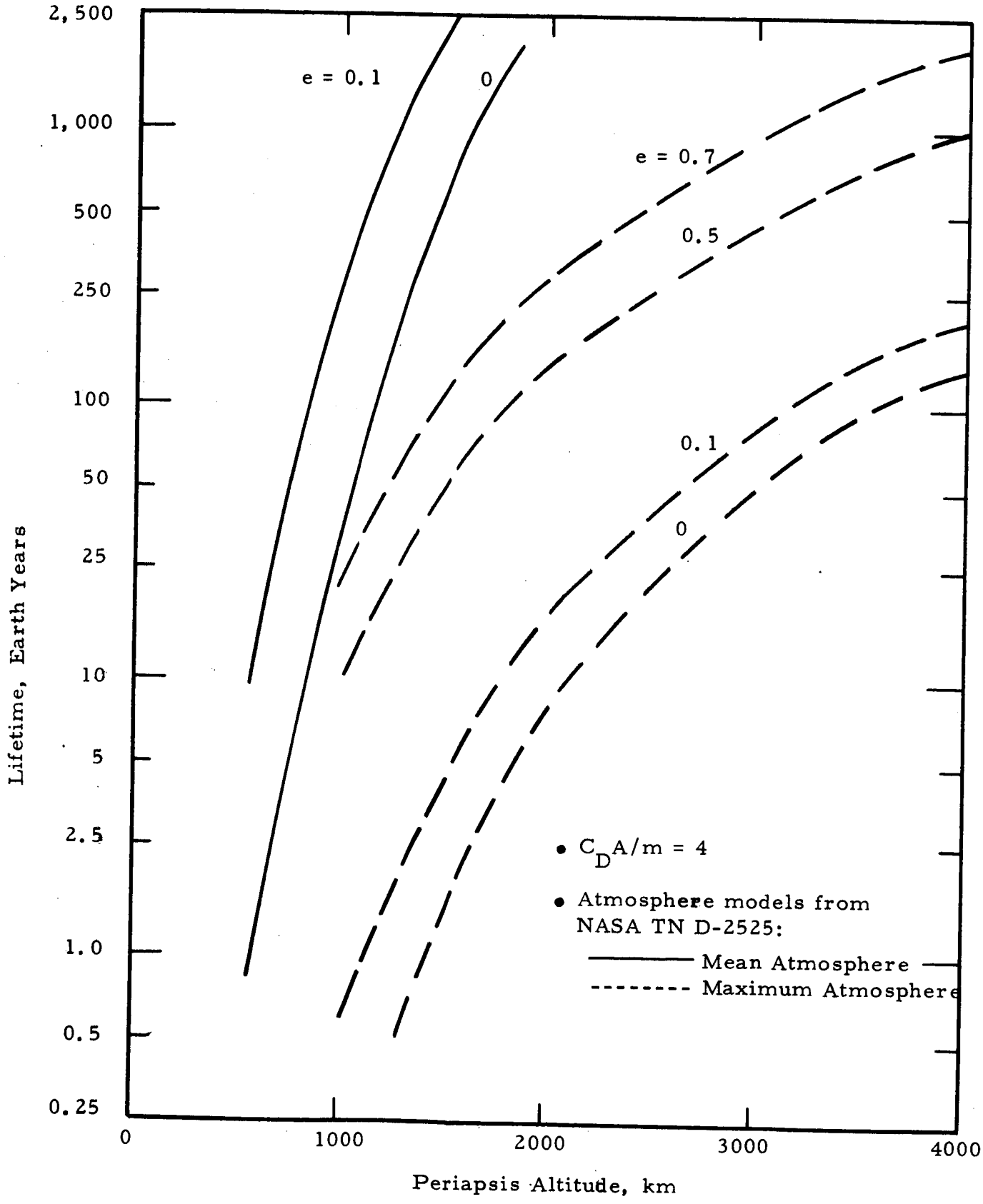

ORBIT LIFETIME VS. PERIAPSIS ALTITUDE

Figure A-12

The successful flight of the Mariner IV past Mars on July 14, 1965, provided data that indicates Mars' atmosphere is most nearly represented by the minimum model. This reinforces the conclusion that drag effects will be significant only for very low altitude, low eccentricity orbits.

Lifetimes estimated in Figure A-12 are based on a ballistic coefficient ($B = C_D A/m$) of 4 $ft^2/slug$, and are inversely proportional to B, where m is the satellite mass, A is the satellite cross-section area, and C_D is the satellite drag coefficient.

A. 5. 2 Solar Gravitational Perturbations - The complete definition of the solar gravitational perturbation effects is quite complex, being dependent upon orbital geometry, mission constraints, and even Martian oblateness. Solar perturbations on orbits with moderate-to-high eccentricity affect lifetime estimates primarily by changing the periapsis altitude, potentially to the extent that: periapsis could be changed (lowered) sufficiently to necessitate complete revision of lifetime estimates based on atmospheric drag effects alone, or periapsis altitude could be perturbed sufficiently to cause impact with the planet's surface, even if no atmosphere existed at all. Alternately, if the periapsis height were increased by the solar perturbation, the result would be to enhance the lifetime estimated for the vehicle. For orbits with very low eccentricity considered for reconnaissance satellites, solar perturbations have essentially negligible effect on lifetime (Ref. A-4). In addition, the effect is considerably less than that due to atmospheric drag for low periapsis orbits.

A. 5. 3 Planetary Oblateness - In accounting for variations in the orbital elements, the effect of planetary oblateness cannot be overlooked or assumed negligible. As is well known, the effect of planetary oblateness is to rotate the orbital plane of the satellite about the planet's north pole (rotating the line of nodes), and also to rotate the line of apsides in the orbital plane. Mean orbital inclination, eccentricity and semi-major axis are unchanged, which means oblateness does not directly change the periapsis height. Because of the coupling with the solar perturbation equation for Δr_p through the location of the ascending node and argument of periapsis, the oblateness indirectly can alter the periapsis height. The location of the periapsis subpoint is, of course, very important for reconnaissance sensor considerations.

The line of nodes always regresses, while the argument of periapsis advances for inclination less than 63 1/2° and regresses for inclinations between 63 1/2° and 90° (Ref. A-4.) (Retrograde orbits are omitted from the present discussion.) Oblateness effects are measured with respect to Mars' equatorial plane, while the solar perturbation reference plane is Mars' ecliptic plane, and these two reference planes have a mutual inclination of about 24°. A Martian orbit having a periapsis radius of 7,380 km, an apoapsis radius of 57,120 km (eccentricity = 0.77) and an inclination with respect to the equator of 44° has been examined (Ref. A-4). For this sample orbit, the rate of change of the ascending node was – 17 1/2° per Martian year, and the rate of change of the argument of periapsis was 19° per Martian year. As oblateness causes the orbital plane to rotate, the ecliptic inclination decreases to 20°, and then increases to a maximum of 68°.

A.5.4 Other Bodies - Gravitational perturbation effects of several other bodies also have been estimated, since all planets and their moons do influence the trajectory of an orbiting satellite, not just the sun. Jupiter's perturbing acceleration is about 10^{-4} that of the Sun; the Earth's perturbing acceleration about 10^{-5} that of the Sun; and Phobos and Deimos, Mars' moons, would have an estimated perturbing acceleration 10^{-5} and 10^{-6} that of the Sun's, respectively, when the satellite was at the estimated surface radius of that moon. Because of this overpowering dominance of the Sun, no other celestial body is usually considered in gravitational perturbation analyses.

A.5.5 Solar Radiation Pressure - Although a vehicle in the vicinity of Mars is subjected to a solar radiation pressure of about 2.0×10^{-5} dynes/cm^2, this radiation pressure is an insignificant source of perturbations when orbiter lifetimes are evaluated (Ref. A-4). A representative value of frontal area to mass ratio for Martian orbiters is 0.20 cm^2/gm. The magnitude of the resultant acceleration due to solar radiation experienced by an orbiter with its solar panels extended and facing the Sun would be 4.0×10^{-6} cm/sec^2, which is roughly an order of magnitude smaller than the level of the solar gravitational perturbing acceleration. Hence, solar radiation pressure effects are assumed negligible in preliminary lifetime analyses.

A.5.6 Perturbation and Lifetime Summary - Estimations of the potential lifetime of a satellite orbiting the planet Mars will range over several orders of magnitude until a better knowledge of the Martian atmosphere is obtained, since the uncertainties in the density profile of Mars' atmosphere directly affect any lifetime prediction. The time history of the periapsis height can be significantly affected by solar gravitational perturbations for orbits with high eccentricities, and the interaction of planetary oblateness with these perturbations cannot be ignored for a physically accurate appraisal of the periapsis variation.

For an accurate analysis of a specific mission, a computer program is necessary to handle all the couplings between the effects of drag, solar perturbations, and oblateness if a high degree of confidence is required in the results; however, fairly good preliminary estimates of perturbational influences can be made for high-eccentricity orbits by assuming that the drag and gravitational perturbations can be treated independently. Characteristics of example orbits examined in more detail for the photoreconnaissance mission and described in Section 4, were calculated with General Electric Company "Planetary Area Seen by a Satellite" computer program which takes into account solar gravitational attraction and Mars oblateness.

A.6 REFERENCES

A-1 "Orbital Photographic Study," Fairchild Space and Defense Systems, P&AP-Q-67-1, June 1967.

A-2 "Study of Applicability of Lunar Orbiter Sub-Systems to Planetary Orbiters," The Boeing Company, Report No. D2-100710-2, March 15, 1967.

A-3 "Summary of the Voyager Program", NASA Office of Space Science and Applications, January, 1967.

A-4 MOLL, R., and KROP, M., "Long Lifetime Orbits About Mars," AIAA Paper No. 66-35, Presented at the 3rd Aerospace Sciences Meeting, January 24-26, 1966.

A-5 LEVIN, G.M., EVANS, D.E., STEVENS, V., "NASA Engineering Models of the Mars Atmosphere for Entry Vehicle Design," NASA TN D-2525, November 1964.

A-6 BREAKWELL, J.V., "Drag-Life Curves for High Eccentricity," Astronautical Sciences Review, January - March 1962.

APPENDIX B

VIEWING GEOMETRY, COVERAGE AND LOCATION ERRORS

This appendix considers the factors influencing the field-of-view of an orbiting sensor, the planet surface covered as a function of both time and sensor field-of-view, and the errors in the location of data acquired by a satellite borne sensor.

B.1 SATELLITE VIEWING GEOMETRY AND COVERAGE

The factors influencing the view of a sensor, from a satellite position which is assumed to be known will now be examined. The development of the following mathematical expressions is presented in Ref. B-1.

A satellite or a satellite sensor, S, is shown in Figure B-1 at a known height, h, over a known subpoint, S_p. The line of sight from the satellite is defined in terms of n, the nadir angle or the angle between the line of sight and the vertical. A point on the planet is defined in terms of its planocentric distance, B, in degrees of great circle arc, from S_p. The angle between the line of sight and the local horizontal at the point on the planet surface is the elevation angle, E.

Considering Figure B-1, the extreme limit of coverage (i.e., the line of sight from the satellite to the horizon) is given by:

$$\sin n_H = \cos B_H = \frac{R}{R+h} = \frac{R}{r}$$

For any arbitrary nadir angle $n, \left(\leq n_H\right)$,

$$\frac{R}{\sin n} = \frac{R+h}{\sin (180^\circ - n - B)}$$

For some purposes, the zenith angle, Z, at the point observed is of significant interest. Simple trigonometry provides Z in terms of either n or B, since:

$$Z = n+B$$

$$Z = \text{arc sin}\left[\left(\frac{R+h}{R}\right) \sin n\right]$$

$$Z = \text{arc cot}\left[\left(\frac{R+h}{R}\right) \csc B - \cot B\right] + B$$

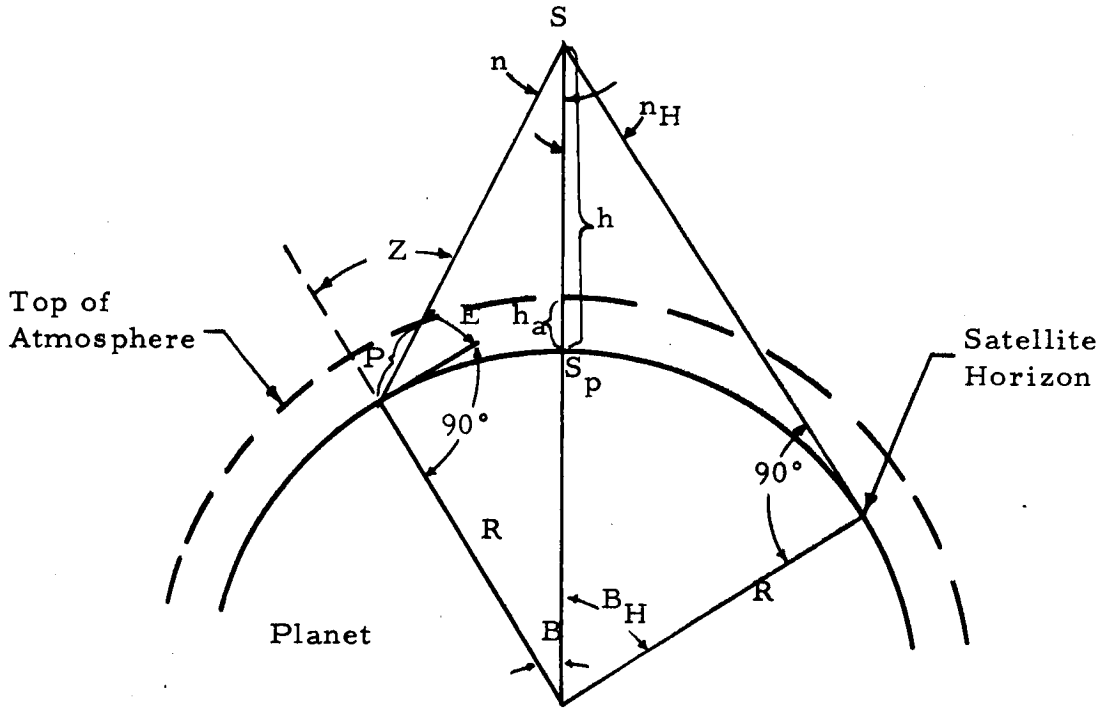

SATELLITE VIEWING GEOMETRY

Figure B-1

The coverage of the planet surface for various nadir and elevation angles is illustrated for circular orbits in Figure B-2, which presents the ratio of viewing area per orbit to total surface area versus the ratio of the altitude of the orbit to the planet radius.

The resolution of a satellite sensor is often expressed in terms of its resolving capability along the ground, at zero nadir angle, for a given satellite altitude. As derived in Ref. B-1, let Δn be the angular resolution; ΔB_o is given by (see Figure B-3):

$$\Delta B_o = 2\left\{\text{arc sin}\left[\left(\frac{R+h}{R}\right) \sin\frac{\Delta n}{2}\right] - \frac{\Delta n}{2}\right\}, \text{ or}$$

$$\Delta B_o = \frac{h}{R}\,\Delta n, \text{ if } \Delta B_o \text{ and } \Delta n \text{ are small.}$$

The ground resolution, ΔB_n, at any other nadir angle, n, is then given by:

$$\Delta B_n = \left(\frac{dB}{dn}\right)_n \Delta n, \text{ or}$$

$$\Delta B_n = \left[\frac{\cos n}{\sqrt{\frac{R^2}{R+h} - \sin^2 n}} - 1\right] \Delta n$$

as long as Δn is not too large. It is obvious that resolution degrades with increasing nadir angle.

The angle between the sensor line of sight and the sun line is an important consideration in selecting periods of data acquisition. The various angles employed in photosystem analyses are illustrated in Figure B-4 and are defined as follows:

i = the angle of incidence between the source (sun) and the local vertical

e = the angle of emittance between the sensor and the local vertical

g = the phase angle between the direction of incident and sensed energy. This could be the same as the angle of incidence (i), if sensor is normal to the surface

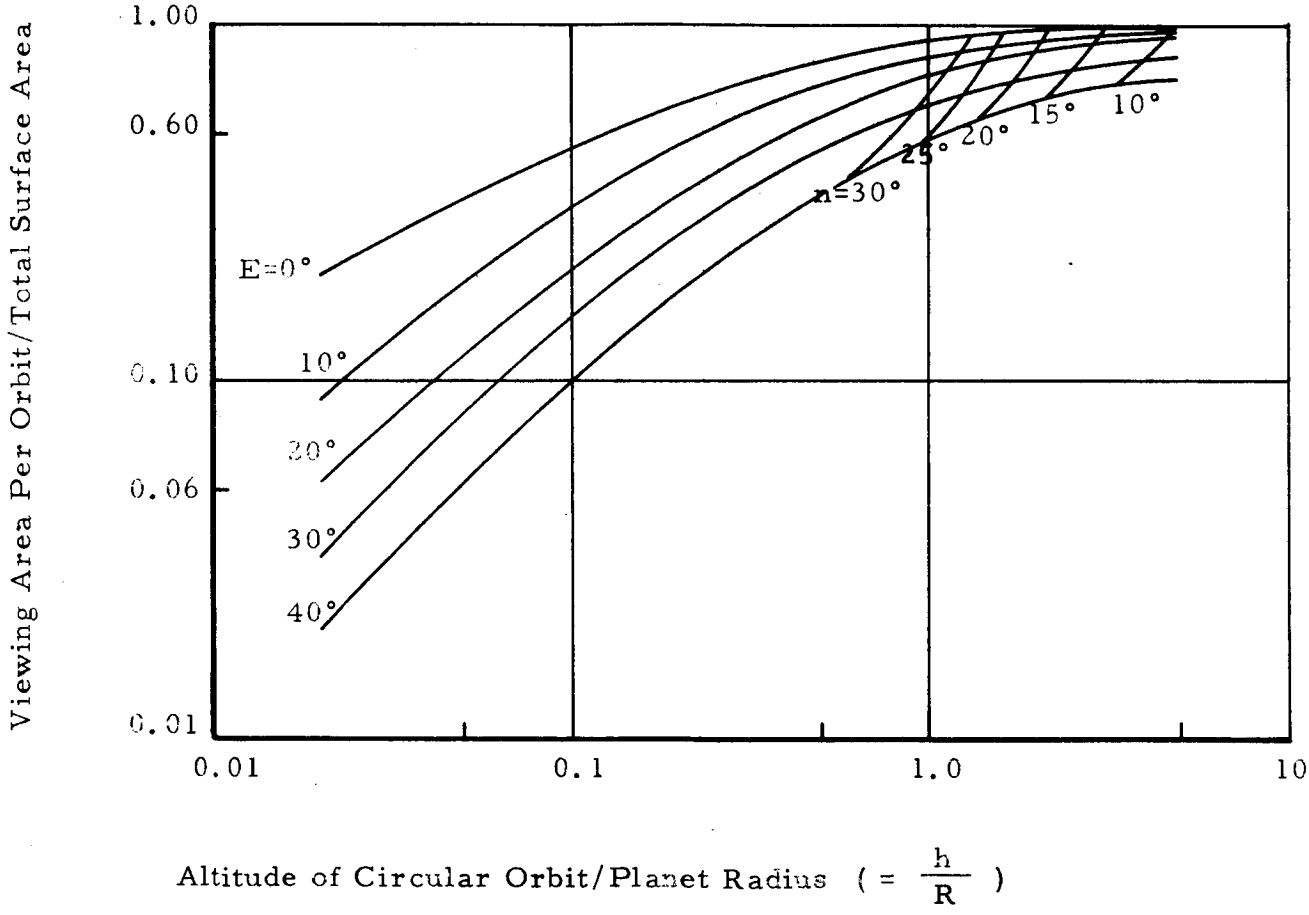

SURFACE AREA COVERED VS. ORBIT ALTITUDE
AS FUNCTION OF VIEWING ANGLES

Figure B-2

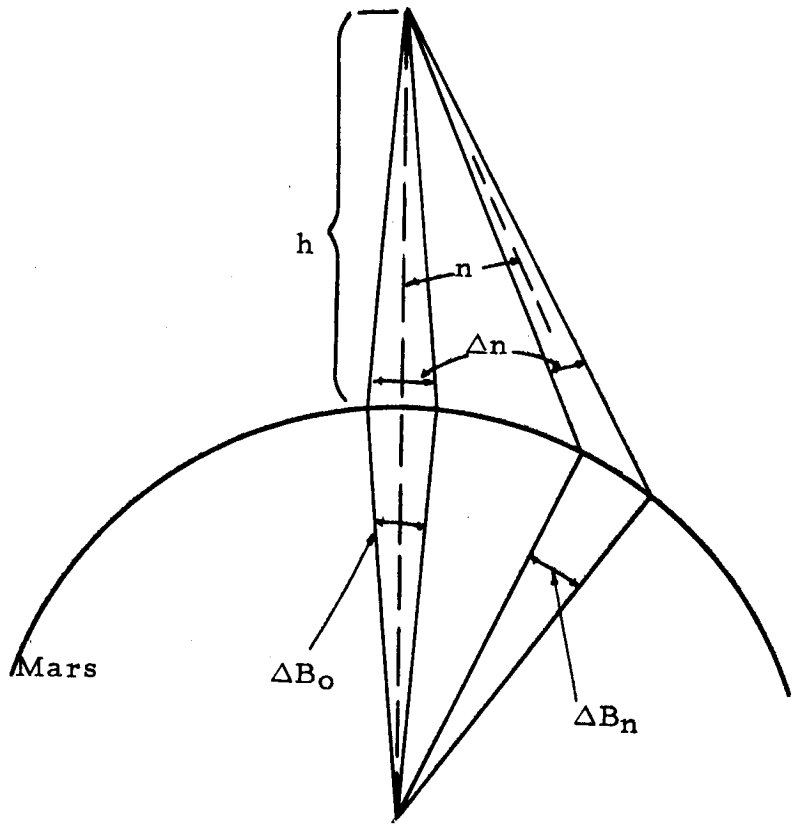

VARIATION OF RESOLUTION WITH NADIR ANGLE

Figure B-3

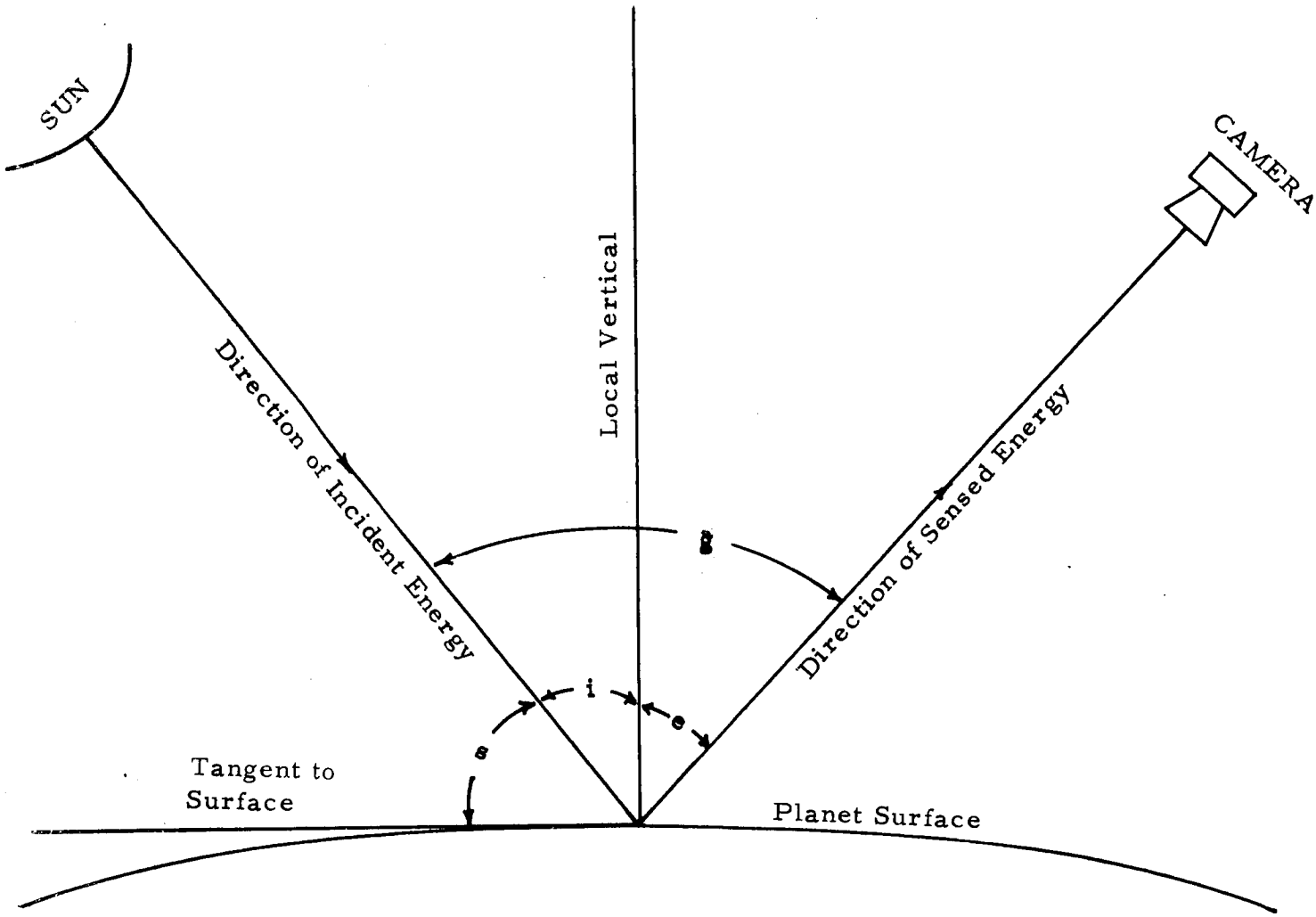

DEFINITION OF DIRECTION OF ILLUMINATION SOURCE AND SENSOR ANGLES

FIGURE B-4

s = the Sun angle between the source (Sun) and the tangent to the surface

Figure B-5 gives angle s as a function of location on planet's surface measured from Sun line and the plane of the ecliptic.

B.2 ERRORS IN GEOGRAPHICAL LOCATIONS OF DATA

Errors in the location of satellite data arise from a number of sources, including errors in (1) subpoint, (2) satellite altitude, and (3) satellite or sensor orientation.

Errors in subpoint position will be directly reflected in data locations. Errors in the subpoints of operationally available ephemerides are estimated to be about five miles for Earth satellites (Ref. B-1).

The effects of altitude errors can be examined by:

$$\frac{dB}{dh} = \frac{\sin n}{R\sqrt{1 - \left(\frac{R+h}{R}\right)^2 \sin^2 n}} = \frac{\sin n}{\sqrt{R^2 - (R+h)^2 \sin^2 n}}$$

The error is zero for n = 0, and increases with increasing n. It is to be noted that there are limits to the practically attainable accuracy due to the variations and uncertainties as to cloud top heights and the height of terrain, and to the variations of the planet's radius with latitude. Fujita (Ref. B-2) cites errors of a few tenths of a degree of great circle arc for Earth satellite height errors of about 10 km.

Errors of satellite or sensor orientation are usually defined in terms of roll, pitch, and yaw. Pitch is a tilting forward or backward (from the vertical) of the spacecraft (the pitch axis is perpendicular to the orbit plane). The roll axis is parallel to the velocity vector. Yaw is a rotation about the vertical axis.

Errors due to pitch or roll can be shown to be,

$$\Delta B_n = \left[\frac{\cos n}{\sqrt{\left(\frac{R}{R+h}\right)^2 - \sin^2 n}} - 1\right] \Delta n$$

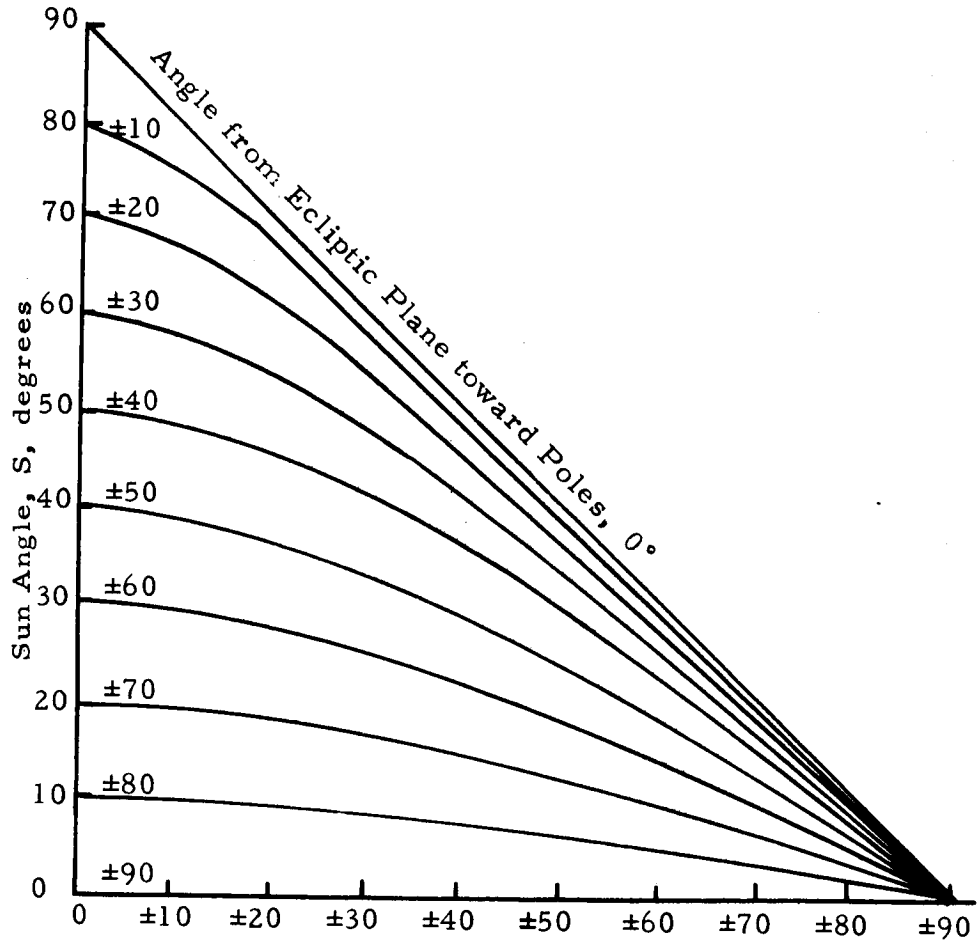

SUN ANGLE VARIATION OVER PLANET SURFACE

FIGURE B-5

where now,

Δn = error in satellite or sensor nadir angle

ΔB_n = error, measured radially from subpoint, in degrees of great circle arc

The linear error of position, Δx, due to yaw error, is

$\Delta x = R \sin B \sin \Delta y$, or

$\Delta x = R(\sin B)\Delta y$, if Δy is small

where Δy is the angular error in yaw, and the error, Δx, is in a direction perpendicular to the line from the point in question to the subpoint. In many cases, a yaw error can be adequately compensated for merely by a relative rotation, around the subpoint, of either the data, or a geographical grid or map.

When errors in pitch, roll, and yaw are small, the neceessary corrections can be considered as mutually independent for many purposes. As they become larger, the errors interact and the correction procedures become complex.

The Voyager spacecraft is expected to employ a "bang-bang" type control system having a limit cycle of 1 degree excursion; a 0.1 degree pointing accuracy is expected (Ref. B-3).

In most present satellites, the direct determination of pitch, roll, and yaw is not as accurate as would be desired. Accordingly, maximum accuracy in the location of the data usually results from the identification and matching of landmarks, or from the use of horizons if they are present and can be identified in the data. In the absence of landmarks, azimuth may be expecially difficult to determine or confirm, and there is often little alternative to the assumption that the satellite or sensor is properly oriented relative to the heading line. If horizons are present, and identifiable in the data, they often provide a good basis for determining errors in pitch and/or roll.

B.3 REFERENCES

B-1 WIDGER, W.K., Jr., "Orbits, Altitudes, Viewing Geometry, Coverage and Resolution Pertinent to Satellite Observations of the Earth and Its Atmosphere", Proceedings of the 4th Symposium on Remote Sensing of the Environment, 1966

B-2 FUJITA, T., "Evaluation of Errors in Graphical Rectification of Satellite Photographs", Journal of Geophysical Research, 1965

B-3 CAMPEN C., Personal Communications, Voyager Interim Project Office, 22 August 1967

APPENDIX C

OTHER ORBITAL CONSIDERATIONS

This appendix presents data which are useful in overall Mars reconnaissance system design considerations, such as: Earth-Mars transfer time, spacecraft hyperbolic excess velocity at Mars encounter, Mars orbit insertion ΔV requirements, relative position of Earth-Mars-Sun, communication distances, maximum possible spacecraft occultation times, Earth-cone angles, etc.

C.1 APPROACH VELOCITY AT MARS

The approach velocity at the planet (hyperbolic excess velocity) determines the velocity increment required to inject the vehicle into the desired satellite orbit. The approach velocity in each opportunity is constrained so that the "tightest" orbit considered can be achieved within the available ΔV for orbit insertion. For the TypeI trajectories, this approach velocity constraint usually determines the earliest arrival date which can be flown, whereas, for the Type II trajectories, it usually determines the latest arrival date which can be flown. Hyperbolic approach velocity is presented for both minimum energy and minimum total hyperbolic velocity in Figure C-1 for 1973 and 1975 Mars missions, respectively (Ref. C-1). The hyperbolic excess velocity at arrival for the Earth-to-Mars 1973 mission is given in Figure C-2 as a function of launch and arrival dates (Ref. C-2).

C.2 TRIP TIME

Trip time is plotted in Figure C-3 as a function of launch date for the 1973 and 1975 Mars opportunities (Ref. C-1). Again Type I and Type II trajectories are shown, and the solid curves represent minimum injection energy transfers, while the dashed curves are for minimum total hyperbolic velocity transfers.

C.3 ORBIT INSERTION ΔV REQUIREMENTS

Figure C-4 shows orbit insertion ΔV's for a hyperbolic excess velocity of 3.26 km/sec (Ref. C-2) which is considered the maximum baseline value for the 1973 Mars mission. The ΔV's shown are the minimum requirements for the orbits, being based on impulsive thrust and coplanar

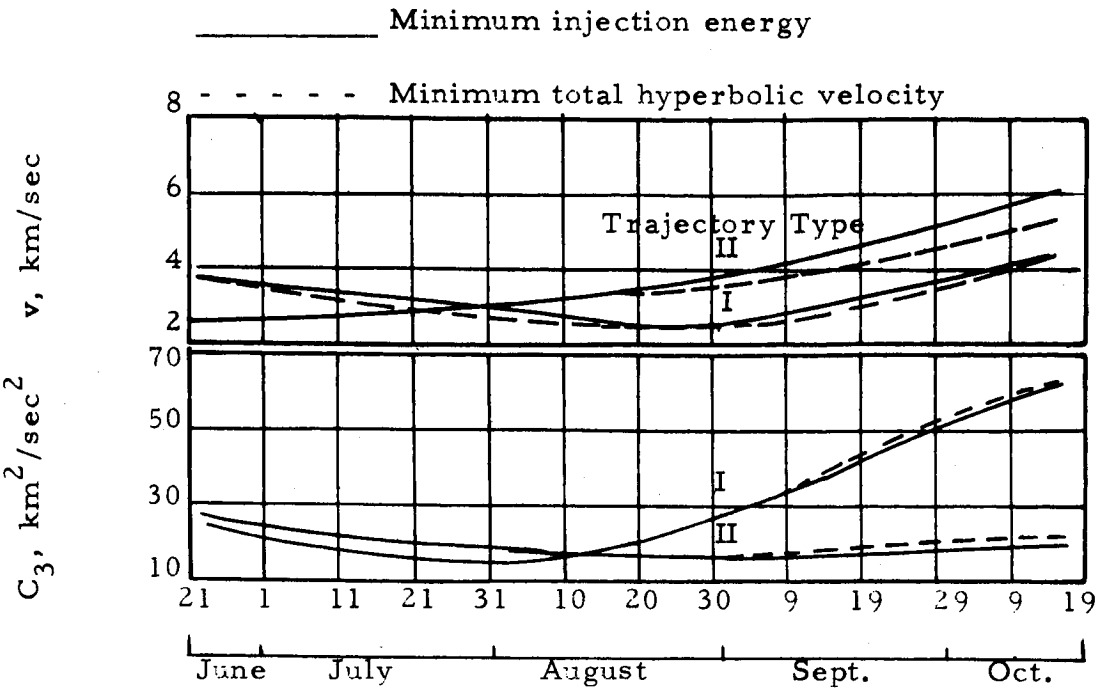

Launch Date, 1973 Opportunity

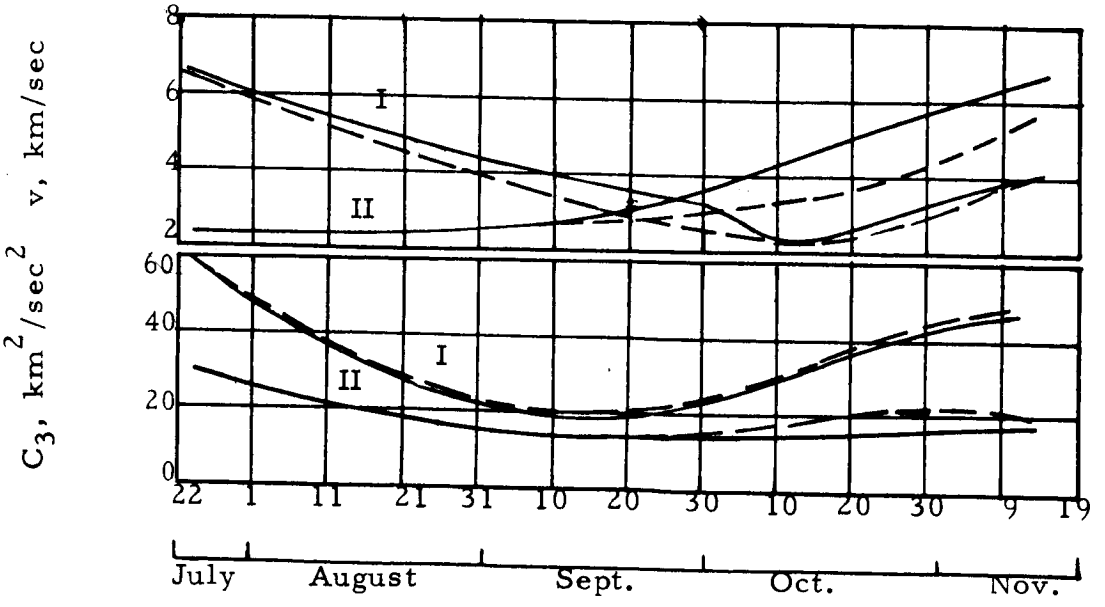

Launch Date, 1975 Opportunity

INJECTION ENERGY (C_3) REQUIREMENTS AND HYPERBOLIC APPROACH VELOCITY (v) FOR MARS MISSIONS

Figure C-1

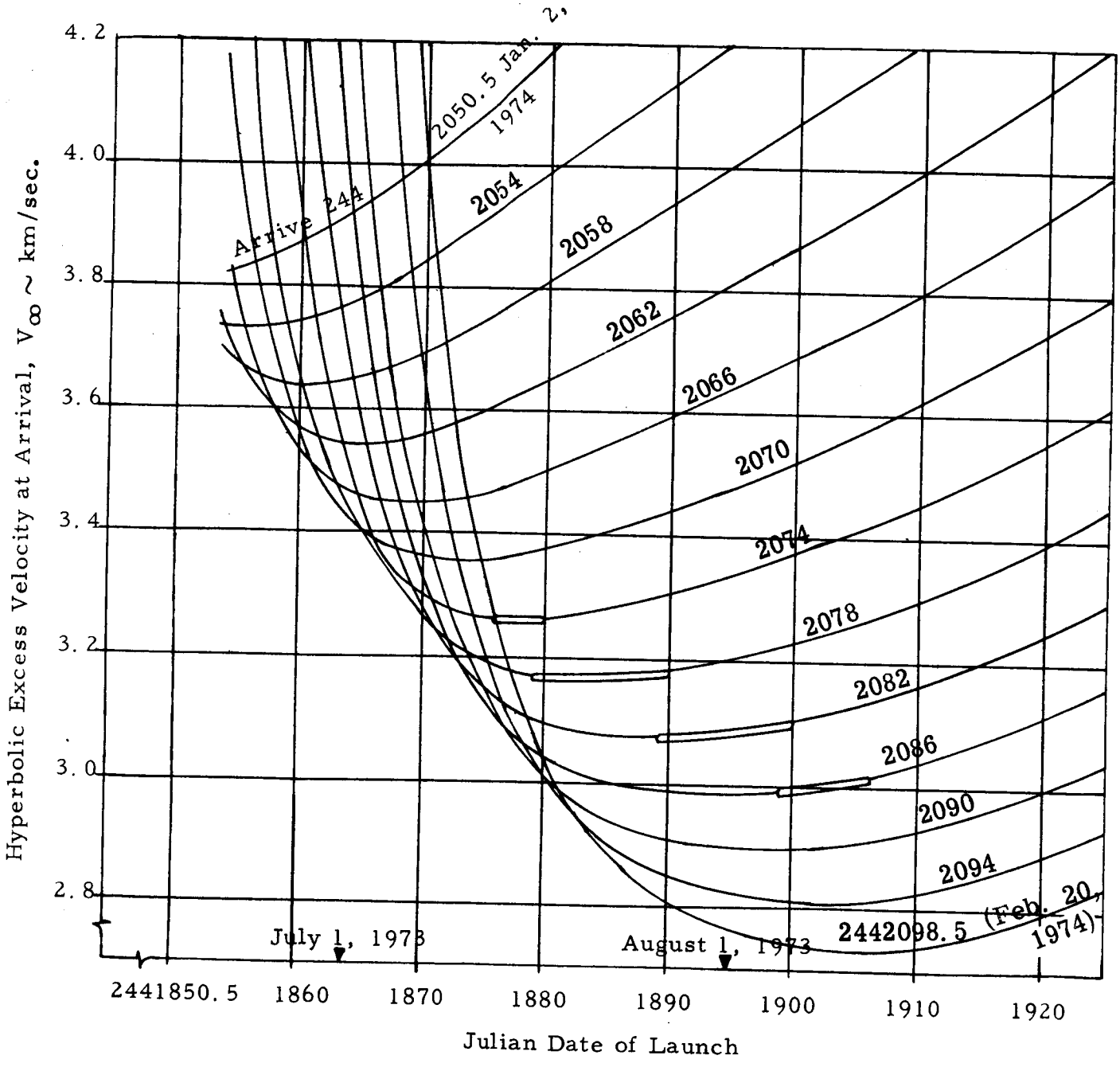

HYPERBOLIC EXCESS VELOCITY AT ARRIVAL; EARTH TO MARS 1973

FIGURE C-2

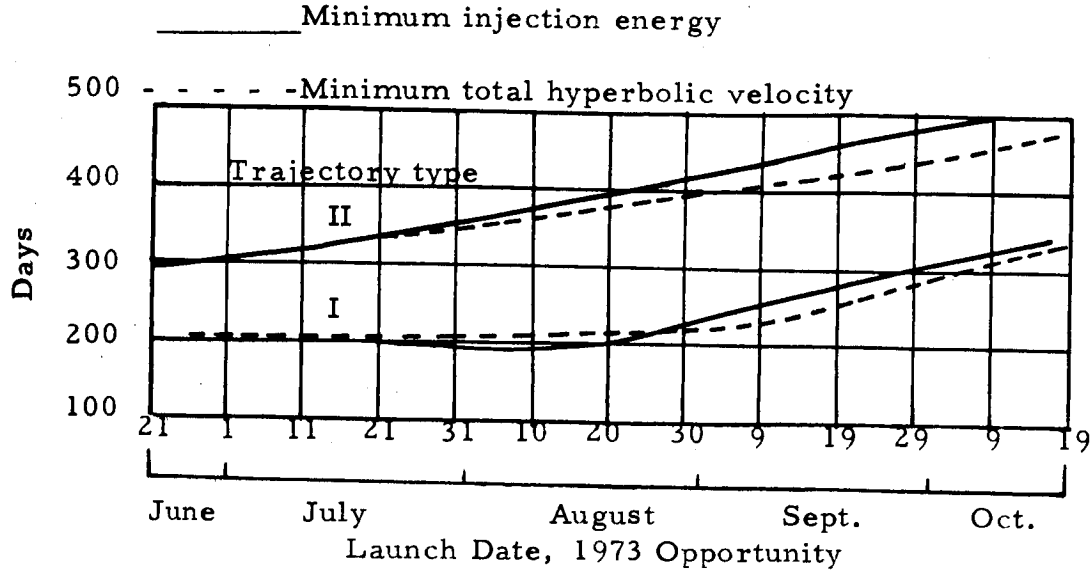

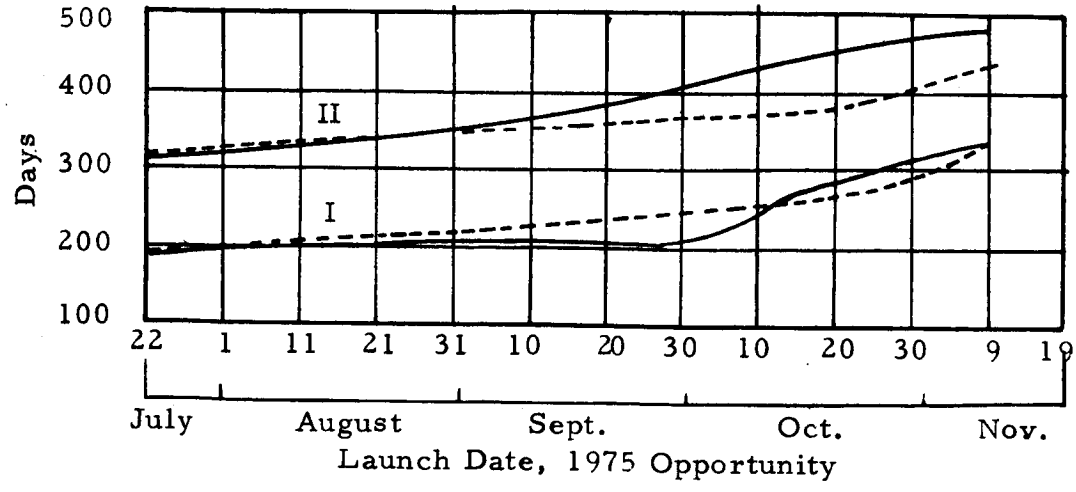

TRIP TIME AS A FUNCTION OF LAUNCH DATE FOR MARS MISSIONS

Figure C-3

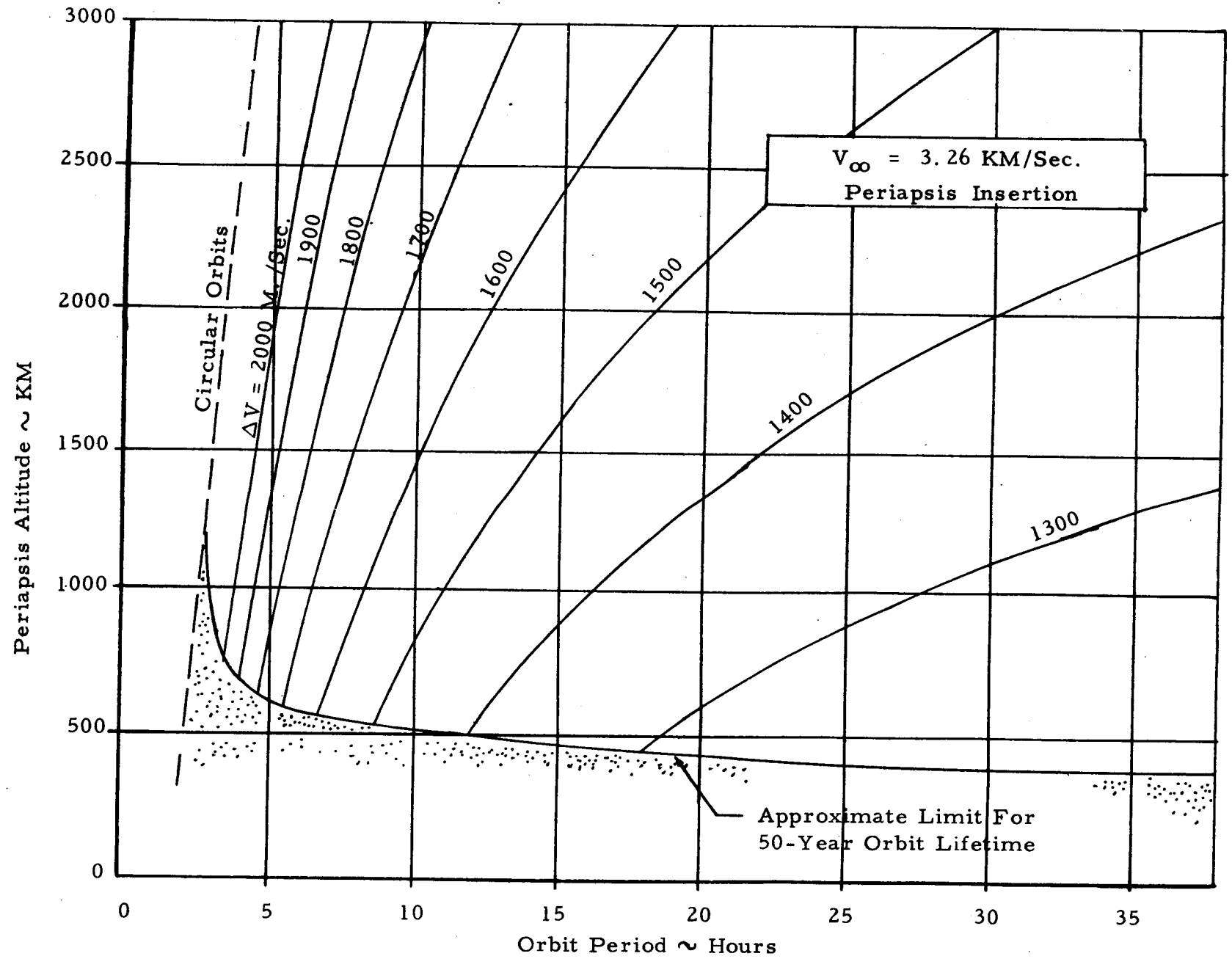

ORBIT INSERTION ΔV'S ~ MARS 1973
FIGURE C-4

periapsis-to-periapsis insertion. Use of finite thrust will increase the requirements somewhat, with the amount of increase being dependent upon periapsis altitude and burn time. An example of finite thrust loss is given in Figure C-5 for insertion into an orbit having a periapsis of 1,000 km.

The propellant mass required to achieve circular capture orbits about Mars for various excess hyperbolic approach velocities is given in Figure C-6 (Ref. C-3).

C.4 RELATIVE POSITIONS OF EARTH-MARS-SUN

Figure C-7 illustrates the relative positions of Earth and Mars for several example arrival dates for the 1973 mission. The illustration is only an approximation, since average orbital rates for Mars and Earth were used to determine their positions as a function of time.

When the spacecraft is in orbit, its distance from the planet is some three orders of magnitude less that its distance from Earth and the Sun. It is possible, therefore, to completely neglect the orbit in computing the apparent positions of Earth and the Sun. Figure C-8 (Ref. C-1) gives communication distance at planet arrival as a function of launch date for both the 1973 and 1975 Mars missions. Figure C-9 shows Earth-spacecraft distance as a function of time after arrival for the 1973 Voyager-Mars mission having an early July launch date. Figure C-10 shows the Earth cone angle for this particular case. The Sun-spacecraft distance is given in Figure C-11. Data shown in Figures C-9 through C-11 were obtained from Ref. C-2.

C.5 OCCULTATION BY MARS

The maximum occultation times for orbits about Mars is given in Figure C-12, and Figure C-13 shows the same times expressed as percentages of the orbit period. These occultation times apply to Sun, Earth, or Canopus occultation, as they are based on a cylindrical shadow zone with a radius of 3,400 km. The maximum possible occultation time occurs when the apoapsis of the orbit lies on the axis of the shadow cylinder. Actual occultation times encountered during a mission are dependent on the orbit orientation; they can vary between zero and the times shown here.

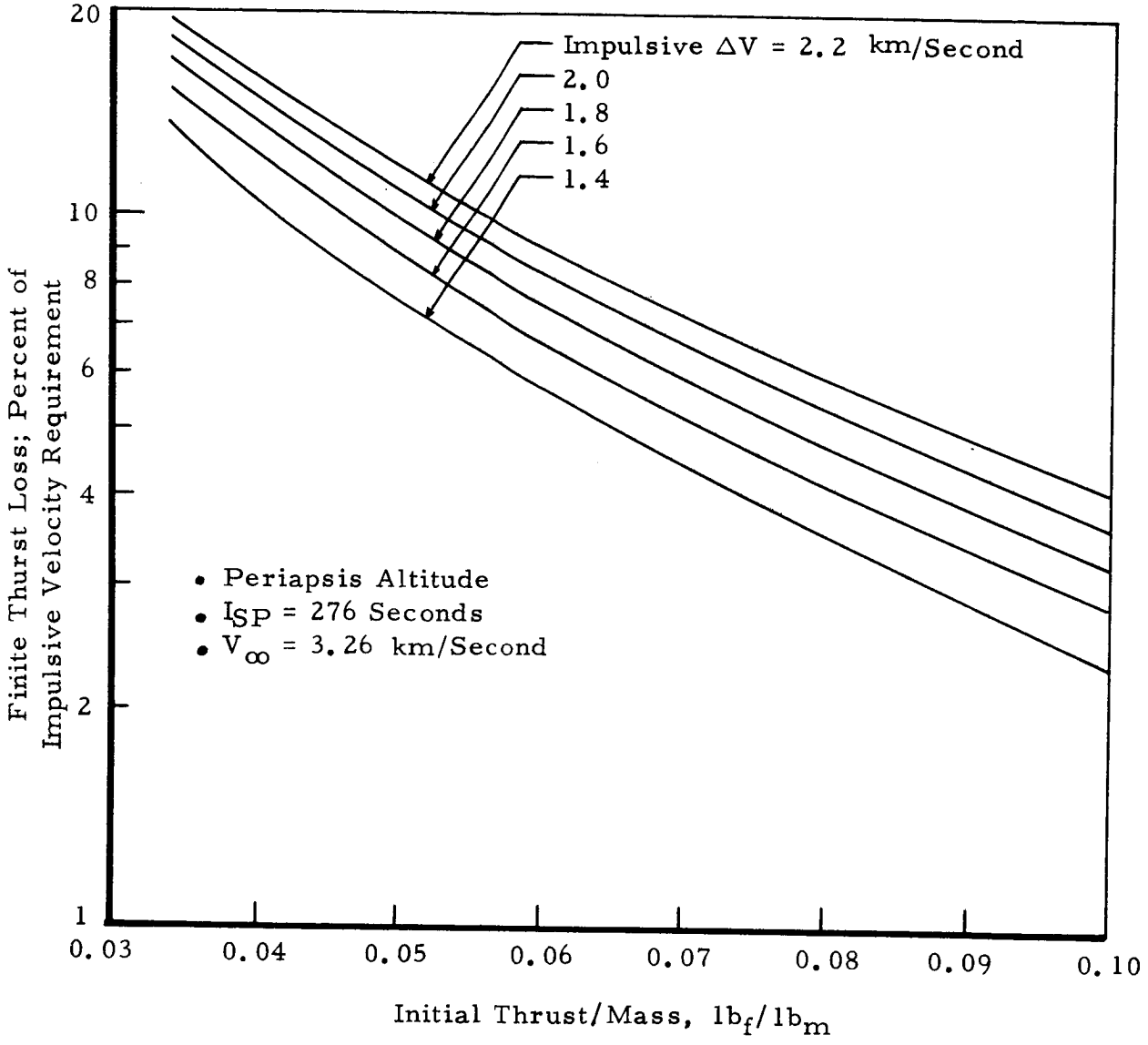

ORBIT INSERTION FINITE BURN EFFECTS~MARS 1973

FIGURE C-5

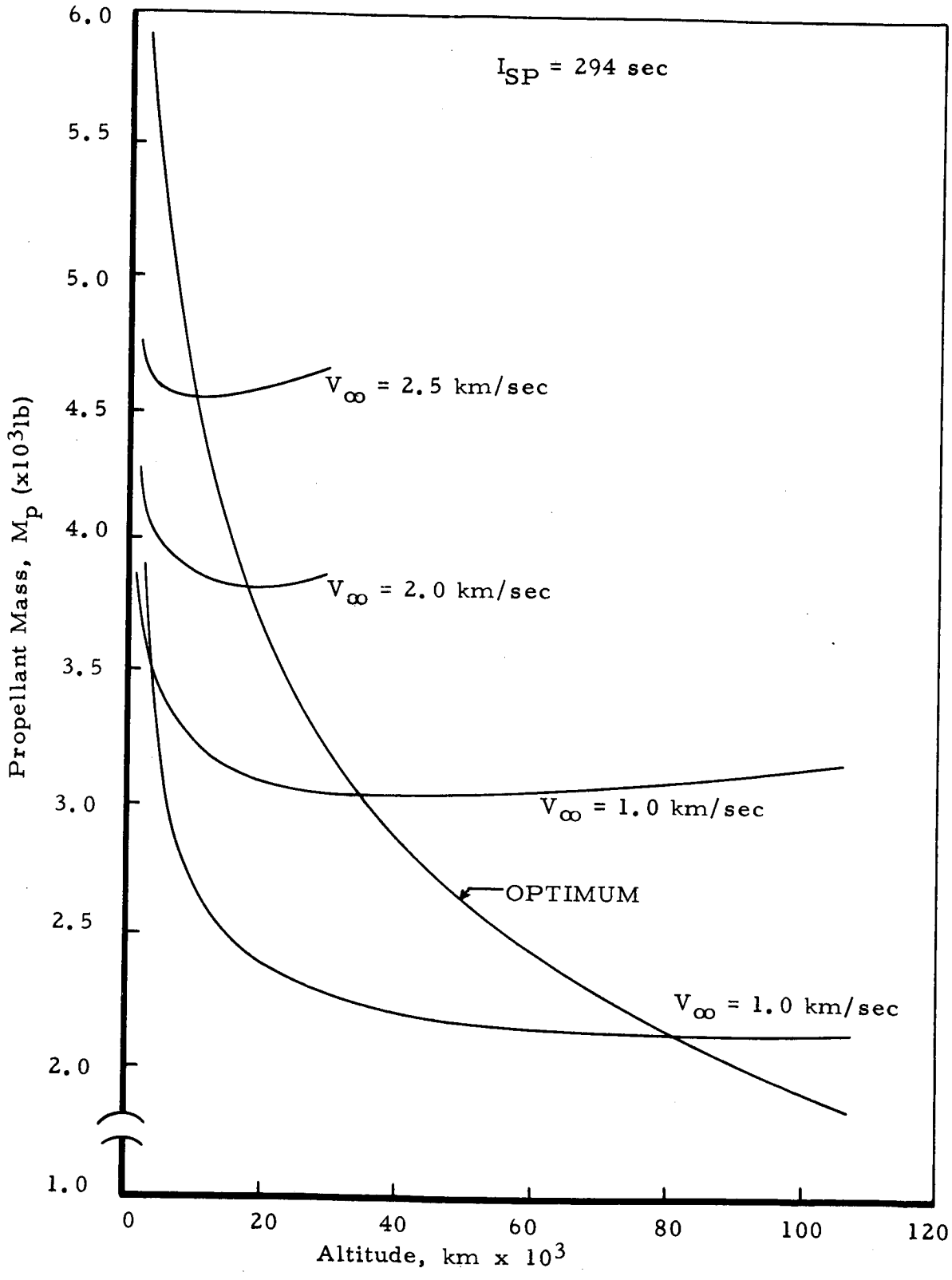

PROPELLANT MASS REQUIRED TO ACHIEVE CIRCULAR CAPTURE ORBITS FOR VARIOUS EXCESS HYPERBOLIC APPROACH VELOCITY

FIGURE C-6

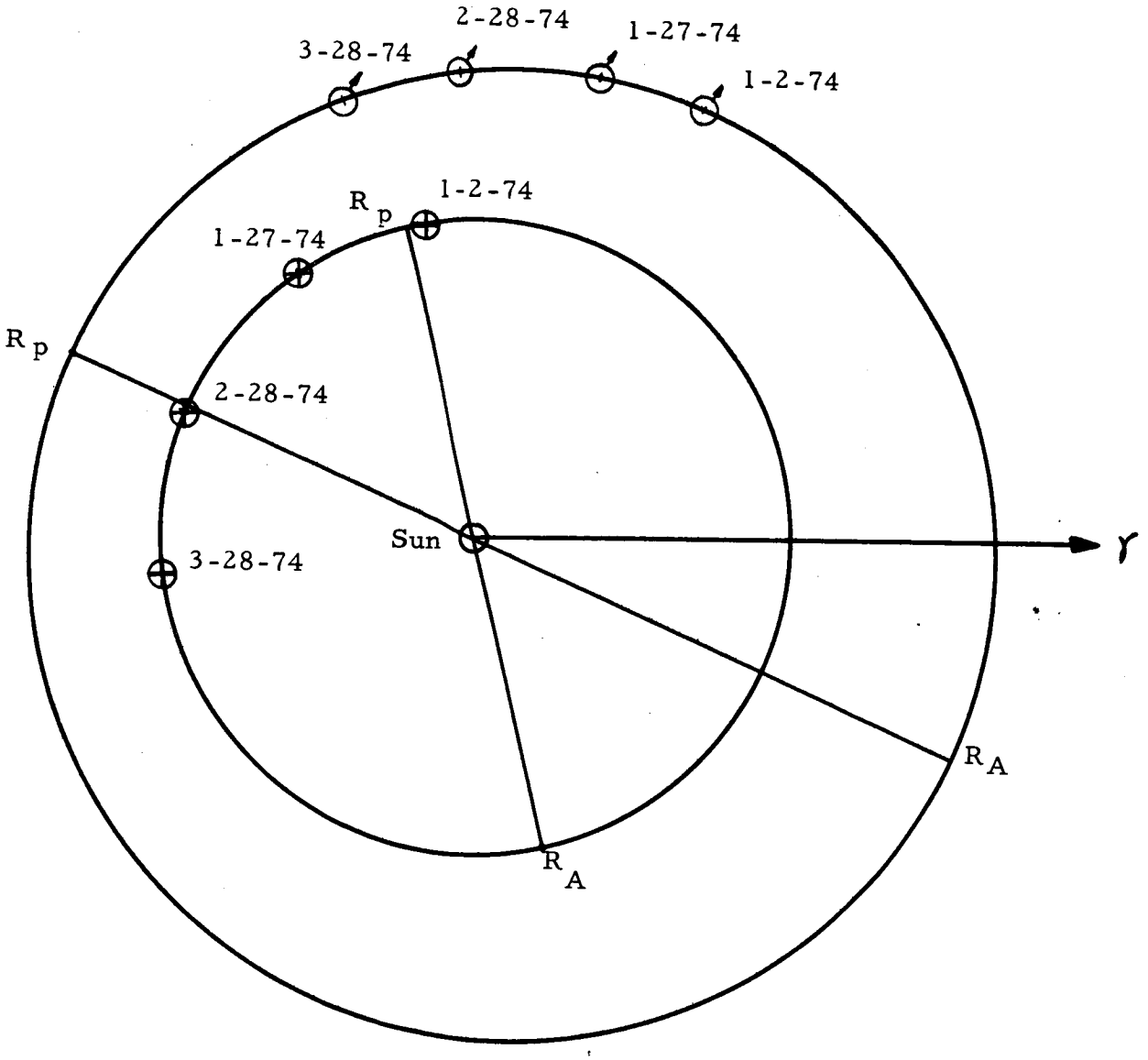

APPROXIMATE RELATIVE POSITIONS OF EARTH AND MARS FOR SEVERAL EXAMPLE MARS ARRIVAL DATES FOR THE 73 MISSION

Figure C-7

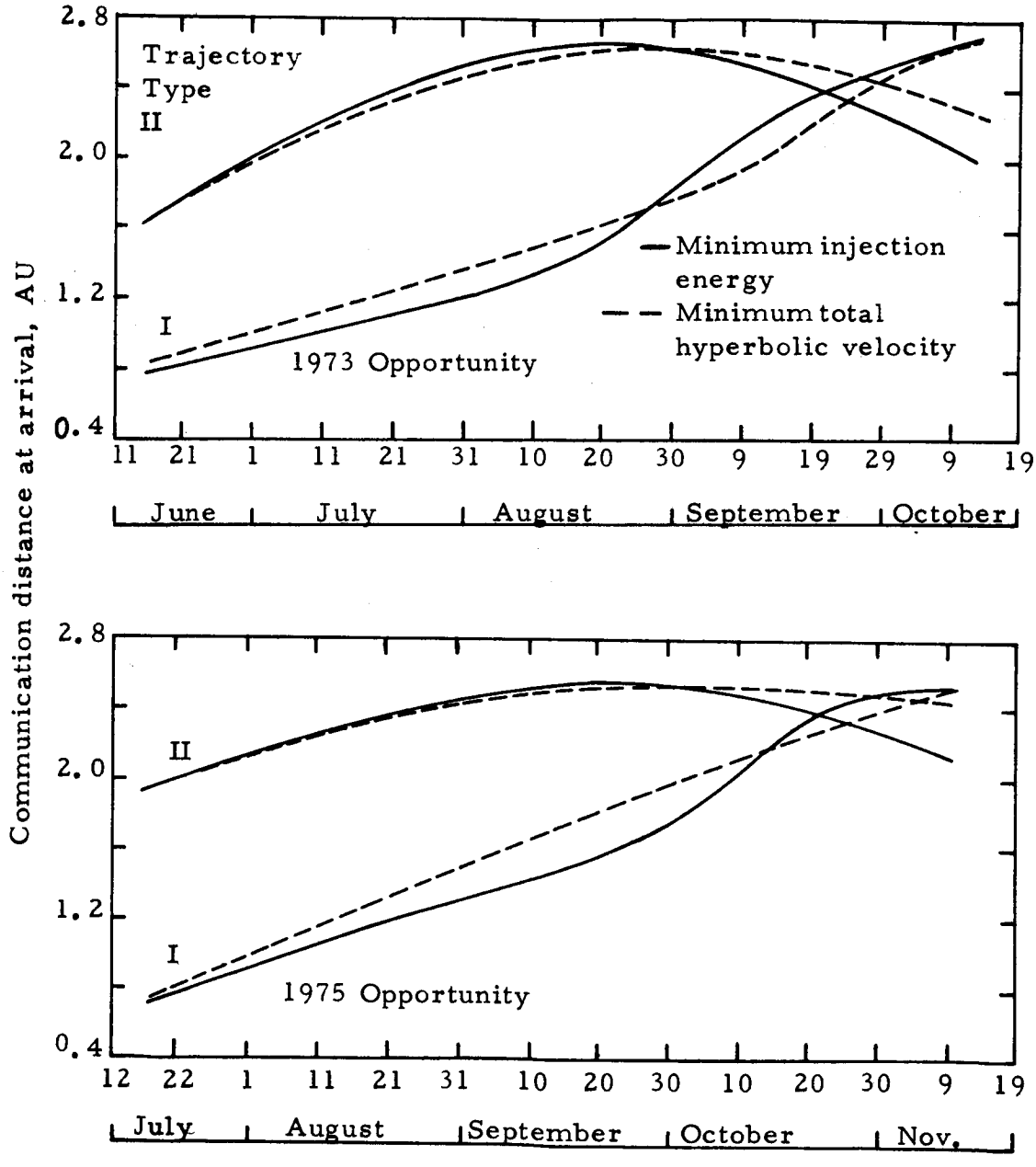

COMMUNICATION DISTANCE AT ARRIVAL AS A FUNCTION OF LAUNCH DATE FOR MARS MISSIONS

Figure C-8

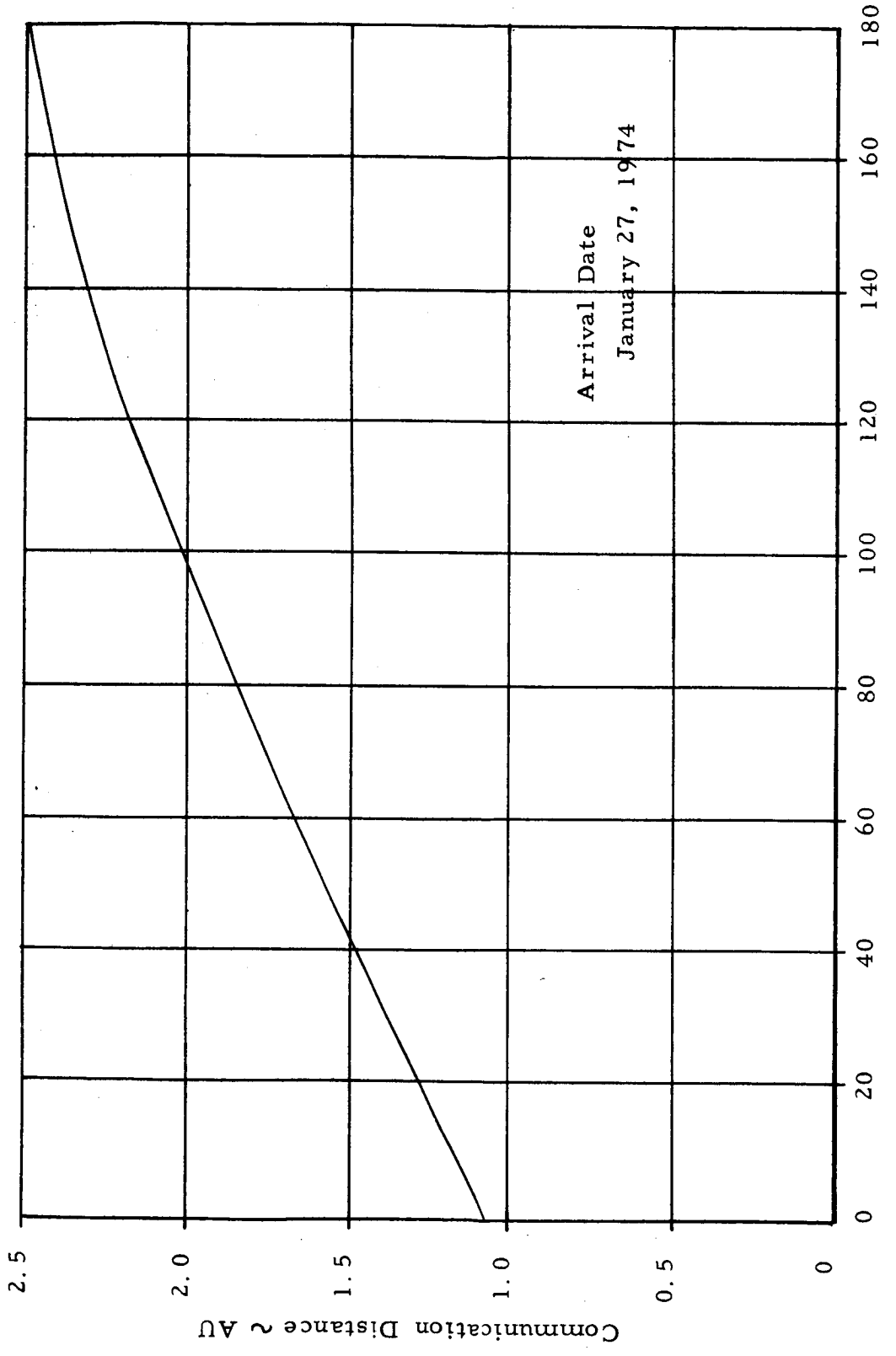

COMMUNICATION DISTANCE ~ MARS ORBITS

FIGURE C-9

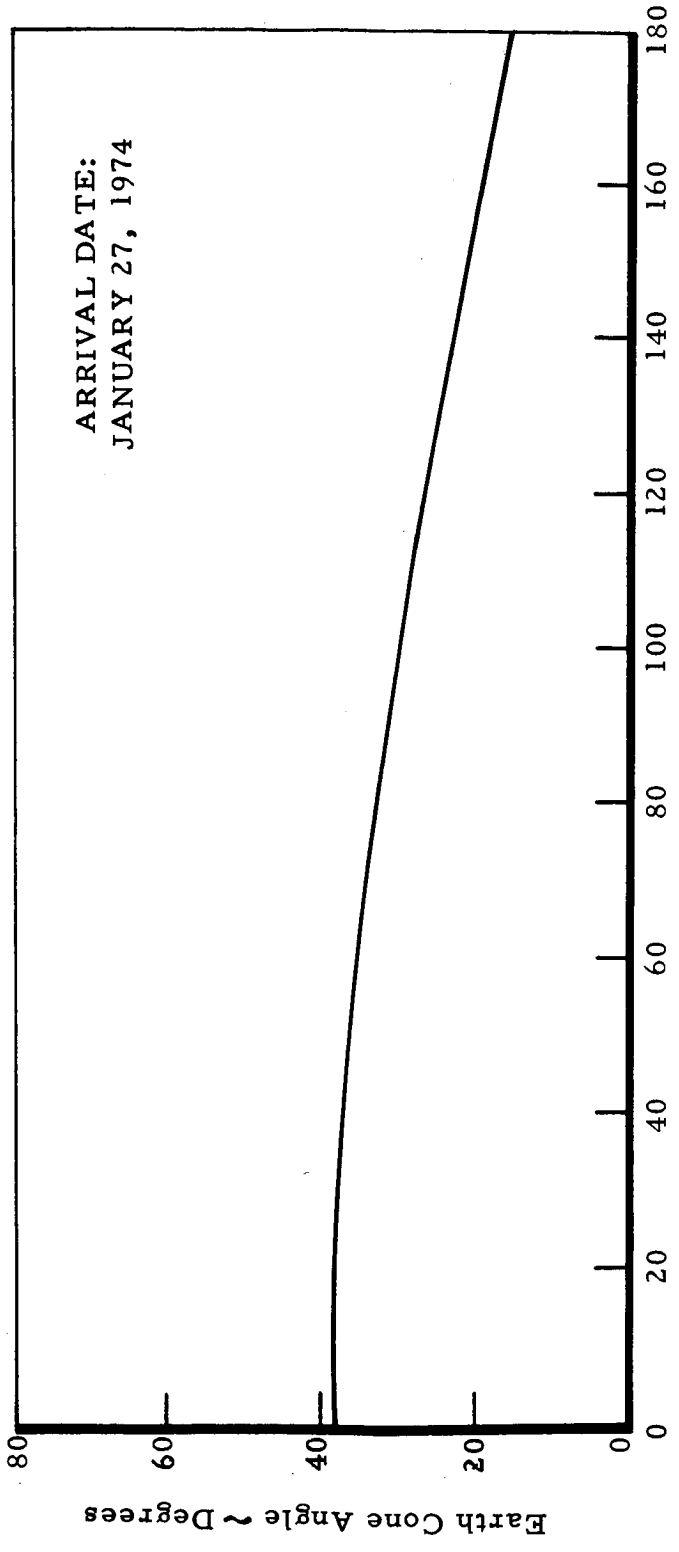

EARTH CONE ANGLE

FIGURE C-10

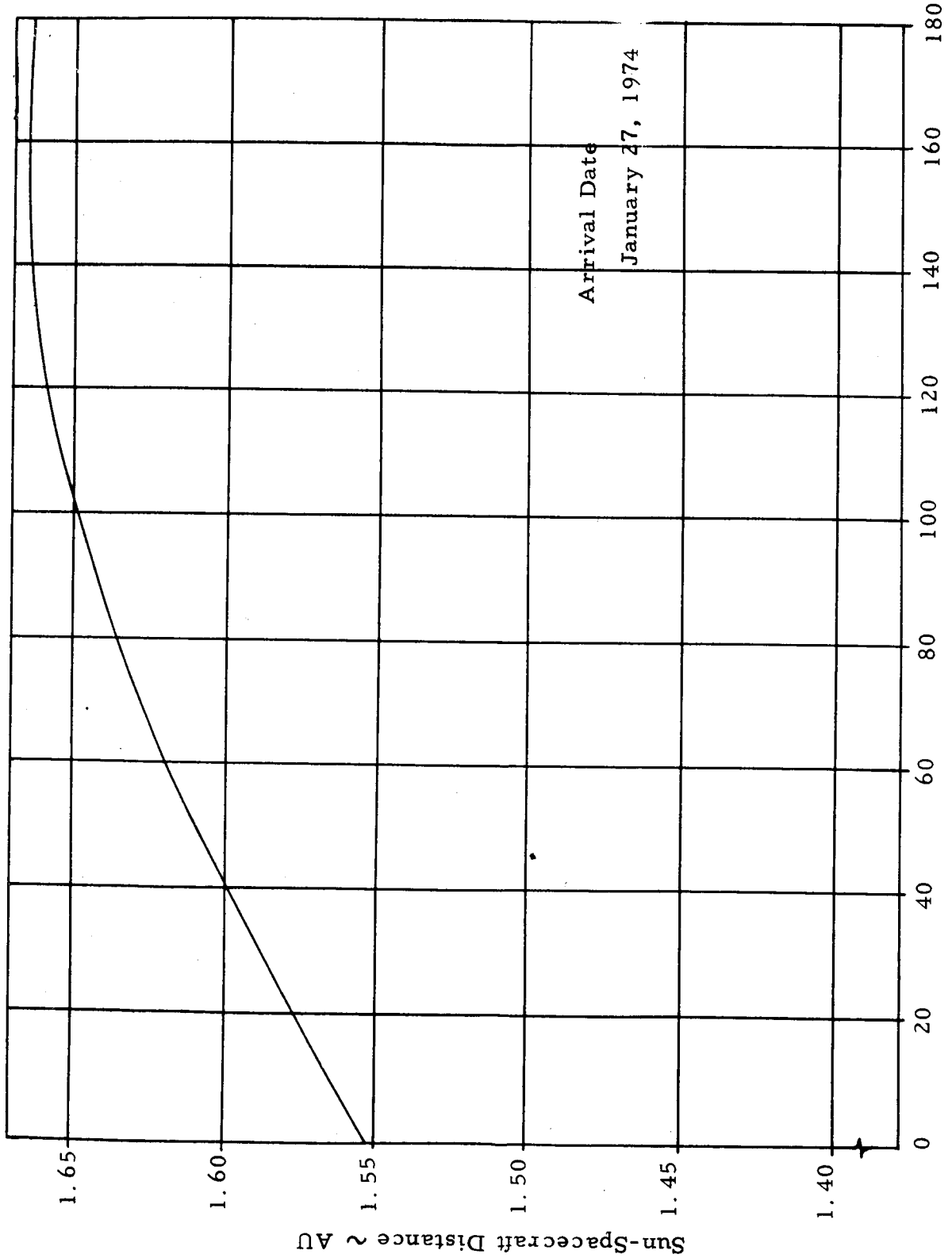

SUN-SPACECRAFT DISTANCE ~ MARS ORBITS

FIGURE C-11

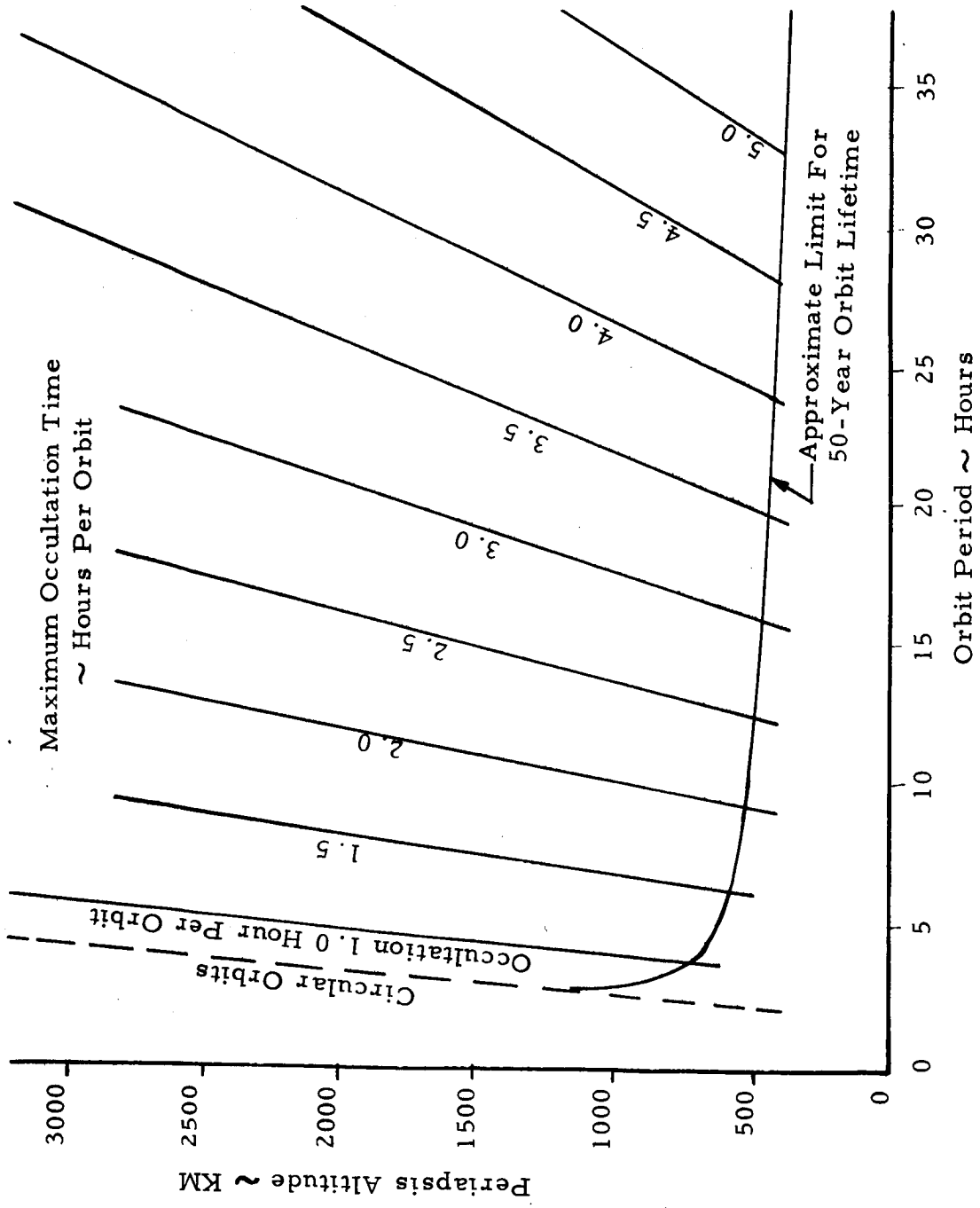

MAXIMUM POSSIBLE OCCULTATION TIMES FOR ORBITS ABOUT MARS

FIGURE C-12

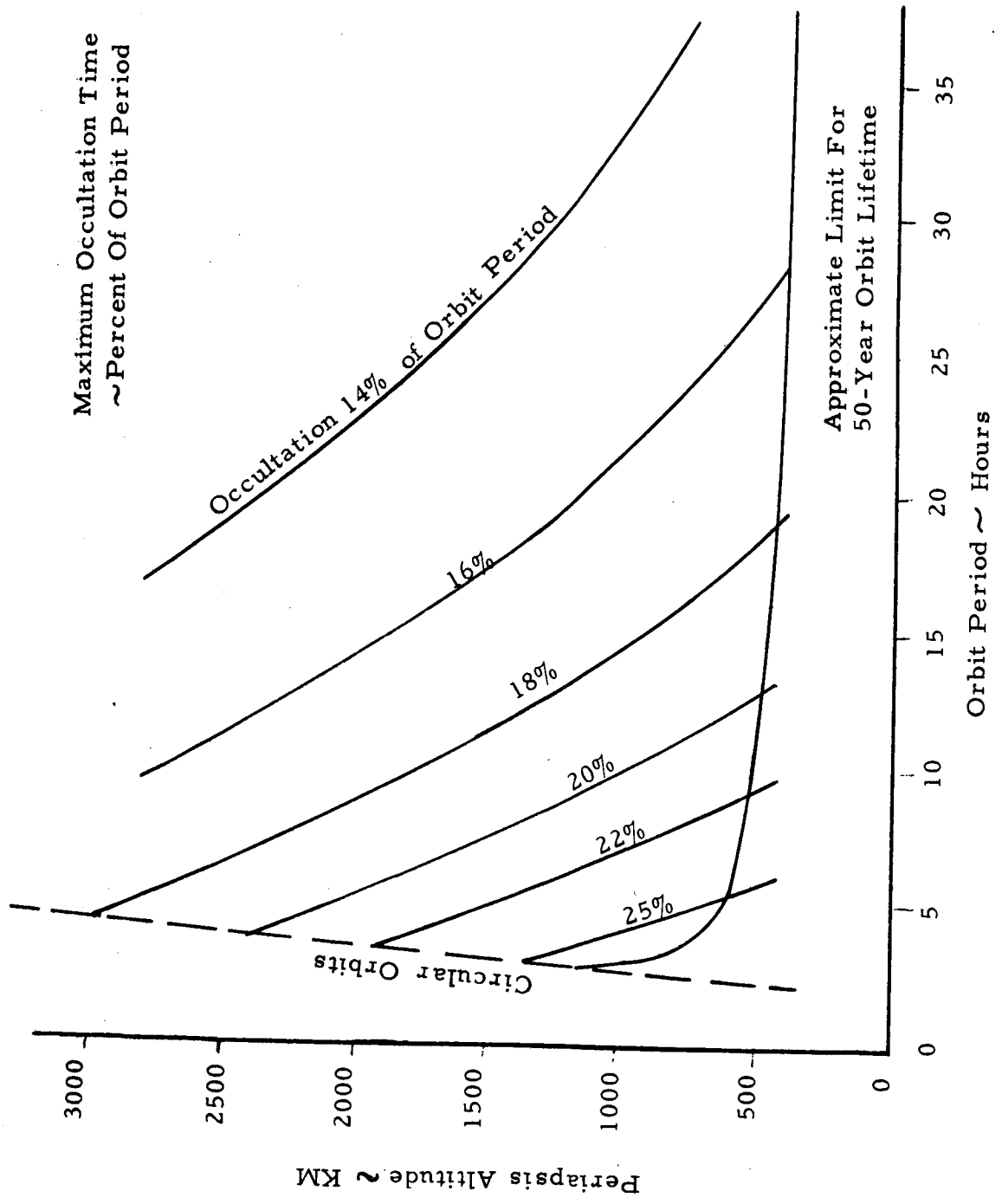

MAXIMUM POSSIBLE OCCULTATION TIMES FOR ORBITS ABOUT MARS

FIGURE C-13

The minimum line-of-sight time is illustrated in Figure C-14 and is defined as the difference between the orbit period and the maximum occultation time. Like occultation times discussed above, this time is applicable to either the Sun or the Earth. Actual times encountered during a mission are dependent on the orbit orientation; the time can vary between the minimum times shown here and the total orbit period. The minimum line-of-sight time is of interest primarily in guidance and communication subsystem design considerations.

C.6 REFERENCES

C-1 SAGERMAN, G. and KREITER, T., "Payload Capabilities of Saturn 1B-Centaur for Launch Opportunities to Mars in 1971, 1973 and 1975 and to Venus in 1972 and 1973", Lewis Research Center, NASA TM X-1327

C-2 "Study of Applicability of Lunar Orbiter Sub-systems to Planetary Orbiters", The Boeing Company, Report No. D2-100710-2, March 1967

C-3 WOOD, L.H., et al, "Planetary Photographic Exploration with Solar-Electric Propulsion", presented at the AIAA Electric Propulsion and Plasmadynamics Specialists Conference, September 1967

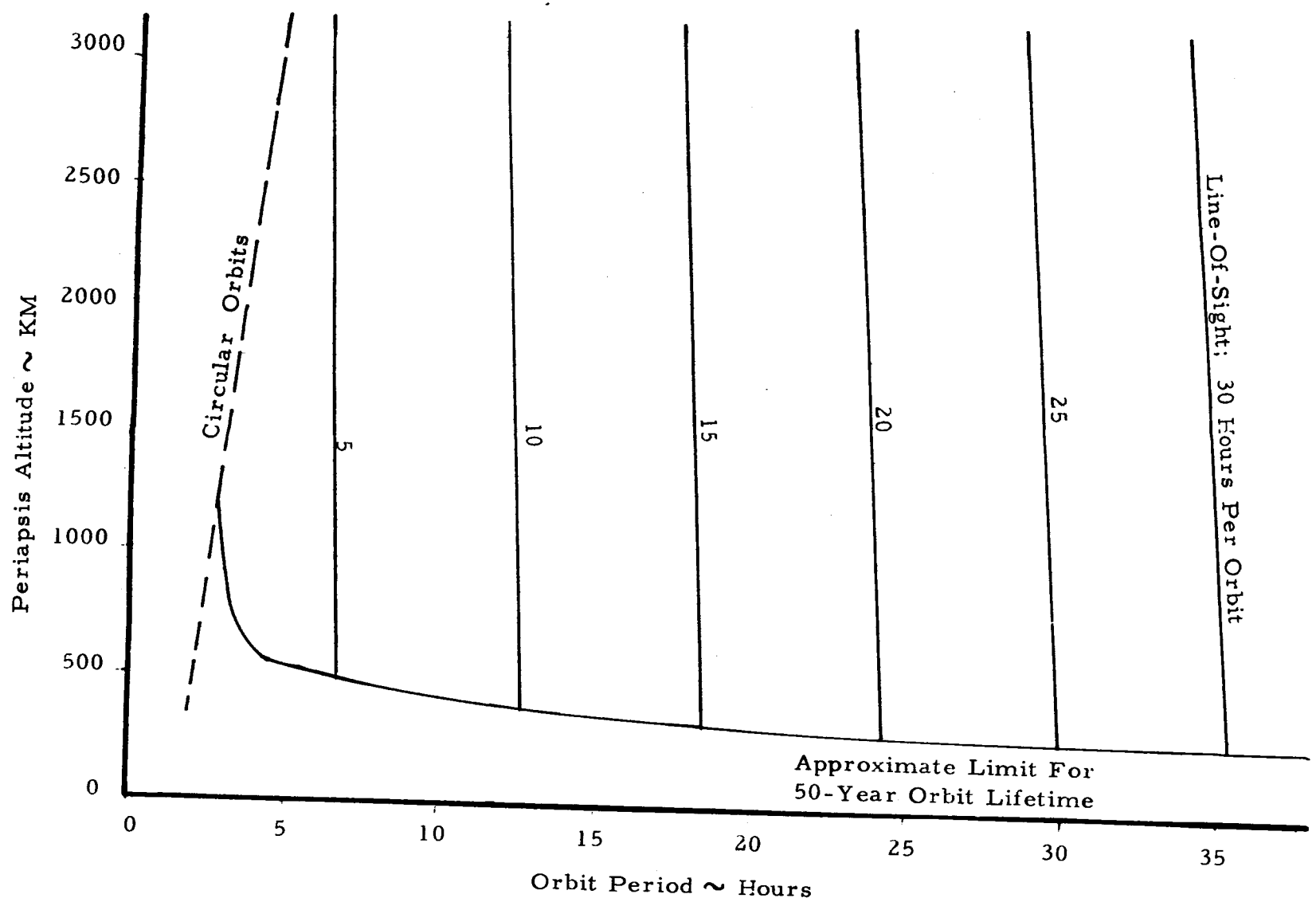

MINIMUM POSSIBLE LINE-OF-SIGHT TIMES FOR ORBITS ABOUT MARS

FIGURE C-14

APPENDIX D

NON-UNIFORM IMAGE MOTION ON PLATE OF CAMERA SYSTEM IN ELLIPTICAL ORBIT*

D.1 STATEMENT OF PROBLEM

To determine the instantaneous image motion at any point of a plane format for the case of an arbitrarily oriented camera system in an elliptical orbit about a rotating spherical planet, including the effect of arbitrary yaw, pitch and roll angular velocities.

D.2 DEFINITIONS

Referring to Figure D-1, in which the angles Θ and i are defined, we have the following additional quantities,

F = camera system focal length
R = radius of planet
ω = angular velocity of planetary rotation
H = instantaneous height above ground
$\dot{H}$ = change in height per unit time. $\dot{H}$ is positive if H is increasing. When $\dot{H} = 0$, the orbit is circular.
lat = instantaneous latitude of camera system
x_{3_p}, y_{3_p} = coordinates of a point on the plate in the x_3, y_3 system.
$\dot{\Theta} \equiv |\vec{\dot{\Theta}}|$
Θ, i, ω, $\dot{\Theta}$, F, R, H are all positive scalars.
α = yaw angle of camera system plate. Specifically, it is the angle between the "horizontal component" of the x_3 axis and the "horizontal component" of the instantaneous flight direction. By horizontal here is meant the instantaneous local horizontal, i.e., as determined by the part of the planet's surface directly below the camera at a given instant. The angle α is taken as positive if it describes a rotation of the $+y_3$ axis "toward" the $+x_3$ axis.

β = pitch angle of plate. β is measured with respect to the instantaneous local horizontal and is positive for rotations of the $+x_3$ axis "towards" the $+z_3$ axis.

* This appendix is a summary of an analysis performed by Paul Reichel, Principal Engineer, Fairchild Space and Defense Systems.

$\vec{\dot{\theta}}$, instantaneous orbital angular velocity, measured with respect to inertial space (rather than with respect to the rotating surface of the planet). For the special case of a circular orbit, $\vec{\dot{\theta}}$ would become constant.

Camera orbit; it is shown as circular for clarity, but the equations given apply to the general elliptical (or hyperbolic fly-by) case.

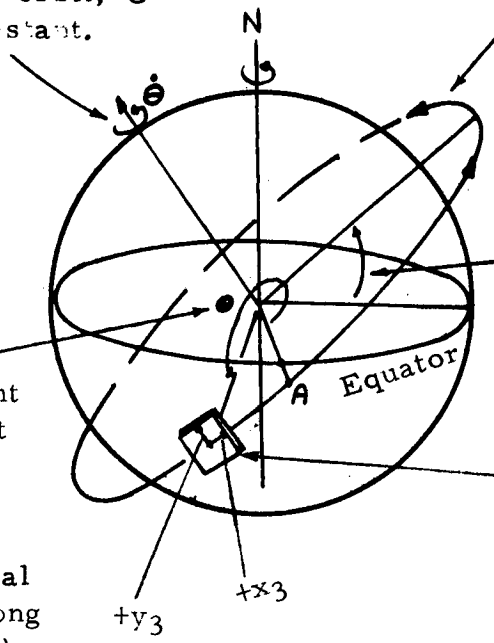

θ, angle of great circle are between passing over equator (point A) and the present sensor position. (For elliptical orbits, θ is not simply proportional to the distance along the elliptical arc.)

i, inclination angle of orbit. It may have any value between 0° and 180°.

Camera system plate (shown for the special case where yaw, elevation and roll angles are zero, i.e., where plate is parallel to local ground.)

Camera system plate coordinates. (Etched into the plate, rather than merely describing the plane of the plate). A third coordinate, z_3, not shown, is normal to the plate and pointed away from the planet.

For the special case of zero yaw, elevation and roll of the plate, the $+x_3$ axis points in the direction of the horizontal component of instantaneous (linear) orbiting velocity. The $+y_3$ axis is, for this special case, parallel to the orbital angular velocity vector .

FIGURE D-1

γ = roll angle of plate. It is measured with respect to the instantaneous local horizontal, being zero is the y_3 axis is locally horizontal. γ is positive for rotations of the $+z_3$ axis "towards" the $+y_3$ axis.

$\dot{\alpha}$, $\dot{\beta}$, $\dot{\gamma}$; Since α, β, γ are defined in terms of the instantaneous local horizontal, it follows that the angular velocities $\dot{\alpha}$, $\dot{\beta}$, $\dot{\gamma}$ are measured with respect to it also. Thus $\dot{\alpha}$, $\dot{\beta}$, $\dot{\gamma}$ are not angular velocities with respect to inertial space. For example, as the camera pursues its elliptical orbit, the x_3 and y_3 axes tumble in inertial space so as to remain locally horizontal throughout and so that the y_3 axis never leaves the orbital plane, then $\dot{\alpha}$, $\dot{\beta}$, $\dot{\gamma} = 0$. (More generally, if x_3, y_3, z_3 maintain the same orientation with respect to $\vec{\Theta}$ and the local horizontal, then $\dot{\alpha}$, $\dot{\beta}$, $\dot{\gamma} = 0$.)

Given the above defined quantities (corresponding to an instantaneous location of the camera system), then for any specified point on the format x_{3p}, y_{3p}, the image velocity components x_{3_p} Total, y_{3_p} Total (or average velocity) of a point on the planet's surface can be computed.

D.3 SOLUTION OF PROBLEM

Given: $i, \Theta, \dot{\Theta}, R, H, \dot{H}, \omega, F, \alpha, \beta, \gamma, \dot{\alpha}, \dot{\beta}, \dot{\gamma}, x_{3_p}, y_{3_p}$

Find: x_{3_p} Total, y_{3_p} Total (and average velocity for case where α, β, γ are random).

(1) Compute: $$\tan\epsilon = \frac{\cos\alpha \sin\beta \cos\gamma - \sin\alpha \sin\gamma}{\cos\beta \cos\gamma}$$

(2) Using (1), compute $$\sin\epsilon = \frac{\tan\epsilon}{\sqrt{1+\tan^2\epsilon}}$$

and $$\cos\epsilon = \frac{1}{\sqrt{1+\tan^2\epsilon}}$$

Thus, it is seen that $$-\frac{\pi}{2} < \epsilon < +\frac{\pi}{2}$$

(3) Compute:

$$\tan\rho = \frac{\cos\alpha \sin\gamma + \sin\alpha \sin\beta \cos\gamma}{\sqrt{(\cos\alpha \sin\beta \cos\gamma - \sin\alpha \sin\gamma)^2 + (\cos\beta \cos\gamma)^2}}$$

(4) Using (3), compute $\sin\rho = \dfrac{\tan\rho}{\sqrt{1+\tan^2\rho}}$

and $\cos\rho = \dfrac{1}{\sqrt{1+\tan^2\rho}}$

Similarly, $-\frac{\pi}{2} < \rho < +\frac{\pi}{2}$

(5) Using (2), compute

$$\sin\sigma = \cos\epsilon \sin\alpha \cos\gamma + \cos\epsilon \cos\alpha \sin\beta \sin\gamma - \sin\epsilon \cos\beta \sin\gamma$$

(6) Using (2), compute $\cos\sigma = \cos\epsilon \cos\alpha\cos\beta + \sin\epsilon \sin\beta$

(7) Using (5), (6) compute $x''_p = x_{3_p} \cos\sigma + y_{3_p} \sin\sigma$

(8) Using (5), (6), compute $y''_p = y_{3_p} \cos\sigma - x_{3_p} \sin\sigma$

(9)
$$B_x = x_{3_p} \cos\epsilon - \left[F\cos\rho - y_{3_p} \sin\rho \right] \sin\epsilon$$

$$B_y = y_{3_p} \cos\rho + F \sin\rho$$

$$B_z = \left[F\cos\rho - y_{3_p} \sin\rho\right] \cos\epsilon + x_{3_p} \sin\epsilon$$

(10) Using (9), compute

$$R_z = \frac{b + \sqrt{b^2 - (m^2+1)(b^2 - R^2m^2)}}{(m^2+1)}$$

where $b = R + H$, and $m = \dfrac{B_z}{\sqrt{B_x^2 + B_y^2}}$

(11) Using (10), compute $D_z = R_z - \left[R+H\right]$

(12) Using (9), (11), compute $D_x = R_x = \dfrac{B_x D_z}{B_z}$

(13) Using (9), (11), compute $D_y = R_y = \dfrac{B_y D_z}{B_z}$

(14) Compute $\omega_y = \omega \cos i$

(15) Compute $\omega_x = (\omega \sin i) \cos \Theta$

(16) Compute $\omega_z = (\omega \sin i) \sin \Theta$

where Θ = great circle angle along orbit since passing over equator.

$$\Theta = \sin^{-1}\left[\frac{\sin \text{lat}}{\sin L_{max}}\right] \quad ; \quad (L_{max} = \text{maximum latitude})$$

(17) Using (11), (12), (13) compute

$$D_{z''} = \left[D_z \cos\epsilon - D_x \sin\epsilon\right] \cos\rho + D_y \sin\rho$$

(18) Using (10), (13), (14), (16), compute

$$\dot{D}_x = R_z (\omega_y - \dot{\Theta}) - R_y \omega_z$$

(19) Using (10), (12), (15), (16), compute

$$\dot{D}_y = R_x \omega_z - R_z \omega_x$$

(20) Using (12), (13), (14), (15), compute

$$\dot{D}_z = R_y \omega_x - R_x (\omega_y - \dot{\Theta}) - \dot{H}$$

(21) Using (18), (19), (20), compute

$$\dot{D}_{z''} = \left[\dot{D}_z \cos\epsilon - \dot{D}_x \sin\epsilon\right] \cos\rho + \dot{D}_y \sin\rho$$

(22) Using (17), (21), compute

$$E = \frac{\dot{D}_{z''} F}{D_{z''}^2}$$

(23) Using (12), (17), (18), (22), compute

$$B_x = D_y \frac{F}{D_{z''}} - E D_x$$

(24) Using (13), (17), (19), (22), compute

$$B_y = D_y \frac{F}{D_z''} - ED_y$$

(25) Using (11), (17), (20), (22), compute

$$B_z = D_z \frac{F}{D_z''} - ED_z$$

(26) Using (23), (24), compute

$$\dot{x}_p'' = \dot{B}_x \cos\epsilon + \dot{B}_y \sin\epsilon$$

(27) Using (23), (24), (25), compute

$$\dot{y}_p'' = \dot{B}_y \cos\rho - \left[\dot{B}_z \cos\epsilon - \dot{B}_x \sin\epsilon\right] \sin\rho$$

(28) Using (23), (24), (25), compute as a check:

$$\dot{z}_p'' = 0 = \left[\dot{B}_z \cos\epsilon - \dot{B}_x \sin\epsilon\right] \cos\rho + \dot{B}_y \sin\rho$$

(29) Using (5), (6), (26), (27), compute

$$\dot{x}_{3_p} = \dot{x}_p'' \cos\sigma - \dot{y}_p'' \sin\sigma$$

(30) Using (5), (6), (26), (27), compute

$$\dot{y}_{3_p} = \dot{y}_p'' \cos\sigma + \dot{x}_p'' \sin\sigma$$

$\dot{y}_{3_p}$ and $\dot{x}_{3_p}$ are the parts of the image velocity exclusive of the effect of $\dot{\alpha}$, $\dot{\beta}$, $\dot{\gamma}$; i.e., they are only "partial image velocity components."

Note: If the plate constitutes a stable platform during exposure, (i.e., if it has zero angular velocity with respect to inertial space), then $\dot{\alpha}$, $\dot{\beta}$, $\dot{\gamma}$ are given by

$$\dot{\alpha} = \dot{\Theta}\left[\sin\alpha \sin\beta \cos\gamma + \cos\alpha \sin\gamma\right]$$

$$\dot{\beta} = \dot{\Theta}\left[\cos\alpha \cos\gamma - \sin\alpha \sin\beta \sin\gamma\right]$$

$$\dot{\gamma} = -\dot{\Theta}\left[\sin\alpha \cos\beta\right]$$

More generally, for arbitrary plate angular velocities, the relation between the inertial space angular velocity components $\dot{A}$, $\dot{B}$, $\dot{\Gamma}$, which are directed along the instantaneous directions of the z_3, y_3, x_3 axes respectively, are related to $\dot{\alpha}$, $\dot{\beta}$, $\dot{\gamma}$ as follows:

$$\dot{A} = -\dot{\alpha} + \dot{\Theta}\left[\sin\alpha \sin\beta \cos\gamma + \cos\alpha \cos\gamma\right]$$

$$\dot{B} = -\dot{\beta} + \dot{\Theta}\left[\cos\alpha \cos\gamma - \sin\alpha \sin\beta \sin\gamma\right]$$

$$\dot{\Gamma} = -\dot{\gamma} - \dot{\Theta}\left[\sin\alpha \cos\beta\right]$$

(31) Compute; $\dot{x}_{3_{p,\dot{\beta}}} = -\dot{\beta}\left[\frac{F^2+x_{3_p}^2}{F}\right]$

(32) Compute $\dot{y}_{3_{p,\dot{\beta}}} = -\dot{\beta}\left[\frac{x_{3_p}\, y_{3_p}}{F}\right]$

(33) Compute $\dot{x}_{3_{p,\dot{\gamma}}} = -\dot{\gamma}\left[\frac{x_{3_p} y_{3_p}}{F}\right]$

(34) Compute $\dot{y}_{3_{p,\dot{\gamma}}} = -\dot{\gamma}\left[\frac{F^2 + y_{3_p}^2}{F}\right]$

(35) Compute $\dot{x}_{3_{p,\dot{\alpha}}} = -\dot{\alpha}\, y_{3_p}$

(36) Compute $\dot{y}_{3_{p,\dot{\alpha}}} = \dot{\alpha}\, x_{3_p}$

(37) Using (30), (31), (32), (35), compute

$$\dot{x}_{3_p}\,\text{Total} = \dot{x}_{3_p} + \dot{x}_{3_{p,\dot{\alpha}}} + \dot{x}_{3_{p,\dot{\beta}}} + \dot{x}_{3_{p,\dot{\gamma}}}$$

(38) Using (29), (32), (34), (36), compute

$$\dot{y}_{3_p}\,\text{Total} = \dot{y}_{3_p} + \dot{y}_{3_p,\dot{\alpha}} + \dot{y}_{3_p,\dot{\beta}} + \dot{y}_{3_p,\dot{\gamma}}$$

$\dot{x}_{3_p}$ Total and $\dot{y}_{3_p}$ Total are the required answers for a specific $\dot{\alpha}$, $\dot{\beta}$, $\dot{\gamma}$; but if $\dot{\alpha}$, $\dot{\beta}$, $\dot{\gamma}$ are random - so that they are negative as often as they are positive, then average values and extreme values of $\dot{x}_{3_p}$ Total and $\dot{y}_{3_p}$ Total would usually be desired.

(39) For the random case, we repeat steps (31) and (39) for all eight possible sign combinations between $\dot{\alpha}$, $\dot{\beta}$, $\dot{\gamma}$.

$\dot{\alpha}$	+	+	+	+	-	-	-	-
$\dot{\beta}$	+	+	-	-	+	+	-	-
$\dot{\gamma}$	+	-	+	-	+	-	+	-

(40) Using (37), (38), compute, for each of the eight cases:

$$\left|\text{VEL}_{\text{Total, 3p}}\right| = \sqrt{\dot{x}_{3p}^{2}{}_{\text{Total}} + \dot{y}_{3p}^{2}{}_{\text{Total}}}$$

(41) Of the eight values obtained in (40), we will have

$\left|\text{VEL}_{\text{Total, 3p}}\right|$ Max Possible, $\left|\text{VEL}_{\text{Total, 3p}}\right|$ Min Possible

(42) Using the eight values obtained in (40), compute

$$\left|\text{VEL}_{\text{Total, 3p}}\right| \text{ Linear Average} = \frac{1}{8} \cdot \sum_{n=1}^{8} \left|\text{VEL}_{\text{Total, 3p}}\right|_n$$

(43) In the general case, any or all of the angular velocities $\dot{\alpha}$, $\dot{\beta}$, $\dot{\gamma}$, may have non-random components, while some may have negligible random components. This can still be handled by the formalism of (39) through (42) by considering all eight cases as having equal weight (keeping as distinct those combinations which, due to zero random components, may have become identical). To illustrate; if $\dot{\alpha}$ were purely non-random and always positive, and $\dot{\beta}$ had a negative non-random component as well as a random part, and $\dot{\gamma}$ were purely random, the eight cases would be tabulated as shown, the first part of each sign pair denoting the non-random component.

$\dot{\alpha}$	+, 0	+, 0	+, 0	+, 0	+, 0	+, 0	+, 0	+, 0
$\dot{\beta}$	-, +	-, +	-, -	-, -	-, +	-, +	-, -	-, -
$\dot{\gamma}$	0, +	0, -	0, +	0, -	0, +	0, -	0, +	0, -

APPENDIX E

GLOSSARY

AEOLIAN - Borne, deposited, produced or eroded by the wind.

AEROSOL - A suspension of insoluble particles in a gas.

ANOMALOUS - Deviating from the general rule or norm.

APHELION - The point in a solar orbit which is most distant from the sun.

APSIDAL - Pertaining to either of the two orbital points nearest or farthest from the center of attraction.

ASPHERIC LENS - A lens in which one or more surfaces depart from a true spherical shape.

ASTIGMATISM - An aberration affecting the sharpness of images for off-axis objects in which the rays passing through different meridians of the lens come to a focus in different planes.

CENTRAL OBSCURATION - The loss of the light gathering capability in the central portion of the primary mirror of a catadioptric or reflective optical system due to the necessity of placing a secondary image forming component on the optical axis.

CHROMATIC ABERRATION - In an optical system, the forming of more than one image, one for each color of light present, caused by the varying refractive index of the glass with different colors (wavelengths).

COMA - In an optical system, a result of spherical aberration in which a point of light, not on the axis, has a blurred, comet-shaped image.

APPENDIX E
(Continued)

GLOSSARY

CURVATURE OF FIELD - An aberration affecting the longitudinal position of images off the axis in such a manner that objects in a plane perpendicular to the axis are imaged in a curved or disk shaped surface.

DIURNAL - Having a period of, occurring in, or related to a day.

ESCARPMENT - A steep slope or cliff.

F/NUMBER - For a photographic or telescopic lens, the ratio of the equivalent focal length to the diameter of the entrance pupil (aperture diameter).

FIDUCIAL MARKERS - Index marks, usually four, used to define the axes whose intersection fixes the principal point of a photograph and fulfills the requirements of interior orientation.

GRABEN - A depressed tract bounded on at least two sides by faults and generally of considerable length as compared with its width.

HORST - A tract or mass of the planets crust separated by faults from surrounding tracts which have been relatively depressed.

IGNEOUS - Resulting from the action of heat from within, usually accompanied by fusion; of rocks, formed by solidification of a molten magma.

JULIAN DATE - The number of mean solar days elapsed since January 1, 4713BC, Greenwich mean noon.

APPENDIX E
(Continued)

GLOSSARY

MESOPAUSE - The base of the inversion at the top of the mesosphere.

MESOSPHERE - The atmospheric shell, in which temperature generally decreases with heights, extending from the stratopause at about 50 to 55 kilometers to the mesopause at about 80 to 85 kilometers.

MONOBATH - A single solution which contains both developer and fixer.

MORPHOLOGY - The science of structural organic types.

OCCULTATION - The disappearance of a body behind another body of larger apparent size.

PARALLAX - The difference in the apparent direction or position of an object when viewed from different points.

PERIHELION - The point in a solar orbit which is closest to the sun.

RETROGRADE - Motion in an orbit opposite to the usual orbital direction of celestial bodies within a given system.

SECULAR - Pertaining to long periods of time on the order of a century.

SPHERICAL ABERRATION - An aberration caused by rays through various zones of a lens coming to focus at different places along the axis.

T/NUMBER - The ratio of the F/number to the square root of the lens transmittance, a measure of the "speed" of a lens.

TECTONIC - Of, pertaining to, or designating, the rock structures and external forms resulting from the deformation of the earth's crust.

TONE - The characteristic of a photographic emulsion which records different target reflectances as different density levels on the film.